

From Small Organic Molecules to Peptides As Tools For Anti-infectives Drug Discovery

Dissertation

zur Erlangung des Grades des Doktors der
Naturwissenschaften der Naturwissenschaftlich-
Technischen Fakultät der Universität des Saarlandes

Von

Dipl.-Pharm.

Ahmed Ashraf Moustafa Kamal

Saarbrücken

2017

Tag des Kolloquiums: 8th Dezember 2017

Dekan: Prof. Dr. Guido Kickelbick

Vorsitz: Prof. Dr. A. K.H. Hirsch

Berichterstatter: Prof. Dr. R. W. Hartmann
Prof. Dr. C. M. Lehr

Akad. Mitarbeiter: Dr. M. Engel

Die vorliegende Arbeit wurde von Januar 2014 bis Septemeber 2017 unter Anleitung von Herrn Univ.-Prof. Dr. Rolf W. Hartmann in der Fachrichtung Pharmazie der Naturwissenschaftlich-Technischen Fakultät der Universität des Saarlandes sowie am Helmholtz-Institut für Pharmazeutische Forschung Saarland (HIPS) in der abetailung Drug design and Optimizationn (DDOP), angefertigt.

Fall seven times, stand up eight

~Japanese proverb

Table of Contents

Abstract	3
Zusammenfassung.....	4
Acknowledgement.....	5
List of Abbreviations.....	7
Papers included in the thesis	8
Contributions report	9
1. Introduction.....	10
1.1. Analysis of drugs discovery in respect of molecular size	10
1.2. Cellular location of targets and its influence on drug class choice	12
1.3. Approaches to overcome biological barriers for drugs addressing intracellular targets .	13
1.3.1 Chemical derivatization according to semi-empirical rules	13
1.3.2 Coupling of “cargo” to peptides/proteins capable of cell penetration	16
2. Aim of thesis.....	19
A) PQS-QS system in <i>Pseudomonas aeruginosa</i>	19
B) <i>E. coli</i> RNA polymerase	20
3. Results	21
3.1 Chapter A: Structure–functionality relationship and pharmacological profiles of <i>Pseudomonas aeruginosa</i> alkylquinolone quorum sensing modulators	21
3.2 Chapter B: Exploring the chemical space of ureidothiophene-2-carboxylic acids as inhibitors of the quorum sensing enzyme PqsD from <i>Pseudomonas aeruginosa</i>	33
3.3 Chapter C: Hit optimization of an α -helical peptide: Ala-scan, truncation, and sidechain-to-sidechain macrocyclization of an RNA polymerase inhibitor	42
4. Conclusion and Outlook	58
4.1 Small organic molecule (PqsR)	58
4.2 Peptide-Small organic molecule conjugates (PqsD).....	59
4.3 Peptides (RNAP)	60
5. References	62
6. Appendix.....	67
6.1 Supporting information chapter A	67
6.2 Supporting information chapter B	138

6.3 Supporting information chapter C	176
7. Curriculum Vitæ.....	223
8. Further publications of the author that is not part of this dissertation	224

Abstract

The increasingly lower discovery rates of novel drugs with a novel mechanism of action are alarming especially anti-infective agents where concurrent increase in resistance rates are reported. This advocates expanding the search for innovative anti-infectives over a wide chemical space range.

Accordingly, two targets are addressed in the novel approach of developing pathoblockers instead of classical antibacterials by quorum sensing inhibition. In the first target (PqsR), the focus is synthesizing small organic molecules to shed more light on the structure-functionality relationship of the compounds. Inverse agonists were shown to be the only pharmacological class to significantly inhibit the virulence factor pyocyanin in addition to identifying distinct amino acids for each drug class interaction. As to the second focus (PqsD), the developed inhibitors suffered from the lack of activity on the cellular level. So, design and linking of small molecule inhibitor to cell penetrating peptides were executed. While one of the conjugates retained its *in vitro* activity, no activity was yet observed *in vivo*.

Lastly, a validated antibacterial target (RNA polymerase) was revisited *via* a novel approach. Macrocyclic peptides with improved α -helical propensities were designed and synthesized in order to improve activity *in vitro* and potentially on the cellular level. Even though this enhancement was not allied with an increase in biological activity, novel SAR insights were disclosed.

Zusammenfassung

Alarmierend ist die Tatsache, dass die Zahl neuer Arzneistoffe mit innovativem Mechanismus ständig abnimmt. Das fällt bei Anti-Infektiva besonders schwer ins Gewicht, da gleichzeitig die Resistenzraten gegenüber verfügbaren Antibiotika steigen. Dies macht die Suche nach neuartigen Anti-Infektiva unter Einbeziehung des gesamten chemischen Strukturraums nötig.

Dementsprechend wurden hier zwei Targets in einem neuartigen Ansatz zur Hemmung der Quorum Sensing Kommunikation adressiert, die zur Entwicklung von Pathoblockern anstelle der klassischen Antibiotika führen sollen. Im Fall des ersten Targets (PqsR) liegt der Fokus auf der Synthese von kleinen organischen Molekülen um den Zusammenhang zwischen Struktur und Funktion der Moleküle besser zu verstehen. Gezeigt werden konnte, dass nur inverse Agonisten in der Lage waren, die Bildung des Virulenzfaktors Pyocyanin signifikant zu hemmen. Außerdem wurden die für die Interaktion jeder Klasse spezifischen Aminosäuren identifiziert. Was das zweite Target (PqsD) anbelangt, hatten die entwickelten Inhibitoren keine Zellaktivität gezeigt. Aus diesem Grunde wurden diese Verbindungen mit Zellpenetrierenden Peptiden verknüpft. Die Konjugate erwiesen sich als *in vitro* aber nicht *in vivo* aktiv.

Des Weiteren wurde auf das validierte antibakterielle Target RNA Polymerase in einem neuartigen Ansatz zurückgekommen. Makrozyklische Peptide mit verbesserten α -helikalen Eigenschaften wurden konzipiert und synthetisiert um die *in vitro* Aktivität und eventuell die Zellaktivität zu erhöhen. Auch wenn die biologische Aktivität nicht gesteigert werden konnte, wurden neue Struktur-Wirkungs-Beziehungen erhalten.

Acknowledgement

First and foremost, my gratitude goes to Allah (the Arabic word for God) for guiding me throughout this last few years and charging me with perseverance to complete this work until the end.

It was my great honor to be one of the last students mentored by Prof. Rolf W. Hartmann. I learned so much from him not only scientifically but on the personal level as well. I am forever in his debt for the continuous support, patience, motivation, and immense knowledge I could not have wished for a better supervisor for my doctoral thesis.

I would like to thank Prof. Claus M. Lehr for accepting me as one of his students and being my second supervisor for the last four years. He always showed care and attention to make sure I am progressing well throughout my Ph.D. and would finish in the time frame set.

I am grateful for working with Dr. Jens Eberhard even for such a short period of time as I got to learn most from him whether it was skills in the lab or in life. He was always a great support and showed faith in me when I didn't have any myself and for that, I thank him endlessly.

I am appreciative of all the efforts and mentorship Dr. Martin Empting has given me starting from my masters till today. I shall carry on the knowledge and lessons he taught me for life.

I believe I was extremely lucky to work with such an amazing group of scientists during my stay at HIPS. Firstly, I would like to thank Dr. Christine K. Maurer for being an outstanding scientist, colleague, and friend. She never seized to give help when needed. Same goes for Dr. Jörg Haupenthal for always having his door open to others seeking his scientific and managerial help. I am grateful for knowing such a great human being and friend Dr. Mostafa Hamed, his easy-going friendly character made him an extraordinary lab mate. I would like to show appreciation to Dr. Matthias Engel for being an outstanding scientific collaborator and scientist. I am grateful for Dr. Samir Yahiaoui's great pieces of advice and unlimited aid he always offered. My due thank goes to Isabell Schnorr, Dr. Jan Henning Sahner and Dr. "Astrein" Benny for their amazing collaborative spirit and sense of humor.

I was even luckier for knowing and working with Jeannine Jung and Simone Amann. You were an unlimited source of joy and fun as well as a second family to me. I would like to thank Ghamdan, Nadia, Federica, Mohamed Salah and Abo Saad for the great time, laughter and companionship we shared. A very special gratitude goes out to all my colleagues at HIPS, Universität des Saarlandes, and Pharmbiotech for their emotional support, advice and providing such a positive working environment.

“It's the friends we meet along life's roads who help us appreciate the journey”. Gogo Allegretta and Antonio Martins, no words can describe how grateful I am to meet you guys. Long live the exp(er)ts.....

Last but not least, my family, mom, dad, and brother, if I start off thanking you from today till the last day of my life it won't be enough to show you appreciation and gratitude. You were always there for me in distress before ease and provided me with a never-ending support during my life.

Without you all, I would not be the person
I am today

Thank you, Danke Schön, Grazie Mille,
Dank je wel, Obrigado, شكرا

List of Abbreviations

SOM	Small organic molecule
Da	Dalton
Mwt	Molecular weight
mAbs	Monoclonal antibodies
CPP	Cell penetrating peptide
ADC	Antibody-drug conjugates
i.v.	Intravenous
s.c.	Subcutaneous
i.m.	Intramuscular
CYP	Cytochrome P450
PPI	Protein-protein interaction
GIT	Gastrointestinal tract
BBB	Blood brain barrier
Ro5	Rule of 5
cLogP	Calculated octanol-water partition coefficient
PSA	Polar surface area
MAS	Minimal active sequence
PEPT	Peptide transporter
DNA	Deoxyribonucleic acid
RNA	Ribonucleic acid
MTX	Methotrexate
SynB1	Protegrin-derived cell penetrating peptide
IC50	Half maximal inhibitory concentration
E2F	E2 factor
HTV	Hantaan virus
Tat	Trans-activator of transcription
SP	Substance P
GPCR	G protein-coupled receptors
NK1R	Neurokinin-1 receptor
GFP	Green fluorescent protein
Cre	Causes recombination
PA	<i>Pseudomonas aeruginosa</i>
PQS	<i>Pseudomonas</i> quinolone signaling
QS	Quorum sensing
RNAP	Ribonucleic acid polymerase
SM	Signaling molecule
PqsR	<i>Pseudomonas</i> quinolone signaling receptor
MvfR	Multiple virulence factor regulator
μM	Micromolar

Papers included in the thesis

This thesis is divided into three publications, which are referred to in the text by their letter:

A) “Structure-functionality relationship and pharmacological profiles of *Pseudomonas aeruginosa* alkylquinolone quorum sensing modulators”

Kamal, A.A.M.; Petrera, L.; Eberhard, J.; Hartmann, R.W. *Organic & biomolecular chemistry* **2017**, *15*, 4620–4630.

B) “Exploring the chemical space of ureidothiophene-2-carboxylic acids as inhibitors of the quorum sensing enzyme PqsD from *Pseudomonas aeruginosa*”

Sahner, J.H.; Empting, M.; Kamal, A.; Weidel, E.; Groh, M.; Börger, C.; Hartmann, R.W. *European journal of medicinal chemistry* **2015**, *96*, 14–21.

Contributions report

The author would like to declare his contributions to the papers **A-B** included in this thesis.

A) The author contributed significantly to the design, organic synthesis, and characterization of the designated compounds. In addition, he performed the underlying molecular docking studies and interpreted the biological results. He conceived and wrote the manuscript.

B) The author synthesized peptide-compound conjugate (**25**) in addition to performing melting point measurements to all compounds.

1. Introduction

A major drive for mankind discoveries has always been curiosity; the urge to find what's lying there in the unknown, crossing barriers and seeking novelty in uncharted regions. Likewise, medicinal and organic chemists have undertaken extensive efforts to explore the drug discovery chemical space and overcome barriers posed by cellular compartments in order to deliver potent, safe, and stable therapies of tomorrow to today's patients.

1.1. Analysis of drugs discovery in respect of molecular size

Upon inspecting currently available drugs on the market according to their molecular sizes, the first evident observation is that all drugs can be categorized into two big classes namely small organic molecules (SOMs) and biologics. Most of the SOMs exist below the 500 Daltons (Da) mark while the molecular weight (Mwt) of biologics is usually a few thousands of Daltons. For example, aspirin has a Mwt of 180 Da in comparison to monoclonal antibodies (mAbs) which usually have a Mwt of ~150,000 Da (Fig. 1). Genentech parallels this to the difference between a bicycle and a business jet. Even though this quite staggering difference in size and complexity both classes effectively exert diverse biological effects on various drug targets [1].

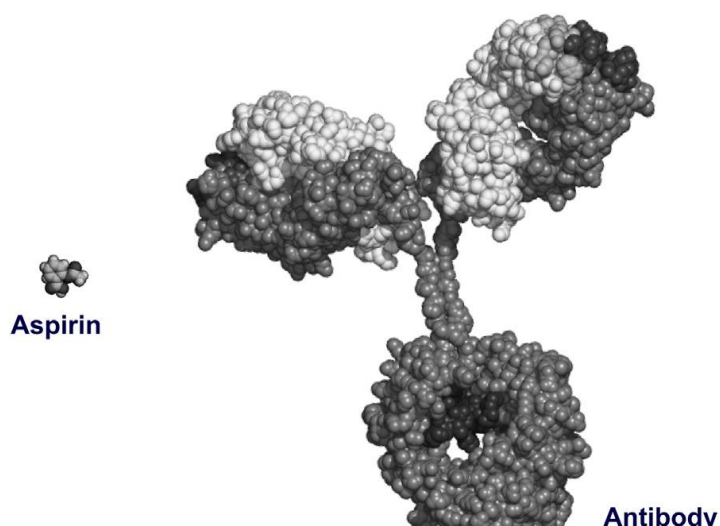


Figure 1. A depiction of aspirin in comparison to a monoclonal antibody [1]

The second observation is the huge gap between the two classes (500-100,000s Da) with Insulin and growth hormones as the most prominent examples of treatments occupying that

space. Peptide-based therapeutics elegantly bridge this gap possessing an amino acid based core as in biologics while maintaining some of the size and cell-penetrability of SOMs [1,2].

A drug doesn't have to be solely composed of one of the aforementioned classes. For example, one can combine SOMs with a cell-penetrating peptide (CPP) or make antibody-drug conjugates (ADCs) [3,4]. The latter have been gaining huge interest as it provides combining the different advantages of both biologics (specificity and safety) with the potency of SOMs. Such techniques would allow the permeation and/or selective delivery of a compound in high concentrations to target cells or cell compartments not accessible by SOMs alone [1–3]. Table 1 provides a comparison of the properties of SOMs, peptides, biologics and mixed conjugates.

	SOMs	Peptides	Biologics	Mixed-conjugates
Composition	Synthetic organic compound	Amino acids	Amino acids	Amino acids/ synthetic organic compounds
Mwt	<700 Da	~ 500 - 2000	>10,000	1000-150,000
Physicochemical properties	Well defined	Fairly defined to complex	Complex	
Preparation	Chemical synthesis	Chemical synthesis / Biotechnological production	Biotechnological production	Chemical synthesis / Biotechnological production
Dosing route	Usually Oral	Typically i.v., s.c., i.m.		
Dose interval	Few hours to days		Days to months	
Serum half-life	Short	Relatively long		
Potency and selectivity	Generally less selective	High selectivity (affinity and potency)		
Immunogenicity	No	Unlikely	Yes	Yes
Distribution	To any combination of organs/cells	Possible to any combination of organs/cells	Usually limited to plasma and extracellular fluids	
Metabolism	Typically <i>via</i> CYP450s	<i>via</i> CYP450s and Proteolytic degradation	Proteolytic degradation	<i>via</i> CYP450s and Proteolytic degradation
Excretion	Mainly biliary and renal		Mostly recycled by body	
Target location	Intracellular and extracellular		Mostly extracellular	Intracellular and extracellular
Off-target activities	By drug or its metabolites	Unlikely		By drug or its metabolites

Table 1. Comparison of properties of small organic molecules, peptides, biologics, and mixed-conjugates. Adopted from [1–4]

Thirty years ago, the rise in biologics led some pharmaceutical companies to focus on developing biologics solely while others remaining with the classical SOMs. However, currently, all “big pharma” are developing both types of drugs. It's not a matter of choosing between the different classes but rather using them alone or in combination in order to discover novel therapies.

1.2. Cellular location of targets and its influence on drug class choice

One of the most important – preferably early – steps in drug discovery is target identification, druggability, and validation [5]. In order to achieve that the target has to be accessible to the molecule and once bound block the site or the production of ligands eliciting an undesirable biological response i.e. the medications have to reach their site of action and be potent enough [6]. Therefore, the target's location and properties of the site of action influence the choice of drug class (size).

Besides Ion channels and transporters, all protein drug targets can be classified into three categories:

- Enzymes: They are proteins required for catalyzing different reactions in the human body. They can be located inside cells or on the surface or in blood.
- Intracellular receptors: For drugs targeting such receptors crossing of the cell membrane is required. Therefore, such molecules must have certain properties. These receptors can be located in the cytoplasm or the nucleus of the cells.
- Extracellular receptors: On the contrary to the previous type, the receptors lay on the cell surface and thus no crossing of cellular barriers are required. Once the drug binds, a signal is transduced to the inside of the cell affecting cellular pathways.

Biologics have long been believed to be too big for cellular penetration. Thus, they were utilized exclusively for extracellular targets on cells surfaces rather than intracellular ones leaving a lot of untapped potential targets [7]. However, recently Ferrone *et al.* were able to show that antibodies can penetrate cell membrane targeting intracellular phosphatases of regenerating liver stopping metastases. Even though, the underlying exact molecular mechanism might still be elusive [8–10].

The assumption (Biologics are too big for cellular penetration) led to bias for using SOMs for targeting intracellular targets [11]. However, targeting protein-protein interactions (PPIs) for example has shown to be impervious to SOMs due to having huge surface areas and small contact points [12]. Thus, even though SOMs are easier to get into cells they are not potent enough to result in a biological response. In contrast, peptides and biologics possess high interaction surface area enabling high affinity as well as specificity to their targets [12]. It is therefore important to consider larger molecules – beyond the 500 Da mark – towards

“challenging” intracellular targets and how to modulate them in order to overcome the hurdle of intracellular penetration [12,13].

1.3. Approaches to overcome biological barriers for drugs addressing intracellular targets

Typically, irrespective of the compound class and route of administration, compounds are challenged by physical barriers such as the gastrointestinal tract (GIT), surface epithelia, blood brain barrier (BBB), and interstitial tissue [14]. In the case of compounds addressing intracellular targets, one or more additional obstacles of human nature (cell membranes and/or mitochondrial membrane) or of other species colonizing the human body i.e. microbes must be overcome.

Molecular weight and size influences cell permeability and the techniques employed to improve drug to target accessibility. Nevertheless, there are three approaches generally pursued:

1. Formulation and drug delivery technologies
2. Chemical derivatization according to semi-empirical rules
3. Coupling of “cargo” to peptides/proteins capable of cell penetration.

The latter two points are discussed more in details in the following subtitles.

1.3.1 Chemical derivatization according to semi-empirical rules

One of the very first attempts to develop empirical correlations for permeation was the seminal work of Lipinski *et al.*. Lipinski’s “Rule of 5” (Ro5) focused on correlating physicochemical properties (polarity and size) of SOMs only and its influence on oral absorption and passive permeation [15]. The rule states mainly four parameters that can decrease permeation and oral absorption:

- >5 H-bond donors
- >10 H-bond acceptors
- Molecular weight >500 Da
- Calculated Log P (cLogP) >5

Other hypotheses were proposed adopting alternative metrics such as polar surface area (PSA), the number of rotatable bonds, and conformational flexibility as better predictors [13,14,16–19]. However, not all permeable compounds conform to those rules and vice versa. Therefore, these physicochemical “rules” should be used more as guidelines rather than absolute criteria. Especially handling natural products and compounds beyond the 500 Da mark (600-1200 Da) where many compounds are characterized by having a ‘chameleonic’ ability [13,19]. A well-known example of this is “cyclosporine A” which in aqueous solution adopts a conformation where its polar groups are exposed to the outside (high PSA) however when crossing the lipid membranes it changes its conformation burying its polar groups (low PSA) [13,14,16].

Drugs for certain indications e.g. anti-infectives display added nonconformity to these rules as they are required to cross dissimilar permeation barriers i.e. the microbe cell wall (bacteria and fungi). In the case of intracellular infections, these drugs need to possess physicochemical properties to cross both barriers [20]. Cell membrane/wall permeation properties might vary immensely from humans to one microorganism and from one microorganism to the other. Thus, several attempts were undertaken to derive semi-empirical guidelines that apply for either single microorganisms or multiple ones e.g. Gram-positive vs. Gram-negative [21–23].

Another example of compounds which need to cross a second additional barrier is drugs targeting the mitochondria. Mitochondria have a further distinct double membrane with a strong internal negative potential. This taken into consideration, the design of molecules possessing a net cationic charge might lead to accumulation inside the negatively charged mitochondrial matrix [24].

Besides passive diffusion, prokaryotic and eukaryotic cells possess a set of transporters that can transport important cell substrates into the cell either with (passive) or against (active) gradient concentration. It also possesses efflux pumps and carrier proteins which expel xenobiotics and/or cellular products to the outside of the cell [14]. In theory, permeation could come about or could improve by designing compounds that mimic the active transporters/protein carriers’ natural substrates structurally rather than using physicochemical properties based models. For instance, if a ligand-based approach is undertaken to concept novel antagonists for an intracellular receptor whose agonist is actively transported, it is possible that the antagonists will be transported *via* the same set of

transporters. However, up till now, it has proven quite difficult to conceive drugs that are transporter specific [14].

A steep drop-off in cellular permeability is observed once the Mwt of molecules exceeds the 1000 Da mark making it unlikely that peptides can passively diffuse through the cellular membrane [13,16–18]. Nevertheless, some peptides are able to translocate into the cells either *via* energy-independent direct penetration or endocytosis [14]. Several techniques have been devolved for converting non-permeable peptides to permeable ones. Those techniques are focused mainly on optimizing two physical parameters (restricting conformation flexibility and decreasing polarity [25]):

A) Macrocyclization:

Cyclization of peptides by insertion of a side-to-side chain “staple” has shown to improve cellular permeability. This is because the polar amide backbone by such modification is shielded from the surrounding milieu hence decreasing polarity. The nature of the covalent stabilization also plays a role. If hydrocarbon side-to-side bridge were to be used, an increase in hydrophobicity occurs enhancing permeability through the lipids membrane. Additionally, stapling might lead to an increase in α -helical content improving peptide-cell membrane interactions and subsequently internalization [25,26].

B) *N*-Methylation:

Backbone *N*-methylation of peptide’s amide *-NH-* has shown to rigidify peptides conformation by stabilizing hydrogen-bonded conformations and decreasing the peptide backbone flexibility. Thus, *N*-methylation may serve to increase membrane permeability by stabilizing intramolecular hydrogen bonding in the membrane-associated state [27,28].

C) Increase net cationic charge

Empirical observations concluded that in order to achieve cell-penetration, a net positive charge is desired for peptides. The overall positive charge is believed to promote better association of the peptides to the negatively charged phospholipid bilayer of cell membranes. Several studies demonstrated that structure guided optimization of peptides and replacement of amino acids not involved in binding to the target with Lysine or Arginine residues induces significant cell permeability. It must be noted that an unmonitored increase in cationic charge might lead to toxic peptides with cell-lysing property [29–32].

Hence, biologics has long been thought incapable of targeting intracellular targets except for a few cases (see subtitle 1.2). Therefore, not many efforts have been pursued into structural modification of biologics for enhancing cellular penetration. The main approach pursued to enhance intracellular delivery is by decreasing the size of biologics to the minimal active sequence (MAS) and coupling the “cargo” to peptides that can translocate across cell membranes. The latter will be further discussed in the next subtitle.

1.3.2 Coupling of “cargo” to peptides/proteins capable of cell penetration

Some molecules have the ability to cross the cell membrane/wall barrier with relative ease compared to others. These could be passively diffused or actively transported substrates, and CPPs [33]. In what’s known as the “Trojan horse” strategy, an impermeable molecule of interest (cargo) can be linked to one of the aforementioned carrier entities granting it cell access [34–36]. However, this is not always straight forward as multiple parameters have to be thoroughly investigated such as the carrier of choice, linker stability (cleavable or not), site of drug conjugation and drug to carrier ratio [37].

A classical application of this approach is design/synthesis of prodrugs by coupling an *in vitro* active drug to a natural transporter substrate such as sugars, amino acids, and bile acids [33]. An example of such “prodrug” approach is Valganciclovir the valyl ester prodrug of Ganciclovir (attached to the amino acid L-valine) that was demonstrated to be better internalized by means of peptide transporters PEPT1 and PEPT2 [38].

Longer amino acid chains namely peptide-based carriers have been shown to be a promising tool for improving intracellular drug delivery e.g. CPPs. These peptides are also known as protein transduction domains and are divided into 3 main classes: 1) Cationic peptides. 2) Hydrophobic peptides derived from secreted growth factors and cytokines. 3) Cell-type specific peptides [31,33,35,36].

Even though the exact mechanistic of how these peptides manage cell membrane penetration is not fully elucidated, the general mechanism has been shown to be receptor-independent pinocytosis [31]. CPPs are very versatile tools in terms of their ability to translocate diverse set of molecules i.e. SOMs, other peptides, plasmids, antigens, enzymes, DNA, RNA, and biologics [36,39].

One of the early attempts for intracellular delivery of CPP-drug conjugates linked methotrexate (MTX) to a poly (L-Lysine) peptide [40]. The conjugate cellular uptake exceeded that of the free drug. Intracellularly, it was found that the carrier peptide is degraded by means of lysosomal enzymes releasing the free drug inside the cells leading to *in vitro* tumor growth inhibition. Another study, coupled Doxorubicin to D-penetratin and SynB1, the vectorized Doxorubicin displayed a 20-fold lower IC₅₀ in Doxorubicin resistant cells due to enhanced uptake [41]. This effect was validated in an *in vivo* mouse model displaying rapid accumulation of the vectorized drug in Doxorubicin-resistant cells, thereby resulting in potent tumor cytotoxicity.

Likewise, the coupling of CPPs to other peptides has been pursued creating a larger sequence capable of both cell penetration and displaying a biological effect. In one study, two peptides were isolated that interfere with the function of the transcription factor E2F (a key factor in the regulation of cell proliferation) displaying an antiproliferative effect in tumor cells [42]. The peptides were fused to a HTV-Tat derived CPP. The Tat containing peptides decreased the level of expression of targeted regulated genes *in vivo* resulting in inhibition of cell proliferation and induction of cell apoptosis.

Although most CPPs have been shown to translocate in a receptor-independent manner and as such lack cell type specificity, some developed vectors have been shown to be receptor mediated. An example of that is substance P (SP) [43]. SP is an eleven-amino acids long peptide that is internalized by means of its natural GPCR cognate (NK1R, neurokinin-1 receptor). NK1R

is known to be over-expressed in glioblastoma. Rizk *et al.* took advantage of this information and covalently associated SP to intracellularly deliver proteins such as GFP, DNA fragments, and polystyrene beads up to 1 μm in diameter in a selective manner to cancerous cells.

Whereas GFP was treated as a cargo in the previous example, a “supercharged” variant of GFP capable of cell membrane penetration has been devised with a net charge of +36 [44]. In a following study, the same lab used the +36 GFP as a transferor for the delivery of functional Cre recombinase enzyme – *in vitro* and *in vivo* – into mammalian cells [45].

In summary, it has been shown that engineered or naturally occurring transporters are capable of internalizing various molecules with a broad span of size and weight. Moreover, the relative size of the drug/cargo (SOM, peptide or protein) compared to its carrier (a single amino acid, peptides or proteins) might not be of utmost importance in determining permeability but rather the common substructures.

2. Aim of thesis

By 2050, deaths attributable to antimicrobial resistance every year are estimated to be around 10 million [46]. That is one fatality every three seconds. Such mortality rates are accelerating due to the concurrent increase in resistance to clinically used antibiotics (Abs) and the lack of innovation in the discovery of novel ones. One of the main microbial threats which this work helps to tackle are Gram negative bacteria namely *Pseudomonas aeruginosa* (PA) and *Escherichia coli*. The strategy adopted for this work aims to help in deaccelerating the aforesaid crisis by targeting:

- a) Novel targets that should not infer resistance but only block the bacterium's pathogenicity [47] (*Pseudomonas* Quinolone signaling quorum sensing system, PQS-QS) and
- b) A previously validated target (*E. coli* RNA polymerase) *via* a novel mode of action.

A) PQS-QS system in *Pseudomonas aeruginosa*

This work intends to tackle two targets in the PQS-QS system namely, PqsD and PqsR (also known as MvfR). In a previous work from our lab, PqsR inhibitors were derived from ligand-based drug design where the natural agonist – a SOM – quinolone scaffold was interconverted into an inhibitor [48–50]. It was observed that the C-3 position might be of great influence on the compound's pharmacology. In order to enable rational hit-to-lead optimization, a synthetic campaign focusing mainly on modifications at position 3 of different biophysical attributes is to be embarked on. The yielded compounds would be subjected to a series of heterologous assays with the aim to elucidate the link between structural variations and compound pharmacological class. Moreover, *in silico* studies are to be devised to gain more insights into protein-ligand interactions on the molecular level. Finally, the effect of the pharmacological profile on the inhibition of virulence factor pyocyanin is to be investigated. The first discovered hits addressing PqsD suffered from low to no activities in cell-based assays that do not correlate with the high potency *in vitro* [51]. In this work, we plan to link one of the top inhibitors by a covalent bond to previously reported PA CPPs to improve cellular permeability. Next, the synthesized SOM-peptide conjugate would be tested *in vitro* on PqsD and if the activity is maintained subsequently in a cell-based assay.

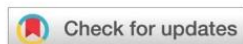
B) *E. coli* RNA polymerase

In order to initiate transcription, the core RNAP enzyme needs to bind to protein factors forming the holoenzyme complex. Thus, the protein-protein interaction (PPI) surface between both proteins represents an attractive new mode/site of action. A previously identified peptide (P07) has been shown to be a micromolar inhibitor of RNAP and sigma factor 70 PPI *in vitro* only [52]. However, for a possible pharmaceutical application, improved activities on the cellular level, oral bioavailability, and resistance to proteolytic degradation are desired. Thus in the frame of this work, peptide sequence and structural modifications by the means of Alanine-scan, truncation, sidechain-to-sidechain macrocyclization are attempted. These modifications aim to first identify the residues suitable for exchange with azide and alkyne bearing un-natural amino acids without compromising activity. These groups will be used as templates for Copper (I)-catalyzed alkyne-azide cycloaddition (CuAAC) forming a triazolyl moiety in order to constrain the peptide in the α -helical form which is assumed to be the bioactive conformation. Thus, leading to a decrease in entropic penalty required to assume the α -helical form required for binding. Moreover, by increasing the α -helical content and decreasing anionic charges might lead to better permeation through *E. coli* cell wall.

In conclusion, these studies aim to conceive and rationally optimise novel anti-infective molecules of different complexity and sizes (SOMs, peptides, SOM-peptide conjugates) addressing various challenges due to target location and nature as well as cell-permeability impediments.

3. Results

3.1 Chapter A: Structure–functionality relationship and pharmacological profiles of *Pseudomonas aeruginosa* alkylquinolone quorum sensing modulators



Cite this: *Org. Biomol. Chem.*, 2017, **15**, 4620

Structure–functionality relationship and pharmacological profiles of *Pseudomonas aeruginosa* alkylquinolone quorum sensing modulators†

Ahmed A. M. Kamal,^a Lucia Petrera,^a Jens Eberhard^a and Rolf W. Hartmann^{*a,b}

An important paradigm in anti-infective research is the antivirulence concept. Pathoblockers are compounds which disarm bacteria of their arsenal of virulence factors. PqsR is a transcriptional regulator controlling the production of such factors in *Pseudomonas aeruginosa*, most prominently pyocyanin. In this work, a series of tool compounds based on the structure of the natural ligand 2-heptyl-4-quinolone (HHQ) were used for probing the structure–functionality relationship. Four different profiles are identified namely agonists, antagonists, inverse agonists and biphasic modulators. Molecular docking studies revealed that each class of the PqsR modulators showed distinctive interactions in the PqsR binding domain. It was found that the substituents in position 3 of the quinolone core act as a switch between the different profiles, according to their ability to donate or accept a hydrogen bond, or form a hydrophobic interaction. Finally, it was shown that only inverse agonists were able to strongly inhibit pyocyanin production.

Received 3rd February 2017,
Accepted 5th May 2017

DOI: 10.1039/c7ob00263g

rsc.li/obc

Introduction

Pseudomonas aeruginosa (PA) is an opportunistic Gram-negative bacterium common in nosocomial infections which has become more and more resistant to clinically used antibiotics.^{1–3} Therefore, there is an urgent need for novel strategies to combat PA infections.^{4–6} The antivirulence concept is very promising in this sense as it is a non-bactericidal approach which should lead to less bacterial resistance.^{7,8}

Bacteria possess chemical signaling networks which are used among them for communication and co-ordination of collective pathogenic behavior.⁹ For PA, the most investigated systems are *rhl*, *las* and *pqs* quorum sensing.^{9–13} One of the main areas of interest in our lab is the *pqs* system with PqsR (also known as MvfR) as the transcriptional regulator orchestrating the production and expression of different QS target genes. Once the circulating amount of PqsR natural ligands 2-heptyl-4-quinolone (HHQ) and *Pseudomonas* quinolone

signal (PQS, Fig. 1) reach a certain threshold, induction of these genes leads to the production of virulence factors such as pyocyanin, extrusion of eDNA, and biofilm formation.^{12,14,15} The biosynthesis of these signaling molecules is accomplished by enzymes of the operon *pqsABCDE*. One strategy to interfere with this system is to block these enzymes. While others focused their efforts on *pqsA*,^{16–18} our group developed several series of potent inhibitors of *pqsD*^{19–27} and *pqsE*.²⁸ Another would be targeting PqsR to decrease the production of signaling molecules and various virulence factors. Over the past few years, several approaches have been used in the attempt of discovering novel compounds blocking PqsR, *i.e.* high-throughput screening (HTS),²⁹ as well as ligand^{30–34} and fragment-based approaches.^{35–37}

In a previous work from our laboratory, the PqsR natural ligand HHQ was modified into a series of potent compounds with different activity profiles. It was discovered that the introduction of an electron withdrawing group such as nitro or CF₃ at position 6 of the quinolone moiety is responsible for activity

^aHelmholtz-Institute for Pharmaceutical Research Saarland, Department of Drug Design and Optimization, Campus E8.1, 66123 Saarbrücken, Germany

^bDepartment of Pharmacy, Pharmaceutical and Medicinal Chemistry, Saarland University, Campus C2.3, 66123 Saarbrücken, Germany.

E-mail: rolf.hartmann@helmholtz-hzi.de; Fax: +49 681 98806-2009;

Tel: +49 681 98806-2000

† Electronic supplementary information (ESI) available. See DOI: 10.1039/c7ob00263g

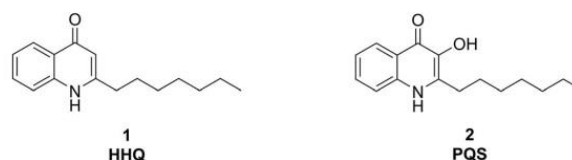


Fig. 1 Structure of PqsR natural ligands.

interconversion from agonists into antagonists.³¹ Additionally, Williams *et al.* have demonstrated with similar compounds (quinazolinones) the importance of an amino group at the 3 position for antagonism.³⁰

Very recently, McGlacken *et al.* also found that substitution at the 3-position of 2-heptyl-6-nitroquinolin-4(1*H*)-one has an impact on the activity profile.³⁴

In this study, we aim to gain further insights into the role of the C-3 position. Therefore, we synthesized a library of compounds with substituents at position 3 possessing different biophysical properties. Interestingly, biological testing revealed not just agonists and antagonists but four different pharmacological classes. Molecular docking experiments elucidated distinct binding modes of each class. Only inverse agonists were able to strongly inhibit pyocyanin formation.

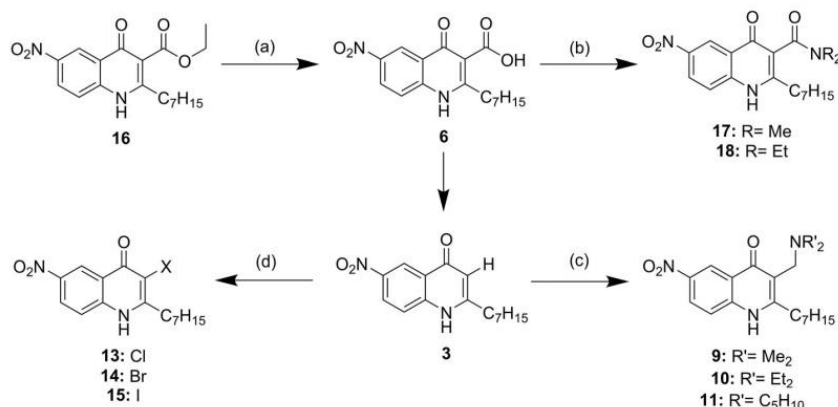
Results and discussion

Design and syntheses of the investigative compounds

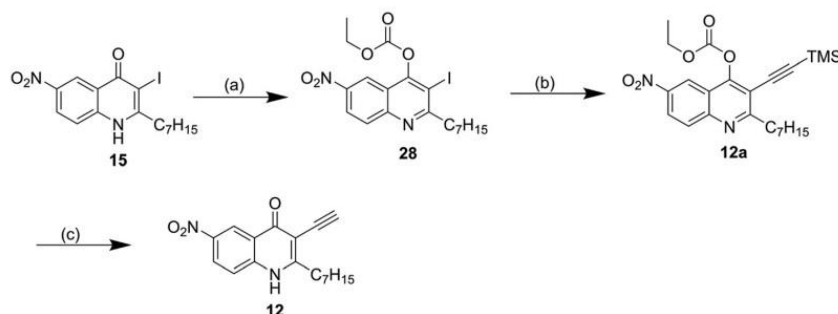
A series of compounds were synthesized in an attempt to elucidate a structure–functionality relationship with the primary

goal to differentiate between the various receptor modulators' profiles. We were especially interested in the outcome of combining the previously identified agonist/antagonist switching behavior *via* the introduction of the nitro group at the 6-position in combination with various position 3 substituents.

Compounds **3–8** and **14–16** were synthesized as previously described.^{31–33,38} Regarding derivatization of the *n*-heptyl class of compounds, **3** was utilized as a common starting point (Scheme 1). Firstly, a Mannich reaction was carried out to yield amino alkylated products **9–11** in low to moderate yields. Secondly, Cl, Br, and I were introduced in the same position by means of *N*-halogen succinimide generating **13–15**. The iodo-derivative **15** was then used for further derivatization employing a Sonogashira coupling to form a carbon–carbon bond (Scheme 2). Protection of the neighboring carbonyl as a carbonate ester was carried out followed by reacting intermediate **28** with a TMS-protected alkyne. Product **12a** was taken as crude and both protecting groups were cleaved off using 5 M KOH to produce **12** in a moderate overall yield of 38%. Finally, tertiary carboxamides **17** and **18** were derived from the carboxylic acid analogue **6** *via* standard amide coupling utilizing EDC and HOBT.



Scheme 1 Synthesis of **9–11**, **13–15**, and **17–18**. Reagents and conditions: (a) NaOH, EtOH, reflux, 6 h; (b) HOBT, EDC, 1 h at RT then NHR₂, N₂, RT, overnight; (c) ETOH, HCHO, HNR₂, reflux, 2–5 days; (d) *N*-halogen succinimide, DMF, N₂, DMF, RT, overnight.

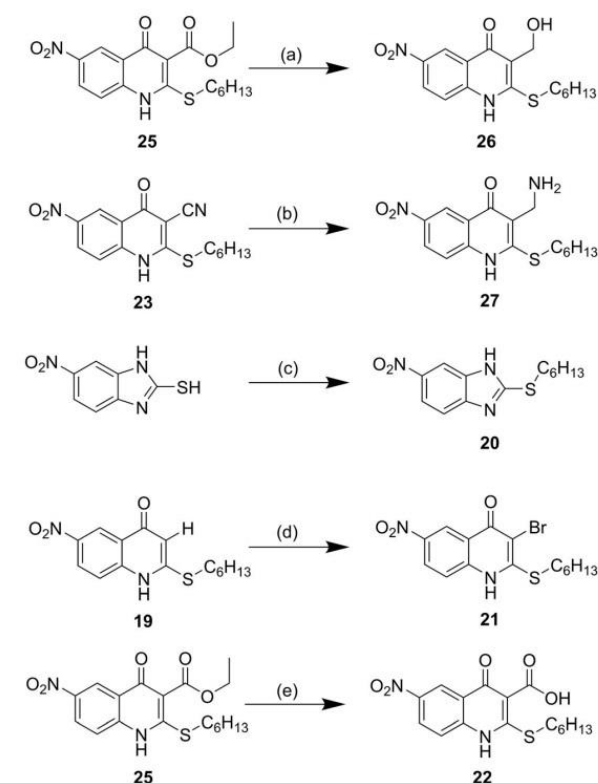


Scheme 2 Synthesis of **12**, **15**, and **28**. Reagents and conditions: (a) *t*-BuOK, THF, RT, 1 h, EtOCOCl, RT, overnight; (b) CuI, PdCl₂(PPh₃)₂, Et₃N, ethynyltrimethylsilane, Ar, RT, overnight; (c) 5 M KOH, RT, overnight.

Additionally, 2-(*n*-hexylthio)-6-nitroquinolin-4(1*H*)-one **19** was synthesized as an isosteric replacement with the aim to extend the search for potent ligands. The literature suggested that an S-motif might be tolerated at this position.²⁹ Derivatives of **19** were synthesized starting from esters of 2-((hexylthio)((4-nitrophenyl)amino)methylene)-3-butanoates. The corresponding position 2-substituted acetate esters were stirred in a suspension of sodium hydride followed by addition of the 4-nitrophenyl isothiocyanate and subsequently 1-iodoalkyl to yield intermediates **19a**, and **23a**–**25a** in a one pot fashion. The latter were subjected to Conrad-Limpach cyclization to generate 3-substituted-2-(hexylthio)-6-nitroquinolin-4(1*H*)-ones (Scheme 3). Interestingly, carboxamide derivative **19a** did not give the 3-carboxamide substituted product but the 3-H analogue quantitatively instead. It seems the carboxamide was cleft off during such harsh cyclization conditions. **21** and **22** were synthesized by the same methodology used for their *n*-heptyl analogues (see above). Compounds **23** and **25** were subjected to different reduction methods in an attempt to yield the aminomethyl and hydroxymethyl compounds **27** and **26**, respectively. However, compound **26** could not be obtained as a pure compound due to stability issues (Scheme 4). Compound **20** was synthesized through reaction of 6-nitro-1*H*-benzo[*d*]imidazole-2-thiol with iodohexane at room temperature.

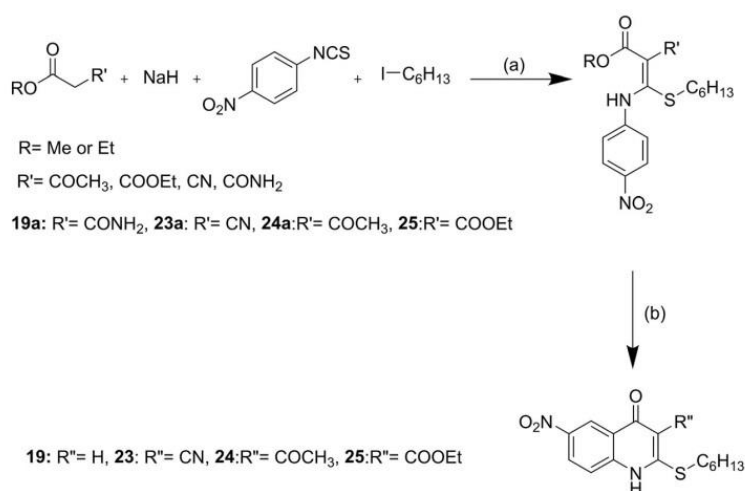
E. coli cell-based assay results and PqsR modulators' grouping

Investigation of PqsR suffers from poor solubility of the protein under *in vitro* conditions hindering the establishment of a functional assay. Therefore, a cell-based assay is needed. As an alternative, a β -galactosidase reporter gene assay in *E. coli* was used where *lacZ* is controlled by the *pqsA* promoter. In *E. coli* impeding factors, such as permeability and efflux, play a much smaller role.³⁹ Using PA as a first assay will not provide a coherent picture due to its high intrinsic



Scheme 4 Synthesis of **20**–**22**, **26**, and **27**. Reagents and conditions: (a) DIBALH, THF, -78 °C then RT, overnight (b) BH_3 .THF, N_2 , reflux, overnight; (c) 1-iodohexane, K_2CO_3 , acetone, RT, overnight; (d) *N*-bromosuccinimide, DMF, N_2 , overnight (e) 10% (w/v) NaOH, EtOH, reflux, overnight.

resistance to chemical compounds as a result of metabolic degradation, efflux, and permeation problems through the thick cell wall.



Scheme 3 Synthesis of **19** and **23**–**25**. Reagents and conditions: (a) DMF, N_2 , RT, overnight; (b) Dowtherm™, 250 °C.

In such an assay, two experimental settings are required to fully address and understand the possible receptor profiles. Firstly, the compound is investigated in different concentrations in the absence of the natural ligand. This experiment shows the intrinsic potential of the compound. Secondly, in a competitive experiment the natural agonist PQS is added together with the compound under evaluation. This provides data about the relative efficacy and compound mode of action.

Within this work, our aim is not only to compare the absolute activities *viz.* IC_{50} or EC_{50} values of the compounds, but also to classify compounds according to their activity profiles (Fig. 2). Thus, dose–response curves were monitored over a broad concentration range. This led to the identification of four main classes. The activity profiles and IC_{50} or EC_{50} values for each class are compiled in Table 1.

Agonists. The two natural ligands, PQS and HHQ, possess agonistic activity. They increase the transcription level in a

dose-dependent manner above the basal level with PQS being more potent. Among the synthetic analogues, the 6-nitro derivative **4** displays activity in the single digit nanomolar range being even more potent than PQS (Fig. 2a).³⁹ Other agonists like **19** and **21** were also active in the nanomolar range while **6**, **22**, **23**, and **24** were weaker showing activities in the single and double-digit micromolar range.

Neutral antagonists. Two compounds were characterized by the ability to antagonise the effect of PQS, reducing the transcriptional level towards basal. In the absence of PQS, they lack an intrinsic pharmacological response (Fig. 2b). Compounds which feature such behavior are **12**, **15** and **20**. Both **12** and **15** possess a hydrophobic group with largely delocalized electron density *viz.* ethynyl and iodide substituents, respectively.

Inverse agonists. Inverse agonists possess a similar behavior to antagonists in the presence of transcriptional induction

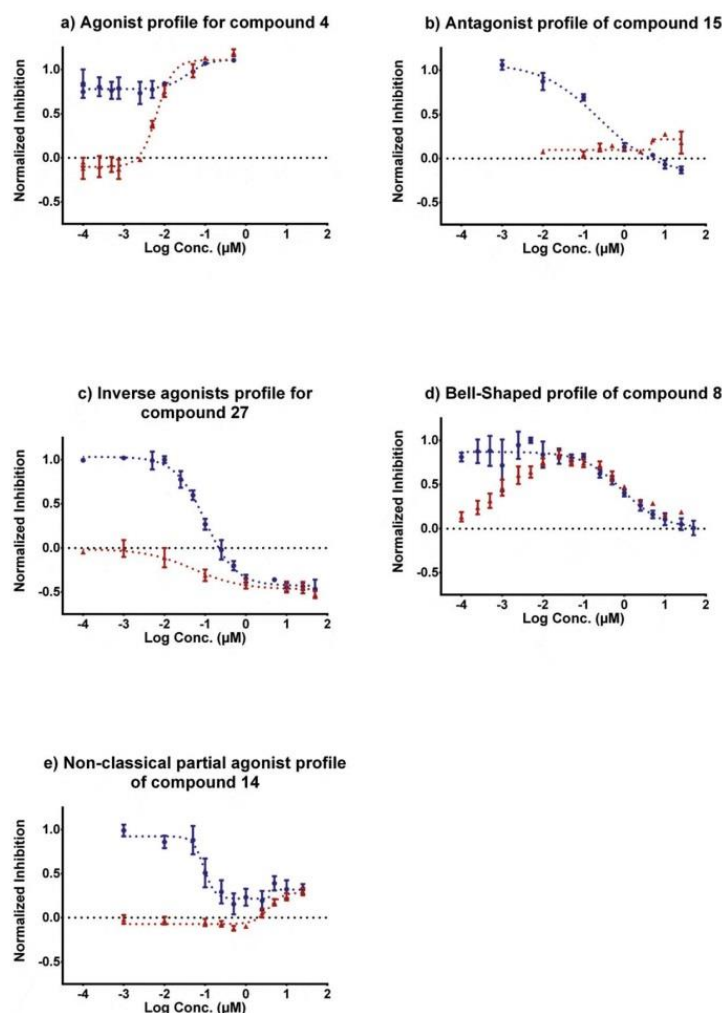
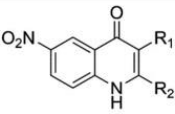
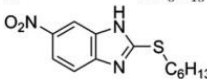


Fig. 2 Dose–response curves for different profiles (agonistic activity in red) (antagonistic activity in blue).

Table 1 Pharmacological profile, IC₅₀, & EC₅₀ values from *E. coli* reporter gene assays


Compound no.	Compound structure		Profile	IC ₅₀ ^a (μM)	95% CI ^d	EC ₅₀ ^b (μM)	95% CI ^d
	R ₁	R ₂					
3*	H	<i>n</i> -C ₇ H ₁₅	Inverse agonist	0.135	0.108–0.169	—	—
4*	OH	<i>n</i> -C ₇ H ₁₅	Agonist	—	—	0.006	0.004–0.011
5 [§]	CH ₂ OH	<i>n</i> -C ₇ H ₁₅	Inverse agonist	0.415	0.101–1.697	—	—
6*	COOH	<i>n</i> -C ₇ H ₁₅	Agonist	—	—	1.028	0.242–4.362
7*	CONH ₂	<i>n</i> -C ₇ H ₁₅	Inverse agonist	0.051	0.032–0.080	—	—
8 [§]	CONHOH	<i>n</i> -C ₇ H ₁₅	Bell-shaped ^f	—	—	0.001	0.0003–0.004
9	CH ₂ NMe ₂	<i>n</i> -C ₇ H ₁₅	Inverse agonist	3.102	0.318–30.29	—	—
10	CH ₂ NEt ₂	<i>n</i> -C ₇ H ₁₅	Inverse agonist	17.13	2.492–117.8	—	—
11	CH ₂ NC ₄ H ₉	<i>n</i> -C ₇ H ₁₅	Inverse agonist	>100	—	—	—
12	HCCH	<i>n</i> -C ₇ H ₁₅	Antagonist	0.667	0.457–0.975	—	—
13 [‡]	Cl	<i>n</i> -C ₇ H ₁₅	Non-classical partial agonist ^c	0.105	0.0579–0.189	—	—
14 [‡]	Br	<i>n</i> -C ₇ H ₁₅	Non-classical partial agonist ^c	0.113	0.047–0.273	—	—
15 [‡]	I	<i>n</i> -C ₇ H ₁₅	Antagonist	0.176	0.074–0.421	—	—
16*	COOEt	<i>n</i> -C ₇ H ₁₅	Inactive	—	—	—	—
17 [‡]	CONMe ₂	<i>n</i> -C ₇ H ₁₅	Inactive	—	—	—	—
18	CONEt ₂	<i>n</i> -C ₇ H ₁₅	Inactive	—	—	—	—
19	H	S-C ₆ H ₁₃	Agonist	—	—	0.034	0.019–0.057
20			Antagonist	2.173	1.008–4.686	—	—
21	Br	S-C ₆ H ₁₃	Agonist	—	—	0.882	0.563–1.380
22	COOH	S-C ₆ H ₁₃	Agonist	—	—	31.74	0.971–1037
23	CN	S-C ₆ H ₁₃	Agonist	—	—	20.31	2.815–146.4
24	COCH ₃	S-C ₆ H ₁₃	Agonist	—	—	3.677	1.502–9.005
25	COOEt	S-C ₆ H ₁₃	Inactive	—	—	—	—
26	CH ₂ OH	S-C ₆ H ₁₃	Unstable	—	—	—	—
27	CH ₂ NH ₂	S-C ₆ H ₁₃	Inverse agonist	0.105	0.089–0.125	—	—

^a IC₅₀ is defined as the concentration of a compound at the half point between the maximal and minimal response. Antagonism dose–response assays were performed for each compound in the presence of 50 nM PQS. ^b EC₅₀ is defined as the concentration of a compound at which the response is 50% of the maximal response. ^c Dose–response exhibited nonmonotonic behavior; for IC₅₀ values concentrations above the turning point were excluded. ^d CI: confidence interval *[†], [§], [‡] are previously reported in ref. 33, 34 and 39 respectively.

where they manage to suppress the activity of the inducer to basal level or below. In contrast to the antagonists, they possess an additional effect in the absence of an inducer and suppress the transcriptional level (Fig. 2c). Synthesized inverse agonists 3, 5, and 27 have shown potent nanomolar activity while compounds 7, 9, 10, and 11 were micromolar inhibitors.

Agonistic/antagonistic mixed profile compounds. This class of compounds possesses a peculiar biphasic dose–response curve in the absence of PQS. However, in the presence of PQS, the compounds at higher concentrations start showing either an agonistic or antagonistic activity. An example for this bell-shaped profile is the hydroxamic acid 8 which antagonizes PQS at higher concentrations (Fig. 2d). Halogen compounds like 13 and 14 – also synthesized by McGlacken *et al.* – interestingly revealed an inverted bell-shaped curve when tested in a broad concentration range. At higher concentrations, they act as agonists (Fig. 2e). In the case of the former, such behavior has been reported for some human receptors, especially GPCRs before.^{40–42} As per the latter, such a phenomenon has been published previously in a study concerning a LasR recep-

tor where the compounds were termed, non-classical partial agonists. It is worth noting that LasR controls another QS system with *N*-acylated L-homoserine lactones as signal molecules.^{43,44}

Two explanations are commonly accepted for compounds possessing such behavior. Firstly, in the presence of the natural ligand and low concentrations of the compound, a mixture of active/inactive heterodimer complexes is formed. This translates into either weak agonism or antagonism. While, in the absence of PQS or at a higher concentration of the compound, it fully displaces the natural ligand and produces its innate pharmacological effect. The second common explanation relies on a second binding event of the compounds on the same or different target with two opposing effects, resulting in a biphasic-shaped activity curve.^{43,45}

Elucidation of the structure–functionality relationship via molecular docking experiments

Intrigued by these biological findings molecular docking experiments were performed, in the hope of finding unique

interactions of the different drug profiles. The structure of the apoprotein (PDB: 4JVC, 2.50 Å) was chosen for the docking procedure as the available co-crystallized structures (PDB 4JVD and 4JVI) have lower resolutions of 2.95 and 2.90 Å, respectively.³⁰ Moreover, the apoprotein possesses two additional water molecules (H₂O-501 & 502) in close proximity to the ligand binding site, which are absent in the co-crystallized structures. In the native X-ray structure, H₂O-501 displays a hydrogen bond network where it acts as a hydrogen bond donor (HBD) to the backbones of Leu208 and Arg209 as well as a hydrogen bond acceptor (HBA) to the side chain of Gln194. This extensive interaction with different protein backbone positions – thereby locking conformation – may point towards a role for this water molecule in understanding the ligands' behavior (see Fig. 3).

The most potent compounds from each activity profile were selected for docking in an attempt to elucidate different key amino acid interactions. The top-ranked docking poses found for each compound were always located at the known binding site except for the weakly active compounds (micromolar activities) and inactive compounds which were used as a negative control. In their docking poses, all compounds possess some common interactions, while other interactions were unique for each class. Among the interactions shared between all compounds is an alkyl-alkyl interaction between the *n*-heptyl/thio-*n*-hexyl chain with Ile186, Leu189, and Tyr258. Additionally, the compounds displayed a π - σ interaction between the quinolone ring system and the side chains of Ile236 and a π -alkyl interaction with Ala186. Finally, the nitro group at the 6-position established a hydrogen bond with H₂O-502 which, in turn, interacts with the backbone of Ile236 in most of the compounds (for exceptions see below).

Agonists 4, 6, and 22 possessing an enolic OH or COOH substituent ($\text{cp}K_a$ values 8.3, 3.6 and 3.6, respectively, Table S1†) displayed a HBA interaction with H₂O-501 in their deprotonated state (Fig. 4). This interaction is assumed to compete with the native engagement of H₂O-501 at the Leu208 and Arg209 backbones. It is notable that this model can also explain the agonistic activity of the recently reported 3-F derivative.³⁴

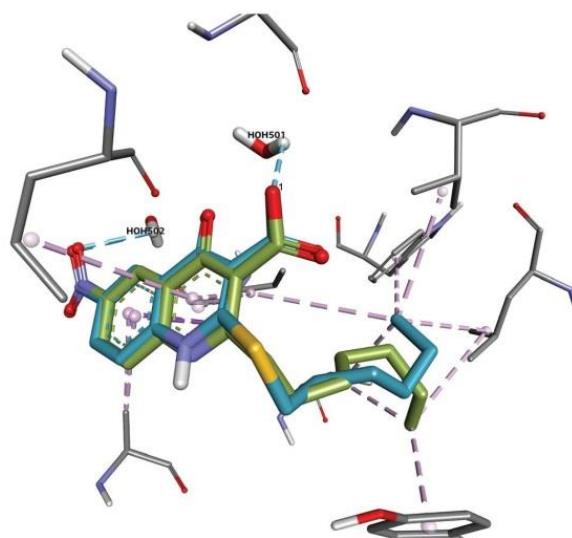


Fig. 4 An overlay of docking poses for compound 6 having an *n*-heptyl chain at position 2 (in dark green) and compound 22 with a thio-*n*-hexyl chain (in cyan) at the same position. Interactions of the 6-NO₂ and the position 3-COOH with H₂O-502 and 501, respectively, are highlighted by dashed lines.

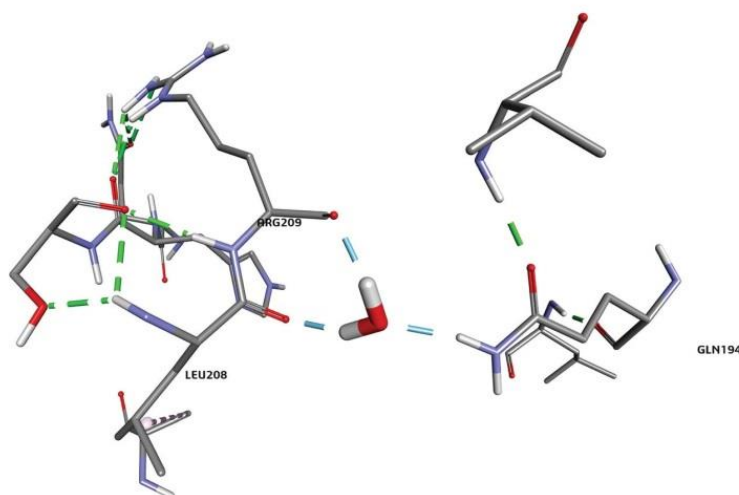


Fig. 3 Hydrogen bond network formed by H₂O-501 with Arg209, Leu208, and Gln194 as seen in the binding pocket of the X-ray structure used for docking (PDB: 4JVC).

In the case of the two agonists **19** and **21** which had shown a different pharmacological profile than their *n*-heptyl counterparts **3** and **14**, molecular docking displays the lack of position 3 mediated interaction, as well as the interaction between the 6-NO₂ and H₂O-502 which is present in their *n*-heptyl analogs.

To further investigate the role of the thiohexyl chain in the observed activity flip, a thio-*n*-hexyl-substituted 6-nitro-1*H*-benzimidazole **20** was synthesized in which the quinolone head group is replaced by a 6-nitrobenzimidazole. This group was inspired by another class of PqsR inverse agonists.²⁹ Compound **20** turned out to be a single digit micromolar antagonist. Therefore, the presence of a thiohexyl chain is not the cause of the activity flip in itself but rather the lack of any inverse agonistic interactions at position 3 and 6 (see below).

In contrast to the agonists, the inverse agonists **7** and **27** are equipped with HBD groups at position 3. Their docking poses showed two exclusive hydrogen bonds between these groups and the backbones of Leu207 and Arg209 while no engagement with H₂O-501 was observed. Replacement of the protons of the primary amide in **7** by alkyl groups leading to compounds **17** and **18** abolished the inverse agonistic activity and led into inactive compounds. This effect has also been observed by McGlacken *et al.*³⁴ In the case of the 3-hydroxymethyl group of compound **5** (alcoholic hydroxyl not acidic in aqueous milieu, compared to agonist **4**), two hydrogen bonds were seen; one with the hydroxyl group being a HBA interacting with H₂O-501, while the other being a HBD interacting with the carbonyl oxygen of Leu207. In conclusion, a HBD bond to either Leu207 and/or Arg209 seems to be essential for achieving inverse agonistic activity (Fig. 5).

Regarding the neutral antagonists, no interaction was found with any of the distinctive amino acids inverse agonists

or agonists engage with. An exclusive alkyl-alkyl interaction of the 3-position substituent of ethynyl derivative **12** and Val211 was observed (Fig. 6). A similar interaction was seen in the case of halogen substituted compounds **13**, **14**, and **15**. However, these findings are not able to shed light on the particular biphasic behavior of **13** and **14**.

As for compound **8** with the unique bell-shaped mixed agonistic-antagonistic behavior, interestingly interactions were observed which had been found in both agonists and inverse agonists. The hydroxamic acid group acts as both a HBA through its hydroxyl group oxygen with H₂O-501 as well as a HBD *via* its amide proton with Arg209.

To sum up, in our computational model position 3 plays a prominent role in the protein-ligand interaction. Agonists' HBA group at position 3 engages with the hydrogen atoms of H₂O-501 which interacts with Arg209 and/or Leu208 in the natural, unbound protein state. In the case of the inverse agonists, their HBD group interacts with the keto group in the backbone(s) of Leu207 and/or Arg209. Finally, antagonists exhibit a hydrophobic interaction with the Val211 side chain. The model is also able to explain the importance of the 6-NO₂ group for the interaction of the compounds, although its role appears to be less important than substituents at position 3.

P. aeruginosa reporter gene assay results

The most potent compounds of each profile were selected to be tested in the PA reporter gene assay to corroborate our results of the *E. coli* assay. Initially, it was confirmed that all compounds showed the same activity profile moving on from *E. coli* to PA with the exception of **12**, which showed no activity in PA. This can be rationalized by pharmacokinetic problems

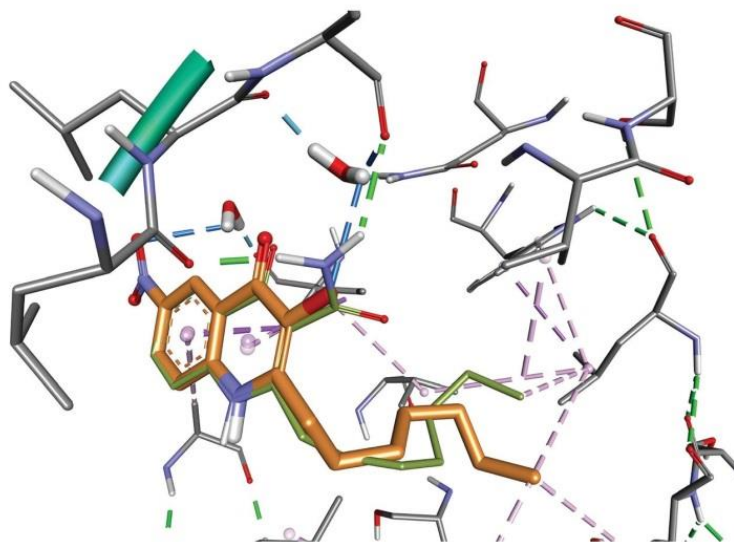


Fig. 5 An overlay of docking poses for compound **4** (agonist, in orange) displaying a HBA bond (blue dashed line) between the substituent at position 3 (OH) with H₂O-501 as opposed to **7** (inverse agonist, in dark green) displaying a HBD bond (green dashed line) *via* the substituent at position 3 (CONH₂).

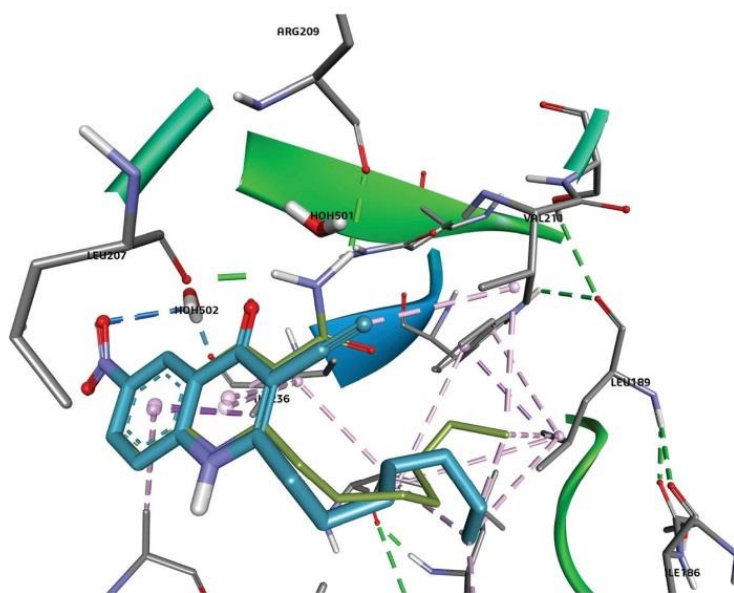


Fig. 6 An overlay of docking poses for compound **12** (antagonist, in cyan) displaying a hydrophobic interaction (pink dashed line) between the substituent at position 3 (C≡CH) with the Val211 side chain, while compound **7** (inverse agonist, in dark green) displays a HBD bond (green dashed line) via the substituent at position 3 (CONH₂).

such as decreased permeability, increased metabolic degradation, and enhanced efflux. Furthermore, **13** and **14** retained their biphasic activity profile excluding it being an artifact of the heterologous *E. coli* experimental setting.

Compounds **13** and **15** showed improved IC₅₀ and EC₅₀ values in PA in comparison to the *E. coli* reporter gene assay while in the other compounds the opposite was observed.

However, comparing the different classes significant differences in the minimal level of expression are observed (see Table 2). The only class of compounds which were able to significantly inhibit the expression below the basal level are the inverse agonists.

Pyocyanin inhibition and its correlation with activity profiles

Pyocyanin is a virulence factor known to be tightly regulated by PqsR genes. Subsequently, as a result of the decrease in PqsR transcriptional activity, a reduction in pyocyanin is expected. Upon inspection of the pyocyanin results, it was observed that only inverse agonists **5**, **7**, and **27** were able to decrease this virulence factor significantly, while the non-classical partial agonists and antagonists showed a mild reduction of pyocyanin. A possible explanation could be that inverse agonists are able to alter the conformation of PqsR in a manner that antagonists and partial agonists do not. In other words, antagonists

Table 2 Pharmacological profile, minimal level of expression, IC₅₀, & EC₅₀ values from PA reporter gene assays

Compound no.	Profile	IC ₅₀ ^a (μM)	95% CI ^d	EC ₅₀ ^b (μM)	95% CI ^d	Minimal level of expression in PA ^e
19	Agonist			0.079	0.059–0.105	—
12	Antagonist	Inactive				—
15 [‡]	Antagonist	0.070	0.0176–0.276			54.3 ± 20.6
13 [‡]	Non-classical partial agonist ^c	0.041	0.005–0.353			30.3 ± 14.4
14 [‡]	Non-classical partial agonist ^c	1.471	0.348–6.224			26.7 ± 12.9
5 [§]	Inverse agonist	0.428	0.245–0.746			–15.2 ± 12.8
7 [*]	Inverse agonist	1.322	0.237–7.380			–10 ± 13.9
27	Inverse agonist	0.365	0.1197–1.115			–53 ± 15.6

^a IC₅₀ is defined as the concentration of a compound at the half point between the maximal and minimal response. Antagonism dose–response assays were performed for each compound in the presence of 50 nM PQS. ^b EC₅₀ is defined as the concentration of a compound at which the response is 50% of the maximal response. ^c Dose–response exhibited nonmonotonic behavior; for IC₅₀ values concentrations above the turning point were excluded. ^d CI: confidence interval. ^e Minimal level inhibition mean values are shown and SD. *[§],[‡] are previously reported in ref. 33, 34 and 39 respectively.

Table 3 Pyocyanin inhibitory values in PA14

Compound no.	Compound profile	IC ₅₀ in pyocyanin ^a (μM)	% production of pyocyanin at the maximal inhibitory concentration ^b
15 [‡]	Antagonist	—	80.1 ± 2.7% @ 25 μM
13 [‡]	Non-classical partial agonist	—	73.7 ± 4.0% @ 25 μM
14 [‡]	Non-classical partial agonist	—	78.5 ± 5.0% @ 25 μM
5 [§]	Inverse agonist	4.4 ± 0.0	
7 [*]	Inverse agonist	1.9 ± 0.0	
27	Inverse agonist	1.9 ± 0.4	

^a Inhibition of the virulence factor pyocyanin was evaluated in the clinical isolate PA14. Non-linear regression analysis to determine IC₅₀ was done using a log (inhibitor) vs. response model with constraints (bottom = 0; top = 100) (GraphPad Prism 6). ^b % production mean values and SD are shown. ^{*}, [§], [‡] are previously reported in ref. 33, 34 and 39 respectively.

and non-classical partial agonists are able to only compete with PQS without being able to induce a global conformational change in the protein. Thus partial agonists and antagonists decrease the level of expression only moderately in PA which is translated into a little decrease in pyocyanin production.

In neuro-receptors it has been shown that different drug classes acting on the same receptor may possess different signal transductions, a finding which is known as functional selectivity or biased agonism.^{46,47} It cannot be excluded that there is a similar mechanism occurring in PqsR. The detailed results of the pyocyanin experiments are shown in Table 3.

Conclusion and outlook

For some receptors, the conventional two-state drug-receptor model may be sufficient to explain their functional behavior. Once the agonist binds to the receptor, specific conformational changes occur which induce protein activity, while, an antagonist only displaces the agonist returning activity to zero. However, recently more receptors have been shown to exhibit a constitutive basal activity like GPCRs.^{48,49} In such cases, it may not be sufficient to only reverse the effect of the agonist to the receptor un-liganded level. Inverse agonists are capable of blocking the basal activity of constitutively active receptors and of inducing conformational changes towards an inactive receptor state. These different conformations are elicited by different binding modes of the different modulators. We have shown through molecular docking that different functional classes of PqsR ligands indeed possess unique interaction hotspots. Interestingly, subtle modifications at one single position of the HHQ moiety were sufficient to elicit dramatic changes in the pharmacological profile of the ligands. Altogether, this study has shown that PqsR – a bacterial transcriptional regulator – behaves in a similar fashion to some human receptors and an inverse agonistic mode of action is required to induce an impactful biological response.

Future molecular biology studies which would investigate the interaction between the different drug-protein complexes and the *pqsA* promoter and how this affects gene expression would be of high impact.

As a general conclusion from this work, we would like to emphasize that in drug discovery it may not be sufficient to

find potent compounds on novel receptors possessing basal activity. Instead, their pharmacological profile should be determined as it might be more important that reduction below basal is obtained rather than the absolute IC₅₀ value.

Experimental

Chemical synthesis and analytical characterization

Reactions that were air and moisture sensitive were performed under a nitrogen atmosphere with oven-dried glassware. Unless otherwise stated, all chemicals and anhydrous solvents used were purchased from commercial vendors and used without further purification. Electrospray ionization (ESI) mass spectrometry and LC-UV purity determination (255 nm) were recorded with a Surveyor LC system coupled to an MSQ electrospray mass spectrometer (both ThermoFisher Scientific) in either positive mode (+) or negative mode (-). If not indicated otherwise, 0.05% formic acid was added to the acetonitrile/water gradient system applied for LC. All compounds tested were obtained with ≥95% purity. High resolution precise mass spectra were recorded on a ThermoFisher Scientific (TF, Dreieich, Germany) Q Exactive Focus system equipped with a heated electrospray ionization (HESI)-II source and Xcalibur (Version 4.0.27.19) software. Mass calibration was done prior to analysis according to the manufacturer's recommendations using external mass calibration. All samples were constituted in methanol and directly injected onto the Q Exactive Focus using the integrated syringe pump. All data acquisition was done in positive ion mode using voltage scans and the data were collected in continuum mode. NMR spectra were recorded on a Bruker Avance AV 300 or a Bruker DRX 500. The residual proton, ¹H, or carbon ¹³C resonances of the >99% deuterated solvents were used for internal reference of all spectra acquired.

Chemistry methodologies and structure elucidation are described in the ESI.†

Reporter gene assays in *E. coli* and *P. aeruginosa*

The assay was performed in *E. coli* DH5α cells containing a pEAL08-2 plasmid, which encodes PqsR under the control of the tac promoter while the β-galactosidase reporter gene lacZ

being controlled by the *pqsA* promoter. As previously reported, the bacterial culture was co-incubated with test compounds only in the case of the agonistic setting while the antagonistic effects of compounds were assayed in the presence of 50 nM PQS.^{31,50} After incubation, β -galactosidase activity was measured spectrophotometrically at OD₄₂₀ using POLARstar Omega (BMG Labtech, Ortenberg, Germany) and expressed as percent stimulation/inhibition of controls. For the determination of EC₅₀ or IC₅₀ values, compounds were tested at least at seven different concentrations. The given data represent mean values of at least two independent experiments.

In the case of *P. aeruginosa*, the PqsR-dependent transcription was evaluated using a β -galactosidase reporter gene assay system. A PA14 strain carrying a non-functional *pqsA* gene to eliminate intracellular HHQ and PQS production was transformed with the same plasmid pEAL08-2 and incubated with the test compound in the presence or absence of 50 nM PQS analogously to the reporter gene assay in *E. coli*.

Pyocyanin assay

Pyocyanin production by *P. aeruginosa* PA14 was assessed as previously described.^{22,51} Briefly, a single colony was removed from agar plates after 16 h of growth at 37 °C and pre-cultured in 10 mL of PPGAS medium. Following 19 h of aerobic growth with shaking at 200 rpm and 37 °C, cultures were centrifuged at 7.450g, washed once with 10 mL of fresh PPGAS medium, and resuspended to a final volume of 5 mL. Afterward, cultures were inoculated and diluted to a starting OD₆₀₀ of 0.02 and grown in the presence of the compounds or DMSO as a control in PPGAS medium at 37 °C, 200 rpm, and under aerobic conditions for 17 h. For pyocyanin determination, cultures were extracted with chloroform and then re-extracted with 0.2 M HCl. The OD₅₂₀ was determined using FLUOstar Omega (BMG Labtech) and normalized to cell growth measured as OD₆₀₀. For each sample, cultivation and extraction were performed in triplicate.

Data analysis

Data analysis was performed using GraphPad Prism 6. The different effect of the compounds was plotted as dose-response curves such that each individual point represents the average of a single experiment. Lines of best fit and associated EC₅₀ and IC₅₀ values as well as the respective 95% confidence intervals (CI) were calculated for each dose-response curve using the nonlinear fit variable slope (four parameters) function of GraphPad Prism 6. Whereas 95% CI means a 0.95 probability of containing the population mean.

Molecular docking experiments

Protein data were collected from the Protein Data Bank (PDB) and prepared using the MOE 2015 LigX function and Amber10:EHT force field. The ligands and proteins were formatted for docking with Auto Dock Tools (ADT). Docking was performed with AutoDock Vina default settings. The dimensions and centers of the grid boxes are center_x = -59.603, center_y = 0.841, center_z = 9.96 and size_x = 54, size_y = 30,

size_z = 28. Afterward, docking poses were visualized using Discovery Studio Visualizer 16.10.

Acknowledgements

We thank our colleagues Christine Maurer and Benjamin Kirsch who provided insight and expertise that greatly assisted the research. We thank Simone Amann for her assistance with the biological assays and Lorenz Siebenbürger for the purification of a few compounds.

References

- 1 P. D. Lister, D. J. Wolter and N. D. Hanson, *Clin. Microbiol. Rev.*, 2009, **22**, 582–610.
- 2 A. Y. Peleg and D. C. Hooper, *N. Engl. J. Med.*, 2010, **362**, 1804–1813.
- 3 M. Porras-Gómez, J. Vega-Baudrit and S. Núñez-Corrales, *J. Biomater. Nanobiotechnol.*, 2012, **3**, 519–527.
- 4 S. Wagner, R. Sommer, S. Hinsberger, C. Lu, R. W. Hartmann, M. Empting and A. Titz, *J. Med. Chem.*, 2016, **59**, 5929–5969.
- 5 A. E. Clatworthy, E. Pierson and D. T. Hung, *Nat. Chem. Biol.*, 2007, **3**, 541–548.
- 6 S. Ruer, N. Pinotsis, D. Steadman, G. Waksman and H. Remaut, *Chem. Biol. Drug Des.*, 2015, **86**, 379–399.
- 7 B. Lasarre and M. J. Federle, *Microbiol. Mol. Biol. Rev.*, 2013, **77**, 73–111.
- 8 S. B. Tay and W. S. Yew, *Int. J. Mol. Sci.*, 2013, **14**, 16570–16599.
- 9 S. Atkinson and P. Williams, *J. R. Soc., Interface*, 2009, **6**, 959–978.
- 10 C. N. Wilder, S. P. Diggle and M. Schuster, *ISME J.*, 2011, **5**, 1332–1343.
- 11 M. Schuster and E. P. Greenberg, *Int. J. Med. Microbiol.*, 2006, **296**, 73–81.
- 12 E. Déziel, S. Gopalan, A. P. Tampakaki, F. Lépine, K. E. Padfield, M. Saucier, G. Xiao and L. G. Rahme, *Mol. Microbiol.*, 2005, **55**, 998–1014.
- 13 D. Maura, A. E. Ballok and L. G. Rahme, *Curr. Opin. Microbiol.*, 2016, **33**, 41–46.
- 14 D. Maura, R. Hazan, T. Kitao, A. E. Ballok and L. G. Rahme, *Sci. Rep.*, 2016, **6**, 34083.
- 15 T. Das, S. K. Kutty, R. Tavallaie, A. I. Ibugo, J. Panchompoo, S. Sehar, L. Aldous, A. W. S. Yeung, S. R. Thomas, N. Kumar, J. J. Gooding and M. Manefield, *Sci. Rep.*, 2015, **5**, 1–9.
- 16 M. W. Calfee, J. P. Coleman and E. C. Pesci, *Proc. Natl. Acad. Sci. U. S. A.*, 2001, **98**, 11633–11637.
- 17 B. Lesic, F. Lépine, E. Déziel, J. Zhang, Q. Zhang, K. Padfield, M.-H. Castonguay, S. Milot, S. Stachel, A. A. Tzika, R. G. Tompkins and L. G. Rahme, *PLoS Pathog.*, 2007, **3**, 1229–1239.

- 18 C. Ji, I. Sharma, D. Pratihari, L. L. Hudson, D. Maura, T. Guney, L. G. Rahme, E. C. Pesci, J. P. Coleman and D. S. Tan, *ACS Chem. Biol.*, 2016, **11**, 3061–3067.
- 19 S. Hinsberger, J. C. de Jong, M. Groh, J. Hauptenthal and R. W. Hartmann, *Eur. J. Med. Chem.*, 2014, **76**, 343–351.
- 20 J. H. Sahner, C. Brengel, M. P. Storz, M. Groh, A. Plaza, R. Müller and R. W. Hartmann, *J. Med. Chem.*, 2013, **56**, 8656–8664.
- 21 A. Steinbach, C. K. Maurer, E. Weidel, C. Henn, C. Brengel, R. W. Hartmann and M. Negri, *BMC Biophys.*, 2013, **6**, 10.
- 22 M. P. Storz, C. K. Maurer, C. Zimmer, N. Wagner, C. Brengel, J. C. de Jong, S. Lucas, M. Müsken, S. Häussler, A. Steinbach and R. W. Hartmann, *J. Am. Chem. Soc.*, 2012, **134**, 16143–16146.
- 23 A. Thomann, C. Brengel, C. Börger, D. Kail, A. Steinbach, M. Empting and R. W. Hartmann, *ChemMedChem*, 2016, **11**, 2522–2533.
- 24 G. Allegratta, E. Weidel, M. Empting and R. W. Hartmann, *Eur. J. Med. Chem.*, 2015, **90**, 351–359.
- 25 M. P. Storz, G. Allegratta, B. Kirsch, M. Empting and R. W. Hartmann, *Org. Biomol. Chem.*, 2014, **12**, 6094.
- 26 J. H. Sahner, M. Empting, A. Kamal, E. Weidel, M. Groh, C. Boerger and R. W. Hartmann, *Eur. J. Med. Chem.*, 2015, **96**, 14–21.
- 27 D. Pistorius, A. Ullrich, S. Lucas, R. W. Hartmann, U. Kazmaier and R. Müller, *ChemBioChem*, 2011, **12**, 850–853.
- 28 M. Zender, F. Witzgall, S. L. Drees, E. Weidel, C. K. Maurer, S. Fetzner, W. Blankenfeldt, M. Empting and R. W. Hartmann, *ACS Chem. Biol.*, 2016, **11**, 1755–1763.
- 29 M. Starkey, F. Lepine, D. Maura, A. Bandyopadhyaya, B. Lesic, J. He, T. Kitao, V. Righi, S. Milot, A. Tzika and L. Rahme, *PLoS Pathog.*, 2014, **10**, e1004321.
- 30 A. Ilangovan, M. Fletcher, G. Rampioni, C. Pustelny, K. Rumbaugh, S. Heeb, M. Cámara, A. Truman, S. R. Chhabra, J. Emsley and P. Williams, *PLoS Pathog.*, 2013, **9**, e1003508.
- 31 C. Lu, B. Kirsch, C. Zimmer, J. C. de Jong, C. Henn, C. K. Maurer, M. Müsken, S. Häussler, A. Steinbach and R. W. Hartmann, *Chem. Biol.*, 2012, **19**, 381–390.
- 32 C. Lu, C. K. Maurer, B. Kirsch, A. Steinbach, R. W. Hartmann, M. P. Storz, C. K. Maurer, C. Zimmer, N. Wagner, C. Brengel, J. C. de Jong, S. Lucas, M. Müsken, S. Häussler, A. Steinbach and R. W. Hartmann, *Angew. Chem., Int. Ed.*, 2014, **53**, 1109–1112.
- 33 C. Lu, B. Kirsch, C. K. Maurer, J. C. de Jong, A. Braunshausen, A. Steinbach and R. W. Hartmann, *Eur. J. Med. Chem.*, 2014, **79**, 173–183.
- 34 R. Shanahan, F. J. Reen, R. Cano, F. O’Gara and G. P. Mcglacken, *Org. Biomol. Chem.*, 2017, **15**, 306–310.
- 35 M. Zender, T. Klein, C. Henn, B. Kirsch, C. K. Maurer, D. Kail, C. Ritter, O. Dolezal, A. Steinbach and R. W. Hartmann, *J. Med. Chem.*, 2013, **56**, 6761–6774.
- 36 T. Klein, C. Henn, J. C. de Jong, C. Zimmer, B. Kirsch, C. K. Maurer, D. Pistorius, R. Müller, A. Steinbach and R. W. Hartmann, *ACS Chem. Biol.*, 2012, **7**, 1496–1501.
- 37 A. Thomann, A. G. G. de Mello Martins, C. Brengel, M. Empting and R. W. Hartmann, *ACS Chem. Biol.*, 2016, **11**, 1279–1286.
- 38 F. J. Reen, S. L. Clarke, C. Legendre, C. M. Mcsweeney, K. S. Eccles, S. E. Lawrence, F. O’Gara and G. P. Mcglacken, *Org. Biomol. Chem.*, 2012, **10**, 8903.
- 39 C. Lu, C. K. Maurer, B. Kirsch, A. Steinbach and R. W. Hartmann, *Angew. Chem., Int. Ed.*, 2014, **53**, 1109–1112.
- 40 K. Sak, E. Barnard and J. Järv, *IUBMB Life*, 2000, **50**, 99–103.
- 41 E. J. Calabrese, *Crit. Rev. Toxicol.*, 2001, **31**, 523–528.
- 42 R. B. Conolly, *Toxicol. Sci.*, 2003, **77**, 151–157.
- 43 J. D. Moore, F. M. Rossi, M. A. Welsh, K. E. Nyffeler and H. E. Blackwell, *J. Am. Chem. Soc.*, 2015, **137**, 14626–14639.
- 44 G. Chen, L. R. Swem, D. L. Swem, D. L. Stauff, C. T. O’Loughlin, P. D. Jeffrey, B. L. Bassler and F. M. Hughson, *Mol. Cell*, 2011, **42**, 199–209.
- 45 E. Szabadi, *J. Theor. Biol.*, 1977, **69**, 101–112.
- 46 T. Kenakin, *J. Pharmacol. Exp. Ther.*, 2011, **336**, 296–302.
- 47 T. Kenakin, *BMC Pharmacol. Toxicol.*, 2012, **13**, 3.
- 48 R. A. F. de Ligt, A. P. Kourounakis and A. P. Ijzerman, *Br. J. Pharmacol.*, 2000, **130**, 1–12.
- 49 Y.-X. Tao, *Pharmacol. Ther.*, 2008, **120**, 129–148.
- 50 C. Cugini, M. W. Calfee, J. M. Farrow, D. K. Morales, E. C. Pesci and D. A. Hogan, *Mol. Microbiol.*, 2007, **65**, 896–906.
- 51 D. W. Essar, L. Eberly, A. Hadero and I. P. Crawford, *J. Bacteriol.*, 1990, **172**, 884–900.

3.2 Chapter B: Exploring the chemical space of ureidothiophene-2-carboxylic acids as inhibitors of the quorum sensing enzyme PqsD from *Pseudomonas aeruginosa*



ELSEVIER

Contents lists available at ScienceDirect

European Journal of Medicinal Chemistry

journal homepage: <http://www.elsevier.com/locate/ejmech>

Original article

Exploring the chemical space of ureidothiophene-2-carboxylic acids as inhibitors of the quorum sensing enzyme PqsD from *Pseudomonas aeruginosa*J. Henning Sahner^a, Martin Empting^a, Ahmed Kamal^a, Elisabeth Weidel^a, Matthias Groh^a, Carsten Börger^b, Rolf W. Hartmann^{a,*}^a Pharmaceutical and Medicinal Chemistry, Saarland University & Helmholtz Institute for Pharmaceutical Research Saarland (HIPS), Department of Drug Design and Optimization, Campus C2 3, 66123 Saarbrücken, Germany^b PharmBioTec GmbH, Science Park 1, 66123 Saarbrücken, Germany

ARTICLE INFO

Article history:

Received 1 October 2014

Received in revised form

1 April 2015

Accepted 2 April 2015

Available online 6 April 2015

Keywords:

Quorum sensing

Pseudomonas aeruginosa

Bacterial cell-to-cell communication

Ureidothiophene-2-carboxylic acids

Antibacterial agents

ABSTRACT

Pseudomonas aeruginosa employs a quorum sensing (QS) communication system that makes use of small diffusible molecules. Among other effects, the QS system coordinates the formation of biofilm which decisively contributes to difficulties in the therapy of *Pseudomonas* infections. The present work deals with the structure-activity exploration of ureidothiophene-2-carboxylic acids as inhibitors of PqsD, a key enzyme in the biosynthetic pathway of signal molecules in the *Pseudomonas* QS system. We describe an improvement of the inhibitory activity by successfully combining features from two different PqsD inhibitor classes. Furthermore the functional groups, which are responsible for the inhibitory potency, were identified. Moreover, the inability of the new inhibitors, to prevent signal molecule formation in whole cell assays, is discussed.

© 2015 Elsevier Masson SAS. All rights reserved.

1. Introduction

Antibiotic therapy is characterized by the everlasting competition between the generation of novel antibacterial substances and the development of the respective bacterial resistances [1,2]. One outstanding example is the opportunistic pathogen *Pseudomonas aeruginosa* which is responsible for severe infections and is a leading cause of death in cystic fibrosis patients [3]. Its ability to rapidly form resistances against the currently used antibiotics necessitates new approaches for antibacterial treatment [4,5]. Typically, antibiotics affect bacterial viability and thus cause a selection pressure that inevitably leads to the development of resistances. In recent years several research groups have been trying to break out of this vicious cycle by reducing the virulence of the pathogens instead of affecting their viability [6]. One approach is the inhibition of the bacterial cell-to-cell communication systems like QS [7]. In QS, bacterial cells release a variety of small diffusible molecules which can be detected by other bacteria. This kind of molecular

signaling allows the bacterial population to assess its cell density and coordinate group behavior. The *Pseudomonas* QS system consists of two *N*-acylhomoserine lactone (AHL) regulatory circuits (*las* and *rhl*) linked to an 2-alkyl-4-quinolone (AQ) system [3]. Whereas the AHL systems are widespread among Gram negative bacteria [8], our group focuses on the so called *Pseudomonas* quinolone signal quorum sensing (PQS-QS) system, an AQ system that exclusively exists in *P. aeruginosa* and some *Burkholderia* strains [9]. It is involved in the production of a number of virulence factors that contribute to their pathogenicity [10]. Moreover, it takes part in regulating the formation of biofilms, a main cause for bacterial resistance against conventional antibiotics in clinical use [11]. The *pqsABCDE* operon, whose expression is controlled by the transcriptional regulator PqsR (MvfR), directs the AQ biosynthesis in *P. aeruginosa*. Molecules, produced upon activity of this operon are among others, 2-heptyl-3-hydroxy-4-quinolone (*Pseudomonas* quinolone signal, PQS) and its biosynthetic precursor 2-heptyl-4-quinolone (HHQ) [12]. HHQ and PQS themselves activate PqsR leading to an auto-induction of the *pqsABCDE* operon [13,14]. Besides, they can modulate the innate immune response of mammalian cells, affecting the first defense barrier of the host

* Corresponding author.

E-mail address: rolf.hartmann@helmholtz-hzi.de (R.W. Hartmann).

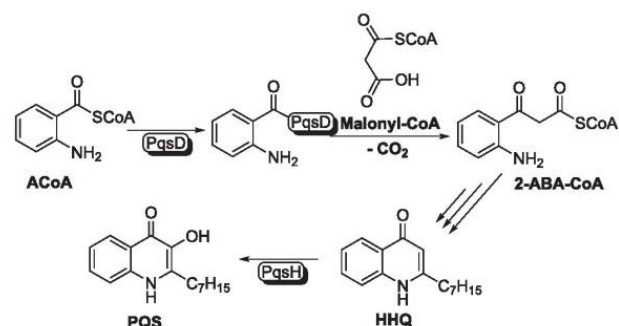
[15,16,17]. Compounds, interfering with the PQS-QS system have proven to be promising candidates for drug development. Treatment with antagonists of the PqsR receptor enabled the survival of *P. aeruginosa* infected *Galleria mellonella* larvae [18]. Furthermore we could show that inhibitors of the enzyme PqsD, a key player in the AQ biosynthesis (Scheme 1), are able to reduce biofilm in *P. aeruginosa* cultures [19]. It was recently reported by Dulcey et al., that PqsD produces 2-aminobenzoylacetate-coenzyme A (2-ABA-CoA), a highly active intermediate in the HHQ biosynthesis, by converting anthraniloyl-coenzyme A (ACoA) with malonyl CoA. Firstly, ACoA is covalently transferred to C112 of PqsD, followed by the reaction with malonyl-CoA. Further conversion of the intermediate 2-ABA-CoA in several enzymatic steps finally results in HHQ and PQS (Scheme 1) [17]. Interestingly, PqsD is also capable of directly producing HHQ by converting ACoA with β -ketodecanoic acid [20]. In the recent past we frequently used this enzymatic reaction to assess the activity of PqsD inhibitors [19,21–25]. For compounds interfering with the first enzymatic step, the formation of the PqsD-CoA complex, this is still a valid method [23,24].

In a recent work, we reported on the class of ureidothiophene-2-carboxylic acids as potent inhibitors of PqsD. Biophysical methods were used to confirm a binding hypothesis derived from molecular docking studies. This approach enabled the structure-based optimization of a screening hit compound resulting in a series of highly active molecules (e.g. **A** and **B** in Chart 1) [21]. According to our docking pose and the results from SPR competition experiments, the most active derivative **B** occupies an area, spanning from the entrance of the binding channel to the active site, leaving a gap of about 6 Å to the bottom of the pocket where the catalytic residues are located. Its carboxylic acid groups are supposed to interact with Asn154 and Arg262 respectively anchoring the inhibitor in the binding channel of PqsD. The phenylalanine residue perfectly fits into a narrow pocket at the channel's entrance delimited by Arg 223 and Phe226 and (Fig. 1).

In this work we describe further exploration of the chemical space, the structure activity relationships (SAR) and the intracellular effects of this class of inhibitors.

2. Results and discussion

According to our binding hypothesis, the carboxylate group of the amino acid part in **A** and **B** interacts with Arg262 at the entrance of the PqsD binding channel (Fig. 1). The natural substrate anthraniloyl CoA (ACoA) builds several ion bridges between its phosphoric acid groups and the arginines on the surface of the protein. Such interactions are considered very potent in literature [26,27]. Inspired by ACoA we replaced the carboxylic acid moiety by a phosphoric acid group (**1**). In comparison to the glycine derivative



Scheme 1. Biosynthetic pathway of the signal molecules HHQ and PQS according to Dulcey et al. [15].

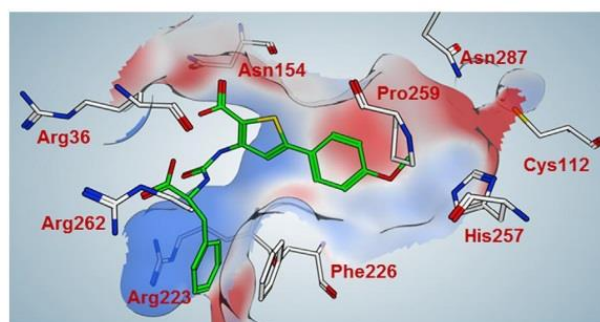


Fig. 1. Docking pose of **B** inside the binding channel of PqsD.

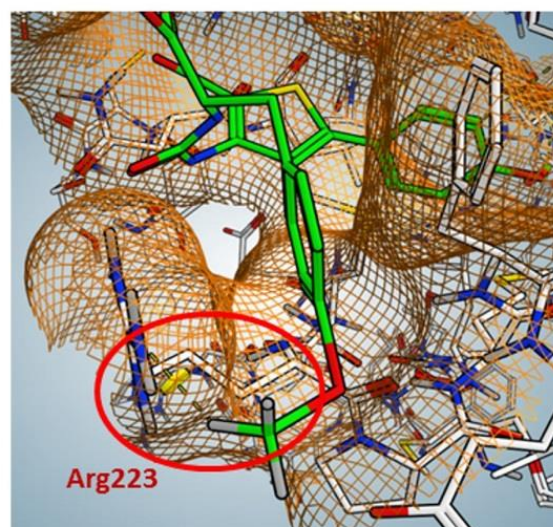


Fig. 2. Illustration of the proposed clash between the additional methoxy group and the protein residue Arg223.

A the activity did not increase. Based on these findings, the phosphoric acid was not considered for further optimization due to synthetic reasons.

The so far most active inhibitor **B** carries a phenylalanine substituent at the ureido motif. In order to fine-tune the electronic properties of the aromatic system we investigated electron donating and electron withdrawing substituents in *para*-position (Table 1). In case of an electron donating hydroxyl function (**2**), the activity dropped to 29 μ M similar to an additional methoxy group (**3**; IC₅₀: 31 μ M). In case of the latter this is probably due to steric reasons, which is in good agreement with our binding hypothesis (Fig. 2).

Introduction of an electron withdrawing and lipophilic chlorine substituent (**4**) also resulted in decreased inhibitory potency (14 μ M). As both kinds of substituents with inverse electronic properties were detrimental to the activity, we considered the unsubstituted ring as most favorable. In the next step we shortened (**5**) and prolonged (**6**) the linker between the α -position and the phenyl ring. In the crystal structure, the entrance to the sub-pocket, delimited by Arg223 and Phe226 and Glu227 is narrow and therefore requires a special conformation. This conformation is obviously only provided by the compound with the methylene linker as both, **5** and **6** displayed significantly weaker inhibitory potency. As a last trial to explore the SAR at this part of the

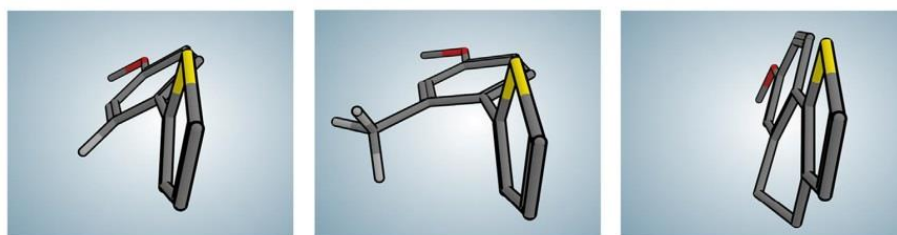


Fig. 3. Energy minimized conformations showing the orientation between the phenyl ring and the thiophene core of **B**, **15** and **16**.

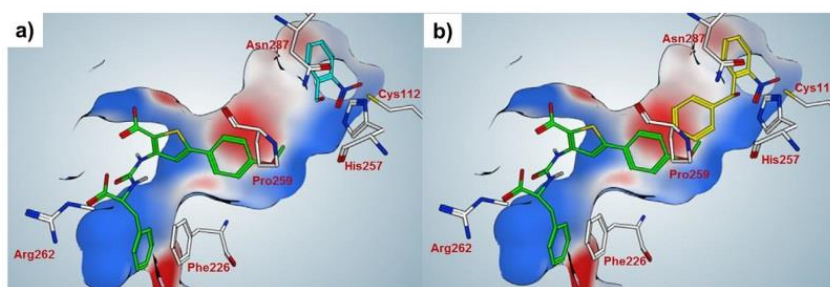


Fig. 4. a) Docking pose of **B** (green) and **C** (turquoise). b) Docking pose of **B** (green) and **D** (yellow). (For interpretation of the references to colour in this figure legend, the reader is referred to the web version of this article.)

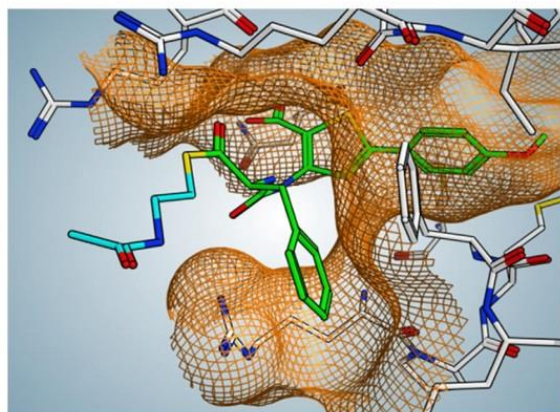


Fig. 5. Docking pose of **B** (green) extended with the NAC moiety (blue) present in **24**, illustrating how the additional residue is directed outside the binding channel of PqsD. (For interpretation of the references to colour in this figure legend, the reader is referred to the web version of this article.)

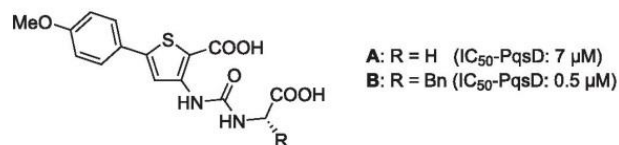


Chart 1. Structures of the PqsD inhibitors **A** and **B**.

molecule, further readily available (*S*)-amino acids were introduced. None of the resulting compounds (**7–11**) outperformed the potency of **B**.

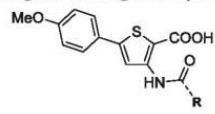
We proceeded, retaining the phenylalanine residue at the ureido-motif, as the most promising moiety and subsequently

focused on the opposite side of the molecule. Firstly parts of the methoxy equipped ring of **B** were removed to determine the essential functional groups (Table 2). Demethylation, resulting in hydroxyl compound **12** decreased the activity. Further omitting this OH-group (**13**) however partially restored it. This leads to the assumption that the oxygen of the methoxy group contributes to the activity to a certain extent, presumably as a hydrogen bond acceptor. In absence of an appropriate interaction partner the hydrogen bond donor of **13** is surrounded by highly ordered water molecules, leading to an entropic loss and, therefore, a lowered activity. Removal of the entire methoxyphenyl ring (**14**) results in a total loss of inhibitory potency. To reveal the bioactive conformation and the orientation of the methoxyphenyl ring towards the thiophene, **15** and **16** were investigated. The methyl group of **15** increased the IC_{50} to 8 μ M suggesting an ortho-effect and thus an unfavorable perpendicular orientation of the two rings or a steric clash of the additional substituent. Rigidification by an ethylene linker (**16**), which directly connects the two aromatic systems causing a planar structure (Fig. 3), did not improve the activity as well. The tight shape of the PqsD binding channel that demands certain flexibility from entering inhibitors can once more be an explanation for these findings.

The proposed interaction between the carboxylic acid at the thiophene core with Asn154 was corroborated by compound **17**. Removal of the carboxylic group decreased the activity by about twentyfold.

By the application of SPR competition experiments in the above mentioned earlier work [21], we were able to narrow down the position of the ureidothiophene-2-carboxylic acids within the binding channel compared to known PqsD inhibitors from the 2-(nitrophenyl)-methanol class (**C** and **D** in Chart 2). Whereas the shorter compound **C** (Fig. 4a turquoise) did not affect the binding affinity of **B**, the longer derivative **D** (Fig. 4b yellow) prevented binding of **B** (data not shown), fitting to our binding hypothesis.

According to the docking pose, a linkage of the two inhibitor classes in order to combine their interactions with PqsD should be

Table 1
Inhibitory activities of **1–11** against *P. aeruginosa* PqsD *in vitro*.


Entry	R	Inhibition of PqsD ^a
1		7.0 ± 0.7 μM
2		29.0 ± 0.01 μM
3		31.3 ± 3.7 μM
4		13.8 ± 1.1 μM
5		~40% @ 50 μM
6		33.7 ± 1.5 μM
7		31.9 ± 3.0 μM
8		19.0 ± 2.6 μM
9		13.2 ± 0.9 μM
10		5.0 ± 0.9 μM
11		30.3 ± 0.3 μM

^a IC₅₀ values of PqsD.

possible. We decided to enlarge the unsubstituted compound **13** step by step to achieve a full combination with **D**. Due to the absence of strong interactions with the protein, docking studies never delivered an unambiguous orientation of the aryl ring at the thiophene core within the pocket. Even though an attachment in 3-position (**18,19**) should be favorable according to the dockings with compound **B** (compare Fig. 4), expansion in 4-position (**20–22**) delivers better results (Table 3). We hypothesized that this is once again due to the tight shape of the binding channel which hampers the entrance of the stronger tilted compounds **18** and **19**. Whereas the introduction of the first phenyl ring (**20**) did not result in better inhibition, elongation with a hydroxy-methyl function (**21**), which is supposed to mimic the one of **C** and **D** increased the activity by twentyfold compared to **13** (factor three compared to **B**). Attachment of the second, nitro-substituted ring (**22**) forfeits parts of the activity gain. A possible explanation could be that the final compound is large and inflexible and, is therefore, incapable of adapting to conformational changes which would be necessary to retain the

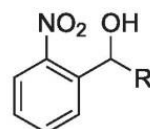
Table 2
Inhibitory activities of **12–17** against *P. aeruginosa* PqsD *in vitro*.

Entry	Structure	Inhibition of PqsD ^a
12		21.6 ± 3.9 μM
13		3.8 ± 1.4 μM
14		no inhibition @ 50 μM
15		7.5 ± 1.8 μM
16		23.7 ± 0.02 μM
17		11.5 ± 2.0 μM

^a IC₅₀ values of PqsD.

sum of interactions of the respective single compounds **B** and **D**. To confirm, that the nitro-substituted ring of **22** reaches deep into the binding channel, SPR experiments were performed. Firstly, the binding responses of **B**, **21** and **22** towards PqsD were recorded in the absence of ACoA. In a second experiment, the PqsD loaded sensor chip was treated with ACoA. According to the catalytic mechanism of PqsD this results in the anthranilate-PqsD complex, in which the anthranilic acid is covalently bound to Cys112. Subsequently the binding responses of **B**, **21** and **22** to this complex were determined. Only the signals of **22** showed significant differences between treated and untreated PqsD (Figure S1 in supporting information). Since this behavior is typical for the 2-nitrophenylmethanol derivatives [22], occupation of the same binding site can be assumed.

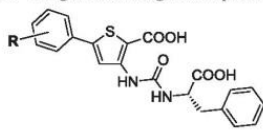
Although the inhibitors displayed high potency in the cell free enzyme assay, none of them was able to reduce the HHQ levels in a whole cell *P. aeruginosa* assay. These findings can be attributed to different reasons like permeation- or efflux problems. Several steps were taken to achieve an intracellular activity.

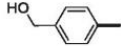
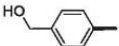
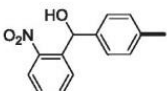


C: R = H (IC₅₀-PqsD: 2 μM)
D: R = Ph (IC₅₀-PqsD: 1 μM)

Chart 2. Structures of the PqsD inhibitors **C** and **D** and their *in vitro* IC₅₀ values against *P. aeruginosa* PqsD.

Table 3
Inhibitory activities of **18–22** against *P. aeruginosa* PqsD *in vitro*.



Entry	3-Position	4-Position	Inhibition of PqsD ^a
18		H	6.2 ± 0.7 μM
19		H	19.4 ± 0.02 μM
20	H		2.7 ± 0.5 μM
21	H		0.14 ± 0.03 μM
22	H		0.36 ± 0.06 μM

^a IC₅₀ values of PqsD.

Fluoroquinolone and β-lactam antibiotics are mostly zwitterionic. According to several reports in literature, this feature significantly contributes to their transport into the cell, which was shown especially for the β-lactams [28,29]. Inspired by that we introduced S-histidine instead of S-phenylalanine, using the imidazole ring as a bioisostere of the phenyl ring while gaining a basic function and therefore a potentially positive charge at the same time. The resulting compound **23** displayed weak activity against PqsD (40% inhibition at 50 μM) but showed for the first time significant but very moderate reduction of HHQ levels in the whole cell assay (Reduction of HHQ at 250 μM: 16 ± 5%). In a second attempt, we made use of an *N*-acetyl thioester (NAC-ester) which is frequently used in mutasynthesis programs. The NAC adducts thereby serve as mimics of coenzyme A esters which improve their acceptance as precursors in biosynthesis and might also facilitate the entrance into bacterial cells in comparison to the free acids [30]. The carboxylic acid moiety of the phenylalanine was considered more suitable for the attachment of an NAC unit than the one at the thiophene core. It is presumably positioned at the entrance of the pocket (Fig. 5) directing the additional substituent outside the binding channel of PqsD, and therefore avoiding steric hindrance. Thus an intracellular cleavage of the thioester to set the active form free might not be mandatory. The resulting compound **24** (Chart 3) still displayed reasonable activity (IC₅₀: 32 μM) but turned out to be inactive in the whole-cell assay. We further examined the introduction of a cell penetrating peptide (**25**) at the same position. Again, the inhibitory activity on the cell free level could be retained, but no inhibitory effect in the whole cell assay was observed at the test concentration.

3. Conclusions

In conclusion, we further explored the chemical space of the ureidothiophene-2-carboxylic acids as inhibitors of PqsD. The pharmacophore of the inhibitor class was determined and the essentiality of several functional groups was clarified. Moreover, two inhibitor classes could be successfully merged without having access to structural information of protein-ligand x-ray structures. The resulting compounds display higher inhibitory activity by profiting from the combined interactions with the protein. Following this approach, the most potent PqsD inhibitors described so far were obtained. Although the potency in cell free assay was high, an intracellular activity could not be achieved even by attachment of a cell penetrating peptide. We assume that the class of inhibitors is subject to efflux causing natural resistance of *P. aeruginosa* towards the newly developed antibacterial agents. Therefore, we consider the ureidothiophene-2-carboxylic acids to be not eligible for further development in the field of *Pseudomonas* quorum sensing inhibitors. The problem could eventually be solved by a combined application with efflux pump inhibitors, or by using pharmaceutical technological methods, but this is beyond the frame of this work. Nevertheless, important interactions of functional groups with the protein were revealed that can be used to improve the inhibitory activity of other PqsD inhibitors with better intracellular effects.

4. Experimental procedures

4.1. Chemistry

4.1.1. Materials and methods

Starting materials were purchased from commercial suppliers and used without further purification. Column flash chromatography was performed on silica gel (40–63 μM), and reaction progress was monitored by TLC on TLC Silica Gel 60 F₂₅₄ (Merck). All moisture-sensitive reactions were performed under nitrogen atmosphere using oven-dried glassware and anhydrous solvents. Preparative RP-HPLC was carried out on a Waters Corporation setup containing a 2767 sample manager, a 2545 binary gradient module, a 2998 PDA detector and a 3100 electron spray mass spectrometer. Purification was performed using a Waters XBridge column (C18, 150 × 19 mm, 5 μm), a binary solvent system A and B (A = water with 0.1% formic acid; B = MeCN with 0.1% formic acid) as eluent, a flow rate of 20 mL/min and a gradient of 60%–95% B in 8 min were applied. ¹H and ¹³C NMR spectra were recorded on a Bruker Fourier spectrometer (500/300 or 125/75 MHz) at ambient temperature with the chemical shifts recorded as δ values in ppm units by reference to the hydrogenated residues of deuterated solvent as internal standard. Coupling constants (*J*) are given in Hz and signal patterns are indicated as follows: s, singlet; d, doublet; dd, doublet of doublets; t, triplet; m, multiplet, br., broad signal. Purity of the final compounds was determined by HPLC. The Surveyor LC system consisted of a pump, an autosampler, and a PDA detector. Mass spectrometry was performed on a MSQ electrospray mass spectrometer (ThermoFisher, Dreieich, Germany). The system was

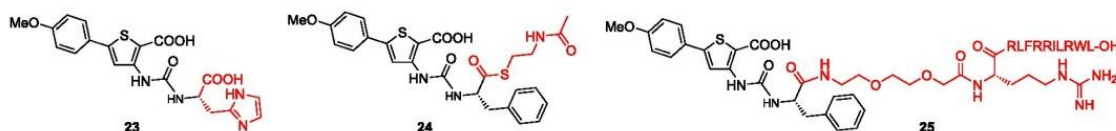


Chart 3. Structures of compound **23–25**, carrying moieties (highlighted in red) which should facilitate the entrance into Gram-negative cells. (For interpretation of the references to colour in this figure legend, the reader is referred to the web version of this article.)

operated by the standard software Xcalibur. A RP C18 NUCLEODUR 100–5 (125 mm × 3 mm) column (Macherey–Nagel GmbH, Dühren, Germany) was used as the stationary phase. All solvents were HPLC grade. In a gradient run the percentage of acetonitrile (containing 0.1% trifluoroacetic acid) was increased from an initial concentration of 0% at 0 min to 100% at 15 min and kept at 100% for 5 min. The injection volume was 10 μ L, and flow rate was set to 800 μ L/min. MS analysis was carried out at a spray voltage of 3800 V and a capillary temperature of 350 °C and a source CID of 10 V. Spectra were acquired in positive mode from 100 to 1000 m/z at 254 nm for the UV trace.

4.1.2. Synthesis and spectroscopic details

The synthesis of most of the 5-aryl-3-ureidothiophene-2-carboxylic acids (Scheme 2) started from readily available acetophenones (**I**) which were converted to the 5-aryl thiophene anthranilic acid methyl esters (**II**) via an Arnold-Vilsmaier-Haack reaction followed by a cyclization using methylmercaptoacetate [31]. The esters (**II**) were then hydrolyzed under basic conditions to afford the thiophene anthranilic acids (**III**) which were converted into the thiaisoic anhydrides (**IV**) [32,33]. The anhydrides (**IV**) were reacted with various amines giving rise to the 5-aryl-3-ureidothiophene-2-carboxylic acids (**V**) [34]. Further substituents at the 5-aryl ring were introduced using boronic acids or esters, respectively, via Suzuki coupling yielding **VI** [35].

Further details on the synthesis and spectroscopic data of final compounds and intermediates can be found in the [Supporting information](#).

4.2. Biology

4.2.1. General procedure for expression and purification of recombinant PqsD WT and R223A mutant in *Escherichia coli*

His6-tagged PqsD (H6-PqsD) and mutants were expressed in *E. coli* and purified using a single affinity chromatography step. Briefly, *E. coli* BL21 (λ DE3) cells containing the pET28b(+)/pqsD (kindly provided by Prof. Rolf Müller, Helmholtz Institute for Pharmaceutical Research Saarland (HIPS), Saarbrücken, Germany) were grown in LB medium containing 50 μ g/mL kanamycin at 37 °C to an OD₆₀₀ of approximately 0.8 units and induced with 0.2 mM IPTG for 16 h at 16 °C. The cells were harvested by centrifugation (5000 rpm, 10 min, 4 °C) and the cell pellet was resuspended in 100 mL binding buffer (10 mM Na₂HPO₄, 2 mM KH₂PO₄ pH 7.4, 3 mM KCl, 137 mM NaCl, 20 mM imidazole, 10% glycerol (v/v)) and lysed by sonication for a total process time of 2.5 min. Cell debris were removed by centrifugation (18500 rpm, 40 min, 4 °C) and the supernatant was filtered through a syringe filter (0.20 μ m). The clarified lysate was immediately applied to a Ni-NTA column, washed with binding buffer and eluted with 500 mM imidazole. The protein containing fractions were buffer-exchanged into

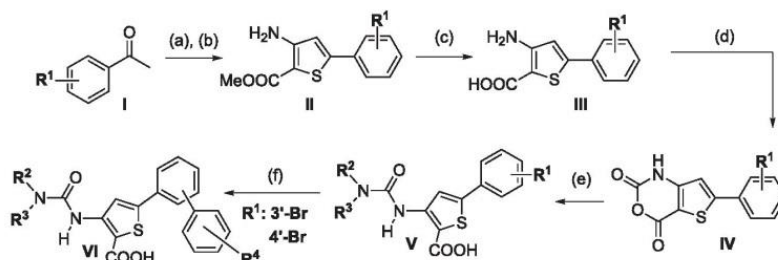
125 mM Na₂HPO₄, 50 mM KH₂PO₄ pH 7.6, 50 mM NaCl, 10% glycerol (v/v), using a PD10 column and judged pure by SDS-PAGE analysis. Then protein was stored in aliquots at –80 °C.

4.2.2. Screening assay procedure for *in vitro* PqsD inhibition [20].

The assay was performed monitoring enzyme activity by measuring HHQ formed by condensation of anthraniloyl-CoA and β -ketodecanoic acid. The reaction mixture contained MOPS buffer (0.05 M, pH 7.0) with 0.005% (w/v) Triton X-100, 0.1 μ M of the purified enzyme and inhibitor. The test compounds were dissolved in DMSO and diluted with buffer. The final DMSO concentration was 0.5%. After 10 min preincubation at 37 °C, the reaction was started by the addition anthraniloyl-CoA to a final concentration of 5 μ M and β -ketodecanoic acid to a final concentration of 70 μ M. Reactions were stopped by addition of MeOH containing 1 μ M amitriptyline as internal standard for LC/MS–MS analysis. HHQ was quantified using a HPLC-MS/MS mass spectrometer (ThermoFisher, Dreieich, Germany) in ESI mode. Ionization of HHQ and the internal standard amitriptyline was optimized in each case. The solvent system consisted of 10 mM ammonium acetate (A) and acetonitrile (B), both containing 0.1% trifluoroacetic acid. The initial concentration of B in A was 45%, increasing the percentage of B to 100% in 2.8 min and keeping it at 98% for 0.7 min with a flow of 500 μ L/min. The column used was a NUCLEODUR-C18, 100–3/125–3 (Macherey Nagel, Dühren, Germany). Control reactions without the inhibitor, but including identical amounts of DMSO, were performed in parallel and the amount of HHQ produced was set to 100%.

4.2.3. Determination of extracellular HHQ and PQS levels

For determination of extracellular levels of HHQ produced by PA14, cultivation was performed in the following way: cultures (initial OD₆₀₀ = 0.02) were incubated with or without inhibitor (final DMSO concentration 1%, v/v) at 37 °C, 200 rpm and a humidity of 75% for 16 h in 24-well Greiner BioOne (Frickenhausen, Germany) Cellstar plates containing 1.5 mL of LB medium per well. For HHQ analysis, according to the method of Lepine et al. [36], 500 μ L of the cultures supplemented with 50 μ L of a 10 μ M methanolic solution of the internal standard (IS) 5,6,7,8-tetradeutero-2-heptyl-4(1H)-quinolone (HHQ-d₄) were extracted with 1 mL of ethyl acetate. After centrifugation (18,620 g, 12 min), 400 μ L of the organic phase were evaporated to dryness and redissolved in methanol. UHPLC-MS/MS analysis was carried out as described in detail by Storz et al. [19] The monitored ions were (mother ion [m/z], product ion [m/z], scan time [s], scan width [m/z], collision energy [V], tube lens offset [V]): HHQ: 244, 159, 0.5, 0.01, 30, 106; HHQ-d₄(IS): 248, 163, 0.1, 0.01, 32, 113. For each sample, cultivation and sample work-up were performed in triplicates. Inhibition values of HHQ formation were normalized to OD₆₀₀.



Scheme 2. Synthesis of 5-aryl-3-ureidothiophene-2-carboxylic acids **V** or **VI**, respectively. Reagents and conditions: (a) POCl₃, DMF, 50 °C to rt, then NH₂OH·HCl, up to 150 °C. (b) Methylthioglycolate, NaOMe, MeOH, reflux. (c) KOH, MeOH, THF, H₂O, reflux. (d) COCl₂, THF. (e) Amine, H₂O, 100 °C then at 0 °C conc. HCl. (f) Na₂CO₃, Pd(PPh₃)₄, boronic acid or ester, THF, H₂O, toluene, 80 °C.

4.2.4. Surface plasmon resonance

4.2.4.1. General. SPR binding studies were performed using a Reichert SR7500DC instrument optical biosensor (Reichert Technologies, Depew, NY, USA) and CMD500M sensor chips obtained from XanTec (XanTec Bioanalytics, Düsseldorf, Germany). Scrubber 2 software (Version 2.0c, 2008, BioLogic Software) was used for proceeding and analyzing the data. Changes in refractive index due to DMSO dependent solvent effects were corrected by use of a calibration curve (seven solutions, 4.25%–5.75% DMSO in buffer).

4.2.4.2. Immobilization of His₆-PqsD. PqsD (38 kDa, >90% pure based on SDS-PAGE) was immobilized at an level of 5919 RU on a CMD500M (carboxymethyl dextran-coated) sensor chip at 18 °C analogous to the method described by Henn et al. [37].

4.2.4.3. Binding studies. The ACoA preincubation studies were performed as previously described using a constant flow rate of 25 µL/min and HEPES buffer as instrument running buffer (10 mM HEPES, pH 7.4, 150 mM NaCl, 5% DMSO (v/v), 0.05% Polysorbat 20 (v/v)) [20]. ACoA (100 µM) was injected for approximately 40 min with a constant flow of 5 µL/min to reach saturation of the ACoA binding site. Afterwards, the flow rate was increased to 50 µL/min for 30 min in order to flush all CoA away. Once the baseline is stable again the compounds were consecutively injected and the responses at equilibrium were compared to those obtained with the untreated surface. Experiments were performed in duplicate. For **B** a concentration series of 250, 125 and 62.5 µM were used. Since stronger binding signal was observed for **21**, the concentration series was decreased to 100, 50 and 25 µM, whereas a series of 25, 12.5, and 6.25 µM was measured for **22**. The compounds were injected for 120 s association times and 300 s dissociation times.

4.3. Computational chemistry

4.3.1. Docking

Inhibitors were built in MOE. The receptor was derived from crystal structure of PqsD in complex with ACoA (PDB Code: 3H77) [10]. The residuals of CoA, the covalently bound anthranilate and H₂O were removed and Cys112 was restored considering its conformation in 3H76 [10]. AutoDockTools V.1.5.6 was used to add polar hydrogens and to save the protein in the appropriate file format for docking with Vina. AutoDockVina was used for docking calculations [38]. The docking parameters were kept at their default values. The docking grid was sized 18 Å × 24 Å × 24 Å, covering the entire ACoA channel.

Acknowledgments

The authors thank Carina Scheidt and Simone Amman for performing the *in vitro* tests. We also appreciate Patrick Fischer's help in performing the synthesis. Furthermore we thank Dr. Werner Tegge (Helmholtz Centre for Infection Research (HZI), Braunschweig, Germany) for kindly providing the cell penetrating peptide. J. Henning Sahner gratefully acknowledges a scholarship from the "Stiftung der Deutschen Wirtschaft" (SDW). This project was funded by BMBF through grant 1616038B.

Appendix A. Supplementary data

Supplementary data related to this article can be found at <http://dx.doi.org/10.1016/j.ejmech.2015.04.007>.

References

- [1] J. Davies, Bacteria on the rampage, *Nature* 383 (1996) 219–220.
- [2] C. Walsh, Molecular mechanisms that confer antibacterial drug resistance, *Nature* 406 (2000) 775–781.
- [3] J.-F. Dubern, S.P. Diggle, Quorum sensing by 2-alkyl-4-quinolones in *Pseudomonas aeruginosa* and other bacterial species, *Mol. Biosyst.* 4 (2008) 882–888.
- [4] N. Bagge, O. Ciofu, L.T. Skovgaard, N. Hoiby, Rapid development *in vitro* and *in vivo* of resistance to ceftazidime in biofilm-growing *Pseudomonas aeruginosa* due to chromosomal β-lactamase, *APMIS* 108 (2000) 589–600.
- [5] A.R.M. Coates, G. Halls, Y. Hu, Novel classes of antibiotics or more of the same? *Brit. J. Pharmacol.* 163 (2011) 184–194.
- [6] F. von Nussbaum, M. Brands, B. Hinzen, S. Weigand, D. Haebich, Antibacterial natural products in medicinal chemistry - exodus of revival? *Angew. Chem. Int. Ed.* 45 (2006) 5072–5129.
- [7] For a recent review see: S. Scutera, M. Zucca, D. Savoia, Novel approaches for the design and discovery of quorum-sensing inhibitors *Expert Opin. Drug. Discov.* 9 (2014) 353–366.
- [8] S. Swift, J.A. Downie, N.A. Whitehead, A.M. Barnard, G.P. Salmond, P. Williams, Quorum sensing as a population-density-dependent determinant of bacterial physiology, *Org. Biomol. Chem.* 12 (2001) 6094–6104.
- [9] S. Diggle, P. Lumjaktase, F. Dipilato, K. Winzer, M. Kunakorn, D.A. Barrett, S.R. Chhabra, M. Cámara, P. Williams, Functional genetic analysis reveals a 2-alkyl-4-quinolone signaling system in the human pathogen *Burkholderia pseudomallei* and related bacteria, *Chem. Biol.* 13 (2006) 701–710.
- [10] A.K. Bera, V. Atanasova, H. Robinson, E. Eisenstein, J.P. Coleman, E.C. Pesci, J.F. Parsons, Structure of PqsD, a *Pseudomonas* quinolone signal biosynthetic enzyme, in complex with anthranilate, *Biochemistry* 48 (2009) 8644–8655.
- [11] L. Yang, M. Nilsson, M. Gjermansen, M. Givskov, T. Toker-Nielsen, Pyoverdine and PQS mediated subpopulation interactions involved in *Pseudomonas aeruginosa* biofilm formation, *Mol. Microbiol.* 74 (2009) 1380–1392.
- [12] L. Gallagher, S.L. McKnight, M.S. Kuznetsova, E.C. Pesci, C. Manoil, Functions required for extracellular quinolone signaling by *Pseudomonas aeruginosa*, *J. Bacteriol.* 184 (2002) 6472–6480.
- [13] D.S. Wade, M. Worth Calfee, E.R. Rocha, E.A. Ling, E. Engstrom, J.P. Coleman, E.C. Pesci, Regulation of *Pseudomonas* quinolone signal synthesis in *Pseudomonas aeruginosa*, *J. Bacteriol.* 187 (2005) 4372–4380.
- [14] G. Xiao, E. Déziel, J. He, F. Lépine, B. Lesic, M.-H. Castonguay, S. Milot, A.P. Tampakaki, S.E. Stachel, L.G. Rahme, MvfR, a key *Pseudomonas aeruginosa* pathogenicity LTTR-class regulatory protein, has dual ligands, *Mol. Microbiol.* 62 (2006) 1689–1699.
- [15] A. Bandyopadhyaya, M. Kesarwani, Y.-A. Que, J. He, K. Padfield, R. Tompkins, L.G. Rahme, The quorum sensing volatile molecule 2-amino acetophenon modulates host immune response in a manner that promotes life with unwanted guests, *PLoS Pathog.* 8 (2012) e1003024.
- [16] K. Kim, Y.U. Kim, B.H. Koh, S.S. Hwang, S.-H. Kim, F. Lépine, Y.-H. Cho, G.R. Lee, HHQ and PQS, two *Pseudomonas aeruginosa* quorum-sensing molecules, down regulate the innate immune responses through the nuclear factor-κB pathway, *Immunology* 129 (2010) 578–588.
- [17] C.E. Dulcey, V. Dekimpe, D.-A. Fauvelle, S. Milot, M.-C. Groleau, N. Doucet, L.G. Rahme, F. Lépine, E. Déziel, The end of an old hypothesis: the *Pseudomonas* signaling molecules 4-hydroxy-2-alkylquinolines derive from fatty acids, not 3-ketofatty acids, *Chem. Biol.* 20 (2013) 1481–1491.
- [18] C. Lu, C.K. Maurer, B. Kirsch, A. Steinbach, R.W. Hartmann, Overcoming unexpected functional inversion of a PqsR antagonist in *Pseudomonas aeruginosa*: an *in vivo* potent antivirulence agent targeting pqs quorum sensing, *Angew. Chem. Int. Ed.* 53 (2014) 1109–1112.
- [19] M.P. Storz, C.K. Maurer, C. Zimmer, N. Wagner, C. Brengel, J.C. de Jong, S. Lucas, M. Müsken, S. Häussler, A. Steinbach, R.W. Hartmann, Validation of PqsD as an anti-biofilm target in *Pseudomonas aeruginosa* by development of small-molecule inhibitors, *J. Am. Chem. Soc.* 134 (2012) 16143–16146.
- [20] D. Pistorius, A. Ullrich, S. Lucas, R.W. Hartmann, U. Kazmaier, R. Müller, Biosynthesis of 2-alkyl-4(1H)-quinolones in *Pseudomonas aeruginosa*: potential for therapeutic interference with pathogenicity, *ChemBioChem* 12 (2011) 850–853.
- [21] J.H. Sahner, C. Brengel, M.P. Storz, M. Groh, A. Plaza, R. Müller, R.W. Hartmann, Combining *in silico* and biophysical methods for the development of *Pseudomonas aeruginosa* quorum sensing inhibitors: an alternative approach for structure-based drug design, *J. Med. Chem.* 56 (2013) 8656–8664.
- [22] E. Weidel, J.C. de Jong, C. Brengel, M.P. Storz, A. Braunshausen, M. Negri, A. Plaza, A. Steinbach, R. Müller, R.W. Hartmann, Structure optimization of 2-Benzamidobenzoic acids as PqsD inhibitors for *Pseudomonas aeruginosa* infections and elucidation of binding mode by SPR, STD NMR, and molecular docking, *J. Med. Chem.* 56 (2013) 6146–6155.
- [23] M. Storz, G. Allegretta, B. Kirsch, M. Empting, R.W. Hartmann, From *in vitro* to *in cellulo*: structure-activity relationship of (2-nitrophenyl)methanol derivatives as inhibitors of PqsD in *Pseudomonas aeruginosa*, *Org. Biomol. Chem.* 12 (2014) 6094–6104.
- [24] M. Storz, C. Brengel, E. Weidel, M. Hoffmann, K. Hollemeyer, A. Steinbach, R. Müller, M. Empting, R.W. Hartmann, Biochemical and biophysical analysis of chiral PqsD inhibitor revealing tight-binding behavior and enantiomers with contrary thermodynamic signatures, *ACS Chem. Biol.* 8 (2013) 2794–2801.
- [25] S. Hinsberger, Johannes C. de Jong, M. Groh, J. Hauptenthal, R.W. Hartmann, Benzamidobenzoic acids as potent PqsD inhibitors for the treatment of *Pseudomonas aeruginosa* infections, *Eur. J. Med. Chem.* 76 (2014) 343–351.
- [26] F.A. Cotton, V.W. Day, E.E. Hazen Jr., S. Larsen, S.T.K. Wong, Structure of bis(methylguanidinium) monohydrogen orthophosphate. A model for the

- arginine-phosphate interactions at the active site of staphylococcal nuclease and other phosphohydrolytic enzymes, *J. Am. Chem. Soc.* 96 (1974) 4471–4478.
- [27] A.S. Woods, S. Ferré, Amazing stability of the arginine-phosphate electrostatic interaction, *J. Proteome Res.* 4 (2005) 1397–1402.
- [28] H. Nikaido, E.Y. Rosenberg, J. Foulds, Porin channels in *Escherichia coli*: studies with β -lactams in intact cells, *J. Bacteriol.* 153 (1983) 232–240.
- [29] F. Yoshimura, H. Nikaido, Diffusion of β -lactam antibiotics through the porin channels of *Escherichia coli* K-12, *Antimicrob. Agents Chemother.* 27 (1985) 84–92.
- [30] A. Kirschning, F. Taft, T. Knobloch, Total synthesis approaches to natural product derivatives based on the combination of chemical synthesis and metabolic engineering, *Org. Biomol. Chem.* 5 (2007) 3245–3259.
- [31] H. Hartmann, J. Liebscher, A simple method for the synthesis of 5-aryl-3-amino-2-alkoxycarbonylthiophenes, *Synthesis* (1984) 275–276.
- [32] F. Fabis, S. Jolivet-Fouchet, M. Robba, H. Landelle, S. Rault, Thiazotico anhydrides: efficient synthesis under microwave heating conditions and study of their reactivity, *Tetrahedron* 54 (1998) 10789–10800.
- [33] L. Foulon, E. Braud, F. Fabis, J.C. Lancelot, S. Rault, Synthesis and combinatorial approach of the reactivity of 6-and 7-arylthieno [3,2-d][1,3] oxazine-2,4-diones, *Tetrahedron* 59 (2003) 10051–10057.
- [34] F.X. Le Foulon, E. Braud, F. Fabis, J.C. Lancelot, S. Rault, Solution-phase parallel synthesis of a 1140-member ureidothiophene carboxylic acid library, *J. Comb. Chem.* 7 (2005) 253–257.
- [35] N. Miyaura, K. Yamada, A. Suzuki, A new stereospecific cross-coupling by palladium-catalyzed reaction of 1-alkenylboranes with 1-alkenyl or 1-alkynyl halides, *Tetrahedron Lett.* 20 (1979) 3437–3440.
- [36] F. Lépine, S. Milot, E. Déziel, J. He, L.G. Rahme, Electrospray/mass spectrometric identification and analysis of 4-hydroxy-2-alkylquinolines (HAQs) produced by *Pseudomonas aeruginosa*, *J. Am. Soc. Mass. Spectrom.* 15 (2004) 862–869.
- [37] C. Henn, S. Boettcher, A. Steinbach, R.W. Hartmann, Catalytic enzyme activity on a biosensor chip: combination of surface plasmon resonance and mass spectrometry, *Anal. Biochem.* 428 (2012) 28–30.
- [38] O. Trott, A.J. Olson, AutoDock Vina: improving the speed and accuracy of docking with a new scoring function, efficient optimization, and multithreading, *J. Comput. Chem.* 31 (2009) 455–461.

3.3 Chapter C: Hit optimization of an α -helical peptide: Ala-scan, truncation, and sidechain-to-sidechain macrocyclization of an RNA polymerase inhibitor

This person contributed to this chapter:

Monica Habib: Synthesis and purification of peptides 27, 28, 31, and 32.

Over the last few years, there has been an increased interest in investigating the underexplored chemical space of peptides beyond Lipinski's rule of five as a source of novel drugs [1]. This can only be emphasized by the presence of more than 140 peptide-based therapeutics in clinical trials in 2014 [2]. The modular assembly of peptides provides high structural diversity combined with the potential to display large interaction surface areas [2,3]. This enables to generate peptides with high affinity as well as specificity to their targets. This specificity jointly with the fact that metabolic degradation products of peptides are amino acids advocates lower risk of toxicity [2,3]. Additionally, peptides are considered superior in pursuing targets perceived as "undruggable" such as protein-protein interactions (PPIs) compared to conventional small organic molecules (SOMs) [4]. Thus, peptides hit a "sweet spot" possessing specificity and potency of larger protein-based biologics yet, being smaller in size. However, peptides still possess some undesirable attributes such as low oral bioavailability, susceptibility to proteolytic degradation, and rapid clearance [5]. Additionally, short peptide sequences stripped from native proteins can unfold, resulting in loss of biological activity. One reason for the loss of the ordered geometry can be the inability of the peptide to retain its secondary structure i.e. α -helix without the stabilizing effect of the protein environment [6–9]. Strategies to overcome such physicochemical and pharmacokinetic deficits have been extensively researched for example truncation, incorporation of unnatural or D-configured amino acids, and macrocyclization [7–9]. In this study, we focus on sidechain-to-sidechain macrocyclization as an approach to enhance conformational stability, biological activity, and proteolytic stability of α -helical peptides.

If installed in a suitable manner, macrocyclization will constrain a peptide structure locking it in the bioactive conformation. Such decrease in the rotational degrees of freedom should lead to the reduction of the entropy "penalty" present upon binding [10,11]. Additionally, a non-natural cross-linkage has been shown to protect the backbone amide moieties improving resistance to degradation *via* proteases [12,13].

Over the years, several approaches for sidechain-to-sidechain macrocyclization have been devised such as disulfide bridges and lactone formations, Ruthenium-catalyzed ring-closing olefin metathesis (RCM), molybdenum-catalyzed ring-closing alkyne metathesis (RCAM) and Copper (I) as well as Ruthenium (II)-catalyzed alkyne-azide cycloaddition (CuAAC and RuAAC, respectively) [14–17]. The latter technique has been used in this study as the strategy of choice as elaborated orthogonal protection schemes are not required when employing the prominent copper-click reaction. Additionally, a triazole moiety as a cross-linkage instead of long hydrocarbon chains would yield peptides with better physicochemical properties [13,18].

The recent surge in antibiotic resistance accompanied with the lack of discovery of new antibiotics possessing novel chemical entities is quite troubling. Thus, the need for "outside of the box" antibiotics with novel mechanisms of action is of high relevance. In a previous study from our lab, we discovered through a peptide-scanning approach a novel nonadecapeptide inhibiting *E. coli* RNA polymerase [19]. The peptide sequence was derived from sigma factor 70 (σ^{70} , region 2.2) and showed activity in the micromolar range (Figure 1). An abortive transcription assay and ELISA demonstrated that P07 obstructs transcription initiation and inhibits binding of σ^{70} to the core enzyme. Additionally, molecular dynamics simulations and mutagenesis studies showed that P07 has the ability to address a new hot spot for the protein-protein interaction inhibition namely the lid-rudder-system (LRS). In this study, we performed Alanine scan and truncation to identify the core sequence for activity and modifiable residues in the peptide sequence. Afterwards, we designed and synthesized macrocyclic derivatives through CuAAC-mediated sidechain-to-sidechain

macrocyclization with the aim to improve potency and conformational stability of the parent peptide.

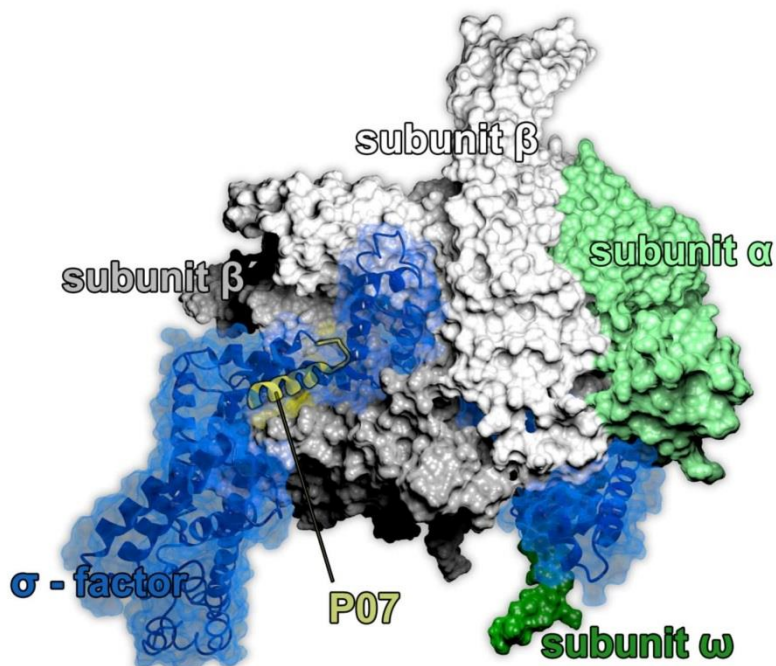


Figure 1. Co-crystal of RNA polymerase and the σ 70 factor (PDB ID: 4YG2) with P07 highlighted in yellow.

Results and Discussion

Alanine-Scan biological results and structural insights

An Ala-scan was undertaken not only to reveal amino acid(s) with high contribution to binding but to additionally give insight into the peptide's binding profile. It is expected that the amino acid(s) key for interaction facing the binding pocket upon substitution to Ala would yield peptides with lower biological activity. Whereas, amino acid(s) exposed to the surface when substituted would retain their activity unless they have an effect on the whole dynamics or conformation of the peptide. Thus, this would provide us with data needed to identify the sequence positions suitable for introduction of unnatural amino acid(s) required for macrocyclization and further optimization.

The yielded peptides did not yield any sequence of improved activity over the original sequence. However, several positions – Met19, Gly17, residues14-12, residues10-5, Asn2 and Thr1 – have been exchanged without a big loss of activity (<2-folds) which could be used for sequence modification or insertion points of unnatural amino acids required for a sidechain-to-sidechain macrocyclization. Peptide 12 has been previously found to have an $IC_{50} > 50 \mu M$ [19]. Key activity loss was observed (>5 folds) upon swapping of Leu18, Ile16, Ile11 and Arg3 (highlighted in red, table 1). In case of Leu18, Ile16, Ile11, this hints towards the importance of the hydrophobic sidechain for protein binding.

While for Arg3 the loss in activity can be attributed to either loss of the hydrophilic and/or basic properties of the side chain. It cannot be excluded that the sidechain also plays a role in stabilizing the whole peptide conformation via intramolecular hydrogen bonding to neighboring residues. Lastly, four peptides showed a moderate loss (2-5 folds). The full biological results from the Ala-scan are compiled in table 1 and illustrated in figure 2.

Peptide name	Sequence ^a	IC ₅₀ (μM) or %inhibition ^b	95% CI ^c
1	<i>H-TNRGLQFLDLIQEGNIGLM-OH</i>	5.17	4.62 - 5.79
2	<i>H-TNRGLQFLDLIQEGNIGLA-OH</i>	7.7	7.02 - 8.46
3	<i>H-TNRGLQFLDLIQEGNIGAM-OH</i>	55.84	38.38 - 81.25
4	<i>H-TNRGLQFLDLIQEGNIALM-OH</i>	5.03	4.62 - 5.46
5	<i>H-TNRGLQFLDLIQEGNAGLM-OH</i>	13.9 ± 0.0 % @ 50μM	
6	<i>H-TNRGLQFLDLIQEGAIGLM-OH</i>	12.78	10.15 - 16.10
7	<i>H-TNRGLQFLDLIQEANIGLM-OH</i>	5.43	4.63 - 6.38
8*	<i>H-TNRGLQFLDLIQAGNIGLM-OH</i>	9.13	6.03 - 13.81
9*	<i>H-TNRGLQFLDLIAEGNIGLM-OH</i>	9.61	8.25 - 11.19
10	<i>H-TNRGLQFLDLLAQEGNIGLM-OH</i>	>50	--
11	<i>H-TNRGLQFLDAIQEGNIGLM-OH</i>	10.78	9.79 - 11.88
12*	<i>H-TNRGLQFLLALIQEGNIGLM-OH</i>	7.09	6.61 - 7.57
13	<i>H-TNRGLQFLADLIQEGNIGLM-OH</i>	8.9	7.28 - 11.1
14	<i>H-TNRGLQALDLIQEGNIGLM-OH</i>	8.24	5.73 - 11.86
15*	<i>H-TNRGLLAFLDLIQEGNIGLM-OH</i>	5.18	4.70 - 5.71
16	<i>H-TNRGAQFLDLIQEGNIGLM-OH</i>	6.52	5.42 - 7.83
17	<i>H-TNRALQFLDLIQEGNIGLM-OH</i>	11.95	10.04 - 14.22
18	<i>H-TNAGLQFLDLIQEGNIGLM-OH</i>	27.94	21.64 - 36.08
19	<i>H-TARGLQFLDLIQEGNIGLM-OH</i>	16.37	13.49 - 19.88
20	<i>H-ANRGLQFLDLIQEGNIGLM-OH</i>	6.18	4.92 to 7.76

Table 1. Alanine scan biological results. ^a) Substituted residues are indicated in bold red ^b) % inhibition mean values and SD are given ^c) 95% CI means a 0.95 probability of containing the population mean. Highlighted in red are results with more than 5-folds loss and in orange between 2-5 folds, loss compared to parent peptide. * are previously reported in [19].

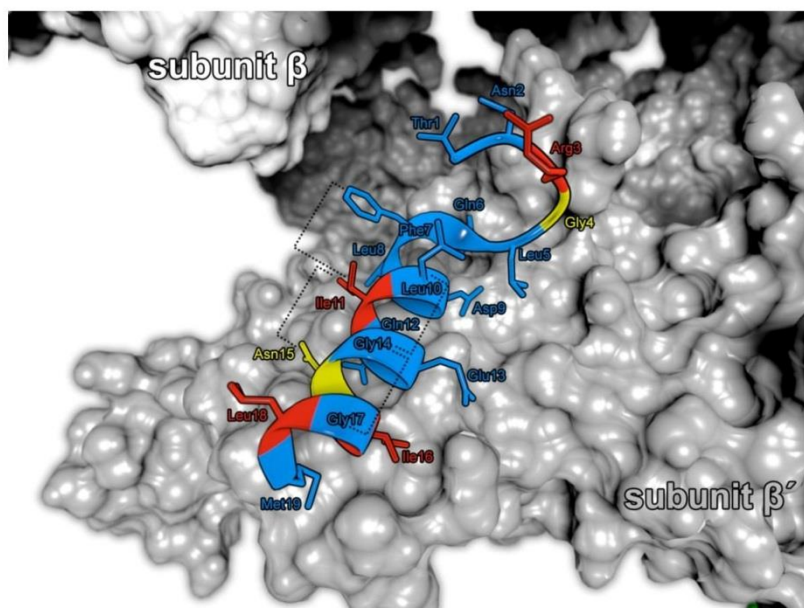


Figure 2. Peptide 1 (P07) bound to RNA polymerase (In red, yellow, and blue are amino acids with 5-, 5-2, <2 folds of activity loss, respectively). Highlighted with black dotted lines are the amino acid positions used for macrocyclization.

Aggregation test

All peptides synthesized so far possessed micromolar activities. Peptides were tested for aggregation to exclude it as the reason for either activity gain or loss. Two peptides were chosen for this test: **5** as an example for inactives and **14** as an example for actives. The measurements were taken at two-time points, after 10 min of incubation (similar to the biological test) and 24 hrs. In both cases, no aggregation was observed *via* light scattering measurements at OD₆₀₀ till the maximum soluble concentration of 100 μM. Values are summarized in table S2.

Shortening of the Peptide Sequence and modifications inspired by other RNAP inhibitors

One by one truncation of the peptide from both the *N*- and *C*- terminus was attempted in order to achieve the minimum active sequence with better physicochemical properties. Deletion of Met¹⁹ led to 3-folds loss of activity as seen in peptide **21** (table 2). This could be attributed to either the importance of the hydrophobic interaction mediated by the methionine side chain or the terminal –COOH position. Replacement of Met¹⁹ with the unnatural amino acid Norleucine **22** possessing a C4-alkyl chain or with shorter methyl **2** led to peptides with IC₅₀s of 7.1 and 7.7, respectively. This lack of large loss/gain in activities upon increasing or decreasing the hydrophobicity of the side chain hints that the importance of the terminal –COOH group at this position. Deletion of Thr¹ at the *N*-terminus led to peptide **24** with similar activity to the parent peptide. Since the Met¹⁹ is important for activity, replacement with another amino acid(s) was considered for further optimization. Literature reports showed that a class of small organic molecules possesses an indole moiety that binds to the same

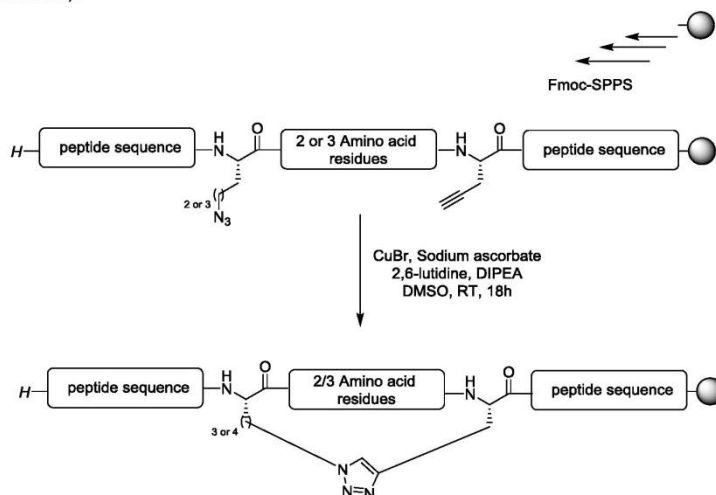
amino acid(s) as the corresponding Methionine residue does in σ^{70} (Met¹⁹) [20]. Hence, we were inspired to synthesize peptide **23** with a Tryptophan instead of Met¹⁹ and deletion of Thr¹ as well. **23** displayed an IC₅₀ of 4.74 μ M similar to peptide **1** without further improvement in activity. As no activity gains were achieved upon deletion of the hydrophilic amino acid Thr¹, or replacement of Met¹⁹, the original sequence was used as a template for further modifications and future syntheses.

Peptide name	Sequence ^a	IC ₅₀ (μ M)	95% CI ^b
1	H-TNRGLQFLDLIQEGNIGLM-OH	5.17	4.62 - 5.79
21	H-TNRGLQFLDLIQEGNIGL----OH	14.09	10.88 - 18.26
22 ^c	H-TNRGLQFLDLIQEGNIGL Nor -OH	7.11	6.18 - 8.17
23	H----NRGLQFLDLIQEGNIGL W -OH	4.74	3.79 - 5.93
24	H----NRGLQFLDLIQEGNIGLM-OH	6.69	5.56 - 8.05

Table 2. Biological activity of terminal amino acid substitutions and truncation^a Substituted residues are indicated in bold red and deleted residues are indicated by bold red dashes^b 95% CI means a 0.95 probability of containing the population mean. ^c Nor stands for un-natural amino acid norleucine.

Macrocyclic peptide syntheses and schemes

Solid-phase peptide syntheses (SPPS) of the desired peptide sequences were carried out incorporating the azide and alkyne bearing amino acids which were used afterward for on-resin CuAAC (Scheme 1).



Scheme 1. Description of the general procedure for on-resin side-chain macrocyclization using CuAAC. Reagents and conditions: CuBr (1.0 eq), sodium ascorbate (1.0 eq) dissolved in water (20 mg/mL), 2, 6-lutidine (10 eq), and DIPEA (10 eq) in 1 ml of degassed DMSO for 18 hr at RT.

In order to prove the formation of the desired triazole moiety, the consumption of the azide functionality is monitored using IR-spectrometry as described before [16]. The azide group gives a

distinctive band around 2100 cm^{-1} , which is well separated from other IR-signals of peptides. Upon triazole formation, this signal will provide an easy method for monitoring progression of the CuAAC reaction. However, there is the possibility of dimer formation (intermolecular reaction) instead of the desired monomer (intramolecular reaction). A successful CuAAC-mediated macrocyclization proceeds with no change in molecular weight compared to the linear precursor, while a possible dimer formation would lead to a doubled mass. Hence, cyclic monomers and triazole-linked dimers can be distinguished through examining the isotope pattern of the MS signals using high-resolution mass spectrometry. In the case of a dimeric product, the distances between individual isotopic species would be half of the monomeric variants with the same m/z ratio (Figure 3 and SI).

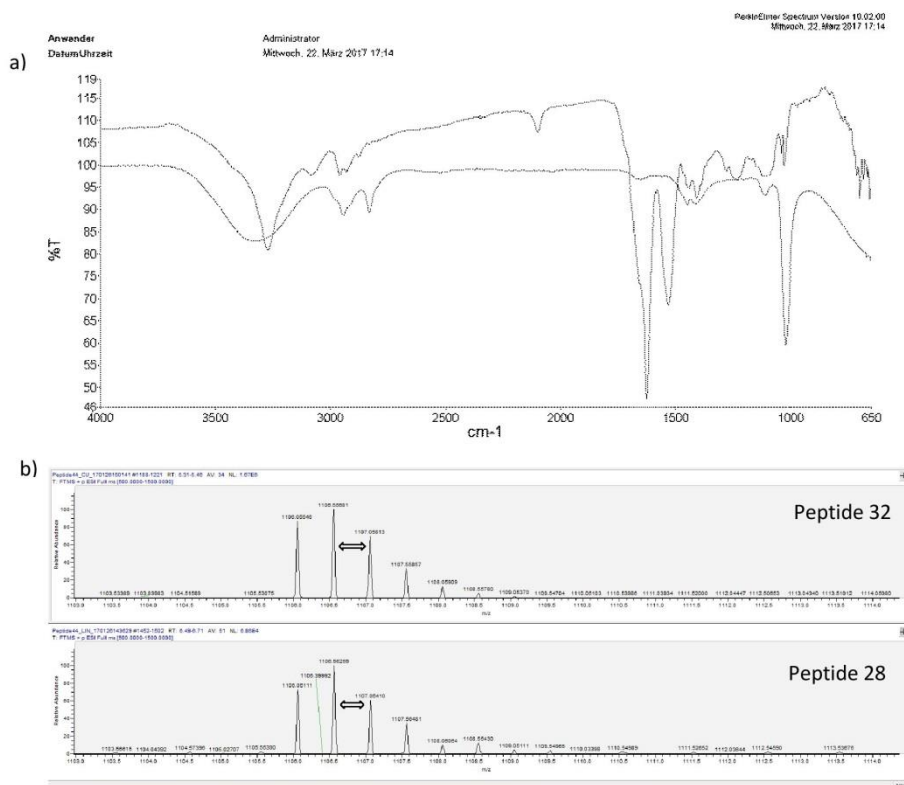


Figure 3. Representative IR-and HR-ESI-MS spectra to illustrate successful intermolecular CuAAC
a) IR-spectra of linear peptide **28** (top) versus macrocyclized peptide **32** (bottom) displaying the depletion of the azide functionality characteristic signal at 2100 cm^{-1} . b) Recorded HR/ESI -MS isotope pattern of linear peptide **28** (top) versus macrocyclized peptide **32** (bottom) showing equidistance (0.5 Da) between different isotopes indicating the formation of intramolecular triazole linkage.

Macrocyclization attempts and their effects on α -helicity and biological activities

According to our hypothesis, stapling of α -helical peptides is expected to increase α -helical content, thus, enhancing peptide affinity and potency *via* reducing entropic costs. However, in order to insert the macrocycle at the appropriate side of the α -helical peptide structural data is required. Attempts at resolving an X-ray of peptide **1** bound to the holoenzyme were not fruitful (unpublished data). So, our design was based on the results from the Ala scan and X-ray structure of the σ factor co-crystal with RNAP (PDB ID: 4YG2) (Figure 2) [21]. Accordingly, four positions were chosen. First, two of these were based on the co-crystal structure: an (i) to (i+4) side-chain-to-side-chain macrocyclization was proposed between Asn¹⁵-Ile¹¹ and Ile¹¹-Phe⁷. The other two proposals were based on the Ala-scan results where amino acids showing no huge loss were assumed to be surface exposed and not involved in binding. Accordingly, Gly¹⁷-Gly¹⁴ and Gly¹⁴-Leu¹¹ were proposed as points for macrocycle insertion. The staple between Gly¹⁷-Gly¹⁴ is an (i) to (i+3) instead of the previously used (i) to (i+4) pattern. Linear precursor peptides harboring non-natural amino acids suitable for CuAAC macrocyclization at the suggested insertion points were synthesized and tested for biological activity. The four proposed linear peptides **25**, **26**, **27** and **28** retained inhibitory activity with IC₅₀s of 8.98, 43.17, 5.14, and 4.16 μ M, respectively. Peptide **26** showed the biggest loss in activity of 10-folds. This fits with the Ala-scan results as Ile¹¹ was firstly replaced with a longer carbon chain bearing an azide moiety **25** and retained some of the activity while greater activity loss was observed when replaced with a shorter less flexible alkyne moiety **26**. Peptides **27** and **28** possessed activities similar to peptide **1** indicating that indeed the amino acid(s) replaced might not be essential for binding. The linear precursor peptides already displayed an increase in α -helicity determined through CD spectroscopy measurement (Table 3 and Figure 4) except for **26** which showed lower content than **1**. Peptide **27** showed almost 2-folds increase in α -helical content (56.7% vs. 24.8%). Hence, the increase/decrease in α -helicity did not correlate with activity at this stage. Upon macrocyclization, almost complete abolishment of activity was observed regardless of the increase in the α -helical content and position of the macrocycle. Activity loss of **29** and **30** can be explained by the constraintment of the alkyl chain(s) in position 10 that was important for interaction as seen from the Ala-scan results. However, this could not explain the activity loss in case of peptides **31** and **32**.

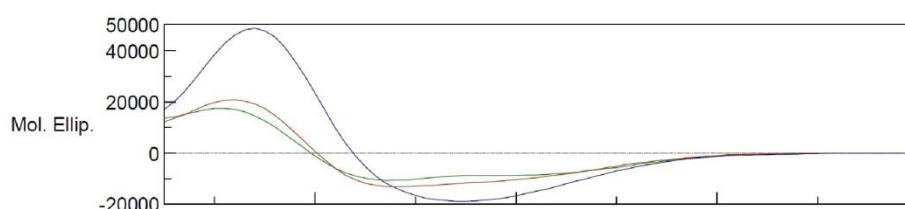


Figure 4. Circular dichroism of peptide **1**, **27** and **31**. Peptide **1**, **27**, and **32** and displayed as green, blue, and red lines, respectively.

Peptide name	Sequence ^a	IC ₅₀ or % inhibition (μM) ^b	95% CI ^c	% α helicity ^d
1	H-TNRGLQ FLDLIQEGNIGLM -OH	5.17	4.62 - 5.79	24.8
25	H-TNRGLQFLDL-N ₃ -QEG-N ₃ -IGLM-OH	8.98	7.90 - 10.21	34.6
26	H-TNRGLQ-N ₃ -LDL-N ₃ -QEGNIGLM-OH	43.17	29.81 - 62.5	6.9
27	H-TNRGLQFLDLNQE-N ₃ -NI-N ₃ -LM-OH	5.14	4.38 - 6.02	56.7
28	H-TNRGLQFLD-N ₃ -IQE-N ₃ -NIGLM-OH	4.52	3.70 - 5.51	36.2
29	H-TNRGLQFLDL-N ₃ -QEG-N ₃ -IGLM-OH	14 ± 0.9% @ 50μM		33.7
30	H-TNRGLQ-N ₃ -LDL-N ₃ -QEGNIGLM-OH	9.8 ± 1.4% @ 50μM		31.8
31 *	H-TNRGLQFLDLNQE-N ₃ -NI-N ₃ -LM-OH	49.95 ± 1.5% @ 25 μM		33
32	H-TNRGLQFLD-N ₃ -IQE-N ₃ -NIGLM-OH	13.7 ± 1.6% @ 50μM		27.9

Table 3. Peptides sequence and results of second macrocyclization attempt. ^a) Substituted residues are indicated in bold red ^b) % inhibition mean values and SD are given ^c) 95% CI means a 0.95 probability of containing the population mean. ^d) Percentage α-helicity was computed *via* CONTIN algorithm. * Results shown are from a 3:2 mixture of 31 and 27.

This complete abolishment of activity upon stapling using CuAAC-mediated (i) to (i+4) side-chain-to-side-chain macrocyclization was rather unexpected. However, it could be reasoned by one of the following explanations:

1. The (perfectly ordered) α-helical conformation might not be the active conformation during binding as seen *via* the presence of an atypical helix turn with extended vertical distances between consecutive turns of the helix bigger than 5.4 Å (PDB ID: 4YG2, see SI) [21]. Thus, a more conformationally flexible peptide might be required for induced-fit binding. This conformational flexibility might be required for such complex multi-subunit machinery which undergoes pronounced structural changes for DNA unwinding and RNA synthesis. However, this hypothesis is difficult to validate experimentally and would be best addressed *via* an X-ray crystallographic analysis of the peptide-protein complex.
2. It could not be excluded that the actual binding mode is different than proposed in both X-ray holoenzyme co-crystal and Ala-scan. In this scenario, the active conformation could still be α-helical as expected but the triazolyl linkage results in a steric clash between the peptide and the enzyme interface.

3. To the best of our knowledge, only a single report in the literature by Czabotar *et al.* had similar findings with stapled peptides having an unexpected reduced affinity for their targets [22]. The loss in affinity was attributed to disruption of a network of intramolecular interactions stabilizing the native peptide. Whereupon stapling this network was disturbed leading to perturbation of the peptide structure.

Materials and Methods

General

Solvents

All solvents were synthesis, or HPLC, or peptide synthesis grade. DMF, MTBE, DIEA, TES, TIS, Anisole, TFA, Acetonitrile, DCM, Methanol and Piperidine obtained from Acros Organics (Heidelberg, Germany), Sigma-Aldrich (Germany), Carl Roth (Karlsruhe, Germany) and VWR (Darmstadt, Germany).

Chemicals and Reagents

All reagents were synthesis or peptide synthesis grade. HATU, HBTU, and TBTU were obtained from IRIS biotech (Marktredwitz, Germany) or Novabiochem (Darmstadt, Germany).

Preloaded resins for SPPS were obtained from Rapp Polymere (Tübingen, Germany).

All Fmoc-protected natural amino acids were obtained from Novabiochem (Darmstadt, Germany) while unnatural Fmoc-protected amino acids were obtained from IRIS biotech (Marktredwitz, Germany).

Instrumentation and Analysis

Microwave synthesis system

Microwave irradiation for SPPS was established using Discover[®] microwave synthesis system from CEM (Kamp-Lintfort, Germany) and an additional external unit was used for solvent removal by suction. The synthesizer was operated using 25 mL polypropylene vessels equipped with polypropylene filters (Roland Vetter, Laborbedarf OHG).

HPLC/MS

Crude and isolated peptides were analyzed using a Thermo Fisher Accela HPLC equipped with a degasser, a quaternary pump, and an autosampler, coupled to an Accela photodiode array detector (PDA) followed by a TSQ Quantum Access Max mass spectrometer with heated electrospray ionization source (HESI-II) (Thermo Fisher). For gradient elution, an Accucore RP-MS column (150 × 2.1 mm, 2.6 μm) was used with a mobile phase consisting of HPLC grade water containing 1% TFA (v/v) and acetonitrile containing 1% TFA (v/v) and a flow rate of 800 μL/min with a gradient of 10% Acetonitrile to 80% in 20 minutes. The injection volumes were 10 and 25 μL. The PDA was operated at 220 and 280 nm wavelength. The MS conditions used were electrospray ionization (ESI) in positive mode. Data acquisition and analysis were achieved using Xcalibur 2.2 software.

LC-HRMS

LC-HRMS data was performed on one of the following machines:

A) A Dionex Ultimate 3000 RSLC system using a Waters BEHC18, 100 x 2.1 mm, 1.7 μ m dp column. All samples were constituted in acetonitrile and water (1:1). Separation of samples was achieved by a linear gradient with (A) H₂O + 0.1 % formic acid to (B) ACN + 0.1 % formic acid at a flow rate of 600 μ l/min and 45 °C. The gradient was initiated after 0.5 min isocratic step at 5 % B, followed by an increase to 95 % B in 18 min to end up with a 2 min step at 95 % B before re-equilibration with initial conditions. UV spectra were recorded by a DAD in the range from 200 to 600 nm. The LC flow was split to 75 μ l/min before entering the maXisr-ToF mass spectrometer Bruker Daltonics (Bremen, Germany) using the standard ESI source.

B) A Dionex Ultimate 3000 RSLC system using a ThermoFisher Scientific Accucore phenyl-hexyl, 100x2.1 mm, 2.6 μ m dp column. All samples were constituted in acetonitrile and water (1:1). Separation of samples was achieved by a linear gradient with (A) H₂O + 0.1 % formic acid to (B) Acetonitrile + 0.1 % formic acid at a flow rate of 500 μ l/min and 40 °C. The gradient was initiated after 0.5 min isocratic step at 5 % B, followed by an increase to 100 % B in 23 min to end up with a 2 min step at 100 % B before re-equilibration with initial conditions. All data acquisition was done in positive ion mode and full-scan mode ranging from 500-1500 m/z at a resolution of 70,000 using a TF (Dreieich, Germany) Q Exactive Focus system equipped with heated electrospray ionization (HESI)-II source and Xcalibur (Version 4.0.27.19) software. Mass calibration was done prior to analysis according to the manufacturer's recommendations using external mass calibration.

Semi-preparative HPLC

Purification of crude peptides was performed using one of the following preparative HPLCs:

A) An Agilent 1200 HPLC system with an automated fraction collector (Agilent Technologies, Inc. Headquarters, Santa Clara, CA, USA) in "time-based" mode. ChemStation® software was used for control, report and data analysis. The sample was manually injected. A Nucleoel 100-7 C18 HD column (250 / 16 mm) was used as stationary phase (Macherey- Nagel GmbH, Dueren, Germany). The solvent system consisted of HPLC grade water containing 1‰ TFA (v/v) (A) and acetonitrile containing 1‰ TFA (v/v) (B). HPLC-Method: Flow rate 5 mL/min with a gradient run from 10% B to 60% in 40 minutes.

B) A Waters HPLC system equipped with a Phenomenex C18 Luna column (5 mm pore size, 100 Å particle size, 250, 21.2 mm) in an acetonitrile/water gradient under acidic conditions. The purified peptide mass was verified by liquid chromatography mass spectroscopy (LCMS; Waters).

Lyophilization

For the removal of RP-HPLC eluents or aqueous solvents from peptidic samples:

A) An Alpha-2- 4-LD plus freeze dryer with condensation temperature of -85 °C (Martin Christ Gefriertrocknungsanlagen GmbH, Osterode, Germany) equipped with a high vacuum pump Ilmvac, type 109012 (Ilmvac GmbH, Ilmenau, Germany) was used.

B) A Labconco freeze dryer.

Centrifuge

Sedimentation and washing of precipitated peptides were performed using a Thermo Fisher Scientific Heraeus Multifuge 15-R centrifuge (Schwerte, Germany).

FT-IR

Fourier-transform infrared (FT-IR) spectrum was recorded on a PerkinElmer (Rodgau, Germany) Spectrum 100 FT-IR spectrometer.

Circular dichroism spectropolarimeter

All single Far-UV-CD spectra were obtained at 24°C using a Jasco-1500 spectropolarimeter (Gross-Umstadt, Germany). All spectra were recorded using a 1-mm pathlength rectangular quartz cell, 1-nm bandwidth, 100 nm/min scan speed, 5 accumulations, within a wavelength range of 185 to 260 nm. Peptides were dissolved to a final concentration of 50µM in deionized water (milliQ, Millipore) containing 30% 2,2,2-trifluoroethanol (TFE). After blank subtraction and smoothing, the percentage of α -helicity of the peptides was computed *via* CONTIN algorithm.

Biological testing

The assay was performed as previously described. The inhibitory effect of our peptides on RNAP transcription and respective IC₅₀ values were measured through a transcription inhibition assay. *E. coli* RNAP holoenzyme is incubated with 3H-UTP, T7A1 promoter PCR fragment as a DNA template to which tested compounds are added afterward. After a while, the transcription reaction is stopped and the residual unincorporated 3H-UTP is quantified by liquid scintillation counting. All peptides were dissolved in a stock solution of 1:1 acetonitrile and MilliQ water before testing. Three different concentrations of a compound/peptide were chosen for the determination of an IC₅₀ value (two samples for each concentration). The calculation of the IC₅₀ value was performed by plotting the percent inhibition versus the concentration of inhibitor. At least two independent determinations were performed for each compound.

Data Analysis

Data analysis was performed using GraphPad Prism 6. The different effect of the compounds was plotted as dose–response curves such that each individual point represents the average of a single experiment. Lines of best fit and associated IC₅₀ values as well as respective 95% confidence intervals (CI) were calculated for dose–response curves using the nonlinear fit variable slope (four parameters) function with a bottom constraint = 0 and top constraint = 1.

Aggregation test

A master mix of *E. coli* RNAP holoenzyme is incubated with T7A1 promoter PCR fragment then mixed with serial dilutions of test compounds into a transparent F-bottom 384-well microtiter plate (Greiner Bio-One, Germany, cat. no. 781901) in duplicates. Absorbance was measured on a PheraStar

FS (BMG Labtech, Germany) plate reader at 600 nm after 10 min at 37 °C and 24 hr at room temperature of incubation. The data were analyzed using BMG Labtech MARS software.

Synthesis

Peptides **1-24** were supplied by our *in-house* peptide platform (HZI Braunschweig). Peptides **25, 26, 29** and **30** were synthesized according to synthesis protocol 1. Peptides **27, 28, 31** and **32** were synthesized according to synthesis protocol 2. Macrocyclization was performed using the protocol described below.

General Protocol for Microwave assisted Fmoc- SPPS

Synthesis protocol #1

The synthesis was performed on a TentaGel[®] S AC-Met-Fmoc resin (scale 0.24/4 mmole) using coupling protocol 1, except in the case of unnatural amino acids, coupling protocol 2 was applied to assure more efficient couplings.

Resin Swelling. Prior to synthesis, the dry resin was allowed to swell in DCM for 30 min followed by washing (3x with DCM and 3 x with DMF).

Deprotection. Removal of the *N*-terminal protecting group was performed *via* the addition of a solution containing 20% (v/v) piperidine in DMF followed by MW-irradiation (40 °C, 30W) for 5 min. After washing and re-addition of 20% piperidine in DMF irradiation was applied for 15 min. Afterward, the reaction mixture was removed *via* filtration and the resin was subsequently washed with DMF (7x).

Coupling protocol 1. First, 4 eq of the Fmoc protected amino acid (scaled to the resin loading) and 3.9 eq of the coupling reagent (HBTU) in a minimal amount of DMF is dissolved. Then, 8 eq DIEA were added for activation. After 15 min of pre-activation, the resulted mixture was added to the *N*-terminal de-protected peptide-resin and irradiated with MW (20min, 40 °C, 30 W). Excess reagents were removed by filtration and the peptide resin was washed thoroughly. These steps were repeated 3 times.

Coupling protocol 2. First, 2 eq of the unnatural Fmoc protected amino acid (scaled to the resin loading) and 1.9 eq of a coupling reagent (HATU) in a minimal amount of DMF is dissolved. Then, 4 eq DIEA were added for activation. After 15 min of pre-activation, the resulted mixture was added to the *N*-terminal de-protected peptide-resin and irradiated with MW (20min, 40 °C, 30 W). Excess reagents were removed by filtration and the peptide resin was washed thoroughly. These steps were repeated 3 times.

Cleavage and workup of the assembled peptide. After completion of synthesis, the resins were washed with DMF (7x), DCM (3x), and diethyl ether (3x) then stored in a desiccator and dried under vacuum. To cleave the assembled peptide off the resin and achieve full deprotection of amino acid side chain protecting groups, the peptide resin is treated with a mixture of TFA/H₂O/TIS 95:3:2 v/v for 3h. The cleaved peptide is precipitated in cold MTBE, centrifuged and washed with MTBE 3 times. At the end, the crude peptide would be stored in a desiccator and dried under vacuum. Crude peptides were purified via semi-preparative HPLC (see above).

Synthesis protocol #2

The synthesis was performed using microwave equipped automated peptide synthesizer (Liberty 1; CEM) on a 0.1mmol scale using standard Fmoc solid phase peptide synthesis techniques. A preloaded Resin with Methionine was used and provided in the reactor.

Resin Swelling. Prior to synthesis, the dry resin was washed with DMF.

Deprotection. Removal of the *N*-terminal protecting group was performed *via* 20% (v/v) piperidine in DMF and initialized by MW-irradiation. The resin was subsequently washed with DMF.

Coupling protocol. Amino acids were added in 2 eq to the reactor, HBTU in 5 eq was dosed into the amino acid solution. After that 2 eq of DIEA was added to the resin. The coupling reaction was irradiated with microwaves for a few minutes then the resin was washed with DMF.

Cleavage and workup of the assembled peptide. After completion of synthesis, the peptides were cleaved in 95% (v/v) trifluoroacetic acid (TFA), 2.5% (v/v) triisopropyl silane (TIS), and 2.5% (v/v) H₂O for one hour. The cleaved peptide is precipitated in cold diethyl ether, centrifuged and washed with diethyl ether. The peptide precipitate was then allowed to dry under vacuum to remove residual ether. Crude peptides were purified *via* semi-preparative HPLC (see above).

On-resin side-chain macrocyclization using CuAAC.

On resin, CuAAC was performed using CuBr (1.0 eq), sodium ascorbate (1.0 eq) dissolved in water (20 mg/mL), 2, 6-lutidine (10 eq), and DIPEA (10 eq) in 1 ml of degassed DMSO for 18 hr at RT to give resin-bound intermediate. Afterward, the solvent was removed *via* lyophilization. Cleavage and workup were performed as described above.

Molecule Modeling

Protein data were collected from the Protein Data Bank (PDB) and prepared using the MOE 2014 LigX function and Amber99 force field. Distance measurements were done using MOE 2014.

Conclusions

In conclusion, we explored the possibility of entropic optimization of previously described peptidic inhibitor (P07, peptide **1**) of RNAP core enzyme to σ^{70} PPI. While sidechain-to-sidechain macrocyclization of peptides proved beneficial for α -helical content, in this case, the reduced flexibility does not translate into biological activity improvement. Nevertheless, these results might change by employing other macrocyclization motifs and lengthier linkers to strike a compromise between flexibility required for induced-fit binding and conformational stability. The Ala-scan results provide basis for future rational optimization with 13 residues (1, 2, 5-10, 12-14, 17, and 19) amenable for medchem-driven modifications. This in combination with the successful insertion of unnatural amino acids in the peptide sequence can be further used for the introduction of new interaction abilities not possible by natural amino acids and combinatorial tuning of the peptide e.g. by decorating it with additional moieties *via* copper-catalyzed click chemistry [23]. Among others CuAAC as well as olefin metathesis mediated sidechain-to-sidechain macrocyclization has been shown to be a valuable tool for peptide optimization [11] and promising cyclic peptides for targeting PPI of RNAP core enzyme to sigma factors have been reported [24]. Thus, targeting protein interaction surfaces is still to be considered an untapped source for novel drugs, yet more efforts

have to be put into better understanding of the exact mechanistic and interaction modes between RNAP as a multi-domain complex and the peptidic inhibitors described herein.

Supplementary Materials

Peptides HPLC chromatograms, mass spectra, characterization, and purities are summarized in supporting information.

Acknowledgments

We are grateful for Werner Tegge for managing our in-house peptide platform operations. We are thankful for Richard Ebright for his attempts in obtaining X-ray co-crystals. We thank Jeanine Jung for her technical assistance and diligence in performing the biological assays. We are appreciative for Michael Hoffmann assistance in obtaining HRMS spectra.

References

1. Doak, B.C.; Over, B.; Giordanetto, F.; Kihlberg, J. Oral druggable space beyond the rule of 5: insights from drugs and clinical candidates. *Chemistry & biology* **2014**, *21*, 1115–1142.
2. Fosgerau, K.; Hoffmann, T. Peptide therapeutics: current status and future directions. *Drug discovery today* **2015**, *20*, 122–128.
3. Craik, D.J.; Fairlie, D.P.; Liras, S.; Price, D. The future of peptide-based drugs. *Chemical biology & drug design* **2013**, *81*, 136–147.
4. Arkin, M.R.; Tang, Y.; Wells, J.A. Small-molecule inhibitors of protein-protein interactions: progressing toward the reality. *Chemistry & biology* **2014**, *21*, 1102–1114.
5. Otvos, L.; Wade, J.D. Current challenges in peptide-based drug discovery. *Frontiers in chemistry* **2014**, *2*, 62.
6. Cardote, T.A.F.; Ciulli, A. Cyclic and Macrocyclic Peptides as Chemical Tools To Recognise Protein Surfaces and Probe Protein-Protein Interactions. *ChemMedChem* **2016**, *11*, 787–794.
7. Driggers, E.M.; Hale, S.P.; Lee, J.; Terrett, N.K. The exploration of macrocycles for drug discovery--an underexploited structural class. *Nature reviews. Drug discovery* **2008**, *7*, 608–624.
8. Goldflam, M.; Ullman, C.G. Recent Advances Toward the Discovery of Drug-Like Peptides De novo. *Frontiers in chemistry* **2015**, *3*, 69.
9. Vlieghe, P.; Lisowski, V.; Martinez, J.; Khrestchatisky, M. Synthetic therapeutic peptides: science and market. *Drug discovery today* **2010**, *15*, 40–56.
10. Marsault, E.; Peterson, M.L. Macrocycles are great cycles: applications, opportunities, and challenges of synthetic macrocycles in drug discovery. *Journal of medicinal chemistry* **2011**, *54*, 1961–2004.
11. Martí-Centelles, V.; Pandey, M.D.; Burguete, M.I.; Luis, S.V. Macrocyclization Reactions: The Importance of Conformational, Configurational, and Template-Induced Preorganization. *Chemical reviews* **2015**, *115*, 8736–8834.
12. Lau, Y.H.; Andrade, P. de; Wu, Y.; Spring, D.R. Peptide stapling techniques based on different macrocyclisation chemistries. *Chemical Society reviews* **2015**, *44*, 91–102.
13. Li, H.; Aneja, R.; Chaiken, I. Click chemistry in peptide-based drug design. *Molecules* **2013**, *18*, 9797–9817.

14. White, C.J.; Yudin, A.K. Contemporary strategies for peptide macrocyclization. *Nature chemistry* **2011**, *3*, 509–524.
15. Avrutina, O.; Empting, M.; Fabritz, S.; Daneschdar, M.; Frauendorf, H.; Diederichsen, U.; Kolmar, H. Application of copper(I) catalyzed azide-alkyne 3+2 cycloaddition to the synthesis of template-assembled multivalent peptide conjugates. *Organic & biomolecular chemistry* **2009**, *7*, 4177–4185.
16. Empting, M.; Avrutina, O.; Meusinger, R.; Fabritz, S.; Reinwarth, M.; Biesalski, M.; Voigt, S.; Buntkowsky, G.; Kolmar, H. "Triazole bridge": disulfide-bond replacement by ruthenium-catalyzed formation of 1,5-disubstituted 1,2,3-triazoles. *Angewandte Chemie* **2011**, *50*, 5207–5211.
17. Tischler, M.; Nasu, D.; Empting, M.; Schmelz, S.; Heinz, D.W.; Rottmann, P.; Kolmar, H.; Buntkowsky, G.; Tietze, D.; Avrutina, O. Braces for the peptide backbone: insights into structure-activity relationships of protease inhibitor mimics with locked amide conformations. *Angewandte Chemie* **2012**, *51*, 3708–3712.
18. Pasini, D. The click reaction as an efficient tool for the construction of macrocyclic structures. *Molecules* **2013**, *18*, 9512–9530.
19. Hüsecken, K.; Negri, M.; Fruth, M.; Boettcher, S.; Hartmann, R.W.; Hauptenthal, J. Peptide-based investigation of the *Escherichia coli* RNA polymerase $\sigma(70)$:core interface as target site. *ACS chemical biology* **2013**, *8*, 758–766.
20. Ma, C.; Yang, X.; Kandemir, H.; Mielczarek, M.; Johnston, E.B.; Griffith, R.; Kumar, N.; Lewis, P.J. Inhibitors of bacterial transcription initiation complex formation. *ACS chemical biology* **2013**, *8*, 1972–1980.
21. Murakami, K.S. X-ray crystal structure of *Escherichia coli* RNA polymerase $\sigma 70$ holoenzyme. *J Biol Chem.* **2013**, 9126–9134.
22. Okamoto, T.; Zobel, K.; Fedorova, A.; Quan, C.; Yang, H.; Fairbrother, W.J.; Huang, D.C.S.; Smith, B.J.; Deshayes, K.; Czabotar, P.E. Stabilizing the pro-apoptotic BimBH3 helix (BimSAHB) does not necessarily enhance affinity or biological activity. *ACS chemical biology* **2013**, *8*, 297–302.
23. Fittler, H.; Avrutina, O.; Glotzbach, B.; Empting, M.; Kolmar, H. Combinatorial tuning of peptidic drug candidates: high-affinity matriptase inhibitors through incremental structure-guided optimization. *Organic & biomolecular chemistry* **2013**, *11*, 1848–1857.
24. El-Mowafi, S.A.; Sineva, E.; Alumasa, J.N.; Nicoloff, H.; Tomsho, J.W.; Ades, S.E.; Keiler, K.C. Identification of inhibitors of a bacterial sigma factor using a new high-throughput screening assay. *Antimicrobial agents and chemotherapy* **2015**, *59*, 193–205.

4. Conclusion and Outlook

The general objective of this thesis is to exploit the rational synthesis and design of novel anti-infectives stemming from diverse starting points and of broad molecular weight range, favorably with a low chance of resistance development. Each drug class was optimized to overcome one or more hurdles interconnected with cellular penetration into bacteria, target topology, and pharmacology.

Compounds discussed in this chapter will be designated by a letter indicating the corresponding manuscript and the Arabic number used in its respective chapter i.e. A1 indicates compound 1 from publication A.

4.1 Small organic molecule (PqsR)

In subchapter 3.1, the main was to investigate structural requirements for functional interconversion and how this translates into pyocyanin inhibition. The testing of the synthesized compounds series in heterologous *E. coli* assay revealed four pharmacological profiles namely, agonist, inverse agonist, antagonist and biphasic modulators. The different pharmacological profiles were found to be controlled by subtle modifications at C-3 of the quinolone scaffold. A structure-functionality relationship was deduced where the presence of hydrogen bond donors, hydrogen bond acceptors, and hydrophobic substituents would yield an inverse agonist, an agonist, and an antagonist, respectively.

E. coli was used as an initial screening step to allow investigation of agonistic and antagonistic activities independent of the pqs system in PA. In addition, due to the higher rates of efflux and metabolism as well as lower membrane permeability that would impede deriving a clear analysis of structure-functionality relationship for the compounds. Thus, these results needed to be validated in PA as well. The top compounds from each class were tested in PA and yielded the same profiles even for the peculiar biphasic compound excluding it as an assay artifact and acting as a validation of our *E. coli* assay. The hypothesis for such behavior has been laid however, an experimental investigation is still missing.

Next, the top compounds were subjected to molecular modeling and docking. The observed computational model corroborated our biological results while identifying key amino acids for interaction with substituent at position 3 for each class of PqsR modulators class. The model

was also able to explain the importance of the 6-NO₂ group for the interaction of the compounds. Yet, it appears that position 3 plays a bigger role in deciding drug modality.

Top compounds from each class were tested for pyocyanin inhibition where it was found that only inverse agonists were able to significantly reduce virulence factor pyocyanin. This was explained by the presence of constitutive basal activity in PqsR in a similar fashion to some GPCRs. Thus, it is not sufficient to only block the effect of the agonist to the receptor to the un-liganded level but the reduction of the receptor activity below basal as well.

Altogether, we are confident this study displayed the utility of ligand-based originating compounds in studying receptors' functional behavior. As well as, it provided novel insights that should be taken into consideration in the future rational design of PqsR inverse agonists. From a drug discovery perspective, this study revealed that pharmacological profile might be of more importance than the absolute IC₅₀ values. Additionally, compound **A27** displayed improved physicochemical attributes, metabolic stability, and toxicity profile (unpublished data), thus, rendering it a possible candidate for future *in vivo* studies.

4.2 Peptide-Small organic molecule conjugates (PqsD)

This study (subchapter 3.2) intended to improve intracellular penetration of *in vitro* active PqsD inhibitor. For achieving that two recently published CPP sequences were linked covalently to a PqsD inhibitor *via* a 3,6-dioxaoctanoic acid linker. Out of the two peptides, conjugate **B25** retained some of the activity on PqsD *in vitro*. However, no activity was observed upon testing in the cell-based setting. From the *in vitro* activity, it can be deduced that the linker and linkage point has been properly chosen.

Regarding the lack of cellular activity further experimentation is required as it could be due to any of the following reasons:

1. The drug is internalized but is rapidly metabolized in the cell. This could be assessed by monitoring metabolic stability in the cell lysate.
2. Blocking the *N*-terminus of the peptide and the lengthy linker abolish the peptide's cell penetrating ability.
3. The free compound as well as the conjugate are efflux pumps substrates and are rapidly expelled outside of the cell. This hypothesis could be tested by concurrent

application of compound and/or conjugate with efflux pump inhibitors, or by using bacterial mutants with attenuated efflux abilities.

Nevertheless, the results of this study shouldn't undermine the utility of compound-CPP conjugates as tools for gaining cellular penetration for drugs lacking activity in the cell as many examples reported the successful application of this approach (section 1.3.2).

4.3 Peptides (RNAP)

The third and last subchapter of this thesis handled the optimization of another class of molecules i.e. peptides. The first step (Alanine-scan) together with the previously published crystal structure, helped identify residues that are most likely solvent exposed. Thus, these residues are assumed to be inconsequential for binding. Next, the four identified spots were successfully exchanged with unnatural amino acids bearing alkyne and azide moieties. A click-chemistry reaction was performed forming a triazole motif, achieving sidechain-to-sidechain macrocyclization. On the one hand, the macrocyclization did result in improved conformational stability and increase of α -helical content which was confirmed experimentally. On the other hand, in contrast to previous reports, this constraint did not translate into improved biological activities. The most likely reason for such discrepancy is that a more conformationally flexible peptide might be required for induced-fit binding as both proteins undergo pronounced changes required for DNA unwinding and RNA synthesis. Due to the unexpected lack of *in vitro* activity, we couldn't further test if the macrocyclization can lead to improved cellular permeability into *E. coli*. Future optimization by means of other macrocyclization motifs and lengthier linkers can produce different results. If such methodology still does not provide beneficial, based on the Ala-scan results exchange of certain residues to positively charged amino acids to convert **C1** into a cell penetrating peptide can be attempted.

The ongoing increase in drug discovery campaigns failure rates urges searching for innovative ideas for novel drugs in underexplored territories. Some indications have been affected by this innovation gap more than others e.g. anti-infectives research. One of the reasons for that was the increased reliance on high-throughput screening campaigns instead of rational drug design. These libraries lacked chemical diversity and were not honed for parameters such as

bacterial cell wall penetration. This thesis aimed to demonstrate the utility of rationally optimizing compounds from a wide drug space spectrum to address different target's needs.

5. References

1. Samanen, J. Similarities and differences in the discovery and use of biopharmaceuticals and small-molecule chemotherapeutics. *Introduction to Biological and Small Molecule Drug Research and Development* **2013**, 161–203.
2. Carton, J.M.; Strohl, W.R. Protein therapeutics (introduction to biopharmaceuticals). *Introduction to Biological and Small Molecule Drug Research and Development* **2013**, 127–159.
3. Smith, A.J. New horizons in therapeutic antibody discovery: opportunities and challenges versus small-molecule therapeutics. *Journal of biomolecular screening* **2015**, *20*, 437–453.
4. Wan, H. An Overall Comparison of Small Molecules and Large Biologics in ADME Testing. *ADMET DMPK* **2016**, *4*, 1.
5. Hughes, J.P.; Rees, S.; Kalindjian, S.B.; Philpott, K.L. Principles of early drug discovery. *British journal of pharmacology* **2011**, *162*, 1239–1249.
6. Thomas Nogrady, Donald F. Weaver. Medicinal Chemistry: A Molecular and Biochemical Approach **2005**, 67–103.
7. Hong, C.W.; Zeng, Q. Tapping the treasure of intracellular oncotargets with immunotherapy. *FEBS letters* **2014**, *588*, 350–355.
8. Guo, K.; Li, J.; Ping Tang, J.; Bobby Tan, C.P.; Wang, H.; Zeng, Q. Monoclonal antibodies target intracellular PRL phosphatases to inhibit cancer metastases in mice. *Cancer Biology & Therapy* **2008**, *7*, 750–757.
9. Ferrone, S. Hidden Immunotherapy Targets Challenge Dogma. *Science Translational Medicine* **2011**, *3*, 99ps38.
10. Malhotra, V. Unconventional protein secretion: an evolving mechanism. *EMBO J* **2013**, *32*, 1660.
11. Gashaw, I.; Ellinghaus, P.; Sommer, A.; Asadullah, K. What makes a good drug target? *Drug discovery today* **2011**, *16*, 1037–1043.

12. Arkin, M.R.; Tang, Y.; Wells, J.A. Small-molecule inhibitors of protein-protein interactions: progressing toward the reality. *Chemistry & biology* **2014**, *21*, 1102–1114.
13. Matsson, P.; Kihlberg, J. How Big Is Too Big for Cell Permeability? *Journal of medicinal chemistry* **2017**, *60*, 1662–1664.
14. Yang, N.J.; Hinner, M.J. Getting across the cell membrane: an overview for small molecules, peptides, and proteins. *Methods in molecular biology* **2015**, *1266*, 29–53.
15. Lipinski, C.A.; Lombardo, F.; Dominy, B.W.; Feeney, P.J. Experimental and computational approaches to estimate solubility and permeability in drug discovery and development settings. *Advanced drug delivery reviews* **2001**, *46*, 3–26.
16. Matsson, P.; Doak, B.C.; Over, B.; Kihlberg, J. Cell permeability beyond the rule of 5. *Advanced drug delivery reviews* **2016**, *101*, 42–61.
17. Doak, B.C.; Over, B.; Giordanetto, F.; Kihlberg, J. Oral druggable space beyond the rule of 5: insights from drugs and clinical candidates. *Chemistry & biology* **2014**, *21*, 1115–1142.
18. Pye, C.R.; Hewitt, W.M.; Schwochert, J.; Haddad, T.D.; Townsend, C.E.; Etienne, L.; Lao, Y.; Limberakis, C.; Furukawa, A.; Mathiowetz, A.M.; *et al.* Nonclassical Size Dependence of Permeation Defines Bounds for Passive Adsorption of Large Drug Molecules. *Journal of medicinal chemistry* **2017**, *60*, 1665–1672.
19. Over, B.; McCarren, P.; Artursson, P.; Foley, M.; Giordanetto, F.; Grönberg, G.; Hilgendorf, C.; Lee, M.D.; Matsson, P.; Muncipinto, G.; *et al.* Impact of stereospecific intramolecular hydrogen bonding on cell permeability and physicochemical properties. *Journal of medicinal chemistry* **2014**, *57*, 2746–2754.
20. Lewis, K. Platforms for antibiotic discovery. *Nature reviews. Drug discovery* **2013**, *12*, 371–387.
21. Richter, M.F.; Drown, B.S.; Riley, A.P.; Garcia, A.; Shirai, T.; Svec, R.L.; Hergenrother, P.J. Predictive compound accumulation rules yield a broad-spectrum antibiotic. *Nature* **2017**, *545*, 299–304.
22. Brown, D.G.; May-Dracka, T.L.; Gagnon, M.M.; Tommasi, R. Trends and exceptions of physical properties on antibacterial activity for Gram-positive and Gram-negative pathogens. *Journal of medicinal chemistry* **2014**, *57*, 10144–10161.

23. O'Shea, R.; Moser, H.E. Physicochemical properties of antibacterial compounds: implications for drug discovery. *Journal of medicinal chemistry* **2008**, *51*, 2871–2878.
24. Frantz, M.-C.; Wipf, P. Mitochondria as a target in treatment. *Environmental and molecular mutagenesis* **2010**, *51*, 462–475.
25. Verdine, G.L.; Hilinski, G.J. Stapled peptides for intracellular drug targets. *Methods in enzymology* **2012**, *503*, 3–33.
26. Bird, G.H.; Crannell, W.C.; Walensky, L.D. Chemical synthesis of hydrocarbon-stapled peptides for protein interaction research and therapeutic targeting. *Current protocols in chemical biology* **2011**, *3*, 99–117.
27. Chatterjee, J.; Gilon, C.; Hoffman, A.; Kessler, H. N-methylation of peptides: a new perspective in medicinal chemistry. *Accounts of chemical research* **2008**, *41*, 1331–1342.
28. Pelay-Gimeno, M.; Glas, A.; Koch, O.; Grossmann, T.N. Structure-Based Design of Inhibitors of Protein-Protein Interactions: Mimicking Peptide Binding Epitopes. *Angewandte Chemie* **2015**, *54*, 8896–8927.
29. Yin, L.M.; Edwards, M.A.; Li, J.; Yip, C.M.; Deber, C.M. Roles of hydrophobicity and charge distribution of cationic antimicrobial peptides in peptide-membrane interactions. *The Journal of biological chemistry* **2012**, *287*, 7738–7745.
30. Shental-Bechor, D.; Haliloglu, T.; Ben-Tal, N. Interactions of cationic-hydrophobic peptides with lipid bilayers: a Monte Carlo simulation method. *Biophysical journal* **2007**, *93*, 1858–1871.
31. Piantavigna, S.; McCubbin, G.A.; Boehnke, S.; Graham, B.; Spiccia, L.; Martin, L.L. A mechanistic investigation of cell-penetrating Tat peptides with supported lipid membranes. *Biochimica et biophysica acta* **2011**, *1808*, 1811–1817.
32. Singh, J.; Joshi, S.; Mumtaz, S.; Maurya, N.; Ghosh, I.; Khanna, S.; Natarajan, V.T.; Mukhopadhyay, K. Enhanced Cationic Charge is a Key Factor in Promoting Staphylocidal Activity of α -Melanocyte Stimulating Hormone via Selective Lipid Affinity. *Scientific reports* **2016**, *6*, 31492.
33. Temsamani, J.; Vidal, P. The use of cell-penetrating peptides for drug delivery. *Drug discovery today* **2004**, *9*, 1012–1019.

34. Ferrari, M.; Onuoha, S.C.; Pitzalis, C. Trojan horses and guided missiles: targeted therapies in the war on arthritis. *Nature reviews. Rheumatology* **2015**, *11*, 328–337.
35. Koren, E.; Torchilin, V.P. Cell-penetrating peptides: breaking through to the other side. *Trends in molecular medicine* **2012**, *18*, 385–393.
36. Lindberg, S.; Copolovici, D.M.; Langel, Ü. Therapeutic delivery opportunities, obstacles and applications for cell-penetrating peptides. *Therapeutic Delivery* **2011**, *2*, 71–82.
37. Lu, J.; Jiang, F.; Lu, A.; Zhang, G. Linkers Having a Crucial Role in Antibody-Drug Conjugates. *International journal of molecular sciences* **2016**, *17*, 561.
38. Sugawara, M.; Huang, W.; Fei, Y.; Leibach, F.H.; Ganapathy, V.; Ganapathy, M.E. Transport of Valganciclovir, a Ganciclovir Prodrug, via Peptide Transporters PEPT1 and PEPT2. *Journal of Pharmaceutical Sciences* **2000**, *89*, 781–789.
39. Torchilin, V.P. Cell penetrating peptide-modified pharmaceutical nanocarriers for intracellular drug and gene delivery. *Biopolymers* **2008**, *90*, 604–610.
40. Ryser, H.J.; Shen, W.C. Conjugation of methotrexate to poly (L-lysine) as a potential way to overcome drug resistance. *Cancer* **1980**, *45*, 1207–1211.
41. Mazel, M.; Clair, P.; Rousselle, C.; Vidal, P.; Scherrmann, J.-M.; Mathieu, D.; Tamsamani, J. Doxorubicin-peptide conjugates overcome multidrug resistance. *Anti-Cancer Drugs* **2001**, *12*, 107–116.
42. Montigiani, S.; Müller, R.; Kontermann, R.E. Inhibition of cell proliferation and induction of apoptosis by novel tetravalent peptides inhibiting DNA binding of E2F. *Oncogene* **2003**, *22*, 4943–4952.
43. Rizk, S.S.; Misiura, A.; Paduch, M.; Kossiakoff, A.A. Substance P derivatives as versatile tools for specific delivery of various types of biomolecular cargo. *Bioconjugate chemistry* **2012**, *23*, 42–46.
44. Lawrence, M.S.; Phillips, K.J.; Liu, D.R. Supercharging proteins can impart unusual resilience. *Journal of the American Chemical Society* **2007**, *129*, 10110–10112.

45. Cronican, J.J.; Thompson, D.B.; Beier, K.T.; McNaughton, B.R.; Cepko, C.L.; Liu, D.R. Potent delivery of functional proteins into Mammalian cells in vitro and in vivo using a supercharged protein. *ACS chemical biology* **2010**, *5*, 747–752.
46. *The Coming Cost of Superbugs: 10 Million Deaths Per Year*. Available online: <https://www.wired.com/2014/12/oneill-rpt-amr/> (accessed on 31 August, 2017).
47. Kamal, Ahmed A. M.; Maurer, C.K.; Allegretta, G.; Haupenthal, J.; Empting, M.; Hartmann, R.W. Quorum Sensing Inhibitors as Pathoblockers for *Pseudomonas aeruginosa* Infections: A New Concept in Anti-Infective Drug Discovery. *Topics in Medicinal Chemistry* **2017**, 1–26.
48. Lu, C.; Kirsch, B.; Zimmer, C.; Jong, J.C. de; Henn, C.; Maurer, C.K.; Müsken, M.; Häussler, S.; Steinbach, A.; Hartmann, R.W. Discovery of antagonists of PqsR, a key player in 2-alkyl-4-quinolone-dependent quorum sensing in *Pseudomonas aeruginosa*. *Chemistry & biology* **2012**, *19*, 381–390.
49. Lu, C.; Maurer, C.K.; Kirsch, B.; Steinbach, A.; Hartmann, R.W. Overcoming the unexpected functional inversion of a PqsR antagonist in *Pseudomonas aeruginosa*: an in vivo potent antivirulence agent targeting pqs quorum sensing. *Angewandte Chemie* **2014**, *53*, 1109–1112.
50. Lu, C.; Kirsch, B.; Maurer, C.K.; Jong, J.C. de; Braunshausen, A.; Steinbach, A.; Hartmann, R.W. Optimization of anti-virulence PqsR antagonists regarding aqueous solubility and biological properties resulting in new insights in structure-activity relationships. *European journal of medicinal chemistry* **2014**, *79*, 173–183.
51. Weidel, E.; Jong, J.C. de; Brengel, C.; Storz, M.P.; Braunshausen, A.; Negri, M.; Plaza, A.; Steinbach, A.; Müller, R.; Hartmann, R.W. Structure optimization of 2-benzamidobenzoic acids as PqsD inhibitors for *Pseudomonas aeruginosa* infections and elucidation of binding mode by SPR, STD NMR, and molecular docking. *Journal of medicinal chemistry* **2013**, *56*, 6146–6155.
52. Hüsecken, K.; Negri, M.; Fruth, M.; Boettcher, S.; Hartmann, R.W.; Haupenthal, J. Peptide-based investigation of the *Escherichia coli* RNA polymerase $\sigma(70)$:core interface as target site. *ACS chemical biology* **2013**, *8*, 758–766.

6. Appendix

6.1 Supporting information chapter A

Supporting Information
for
Structure-functionality relationship and pharmacological profiles of
***Pseudomonas aeruginosa* alkylquinolone quorum sensing**
modulators

Ahmed A.M. Kamal^a, Lucia Petrera^a, Jens Eberhard^a, Rolf W. Hartmann^{a,b}

Author information:

^{a)} Helmholtz-Institute for Pharmaceutical Research Saarland, Department for Drug Design and Optimization, Campus E8.1, 66123 Saarbrücken, Germany

^{b)} Department of Pharmacy, Pharmaceutical and Medicinal Chemistry, Saarland University, Campus C2.3, 66123 Saarbrücken, Germany.

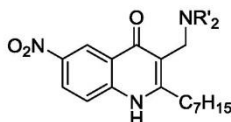
To whom correspondence should be addressed: Rolf W. Hartmann, Helmholtz Institute for Pharmaceutical Research Saarland, Department for Drug Design and Optimization, Campus E8.1, 66123 Saarbrücken, Germany, E-Mail: rolf.hartmann@helmholtz-hzi.de
Tel.: +49 681 98806-2000. Fax: +49 681 98806-2009

Contents

1. General experimental information – Chemistry.....	3
General procedure (A) for synthesis of 3-((dialkylamino)methyl)-2-heptyl-6-nitroquinolin-4(1H)-one via Mannich reaction:	3
General procedure (B) for synthesis of 3-halo-2-heptyl or 2-(hexylthio)--6-nitroquinolin-4(1H)-one.....	5
General procedure (C) for synthesis of 2-heptyl-N,N-dialkyl-6-nitro-4-oxo-1,4-dihydroquinoline-3-carboxamide:	8
Synthesis of ethyl (2-heptyl-3-iodo-6-nitroquinolin-4-yl) carbonate (28):.....	10
Synthesis of intermediate compound ethyl (2-heptyl-6-nitro-3-((trimethylsilyl)ethynyl)quinolin-4-yl) carbonate (12a):.....	11
Synthesis of 3-ethynyl-2-heptyl-6-nitroquinolin-4(1H)-one (12):.....	11
Synthesis of analogs 19 and 23-25 and their intermediates	12
General Procedure (D) for methyl or ethyl (E/Z)-2-((hexylthio)((4-nitrophenyl)amino)methylene)-3-butanoates:	12
General procedure (E) for synthesis of 3-substituted-2-(hexylthio)-6-nitroquinolin-4(1H)-one....	16
Synthesis of compound 2-(hexylthio)-6-nitro-1H-benzof[d]imidazole (20):.....	18
Synthesis of compound ethyl 2-(hexylthio)-6-nitro-4-oxo-1,4-dihydroquinoline-3-carboxylate (25):	18
Synthesis of compound 2-(hexylthio)-3-(hydroxymethyl)-6-nitroquinolin-4(1H)-one (26):	19
Synthesis of compound 2-(hexylthio)-6-nitro-4-oxo-1,4-dihydroquinoline-3-carboxylic acid (22):	20
2. General experimental information – Biology.....	21
2.1 Chemicals, bacterial strains, and media	21
2.2 <i>E. coli</i> reporter gene assay: dose-response curves	21
2.3 <i>P. aeruginosa</i> reporter-gene assay: dose-response curves.....	24
2.4 Effects on pyocyanin in <i>P. aeruginosa</i>	26
3. Additional tables and graphs	26
Table 1. C _p K _a and percentage of ionization for ionizable substituents at position 3.....	26
4. Graphical representation of ¹ H and ¹³ C spectra of compounds.....	27

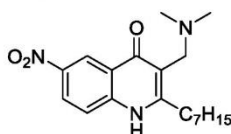
1. General experimental information – Chemistry

General procedure (A) for synthesis of 3-((dialkylamino)methyl)-2-heptyl-6-nitroquinolin-4(1H)-one *via* Mannich reaction:



In a round-bottom flask 2-heptyl-6-nitroquinolin-4(1H)-one (3) in EtOH was dissolved, then formaldehyde solution (37% in water) and the secondary amine were added and stirred at reflux for 48 hours. The volatile components of the reaction solution were then removed *in vacuo* and the mixture was extracted with ethyl acetate/water three times. The combined organic fractions were dried over Na₂SO₄ and dried *in vacuo*. The product was purified *via* preparative RP-HPLC or flash chromatography.

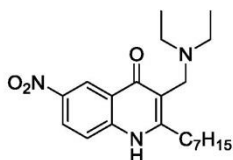
Synthesis of 3-((dimethylamino)methyl)-2-heptyl-6-nitroquinolin-4(1H)-one (9):



Compound **9** was synthesized according to the general procedure (A) from 2-heptyl-6-nitroquinolin-4(1H)-one (0.52 mmol, 150 mg), formaldehyde sol. (5.20 mmol, 192 μ L), dimethylamine 2 M in THF (10.4 mmol, 5.2 mL), and 10 mL of EtOH. The crude product was purified *via* preparative HPLC to give 3-((dimethylamino)methyl)-2-heptyl-6-nitroquinolin-4(1H)-one (62 mg, 0.18 mmol, 34% yield) as an orange resin. ¹H NMR (500 MHz, DMSO-*d*₆) δ 12.57 (s, 1H), 9.06 (s, 1H), 8.85 (d, *J* = 2.7 Hz, 1H), 8.50 (dd, *J* = 9.1, 2.7 Hz, 1H), 7.84 (d, *J* = 9.2 Hz, 1H), 4.26 (d, *J* = 5.5 Hz, 2H), 2.88 – 2.82 (m, 2H), 2.79 (d, *J* = 4.9 Hz, 6H), 1.68 – 1.58 (m, 2H),

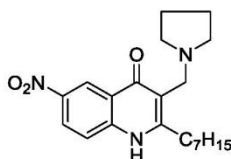
1.45 – 1.21 (m, 9H), 0.92 – 0.80 (m, 3H); ^{13}C NMR (126 MHz, $\text{DMSO-}d_6$) δ 176.4, 156.5, 143.3, 143.1, 126.6, 122.2, 121.2, 120.2, 109.7, 52.5, 42.2, 31.1, 31.1, 29.2, 28.7, 28.5, 22.0, 13.9. MS (ESI⁺): m/z 346.18 (M+H)⁺. HRMS calcd. (%) for $\text{C}_{19}\text{H}_{28}\text{N}_3\text{O}_3$ ⁺: 346.21252; found: 346.21228.

Synthesis of 3-((diethylamino)methyl)-2-heptyl-6-nitroquinolin-4(1H)-one (10):



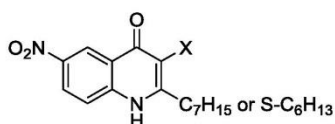
Compound **10** was synthesized according to the general procedure (A) from 2-heptyl-6-nitroquinolin-4(1H)-one (0.50 mmol, 144 mg), formaldehyde sol. (8 mmol, 294 μL), diethylamine (16 mmol, 1.16 g), and 10 mL of EtOH. The crude product was purified *via* flash chromatography using a gradient system of $\text{CHCl}_3/\text{MeOH}$ (0 \rightarrow 9% with 1 vol% of trimethylamine) and finally recrystallized from a mix of ethanol and water. The obtained solid was isolated by filtration and dried under vacuum to give 3-((diethylamino)methyl)-2-heptyl-6-nitroquinolin-4(1H)-one (79 mg, 0.21 mmol, 42% yield) as an orange resin. ^1H NMR (500 MHz, $\text{DMSO-}d_6$) δ 8.84 (d, $J = 2.7$ Hz, 1H), 8.39 (dd, $J = 9.1, 2.7$ Hz, 1H), 8.19 (s, 1H), 7.74 (d, $J = 9.2$ Hz, 1H), 3.71 (s, 2H), 2.83 – 2.77 (m, 2H), 2.61 (q, $J = 7.1$ Hz, 4H), 1.74 – 1.65 (m, 2H), 1.43 – 1.36 (m, 2H), 1.34 – 1.25 (m, 6H), 1.05 (t, $J = 7.1$ Hz, 6H), 0.89 – 0.82 (m, 3H); ^{13}C NMR (126 MHz, $\text{DMSO-}d_6$) δ 175.9, 163.4, 142.3, 125.4, 122.0, 46.2, 44.0, 31.3, 31.1, 29.1, 29.0, 28.4, 22.0, 13.9, 11.2. MS (ESI⁺): m/z 374.16 (M+H)⁺ HRMS calcd. (%) for $\text{C}_{21}\text{H}_{32}\text{N}_3\text{O}_3$ ⁺: 374.24382; found: 374.24408.

Synthesis of 2-heptyl-6-nitro-3-(pyrrolidin-1-ylmethyl)quinolin-4(1H)-one (11):



Compound **11** was synthesized according to the general procedure (A) from 2-heptyl-6-nitroquinolin-4(1H)-one (0.37 mmol, 107 mg), formaldehyde sol. (5.20 mmol, 192 μ L pyrrolidine (14.8 mmol, 1.31 mL) dissolved in 20 mL of EtOH. The crude product was purified *via* preparative HPLC to give 2-heptyl-6-nitro-3-(pyrrolidin-1-ylmethyl)quinolin-4(1H)-one (25 mg, 0.067 mmol, 18% yield) as an orange resin. ^1H NMR (500 MHz, MeOD- d_4) δ 9.10 (d, J = 2.5 Hz, 1H), 8.50 (dd, J = 9.2, 2.6 Hz, 1H), 7.76 (d, J = 9.2 Hz, 1H), 4.29 (s, 2H), 2.98 – 2.87 (m, 2H), 2.07 (s, 4H), 1.75 (dt, J = 15.7, 7.8 Hz, 2H), 1.54 – 1.38 (m, 4H), 1.37 – 1.29 (m, 2H), 0.92 (t, J = 6.9 Hz, 3H); ^{13}C NMR (126 MHz, MeOD- d_4) δ 179.2, 169.7, 157.9, 145.4, 144.7, 127.9, 124.1, 122.9, 120.9, 55.1, 52.2, 33.0, 32.9, 31.0, 30.6, 30.2, 24.1, 23.7, 14.4. MS (ESI $^+$): m/z 372.06 (M+H) $^+$. HRMS calcd. (%) for C $_{21}$ H $_{30}$ N $_3$ O $_3$ $^+$: 372.22817; found: 372.22836.

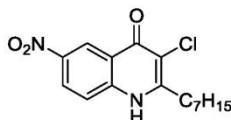
General procedure (B) for synthesis of 3-halo-2-heptyl or 2-(hexylthio)-6-nitroquinolin-4(1H)-ones



In a round-bottom flask intermediate **3** or **20** (2 mmol) was added and 1.1 eq. of the corresponding *N*-halosuccinamide (2.2 mmol) in 7.5 mLs of dry DMF under a N $_2$ atmosphere and left stirring overnight at room temperature. The reaction mixture was poured into water and then extracted three times with EtOAc (3 \times 15 mL). The combined organic fractions were dried over Na $_2$ SO $_4$ and dried *in vacuo*. The crude product was purified *via* flash chromatography using

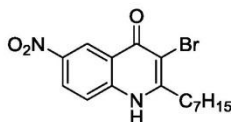
the binary system of $\text{CHCl}_3/\text{MeOH}$ (0→5%). In some cases preparative HPLC was used instead.

Synthesis of 3-chloro-2-heptyl-6-nitroquinolin-4(1H)-one (13):



Compound **13** was synthesized according to the general procedure (B) from 2-heptyl-6-nitroquinolin-4(1H)-one (50 mg, 0.17 mmol), *N*-chlorosuccinimide (35 mg, 0.19 mmol). The crude product was purified *via* preparative HPLC to give 3-chloro-2-heptyl-6-nitroquinolin-4(1H)-one (33 mg, 0.1 mmol, 55% yield) as yellow solid. ^1H NMR (500 MHz, $\text{DMSO}-d_6$) δ 12.54 (s, 1H), 8.84 (d, $J=2.7$ Hz, 1H), 8.44 (dd, $J=9.2, 2.7$ Hz, 1H), 7.76 (d, $J=9.2$ Hz, 1H), 2.90 – 2.82 (m, 2H), 1.75 – 1.66 (m, 2H), 1.42 – 1.21 (m, 8H), 0.89 – 0.82 (m, 3H). ^{13}C NMR (126 MHz, Acetone- d_6) δ 171.8, 152.7, 143.4, 126.7, 124.0, 123.2, 120.6, 116.8, 33.6, 32.4, 28.5, 23.2, 14.3. MS (ESI+): m/z 323.04 ($\text{M}+\text{H}$) $^+$. HRMS calcd. (%) for $\text{C}_{16}\text{H}_{20}\text{ClN}_2\text{O}_3$: 323.11570; found: 323.11600.

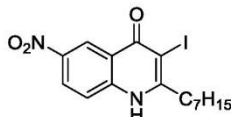
Synthesis of 3-bromo-2-heptyl-6-nitroquinolin-4(1H)-one (14):



Compound **14** was synthesized according to the general procedure (B) from 2-heptyl-6-nitroquinolin-4(1H)-one (100 mg, 0.35 mmol), *N*-bromosuccinimide (68 mg, 0.38 mmol). The crude product was purified *via* preparative HPLC to give 3-bromo-2-heptyl-6-nitroquinolin-4(1H)-one (79 mg, 0.2 mmol, 57% yield) as brown solid. ^1H NMR (300 MHz, $\text{DMSO}-d_6$) δ 12.55 (s, 1H), 8.84 (d, $J=2.6$ Hz, 1H), 8.44 (dd, $J=9.2, 2.7$ Hz, 1H), 7.76 (d, $J=9.2$ Hz, 1H), 2.89 (dd, $J=$

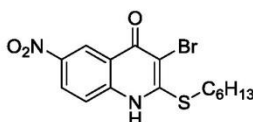
9.2, 6.6 Hz, 2H), 1.71 (p, $J=7.2$ Hz, 2H), 1.48 – 1.19 (m, 8H), 0.93 – 0.80 (m, 3H). ^{13}C NMR (75 MHz, $\text{DMSO-}d_6$) δ 171.5, 154.1, 143.5, 142.8, 126.6, 122.5, 122.2, 120.4, 107.7, 35.2, 31.6, 29.1, 28.8, 28.0, 22.5, 14.4. MS (ESI+): m/z 367.00 ($\text{M}+\text{H}$) $^+$. HRMS calcd. (%) for $\text{C}_{16}\text{H}_{20}\text{BrN}_2\text{O}_3$: 367.06518; found: 367.06537.

Synthesis of 3-iodo-2-heptyl-6-nitroquinolin-4(1H)-one (15):



Compound **15** was synthesized according to the general procedure (B) from 2-heptyl-6-nitroquinolin-4(1H)-one (680 mg, 2.4 mmol), *N*-iodosuccinimide (594 mg, 2.64 mmol). The crude product was purified *via* preparative HPLC to give 3-iodo-2-heptyl-6-nitroquinolin-4(1H)-one (680 mg, 1.64 mmol, 68% yield) as brown solid. ^1H NMR (500 MHz, $\text{DMSO-}d_6$) δ 12.54 (s, 1H), 8.82 (d, $J=2.7$ Hz, 1H), 8.44 (dd, $J=9.1, 2.7$ Hz, 1H), 7.75 (d, $J=9.2$ Hz, 1H), 2.99 – 2.90 (m, 2H), 1.69 (p, $J=7.4$ Hz, 2H), 1.41 (p, $J=7.0$ Hz, 2H), 1.36 – 1.26 (m, 6H), 0.90 – 0.83 (m, 3H). ^{13}C NMR (126 MHz, $\text{DMSO-}d_6$) δ 173.0, 156.2, 143.1, 142.7, 126.2, 122.3, 119.8, 119.5, 87.5, 31.1, 28.7, 28.3, 27.8, 22.1, 14.0. MS (ESI+): m/z 415.08 ($\text{M}+\text{H}$) $^+$. HRMS calcd. (%) for $\text{C}_{16}\text{H}_{20}\text{IN}_2\text{O}_3$: 415.05131; found: 415.05161.

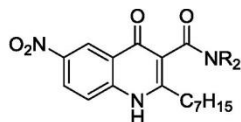
Synthesis of 3-bromo-2-(hexylthio)-6-nitroquinolin-4(1H)-one (21):



Compound **21** was synthesized according to the general procedure (B) from 2-(hexylthio)-6-nitroquinolin-4(1H)-one (102 mg, 0.3 mmol), *N*-bromosuccinimide (59 mg, 0.33 mmol). The crude product was purified *via* preparative HPLC to give 3-bromo-2-heptyl-6-nitroquinolin-4(1H)-

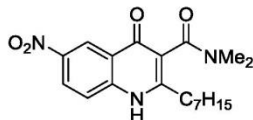
one (101 mg, 0.26 mmol, 87% yield) as brown solid. IR (cm⁻¹) 3315, 2950, 2834, 1020. ¹H NMR (500 MHz, DMSO-*d*₆) δ 8.90 (s, 1H), 8.38 (ddd, *J* = 9.2, 4.5, 2.6 Hz, 1H), 7.90 (dd, *J* = 9.2, 3.2 Hz, 1H), 1.67 (p, *J* = 7.3 Hz, 2H), 1.43 (t, *J* = 7.4 Hz, 2H), 1.27 (dt, *J* = 12.6, 6.1 Hz, 4H), 0.87 – 0.81 (m, 3H). ¹³C NMR experiments were performed using Bruker Avance AV 300 or a Bruker DRX 500 at ambient as well as higher temperatures (100 °C). ¹³C NMR (126 MHz, CDCl₃) δ 143.0, 143.0, 124.9, 120.6, 30.2, 28.3, 28.2, 27.2, 21.4, 13.2. MS (ESI+): *m/z* 384.97 (M+H)⁺. HRMS calcd. (%) for C₁₅H₁₈BrN₂O₃S⁺: 385.02160; found: 385.02153.

General procedure (C) for synthesis of 2-heptyl-N,N-dialkyl-6-nitro-4-oxo-1,4-dihydroquinoline-3-carboxamides:



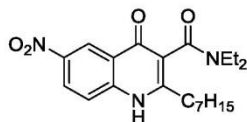
In a round-bottom flask 2-heptyl-6-nitro-4-oxo-1,4-dihydroquinoline-3-carboxylic acid **6** (0.50 mmol, 165 mg) was suspended with HOBt (2.50 mmol, 338 mg) and EDC (2.50 mmol, 388 mg) in anhydrous THF (9 mL) and anhydrous DMF (2 mL) under nitrogen atmosphere. The reaction mixture was left to stir for 1 hr at room temperature. Afterward, the secondary amine (1.25 mmol, 2.5 eq.) was added and the reaction left to stir overnight at room temperature. The reaction solution was evaporated to dryness *in vacuo*, uptaken in ethyl acetate/water and extracted three times. The combined organic fractions were dried over Na₂SO₄, filtered by gravity and the solvent removed *via* rotary evaporation *in vacuo*. The crude product was purified *via* preparative HPLC.

Synthesis of 2-heptyl-*N,N*-dimethyl-6-nitro-4-oxo-1,4-dihydroquinoline-3-carboxamide (17):



Compound **17** was synthesized according to the general procedure (C) from 2-heptyl-6-nitro-4-oxo-1,4-dihydroquinoline-3-carboxylic acid **6** (0.50 mmol, 165 mg). The crude product was purified via preparative HPLC to give *N,N*-dimethyl-2-heptyl-6-nitro-4-oxo-1,4-dihydroquinoline-3-carboxamide (85 mg, 0.24 mmol, 47% yield) as yellow solid. ^1H NMR (500 MHz, $\text{DMSO-}d_6$) δ 0.81 - 0.89 (m, 3 H) 1.22 - 1.34 (m, 8 H) 1.57 - 1.74 (m, 2 H) 2.36 - 2.48 (m, 1 H) 2.70 (ddd, $J = 13.4, 10.0, 6.2$ Hz, 1 H), 2.84 (s, 3 H) 2.98 (s, 3 H) 7.76 (d, $J = 9.1$ Hz, 1 H) 8.43 (dd, $J = 9.1, 2.5$ Hz, 1 H) 8.81 (d, $J = 2.8$ Hz, 1 H); ^{13}C NMR (126 MHz, $\text{DMSO-}d_6$) δ 172.9, 166.1, 143.2, 152.5, 142.7, 126.1, 123.2, 121.6, 119.9, 119.1, 109.5, 37.2, 34.1, 31.7, 31.0, 28.7, 28.2, 22.0, 13.9. MS (ESI+): m/z 360.15 (M+H) $^+$. HRMS calcd. (%) for $\text{C}_{19}\text{H}_{18}\text{N}_3\text{O}_4$: 360.19178; found: 360.19186.

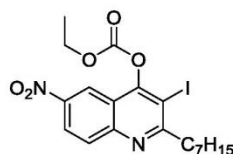
Synthesis of *N,N*-diethyl-2-heptyl-6-nitro-4-oxo-1,4-dihydroquinoline-3-carboxamide (18):



Compound **18** was synthesized according to the general procedure (C) from 2-heptyl-6-nitro-4-oxo-1,4-dihydroquinoline-3-carboxylic acid (**6**) (0.50 mmol, 165 mg). The crude product was purified via preparative HPLC to give *N,N*-diethyl-2-heptyl-6-nitro-4-oxo-1,4-dihydroquinoline-3-carboxamide (51 mg, 0.14 mmol, 27% yield) as yellow solid. ^1H NMR (500 MHz, $\text{DMSO-}d_6$) δ 12.22 (s, 1H), 8.81 (d, $J = 2.7$ Hz, 1H), 8.43 (dd, $J = 9.2, 2.7$ Hz, 1H), 7.75 (d, $J = 9.2$ Hz, 1H), 3.62 (dq, $J = 14.0, 7.1$ Hz, 1H), 3.25 - 3.09 (m, 3H), 2.64 (ddd, $J = 13.4, 10.7, 5.4$ Hz, 1H), 2.48

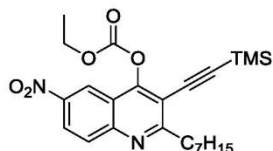
– 2.41 (m, 1H), 1.66 (ddt, $J = 38.1, 11.9, 6.0$ Hz, 2H), 1.35 – 1.30 (m, 2H), 1.28 – 1.22 (m, 6H), 1.13 (t, $J = 7.0$ Hz, 3H), 1.03 (t, $J = 7.1$ Hz, 3H), 0.87 – 0.84 (m, 3H). ^{13}C NMR (126 MHz, $\text{DMSO-}d_6$) δ 173.1, 165.2, 151.9, 143.2, 142.6, 126.1, 123.2, 121.6, 119.9, 119.3, 42.5, 38.2, 31.8, 31.0, 28.9, 28.3, 28.2, 22.0, 14.1, 13.9, 12.6. MS (ESI+): m/z 388.17 (M+H) $^+$. HRMS calcd. (%) for $\text{C}_{21}\text{H}_{30}\text{N}_3\text{O}_4$: 388.22308; found: 388.22336.

Synthesis of ethyl (2-heptyl-3-iodo-6-nitroquinolin-4-yl) carbonate (28):



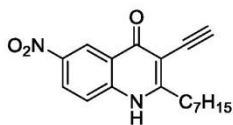
In a round-bottom flask compound (**15**) 3-iodo-2-heptyl-6-nitroquinolin-4(1H)-one (650 mg, 1.57 mmol), potassium tert-butoxide (224 mg, 1.25 mmol) were stirred for 1 h at room temperature in anhydrous THF. Afterwards, ethylchloroformate (165 μL , 1.1 mmol) was added. After 4 h, reaction was quenched with 5 mL of H_2O then evaporated *in vacuo*. Afterwards, 10 mL of H_2O was added and extracted with EtOAc (3 \times 25 mL), the combined organic fractions were dried over Na_2SO_4 and dried *in vacuo*. The crude compound was purified *via* flash chromatography with a gradient of hexane/EtOAc (0 \rightarrow 12.5%) to yield the desired compound as yellow solid (680 mg, 89% yield). ^1H NMR (500 MHz, $\text{DMSO-}d_6$) δ 8.72 (d, $J = 2.5$ Hz, 1H), 8.48 (dd, $J = 9.2, 2.6$ Hz, 1H), 8.21 (d, $J = 9.2$ Hz, 1H), 4.41 (q, $J = 7.1$ Hz, 2H), 3.22 – 3.12 (m, 2H), 1.76 (p, $J = 7.4$ Hz, 2H), 1.42 – 1.26 (m, 11H), 0.89 – 0.82 (m, 3H). ^{13}C NMR (126 MHz, $\text{DMSO-}d_6$) δ 168.2, 156.2, 150.5, 149.4, 145.6, 130.7, 124.3, 120.1, 118.1, 94.3, 66.4, 41.8, 31.2, 28.7, 28.5, 28.1, 22.1, 14.1. MS (ESI+): m/z 486.46 (M+H) $^+$. HRMS calcd. (%) for $\text{C}_{19}\text{H}_{24}\text{IN}_2\text{O}_5$: 487.07244; found: 487.07306.

Synthesis of intermediate compound ethyl (2-heptyl-6-nitro-3-((trimethylsilyl)ethynyl)quinolin-4-yl) carbonate (12a):



Compound **(28)** ethyl-(2-heptyl-3-iodo-6-nitroquinolin-4-yl)-carbonate (680 mg, 1.4 mmol), copper(I) iodide (27 mg, 0.1 mol-%), and bis(triphenylphosphine)palladium(II) dichloride (50 mg, 0.05 mol-%) were added together into a 3 necked round-bottom flask. Afterward, the reaction vessel was evacuated then backfilled with Argon for three times. Under Argon atmosphere, dry DMF (4 mL) and dry triethylamine (380 μ L, 2.73 mmol), Ethynyltrimethylsilane (579 μ L, 4.1 mmol) were added. The brown reaction mixture was left to stir at room temperature overnight. TLC showed the disappearance of compound **16**. Thus, the reaction was stopped and the volatiles of the solution removed *in vacuo*. The crude product was used in the next step without further purification.

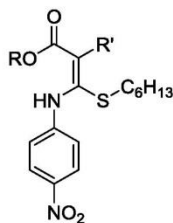
Synthesis of 3-ethynyl-2-heptyl-6-nitroquinolin-4(1H)-one (12):



Crude intermediate **(12a)** was dissolved in aq. 5 N KOH (5 mL) and EtOH (10 mL) at room temperature and left stirring overnight. The reaction solution was neutralized with acetic acid then extracted with EtOAc (3 \times 25 mL). The combined organic fractions were dried over Na₂SO₄ filtered and all volatile materials were removed *in vacuo*. The crude compound was purified *via* preparative HPLC to yield the desired compound as yellow solid (148 mg, 38% yield (for 2 steps)). ¹H NMR (500 MHz, Acetone-*d*₆) δ 8.99 (d, *J*= 2.7 Hz, 1H), 8.41 (dd, *J*= 9.0, 2.7 Hz, 1H),

7.79 (d, $J=9.1$ Hz, 1H), 3.86 (s, 1H), 3.00 – 2.95 (m, 3H), 1.84 (p, $J=7.6$ Hz, 2H), 1.47 – 1.27 (m, 10H), 0.88 – 0.84 (m, 3H). ^{13}C NMR (126 MHz, Acetone- d_6) δ 176.2, 159.8, 144.4, 143.7, 126.8, 124.4, 122.9, 120.8, 105.9, 86.0, 78.4, 34.4, 32.4, 30.2, 29.2, 23.3, 14.3. MS (ESI+): m/z 313.12 (M+H) $^+$. HRMS calcd. (%) for $\text{C}_{18}\text{H}_{21}\text{N}_2\text{O}_3$: 313.15467; found: 313.15488.

Synthesis of analogs 19 and 23-25 and their ketene-S/N-acetal intermediates

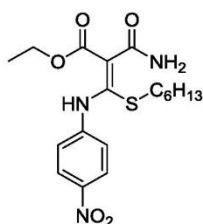


General Procedure (D) for methyl or ethyl (E/Z)-2-((hexylthio)((4-nitrophenyl)amino)methylene)-3-butanoates:

In a three-neck round-bottom flask, NaH (460 mg, 12 mmol, 60% dispersion in mineral oil) was dispersed into 50 mL of dry DMF. Afterward, the corresponding pos. 2-substituted acetates (10 mmol) were added portionwise with vigorous stirring with some effervescence being observed. After 30 min., 1-isothiocyanato-4-nitrobenzene (10 mmol) dissolved in 10 mL of DMF was added dropwise over 30 min. The color of the reaction mixture usually changed from transparent to yellow or dark red and left to stir at room temperature overnight. Last, 1-iodohexane (10 mmol) was added dropwise and left stirring for an additional 4 h at room temperature. It was observed that the reaction solution would become more transparent with the progression of time. The reaction solution was concentrated *in vacuo*, then extracted with EtOAc (3 \times 50 mL), the combined organic fractions were dried over Na_2SO_4 , filtered by gravity and all volatile materials removed *in vacuo*. The crude compound was purified *via* flash chromatography with a binary

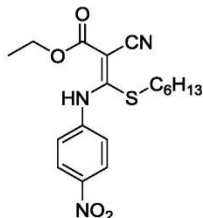
gradient system consisting of Hexane/EtOAc (0→33%) to yield the desired compounds as yellow to orange oils in yields between (39% and 79%). Depending on functional groups, the compounds were obtained as a isomere mixture (E/Z and tautomers) but directly used for cyclization. It's worth mentioning that no mass spectra could be obtained for these class of compounds due their ease of fragmentation using both single quad ESI and the high-resolution Orbitrap.

Synthesis of intermediate ethyl (E/Z)-2-carbamoyl-3-(hexylthio)-3-((4-nitrophenyl)amino)acrylate (19a):



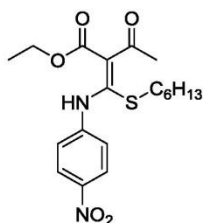
Compound **19a** was synthesized according to the general procedure (D) from ethyl 3-amino-3-oxopropanoate (983 mg, 7.50 mmol), NaH (290 mg, 7.50 mmol, 60% dispersion in oil), 1-isothiocyanato-4-nitrobenzene (1.35g, 7.50 mmol) and 1-iodohexane (1.43 mL, 7.50 mmol). The crude product was purified *via* flash chromatography using a gradient of hexane/EtOAc (0→10%) to give ethyl-(E/Z)-2-carbamoyl-3-(hexylthio)-3-((4-nitrophenyl)amino)acrylate (1.43 g, 3.6 mmol, 48% yield) as yellow oil. ¹H NMR (500 MHz, Chloroform-d) δ 8.22 – 8.15 (m, 2H), 7.41 – 7.35 (m, 1H), 6.93 – 6.85 (m, 1H), 4.22 – 4.09 (m, 2H), 3.37 (s, 1H), 3.04 (t, *J*= 7.4 Hz, 1H), 2.81 (t, *J*= 7.4 Hz, 1H), 1.67 (p, *J*= 7.5 Hz, 2H), 1.44 – 1.21 (m, 9H), 0.93 – 0.83 (m, 3H). ¹³C NMR (126 MHz, Chloroform-d) δ 169.0, 167.3, 159.2, 156.2, 145.6, 144.1, 144.3, 125.2, 121.6, 120.5, 88.4, 61.9, 59.8, 32.5, 31.4, 31.3, 28.7, 28.1, 22.6, 22.6, 14.6, 14.1.

Synthesis of intermediate ethyl (E/Z)-2-cyano-3-(hexylthio)-3-((4-nitrophenyl)amino)acrylate (23a):



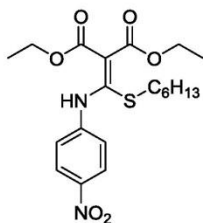
Compound **23a** was synthesized according to the general procedure (D) from ethyl 2-cyanoacetate (1.5 mL, 15 mmol), NaH (720 mg, 18 mmol, 60% dispersion in oil), 1-isothiocyanato-4-nitrobenzene (2.7g, 15 mmol) and 1-iodohexane (2.2 mL, 15 mmol). The crude product was purified via flash chromatography using a gradient hexane/EtOAc (0→10%) to yield ethyl-(E/Z)-2-cyano-3-(hexylthio)-3-((4-nitrophenyl)amino)acrylate (1.43 g, 3.6 mmol, 48% yield) as yellow oil. ^1H NMR (300 MHz, Chloroform-d) δ 11.66 (s, 1H), 8.33 – 8.21 (m, 2H), 7.56 – 7.44 (m, 2H), 4.29 (q, J = 7.1 Hz, 2H), 2.80 – 2.68 (m, 2H), 1.65 – 1.45 (m, 2H), 1.36 (t, J = 7.1 Hz, 3H), 1.35 – 1.10 (m, 6H), 0.96 – 0.78 (m, 3H). ^{13}C NMR (126 MHz, Chloroform-d) δ 167.5, 167.4, 145.5, 143.7, 125.2, 124.1, 116.7, 82.7, 77.4, 62.0, 60.5, 35.1, 31.2, 29.3, 28.2, 22.5, 14.4, 14.0.

Synthesis of intermediate ethyl (E/Z)-2-((hexylthio)((4-nitrophenyl)amino)methylene)-3-oxobutanoate (24a):



Compound **24a** was synthesized according to the general procedure (D) from ethyl 3-oxobutanoate (1.3g, 10 mmol), NaH (460 mg, 10 mmol, 60% dispersion in oil), 1-isothiocyanato-4-nitrobenzene (1.8g, 10 mmol) and 1-iodohexane (1.47 mL, 10 mmol). The crude product was purified *via* flash chromatography using a gradient Hexane/EtOAc (0→25%) to give ethyl-(E/Z)-2-((hexylthio)((4-nitrophenyl)amino)methylene)-3-oxobutanoate (3.1 g, 7.85 mmol, 79% yield) as yellow oil. ¹H NMR (300 MHz, Chloroform-d) δ 12.73 (s, 1H), 8.26 – 8.07 (m, 2H), 6.85 (dd, *J*= 28.3, 8.7 Hz, 2H), 4.37 – 4.08 (m, 2H), 3.05 (d, *J*= 8.4 Hz, 2H), 2.28 (s, 1H), 2.04 (s, 2H), 1.69 (q, *J*= 7.5 Hz, 2H), 1.51 – 1.24 (m, 9H), 0.88 (td, *J*= 4.8, 2.0 Hz, 3H). ¹³C NMR (126 MHz, Chloroform-d) δ 175.4, 169.5, 165.5, 156.7, 143.8, 125.0, 125.0, 120.3, 120.1, 61.5, 61.3, 33.9, 31.3, 31.2, 29.0, 28.5, 22.5, 20.1, 14.2, 14.1, 14.0.

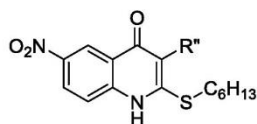
Synthesis of intermediate diethyl 2-((hexylthio)((4-nitrophenyl)amino)methylene)malonate (25a):



Compound **25a** was synthesized according to the general procedure (D) from diethyl malonate (1.15 mL, 7.5 mmol), NaH (290 mg, 7.5 mmol, 60% dispersion in oil), 1-isothiocyanato-4-nitrobenzene (1.35g, 7.5 mmol) and 1-iodohexane (1.43 mL, 7.5 mmol). The crude product was purified *via* flash chromatography using a gradient hexane/EtOAc (0→10%) to give diethyl-2-((hexylthio)((4-nitrophenyl)amino)methylene)malonate (1.24 g, 2.92 mmol, 39% yield) as an orange oil. ¹H NMR (300 MHz, Chloroform-d) δ 10.59 (s, 1H), 8.26 – 8.16 (m, 2H), 7.58 – 7.46 (m, 1H), 6.92 – 6.84 (m, 1H), 4.39 – 4.10 (m, 4H), 3.18 (s, 1H), 3.08 – 2.93 (m, 0H), 2.50 – 2.34 (m, 1H), 1.52 – 1.07 (m, 12H), 0.97 – 0.60 (m, 3H). ¹³C NMR (126 MHz, DMSO-*d*₆) δ 166.5,

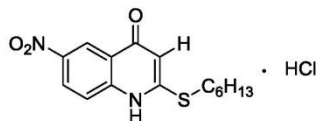
156.8, 152.8, 148.4, 141.0, 125.2, 124.8, 121.4, 120.0, 117.6, 73.7, 70.4, 61.9, 60.8, 60.5, 41.2, 32.0, 31.7, 30.5, 29.1, 27.2, 21.8, 18.8, 13.9, 13.8, 13.7.

General procedure (E) for synthesis of 3-substituted-2-(hexylthio)-6-nitroquinolin-4(1H)-ones



In a three-neck round-bottom flask equipped with a thermometer and a dean stark apparatus, the corresponding intermediates were added dropwise on 25 mL of refluxing Dowtherm™ over 30 min. After completion of addition, the reaction mixture was allowed to reflux for another 30 min. The reaction was let to cool down to room temperature and then poured on ice cold diethyl ether saturated with HCl to give the corresponding HCl salt. The precipitate was then filtered and washed with hexane (50 mL) and diethyl ether (50 mL) unless stated otherwise.

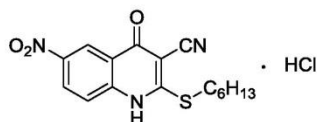
Synthesis of compound 2-(hexylthio)-6-nitroquinolin-4(1H)-one hydrochloride (19):



Compound **19** was synthesized according to the general procedure (E) from ethyl-(E)-2-carbamoyl-3-(hexylthio)-3-((4-nitrophenyl)amino)acrylate (**19a**). The desired compound was yielded as brown solid (990 mg, 2.88 mmol, 80% yield). ¹H NMR (300 MHz, DMSO-*d*₆) δ 12.04 (s, 1H), 8.76 (d, *J*= 2.7 Hz, 1H), 8.41 (dd, *J*= 9.2, 2.7 Hz, 1H), 7.87 (d, *J*= 9.2 Hz, 1H), 6.57 (s, 1H), 3.20 (t, *J*= 7.3 Hz, 2H), 1.67 (ddd, *J*= 12.4, 8.3, 6.4 Hz, 2H), 1.49 – 1.34 (m, 2H), 1.26 (tdd, *J*= 7.9, 6.6, 5.4, 2.8 Hz, 4H), 0.91 – 0.80 (m, 3H). ¹³C NMR (75 MHz, DMSO) δ 170.7, 158.8, 145.9, 143.4, 143.4, 126.3, 122.0, 121.6, 121.1, 105.8, 100.0, 40.8, 40.5, 40.3, 40.0, 39.8, 39.7,

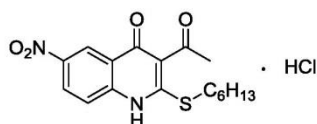
39.4, 39.1, 31.1, 31.1, 28.6, 28.3, 22.5, 14.3. MS (ESI+): m/z 307.10 (M+H)⁺. HRMS calcd. (%) for C₁₅H₁₉N₂O₃S⁺: 307.11109; found: 307.11115.

Synthesis of compound 2-(hexylthio)-6-nitro-4-oxo-1,4-dihydroquinoline-3-carbonitrile hydrochloride (23):



Compound **23** was synthesized according to the general procedure (E) ethyl-(E)-2-cyano-3-(hexylthio)-3-((4-nitrophenyl)amino)acrylate (**23a**). The desired compound was yielded as brown solid (1.28g, 3.47 mmol, 97% yield). IR (cm⁻¹) 2926, 2855, 2223, 1502, 1337. ¹H NMR (500 MHz, DMSO-*d*₆) δ 12.65 (s, 1H), 8.71 (d, *J* = 2.7 Hz, 1H), 8.50 (dd, *J* = 9.1, 2.8 Hz, 1H), 7.90 (d, *J* = 9.1 Hz, 1H), 3.41 (t, *J* = 7.3 Hz, 2H), 1.71 – 1.61 (m, 2H), 1.41 (dtdd, *J* = 9.1, 6.9, 4.6, 2.1 Hz, 2H), 1.27 (tt, *J* = 6.7, 5.9, 2.0 Hz, 4H), 0.90 – 0.79 (m, 3H). ¹³C NMR (126 MHz, DMSO-*d*₆) δ 172.8, 159.5, 143.8, 127.3, 123.1, 121.0, 115.1, 32.8, 30.6, 28.6, 27.5, 21.9, 13.8. MS (ESI+): m/z 332.11 (M+H)⁺. HRMS calcd. (%) for C₁₆H₁₈N₃O₃S⁺: 3032.10634; found: 332.10648.

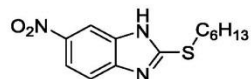
Synthesis of compound 3-acetyl-2-(hexylthio)-6-nitroquinolin-4(1H)-one hydrochloride (24):



Compound **24** was synthesized according to the general procedure (E) ethyl-(E)-2-((hexylthio)((4-nitrophenyl)amino)methylene)-3-oxobutanoate (**24a**). The desired compound was yielded as brown solid (1.1g, 2.9 mmol, 37% yield). ¹H NMR (500 MHz, DMSO-*d*₆) δ 11.74 (s, 1H), 8.78 (d, *J* = 2.7 Hz, 1H), 8.46 (dd, *J* = 9.1, 2.7 Hz, 1H), 7.92 (d, *J* = 9.2 Hz, 1H), 3.23 (t, *J* = 7.3 Hz, 2H), 2.49 (s, 3H), 1.57 (p, *J* = 7.4 Hz, 2H), 1.37 (dq, *J* = 14.3, 6.9, 6.0, 2.9 Hz, 2H), 1.25

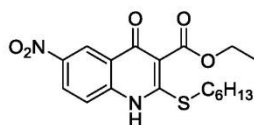
(ddd, $J = 7.3, 4.4, 2.7$ Hz, 4H), 0.87 – 0.80 (m, 3H). ^{13}C NMR (126 MHz, $\text{DMSO-}d_6$) δ 199.0, 173.2, 153.4, 143.3, 126.6, 124.2, 123.3, 121.4, 120.0, 56.0, 31.9, 31.3, 30.6, 28.2, 27.7, 21.9, 13.8. MS (ESI+): m/z 349.04 (M+H) $^+$. HRMS calcd. (%) for $\text{C}_{17}\text{H}_{21}\text{N}_2\text{O}_4\text{S}^+$: 349.12165; found: 349.12198.

Synthesis of compound 2-(hexylthio)-6-nitro-1H-benzo[d]imidazole (20):



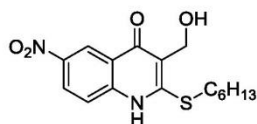
In a round-bottom flask, 6-nitro-1H-benzo[d]imidazole-2-thiol (195 mg, 1 mmol), potassium carbonate (152 mg, 1.1 mmol) and 1-iodohexane (156 μL , 1.1 mmol) was dissolved in acetone (7 mLs). The reaction mixture was left stirring at room temperature for 4 h and evaporated to dryness afterwards. The crude product was purified *via* flash chromatography using a gradient $\text{CHCl}_3/\text{MeOH}$ (0 \rightarrow 2.5%) to give 2-(hexylthio)-6-nitro-1H-benzo[d]imidazole (225 mg, 0.80 mmol, 80% yield) as a yellow oil. ^1H NMR (300 MHz, $\text{Acetone-}d_6$) δ 8.33 (d, $J = 2.3$ Hz, 1H), 8.09 (dd, $J = 8.8, 2.2$ Hz, 1H), 7.59 (d, $J = 8.8$ Hz, 1H), 3.39 (dd, $J = 7.7, 6.9$ Hz, 2H), 3.05 (s, 1H), 1.88 – 1.73 (m, 2H), 1.54 – 1.40 (m, 2H), 1.38 – 1.23 (m, 4H), 0.93 – 0.82 (m, 3H). ^{13}C NMR were performed using Bruker Avance AV 300 or a Bruker DRX 500. ^{13}C NMR (75 MHz, $\text{Acetone-}d_6$) δ 156.8, 142.9, 117.4, 112.0, 40.3, 31.4, 31.1, 29.0, 28.2, 22.3, 13.4. MS (ESI+): m/z 280.04 (M+H) $^+$. HRMS calcd. (%) for $\text{C}_{13}\text{H}_{18}\text{N}_3\text{O}_2\text{S}^+$: 280.11142; found: 280.11157.

Synthesis of compound ethyl 2-(hexylthio)-6-nitro-4-oxo-1,4-dihydroquinoline-3-carboxylate (25):



Compound **25** was synthesized according to the general procedure (E) diethyl-2-((hexylthio)((4-nitrophenyl)amino)methylene)malonate (**25a**). Upon standard work-up procedure, only a little amount of precipitate was obtained and later found to be compound **22** instead. Whereas, the desired compound was obtained *via* evaporation of the filtrate *in vacuo* followed by flash chromatography hexane/EtOAc gradient (0→50%). The desired compound was obtained as slightly yellow solid (500 mg, 1.32 mmol, 17% yield). ¹H NMR (500 MHz, DMSO-*d*₆) δ 8.83 (d, *J*= 2.8 Hz, 1H), 8.20 (dd, *J*= 9.1, 2.8 Hz, 1H), 7.56 (d, *J*= 9.2 Hz, 1H), 7.18 (s, 1H), 4.19 (q, *J*= 7.1 Hz, 2H), 3.15 (t, *J*= 7.3 Hz, 2H), 1.64 – 1.54 (m, 2H), 1.36 (tt, *J*= 8.8, 7.0 Hz, 2H), 1.28 – 1.23 (m, 7H), 0.88 – 0.78 (m, 3H). ¹³C NMR (126 MHz, DMSO-*d*₆) δ 171.3, 167.5, 150.6, 141.0, 125.8, 124.8, 123.8, 121.9, 59.9, 30.8, 30.1, 29.4, 28.0, 22.1, 14.2, 13.9. MS (ESI+): *m/z* 379.12 (M+H)⁺. HRMS calcd. (%) for C₁₈H₂₃N₂O₅S⁺: 379.13222; found: 379.13257.

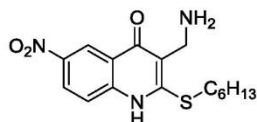
Synthesis of compound 2-(hexylthio)-3-(hydroxymethyl)-6-nitroquinolin-4(1H)-one (26):



In a two-neck round-bottom flask compound (**25**) ethyl 2-(hexylthio)-6-nitro-4-oxo-1,4-dihydroquinoline-3-carboxylate (242 mg, 0.64 mmol) was dissolved in 15 mL anhydrous THF. The reaction vessel was then cooled down to -78 °C, where DIBAL (1 M in hexane, 2.6 mmol) was added dropwise. The reaction mixture was then allowed to warm to room temperature and left to stir overnight. The reaction was monitored *via* TLC till the disappearance of starting material was complete. Any excess DIBAL was quenched with few milliliters of Rochelle salt solution. The reaction solution was then extracted with EtOAc (3× 25 mL). The combined org. phase was washed with Saturated NaHCO₃ (10 mLs), dried over Na₂SO₄, filtered and the volatiles was removed *in vacuo*. The *m/z* value of the desired compound was confirmed *via* MS

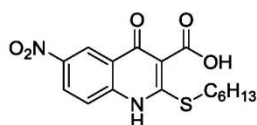
(ESI+) but couldn't be obtained as a pure compound after flash chromatography due to stability issues. MS (ESI+): m/z 337.11 (M+H)⁺.

Synthesis of compound 3-(aminomethyl)-2-(hexylthio)-6-nitroquinolin-4(1H)-one (27):



In a two neck round-bottom flask compound (25) 2-(hexylthio)-6-nitro-4-oxo-1,4-dihydroquinoline-3-carbonitrile hydrochloride (218 mg, 0.66 mmol) was dissolved in anhydrous THF (7 mLs). Borane.THF complex solution (1 mL, 1 mmol) was then added dropwise with effervescence being observed upon addition. After completion of the addition, the reaction mixture was allowed to reflux for 6 h. The reaction was then stopped, cooled to room temperature and 1 M HCl (10 mLs) was added. Afterwards, the reaction solution was evaporated to dryness *in vacuo*. The crude compound was purified *via* preparative HPLC to yield the desired compound as orange solid (42 mg, 0.13 mmol, 20% yield). IR (cm⁻¹) 2953, 2923, 2854, 1324, 1015. ¹H NMR (300 MHz, DMSO-*d*₆) δ 8.87 (d, J = 2.8 Hz, 1H), 8.20 – 7.97 (m, 3H), 7.49 (d, J = 9.2 Hz, 1H), 3.98 (s, 2H), 3.26 (t, J = 7.3 Hz, 2H), 1.67 (ddd, J = 14.8, 8.2, 6.5 Hz, 2H), 1.41 (q, J = 7.0, 6.5 Hz, 2H), 1.33 – 1.19 (m, 4H), 0.93 – 0.79 (m, 3H). ¹³C NMR (75 MHz, DMSO-*d*₆) δ 172.8, 163.1, 160.7, 152.4, 140.1, 127.5, 123.9, 122.3, 121.6, 108.4, 37.1, 30.8, 29.5, 29.0, 28.1, 22.0, 13.9. MS (ESI+): m/z 336.12 (M+H)⁺. HRMS calcd. (%) for C₁₆H₂₂N₃O₃S⁺: 336.13764; found: 336.13779.

Synthesis of compound 2-(hexylthio)-6-nitro-4-oxo-1,4-dihydroquinoline-3-carboxylic acid (22):



In a round-bottom flask compound (**25**) ethyl 2-(hexylthio)-6-nitro-4-oxo-1,4-dihydroquinoline-3-carboxylate (500 mg, 1.32 mmol) was dissolved in 25 mLs of 10% (w/v) NaOH and a few drops of EtOH. The reaction was allowed to reflux overnight. Afterward, the reaction was cooled to room temperature and extracted with EtOAc (3× 10 mL). The aqueous layer was acidified with conc. HCl in an ice bath. The color change from red to yellow and precipitate formation was observed. The aqueous solution was then extracted with EtOAc (3× 50 mL), the combined organic fractions were dried over Na₂SO₄, filtered and all volatile material removed *in vacuo*. The desired compound was obtained as yellow solid without further purification (420 mg, 1.2 mmol, 91% yield). IR (cm⁻¹) 3315 (broad), 2952, 2926, 2854, 1555, 1512, 1330. ¹H NMR (300 MHz, MeOD-*d*₄) δ 8.98 (d, *J*= 2.6 Hz, 1H), 8.37 – 8.27 (m, 1H), 7.73 (d, *J*= 9.1 Hz, 1H), 3.18 (t, *J*= 7.3 Hz, 2H), 1.71 (q, *J*= 7.2 Hz, 2H), 1.50 (p, *J*= 6.8 Hz, 2H), 1.35 (dq, *J*= 6.6, 3.5 Hz, 4H), 0.99 – 0.86 (m, 3H). ¹³C NMR (75 MHz, DMSO-*d*₆) δ 175.1, 172.0, 168.5, 141.8, 124.6, 121.8, 121.8, 121.5, 105.9, 39.5, 30.9, 29.6, 28.6, 28.4, 22.1, 13.9. MS (ESI-): *m/z* 348.96 (M-H)⁻. HRMS calcd. (%) for C₁₆H₁₉N₂O₅S⁺: 351.10092; found: 351.10141.

2. General experimental information – Biology

2.1 Chemicals, bacterial strains, and media

Yeast extract was obtained from Fluka, peptone and casein from Merck, Bacto™ Tryptone from BD Biosciences, and Gibco® PBS from Life Technologies. Salts and organic solvents of analytical grade were obtained from VWR.

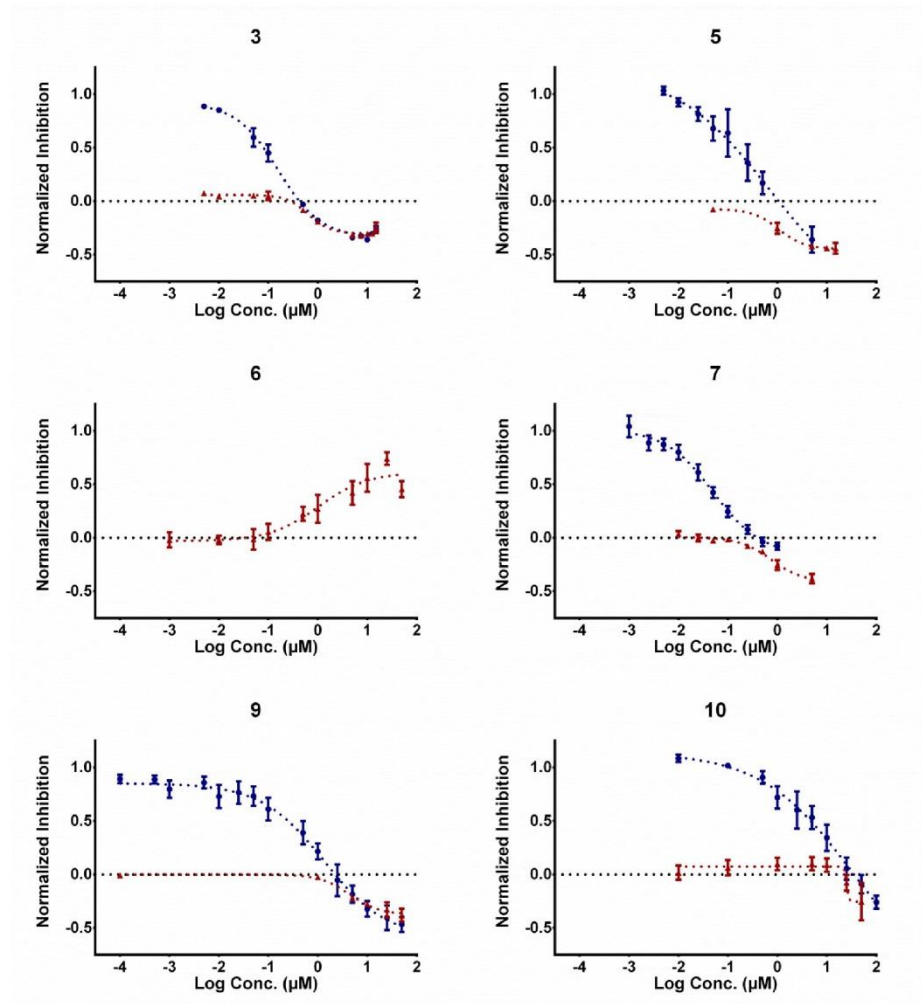
P. aeruginosa PA14 strain and isogenic *pqsR* knockout mutant were stored in glycerol stocks at -80 °C.

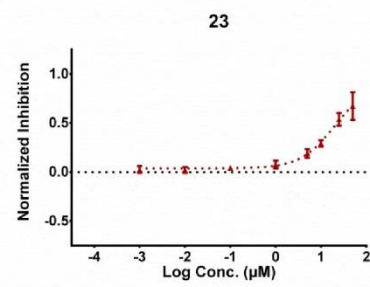
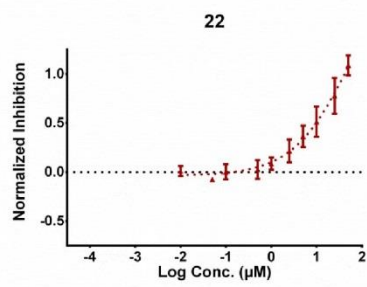
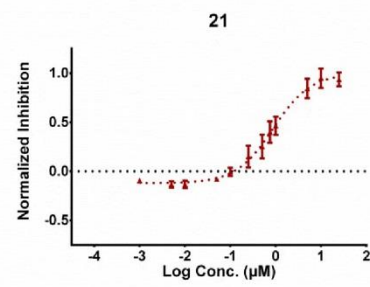
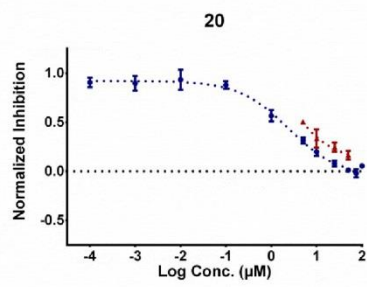
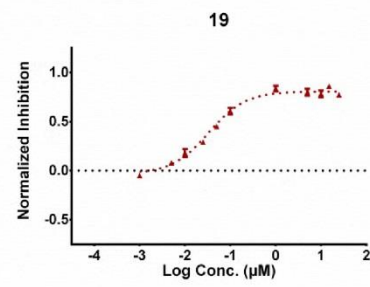
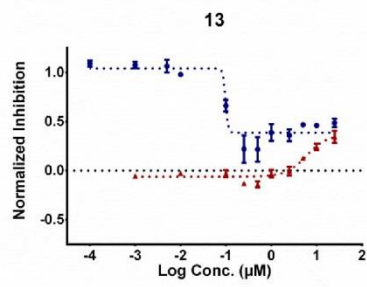
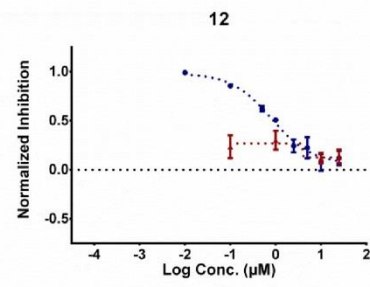
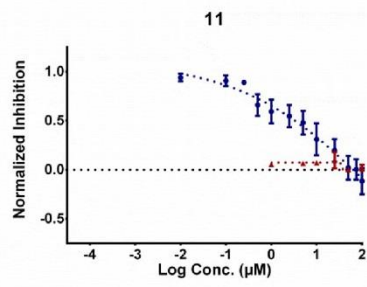
Minimal medium PPGAS3 and Luria-Bertani (LB) were used as bacterial growth media.

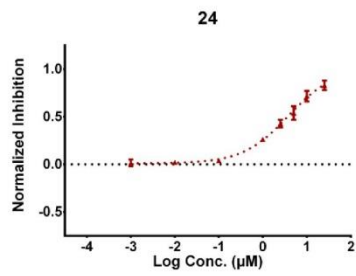
2.2 *E. coli* reporter gene assay: dose-response curves

Shown below are dose-response curves from *E. Coli* reporter gene assay in both experimental settings, namely agonistic (no PQS in red) and antagonistic settings (+50 nM PQS in blue).

Curves were plotted via GraphPad Prism. Error bars represent standard error of the mean of at least n = 2 trials.

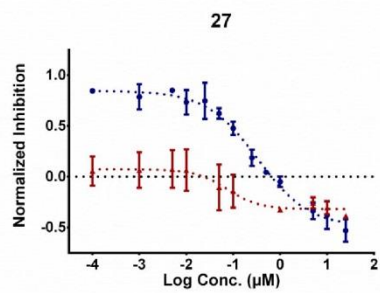
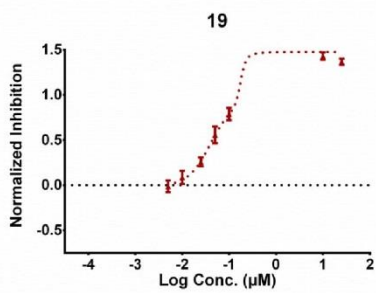
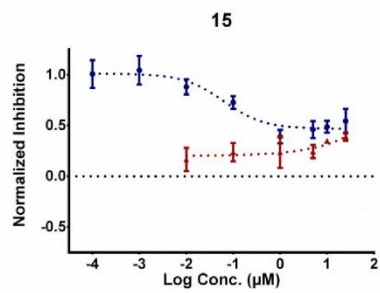
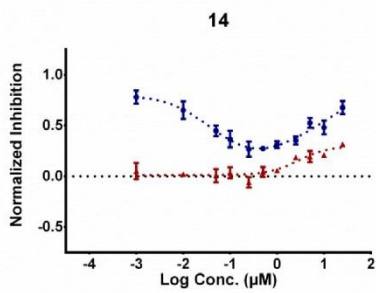
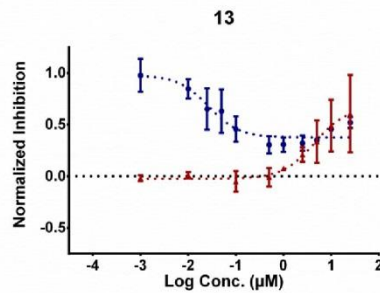
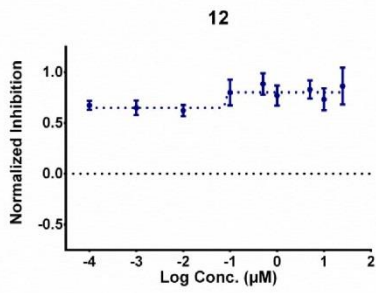
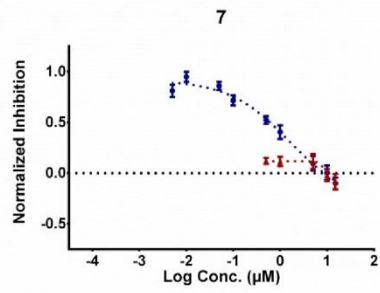
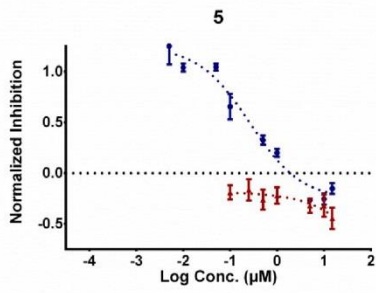






2.3 *P. aeruginosa* reporter-gene assay: dose-response curves

Shown below are dose-response curves from *P. aeruginosa* reporter gene assay in both experimental settings. Color scheme as for the *E. coli* experiment (*vide supra*), viz. agonistic (no PQS in red) and antagonistic settings (+50 nM PQS in blue). Software and statistics correspond to the settings of above.



2.4 Effects on pyocyanin in *P. aeruginosa*

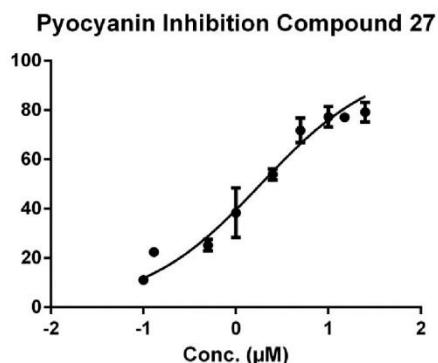


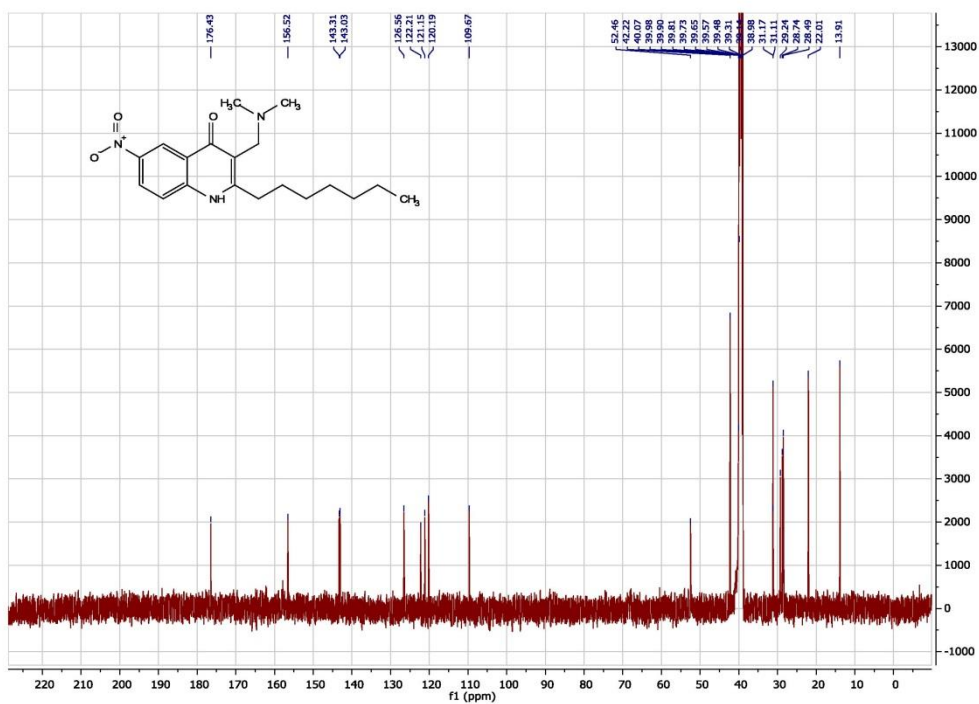
Figure S1. Inhibition of virulence factor pyocyanin was evaluated in the clinical isolate PA14. Representative dose-response curve of compound **27**. Black dots represent the reduction of pyocyanin in presence of a given compound concentration relative to DMSO control (which equals 0%). The continuous black line is the non-linear regression analysis to determine IC₅₀ values using a log (inhibitor) versus response model with constrains (bottom = 0%; top = 100%). Non-linear regression was performed with the aid of Graph Pad Prism 6.

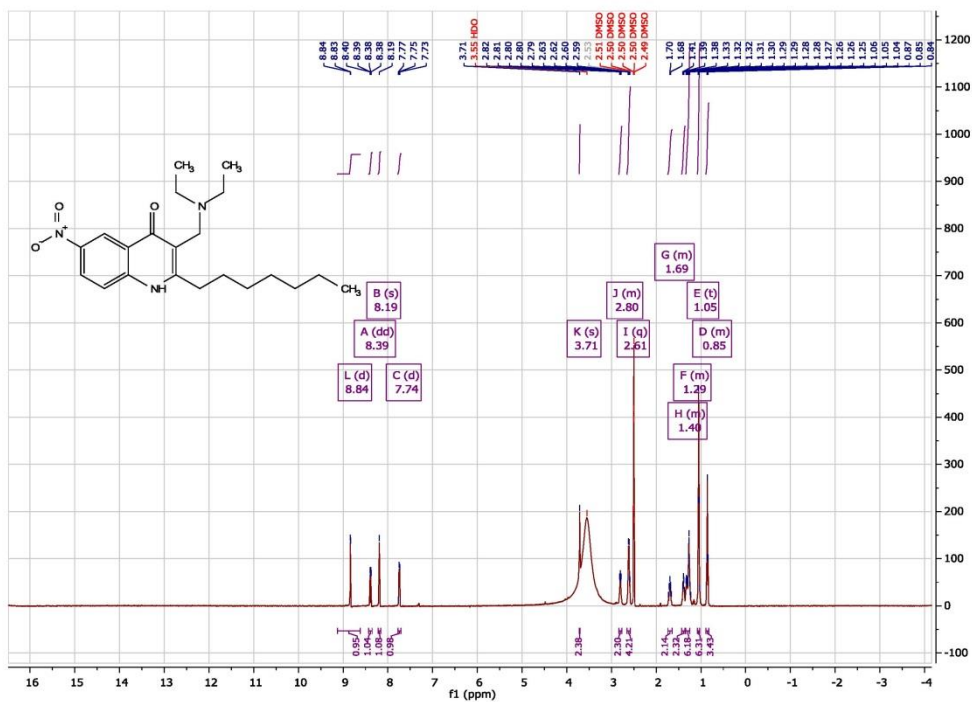
3. Additional tables and graphs

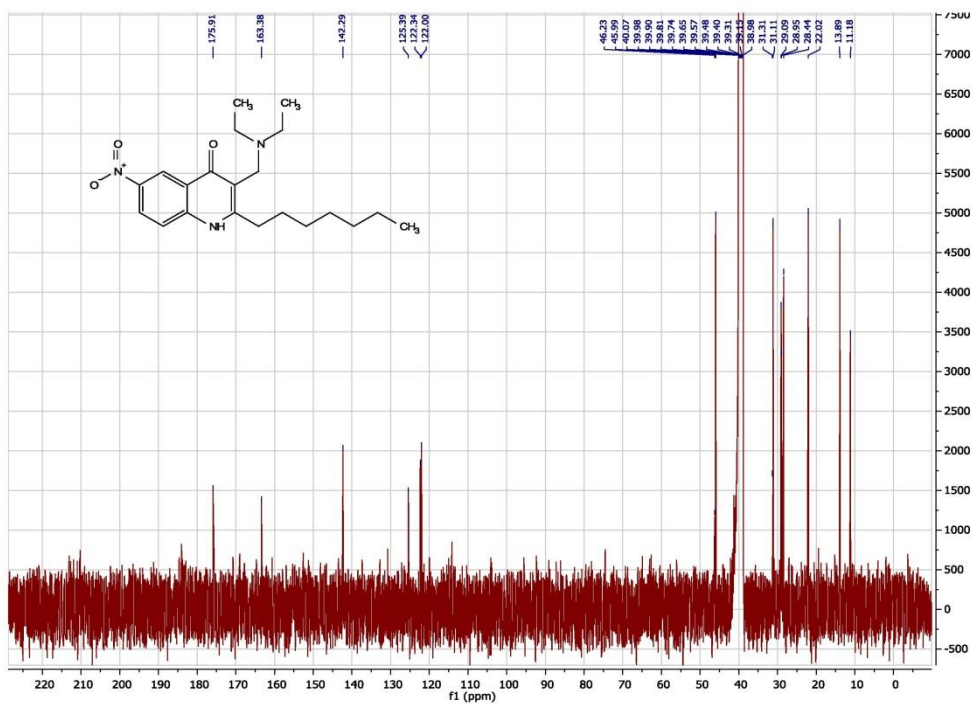
Table S1. CpK_a and percentage of ionization for ionizable substituents at position 3

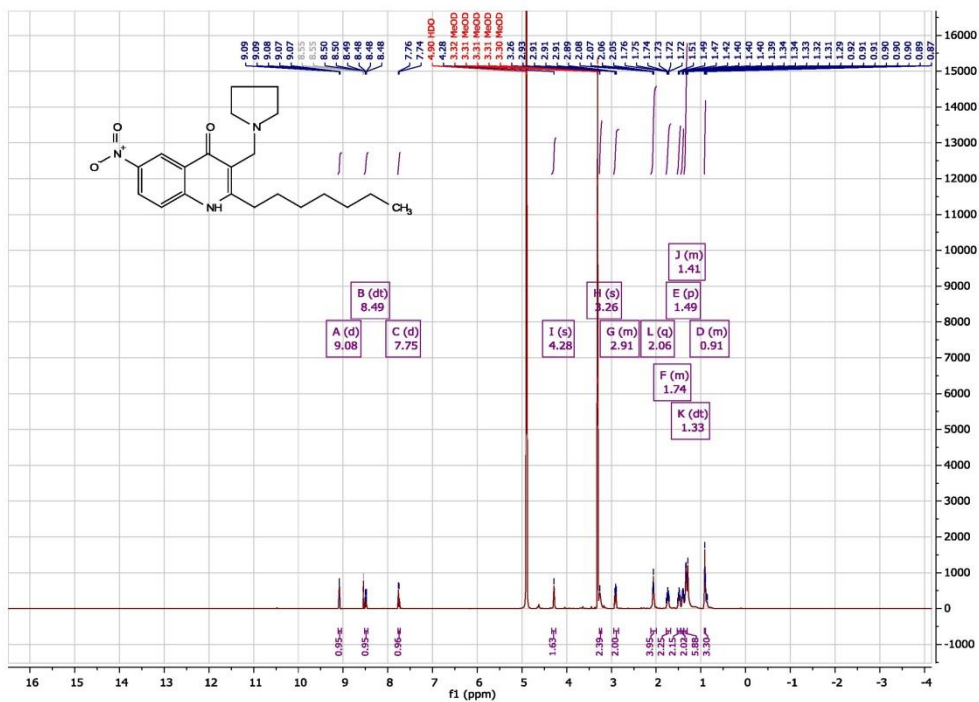
Compound No.	Calculated % ionization of position 3 substituent @ pH 6.5		CpK _a	Position 3 chemical group
4	1%		8.3 ± 0.8	OH
6	100%		3.6 ± 0.8	COOH
22	100%		3.6 ± 0.8	COOH
9	83%		12.0 ± 0.9	CH ₂ NMe ₂
10	83%		11.9 ± 0.5	CH ₂ NEt ₂
11	83%		11.8 ± 0.5	CH ₂ NC ₄ H ₉
27	83%		12.0 ± 0.9	CH ₂ NH ₂

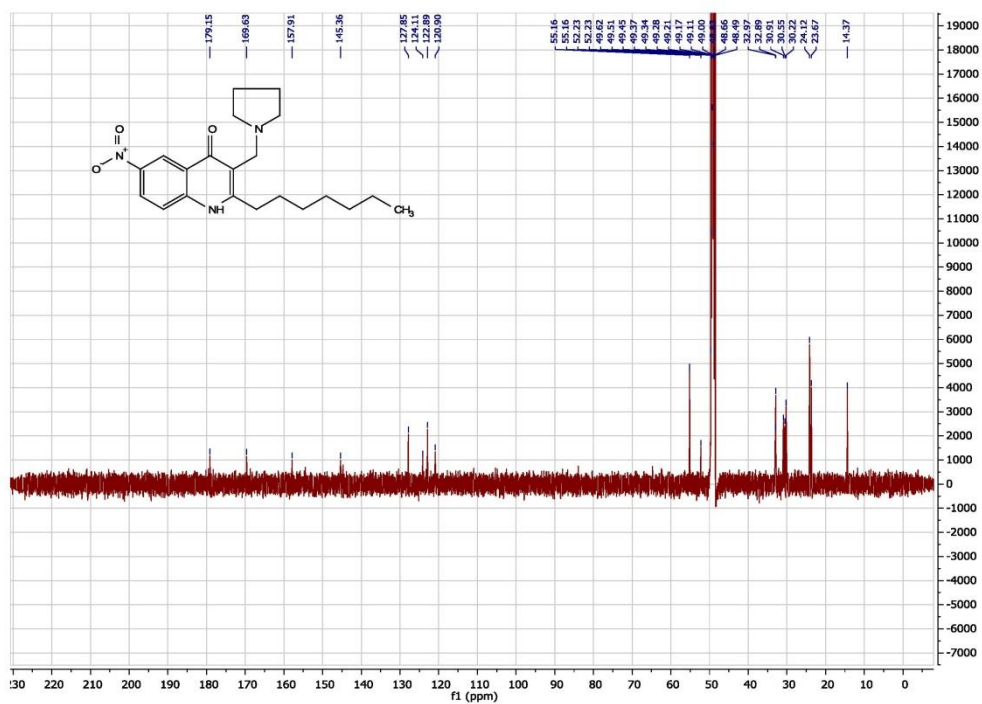
Values were calculated by the use of GALAS algorithm as implemented in ACDLabs (Build 2911. 12 Jul 2016) for CpK_a determination.

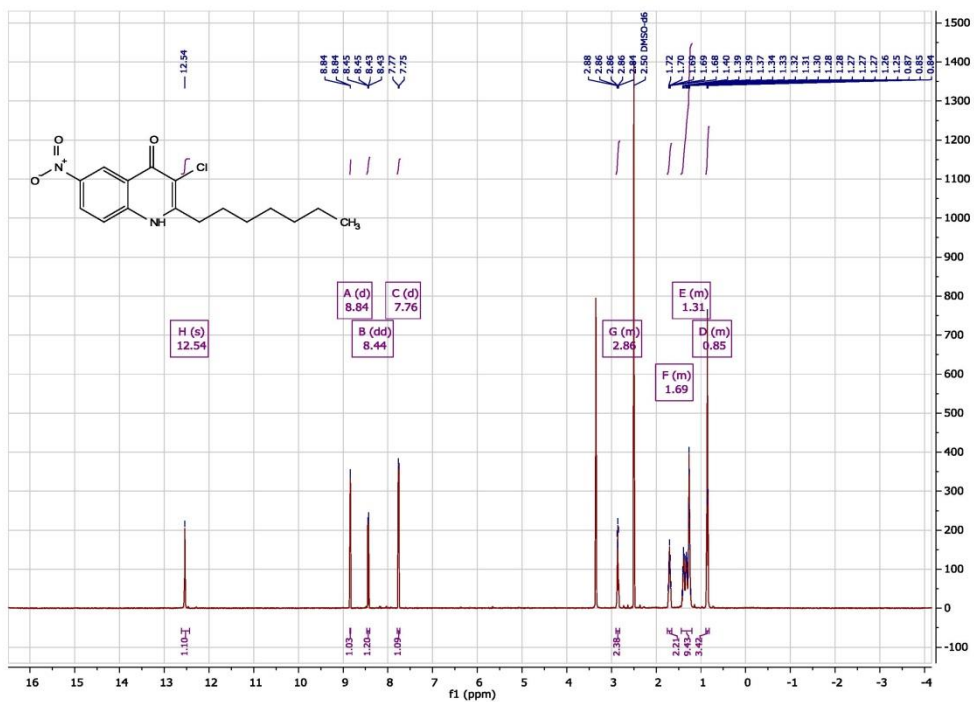


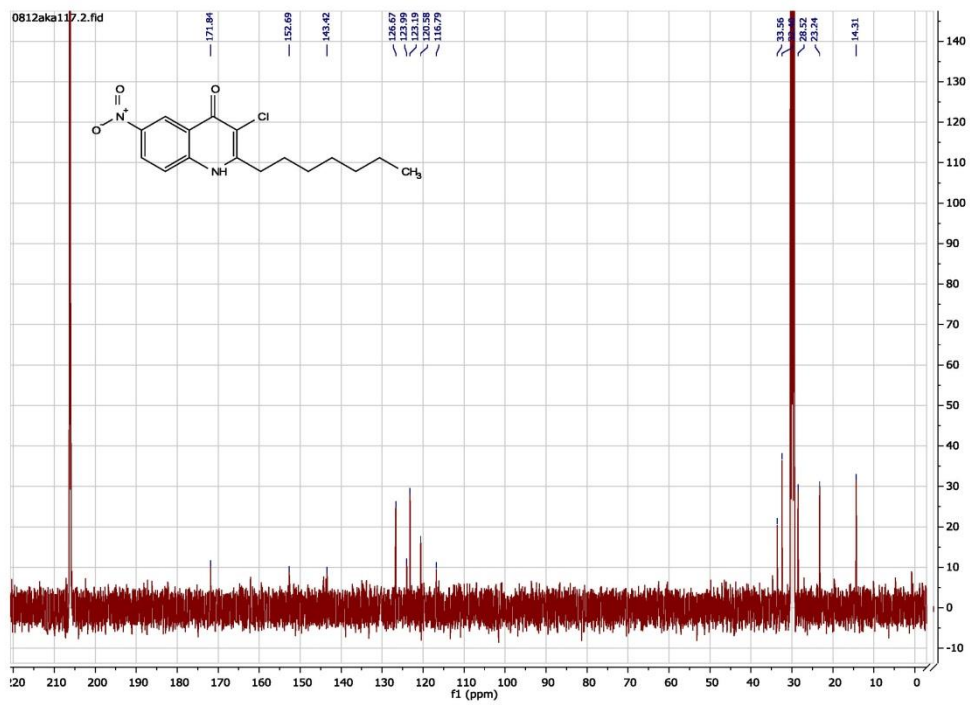


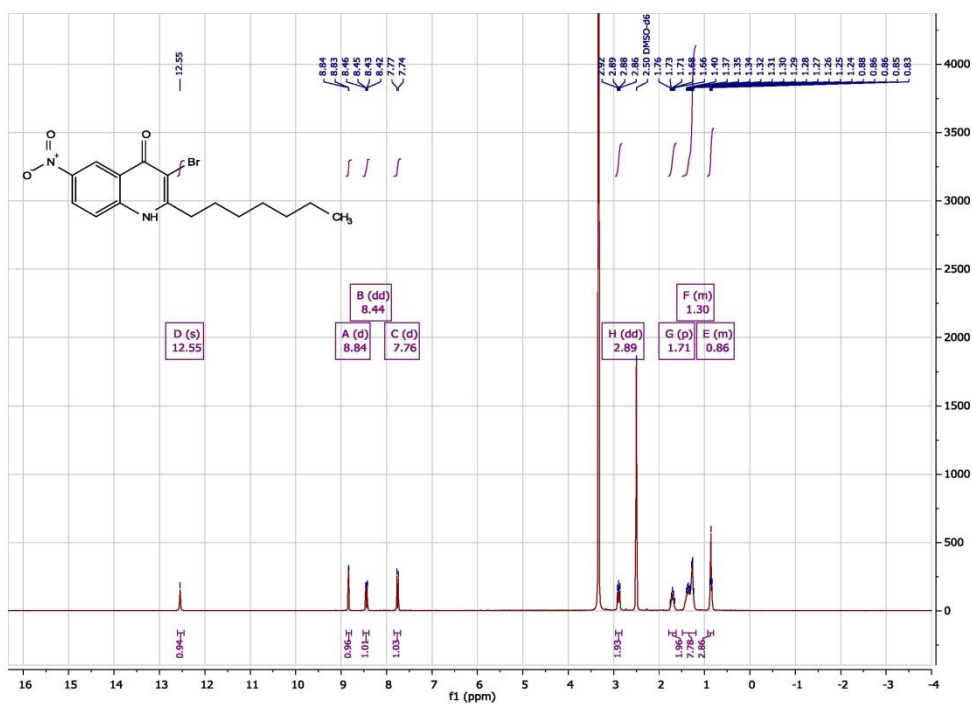


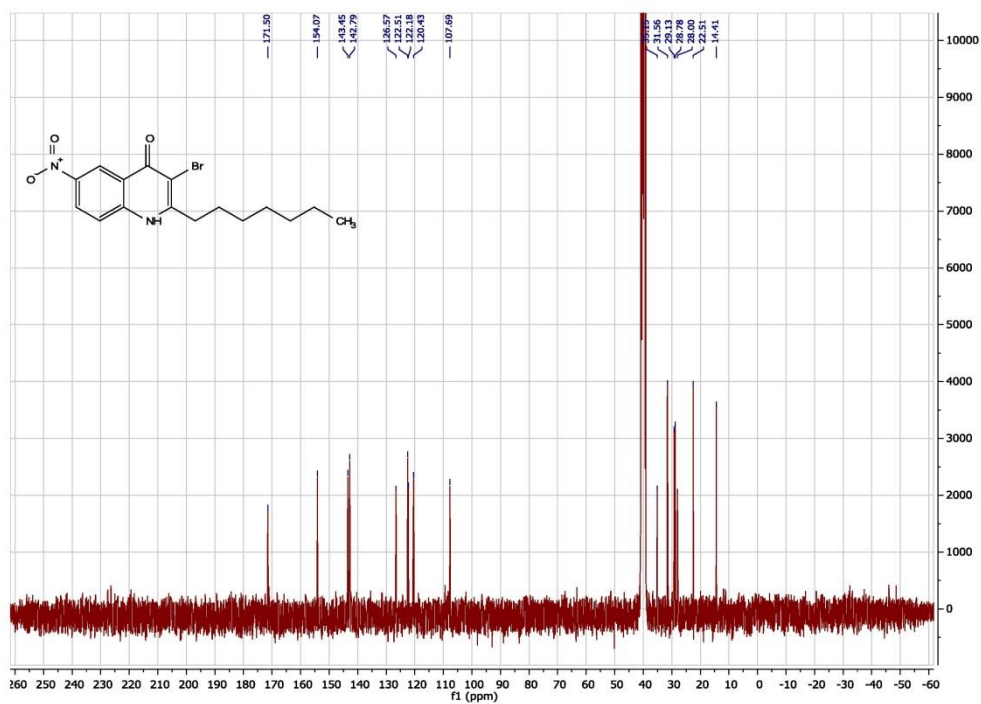


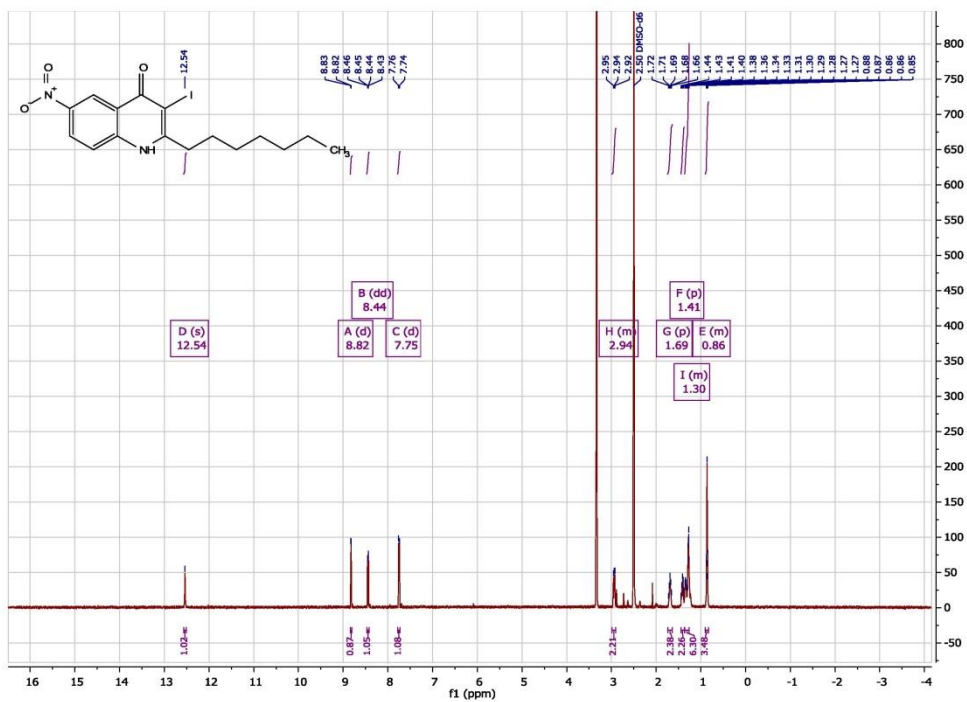


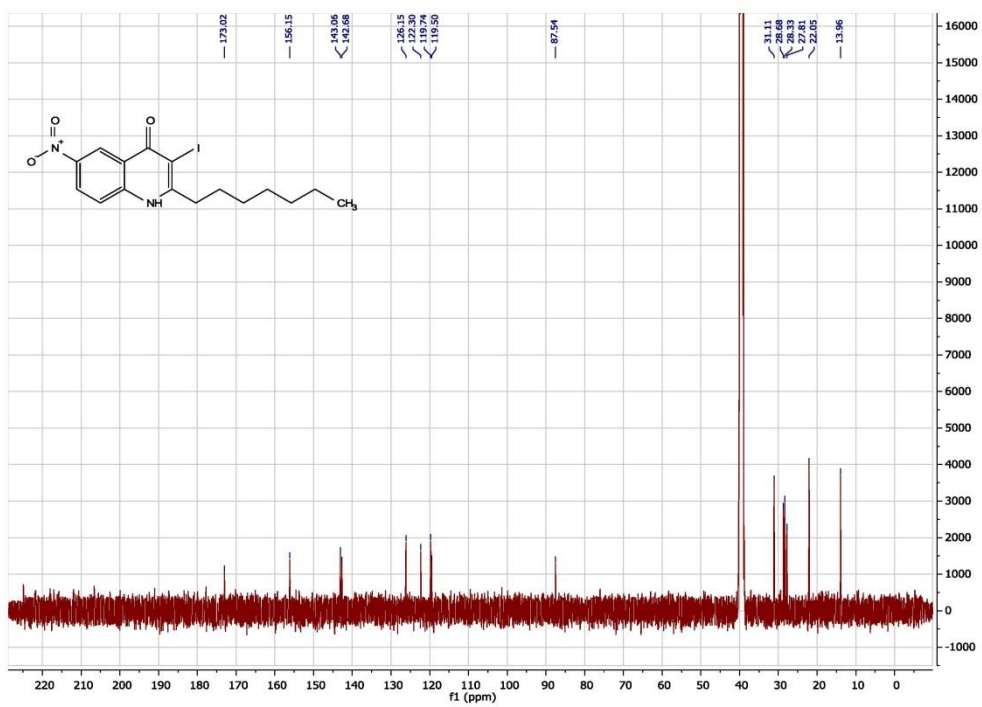


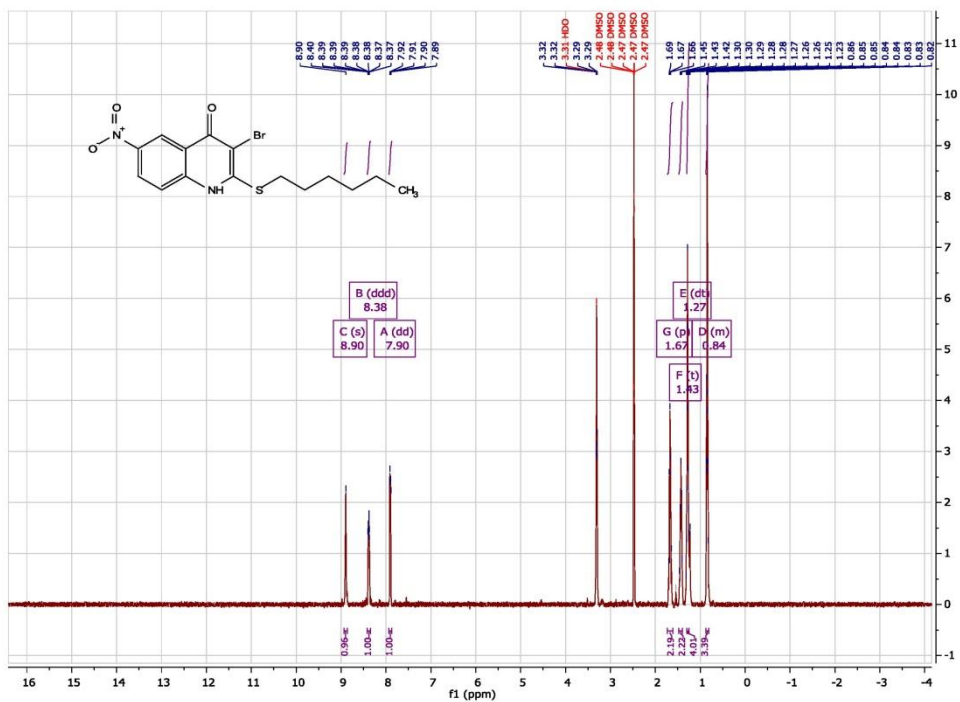


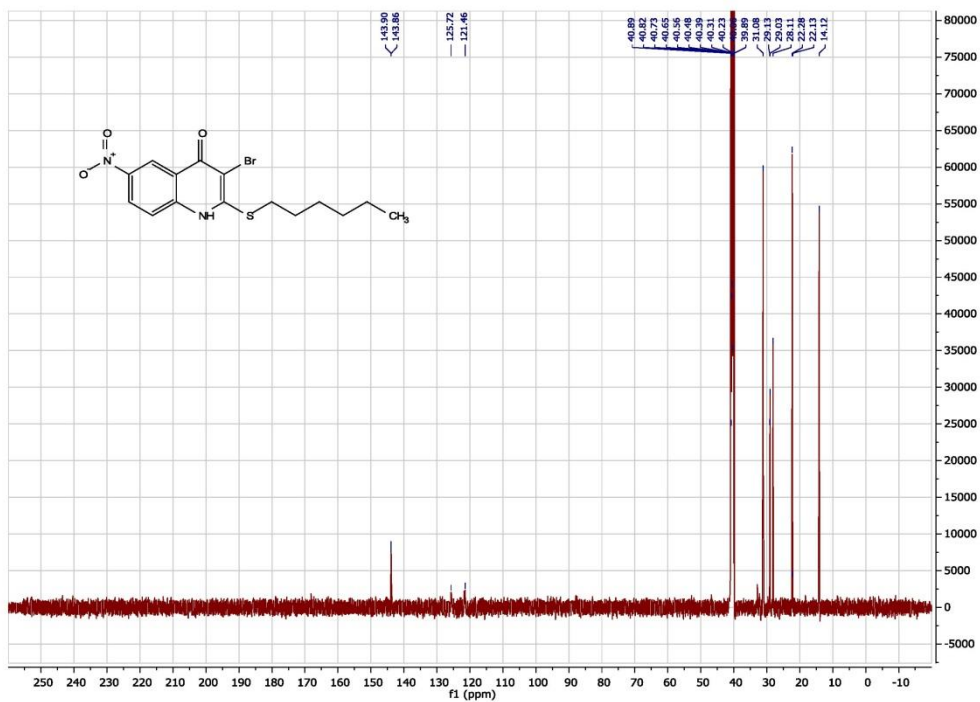


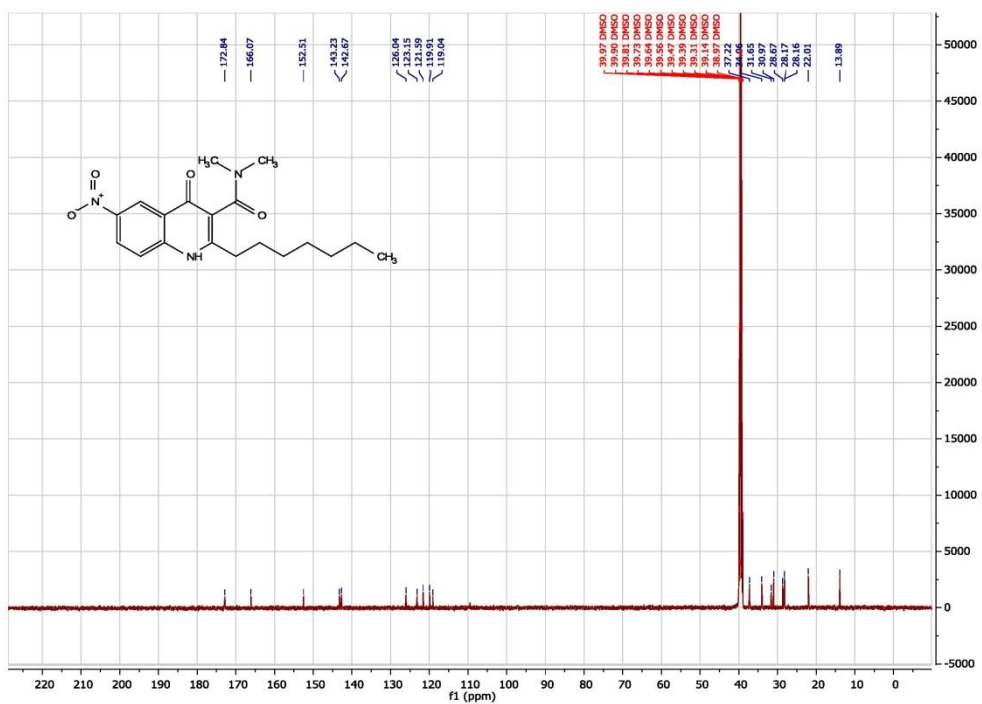


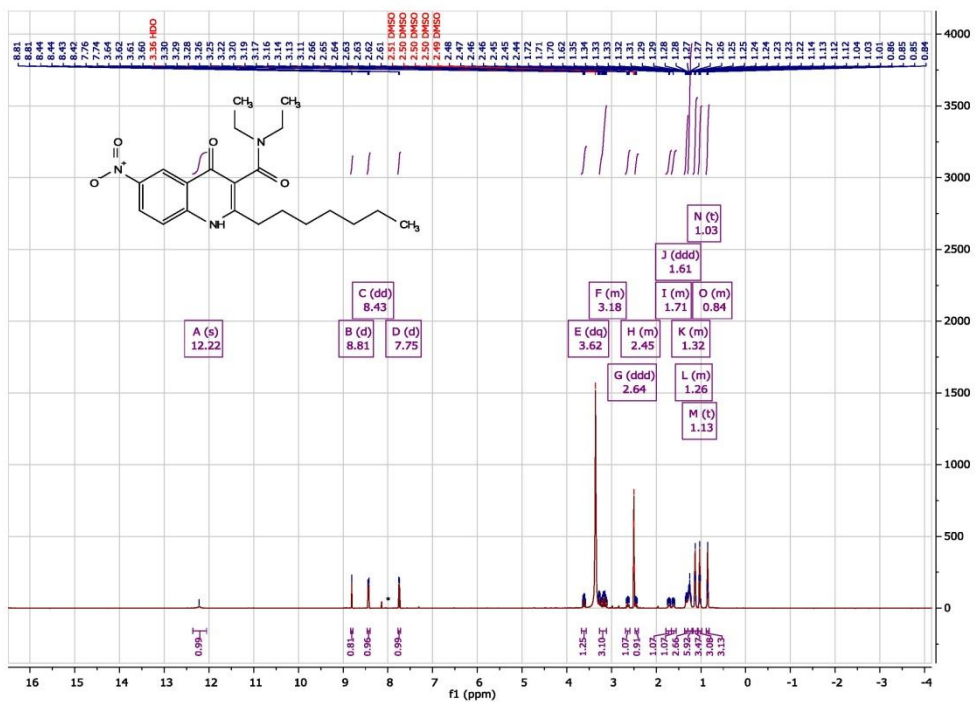


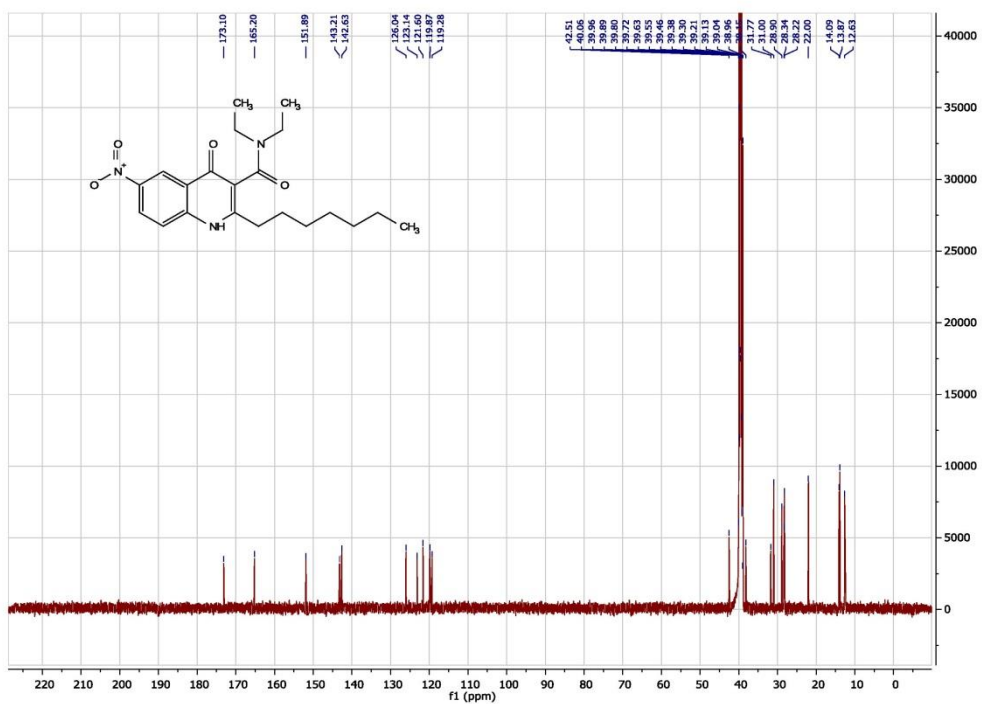


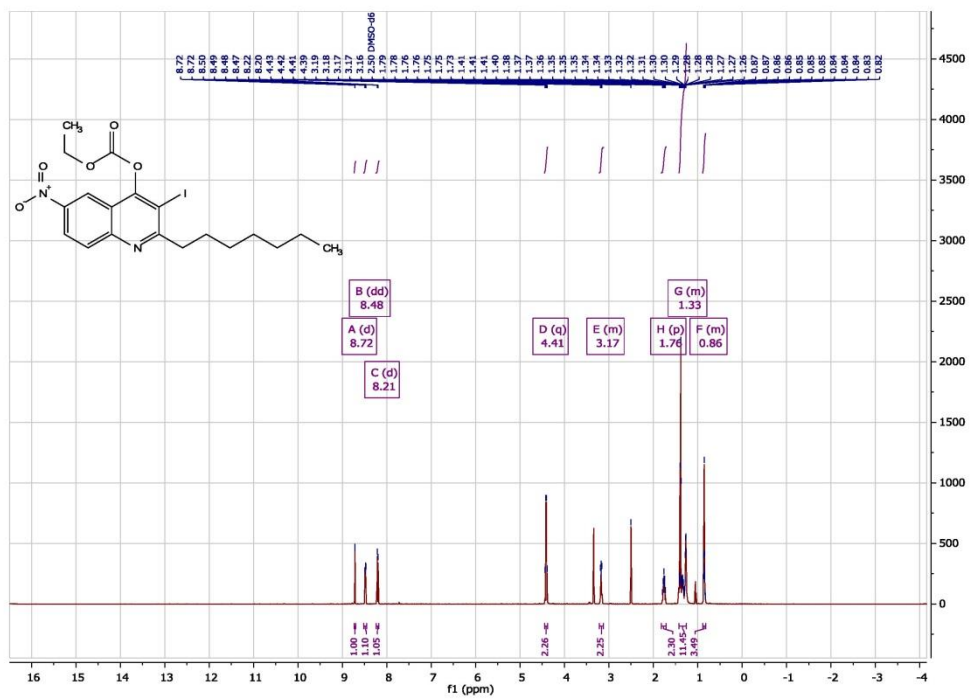


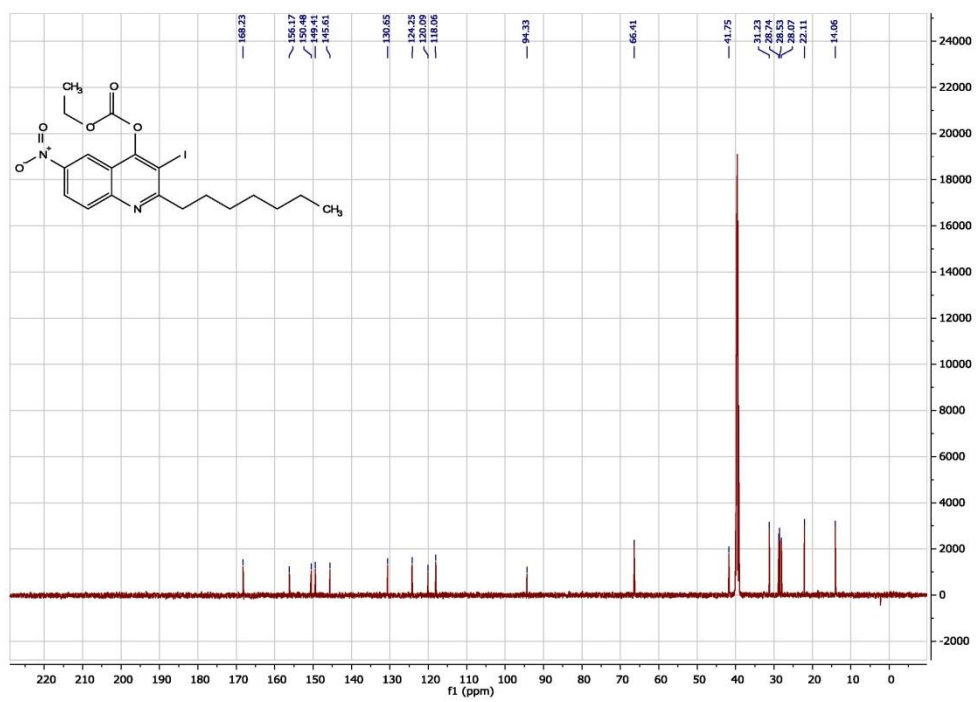


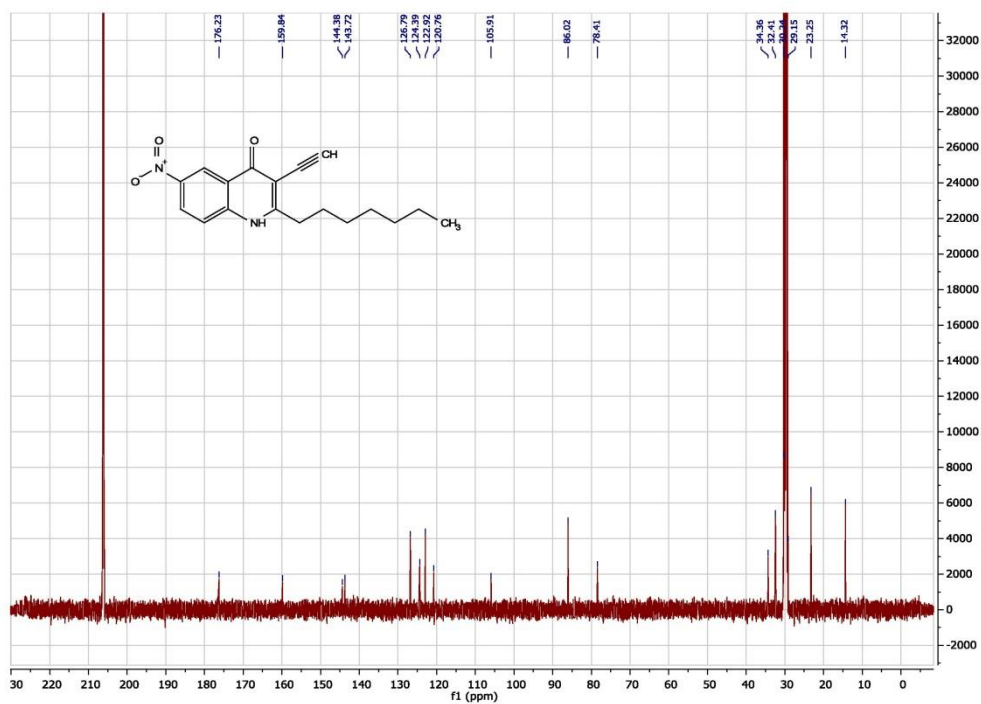


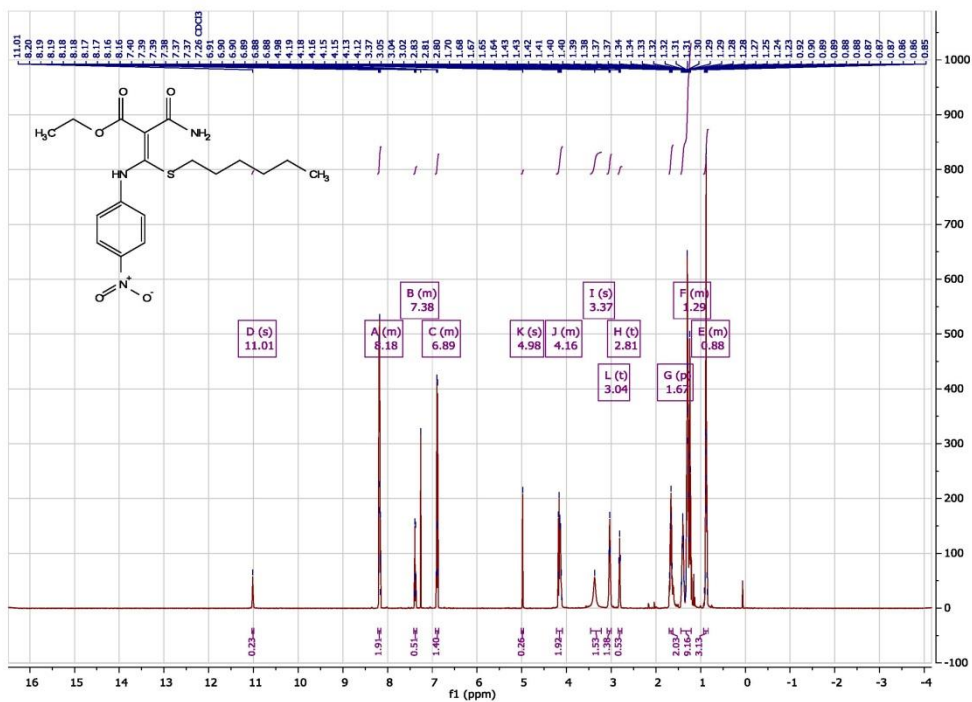


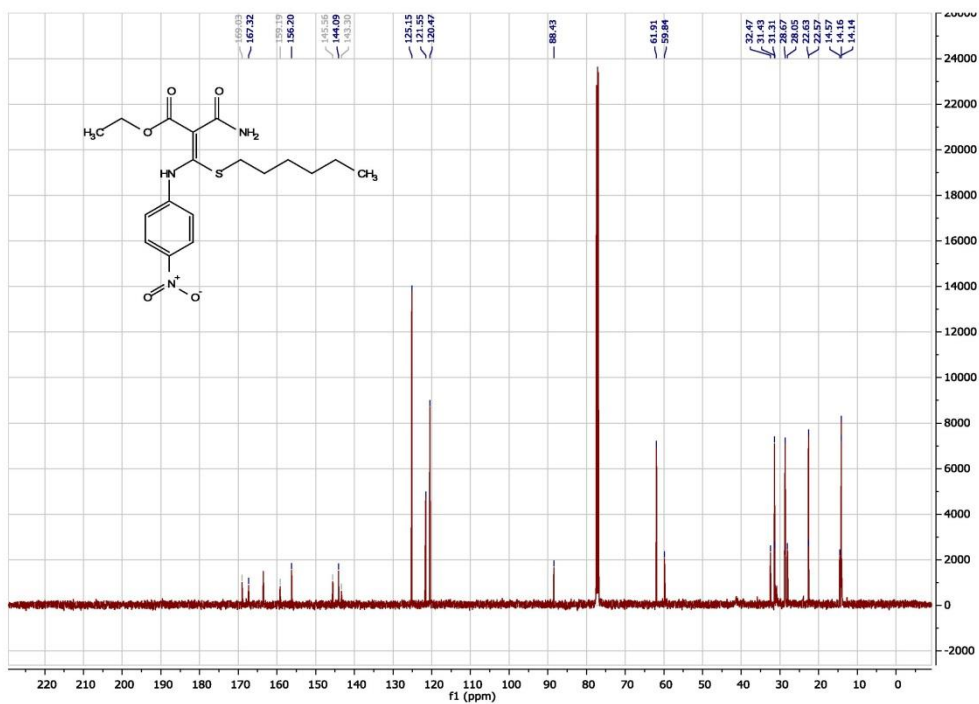


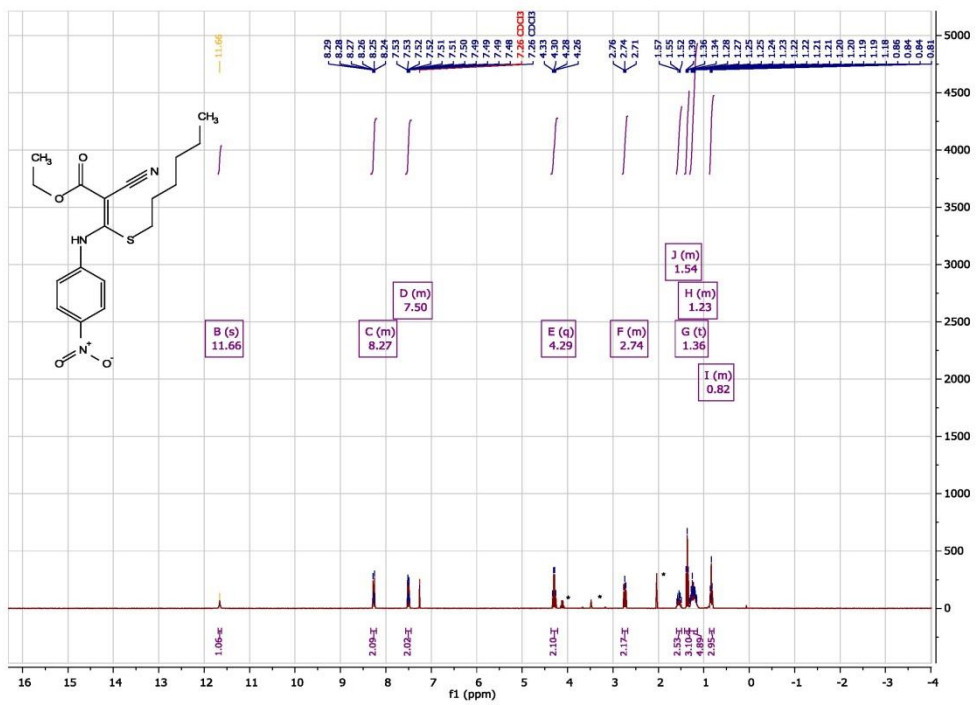


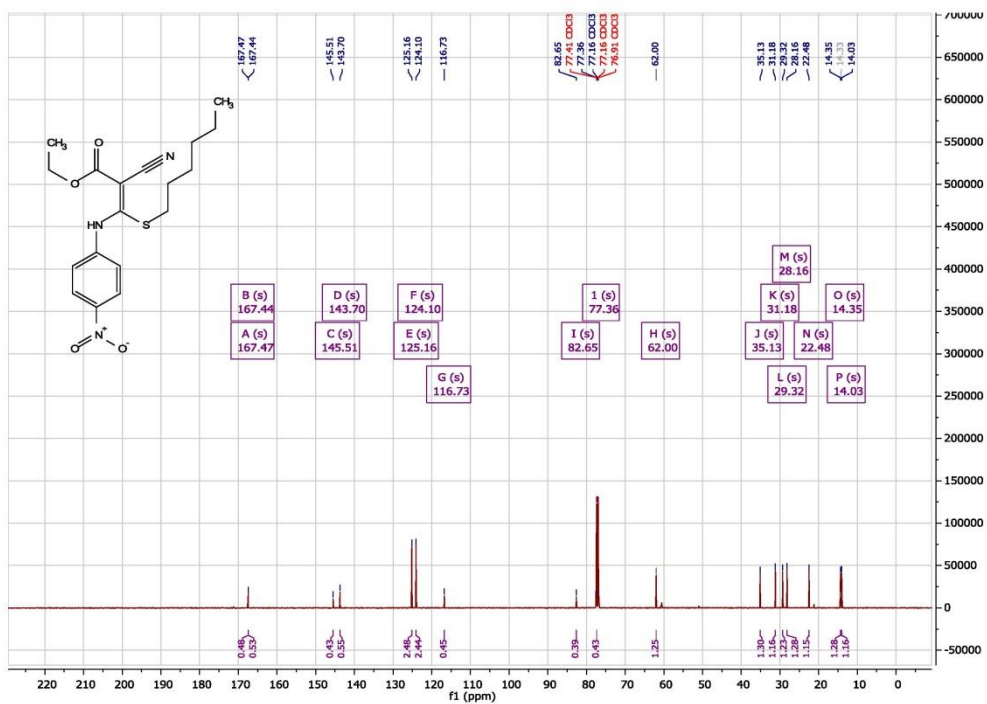


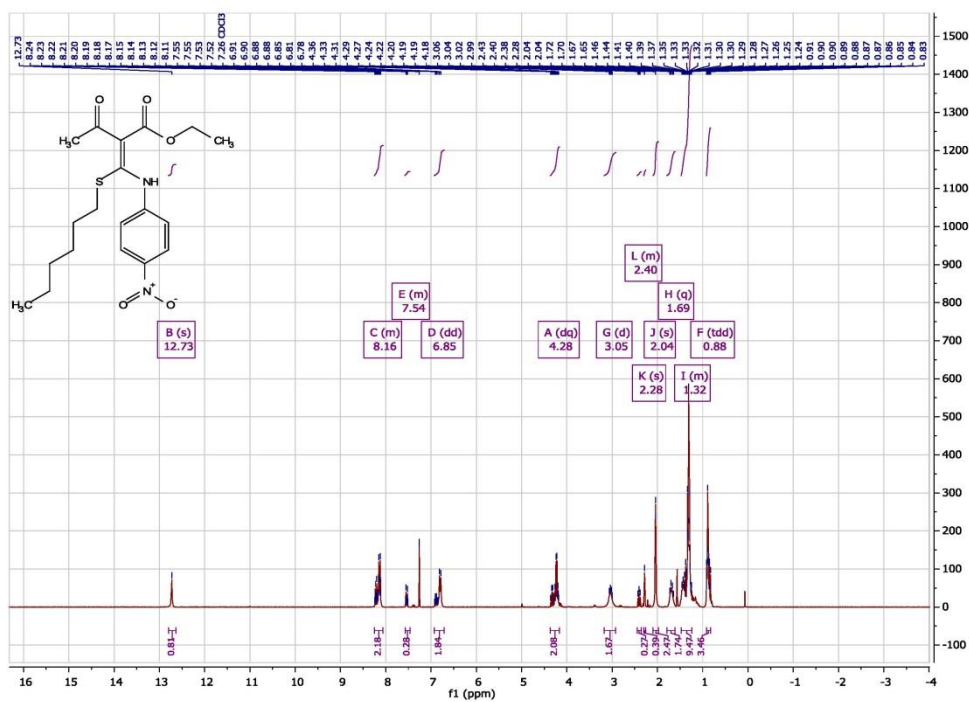


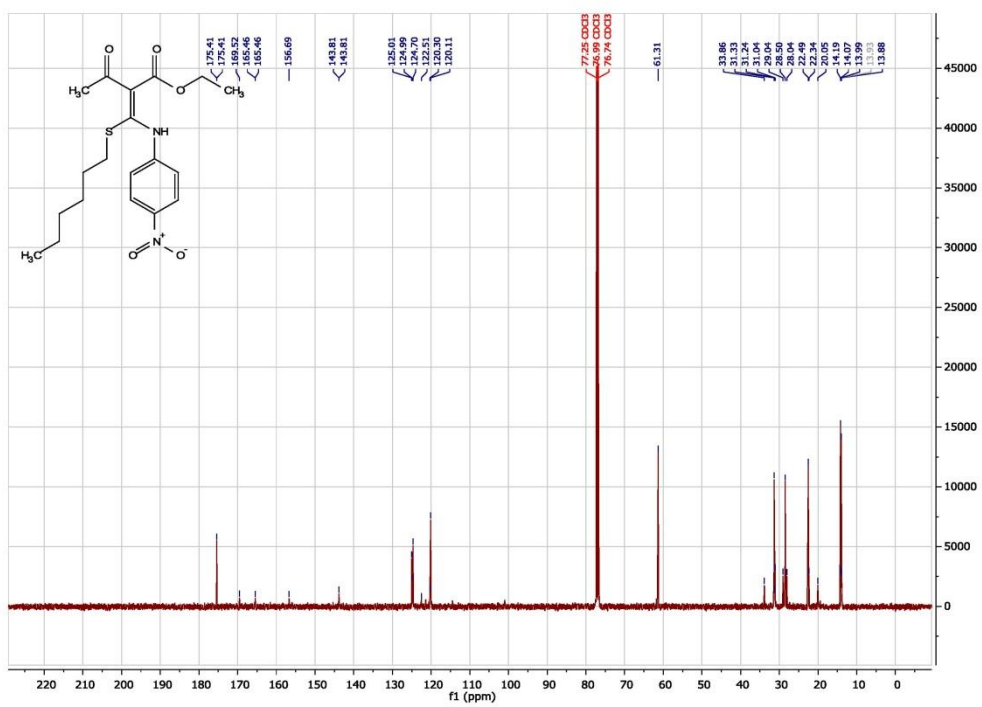


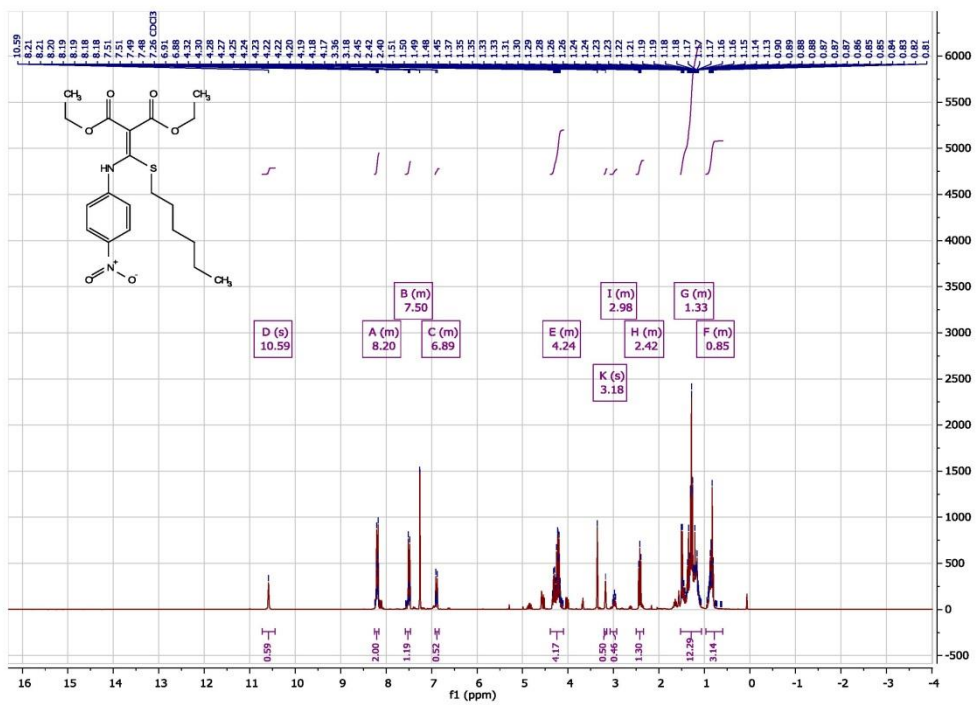


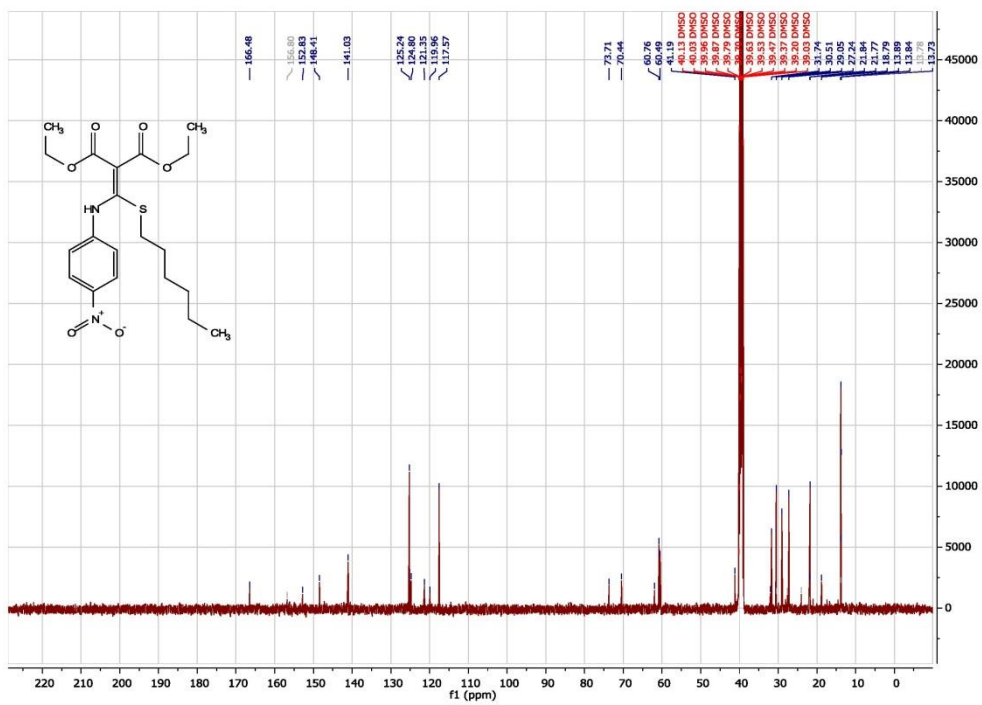


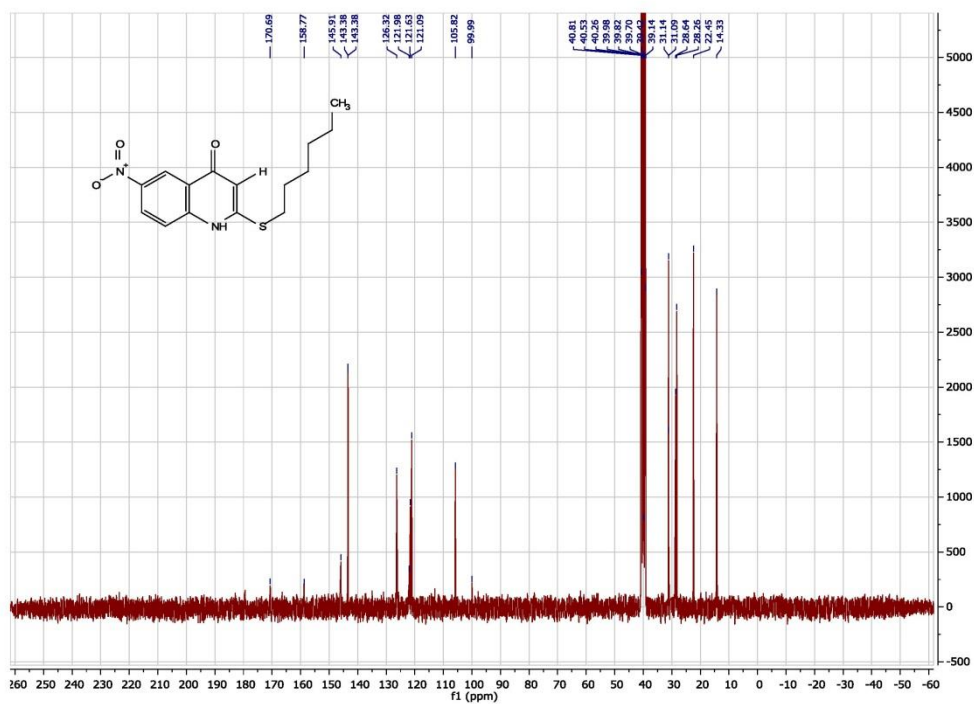


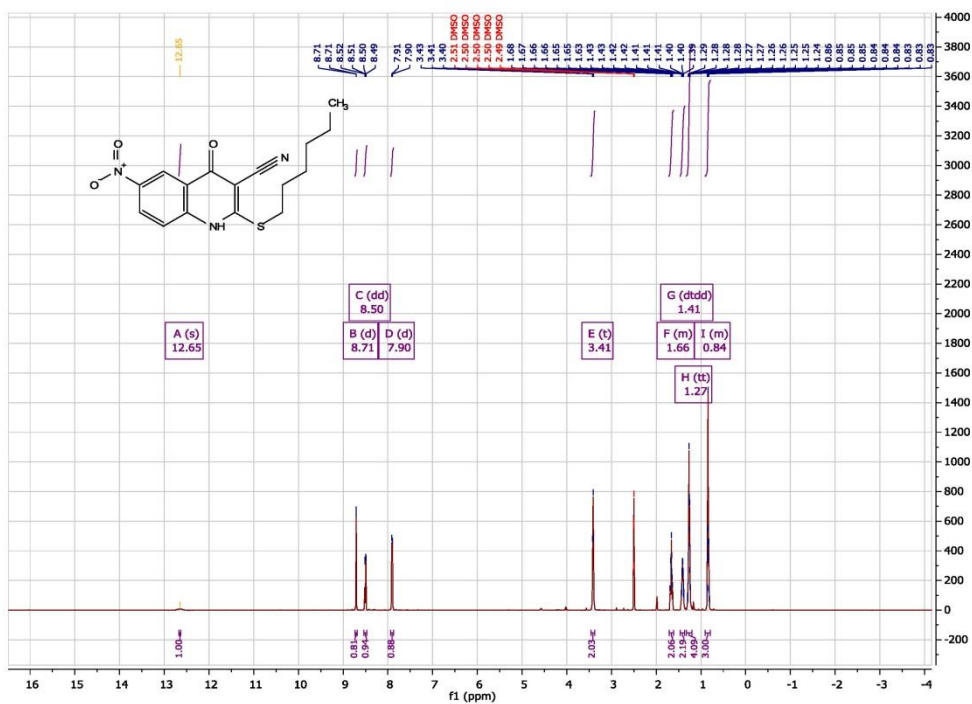


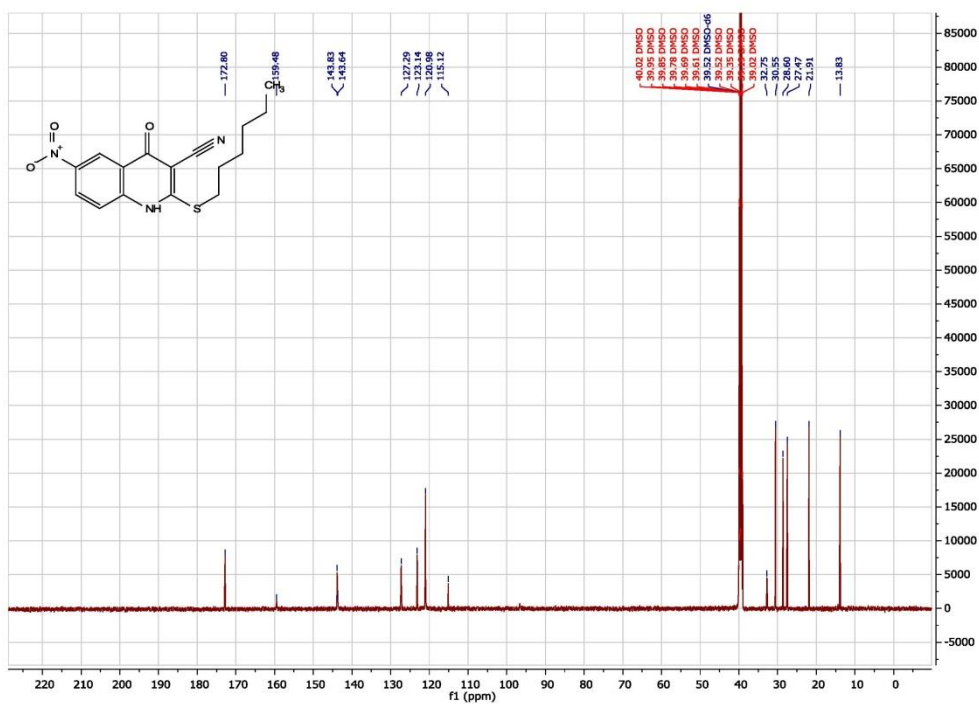


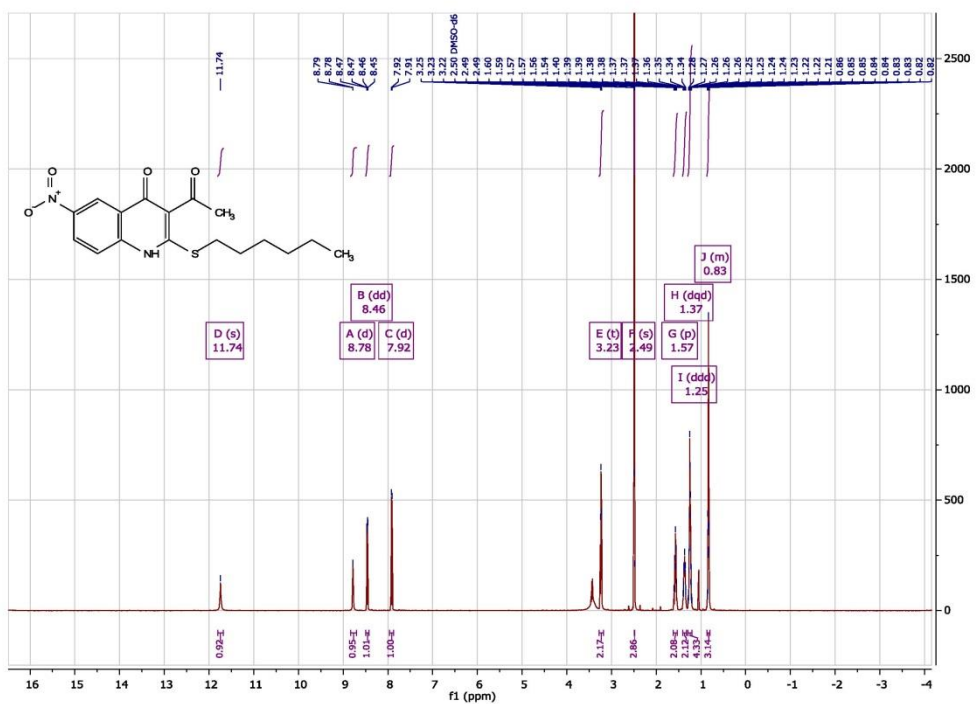


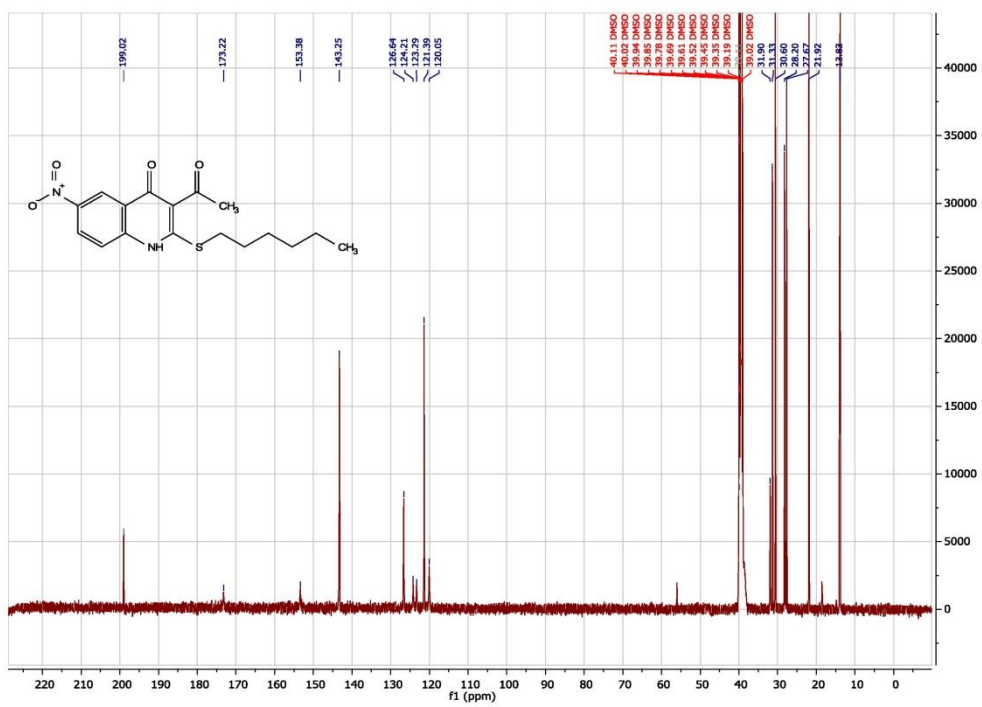


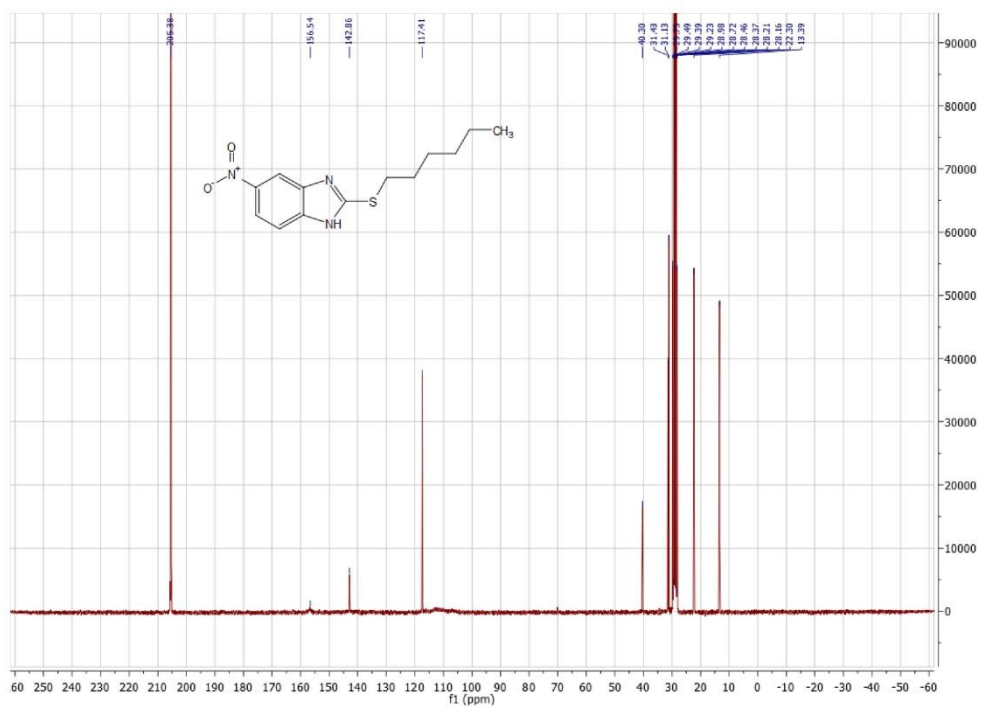


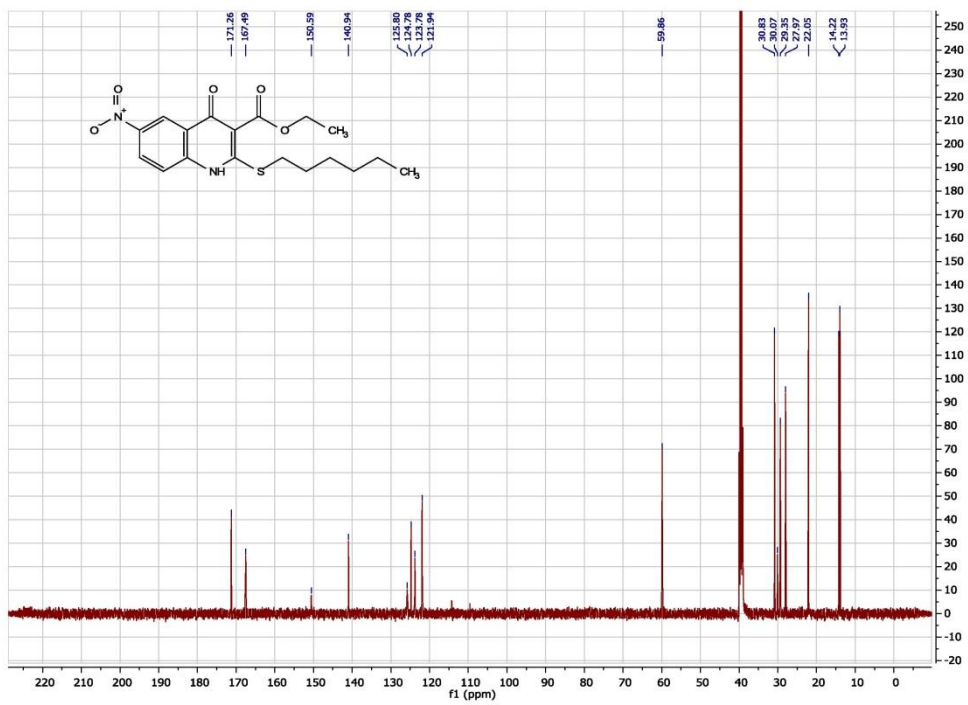


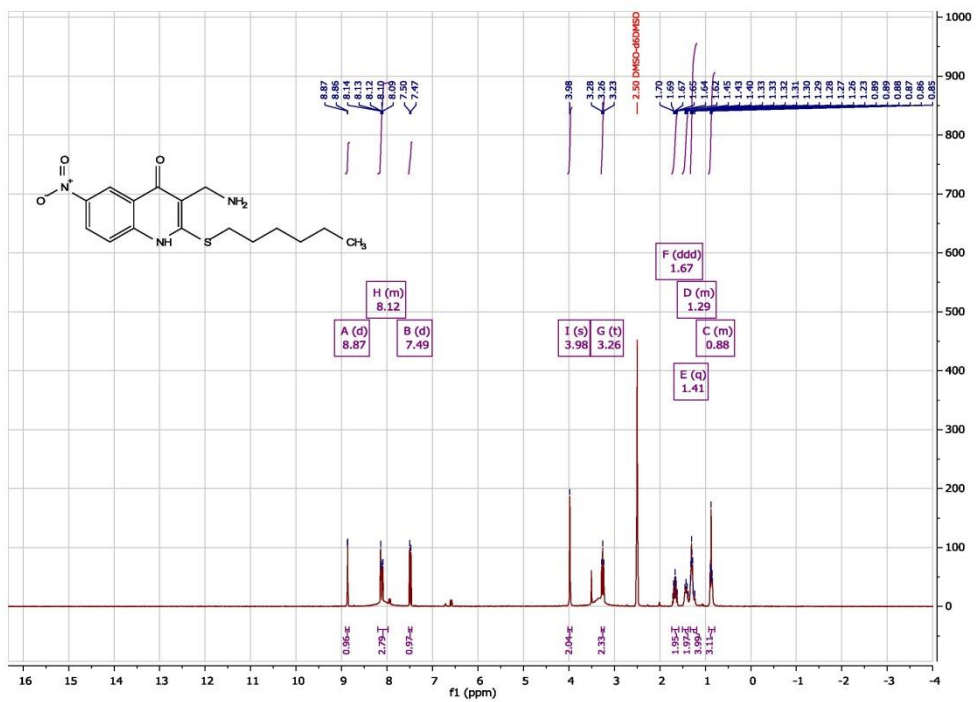


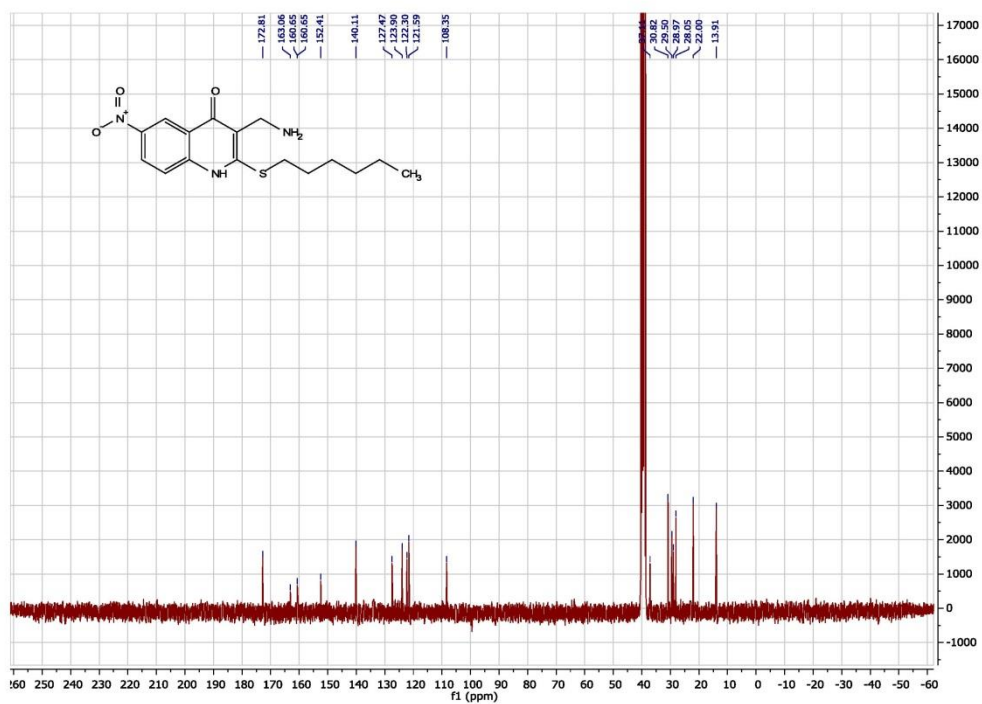


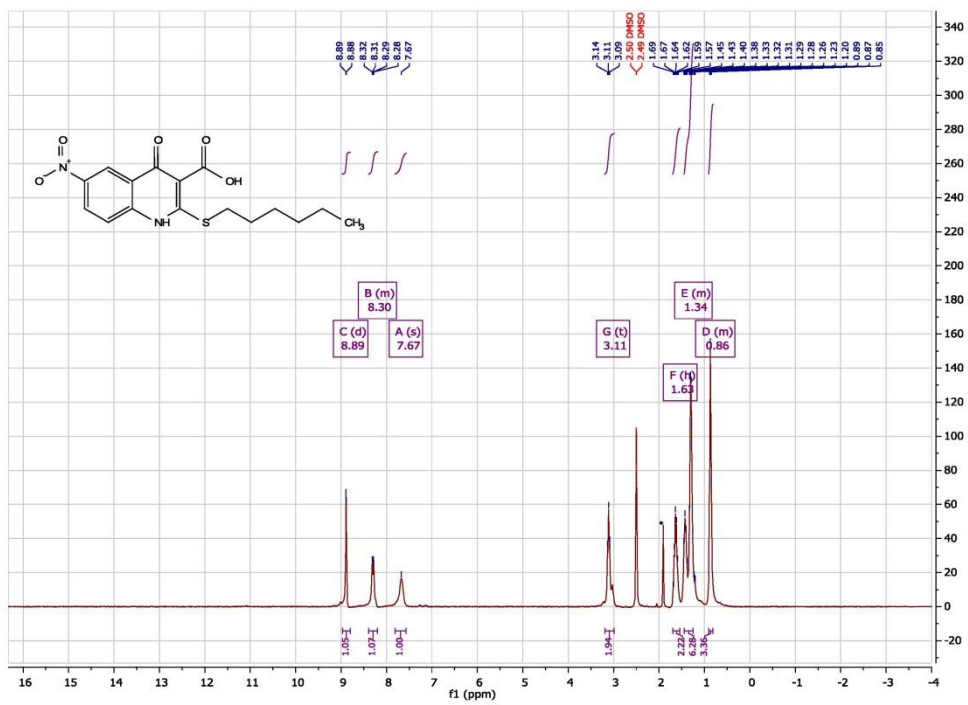


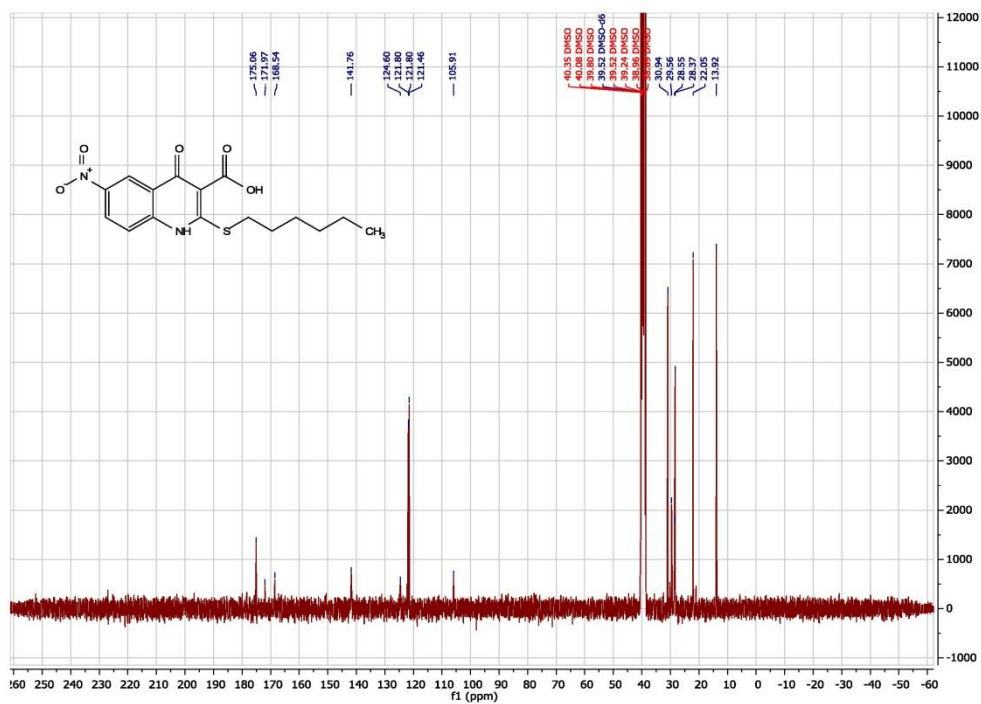












6.2 Supporting information chapter B

Supporting information

Exploring the chemical space of ureidothiophene-2-carboxylic acids as inhibitors of the quorum sensing enzyme PqsD from *Pseudomonas aeruginosa*

J. Henning Sahner,[‡] Martin Empting,[‡] Ahmed Kamal,[‡] Elisabeth Weidel,[‡] Matthias Groh,[‡] Carsten Börger,^{‡*} and Rolf W. Hartmann^{‡,*}

[‡]Pharmaceutical and Medicinal Chemistry, Saarland University & Helmholtz Institute for Pharmaceutical Research Saarland (HIPS), Department of Drug Design and Optimization, Campus C2 3, 66123 Saarbrücken, Germany

^{*}PharmBioTec GmbH, Science Park 1, 66123 Saarbrücken, Germany

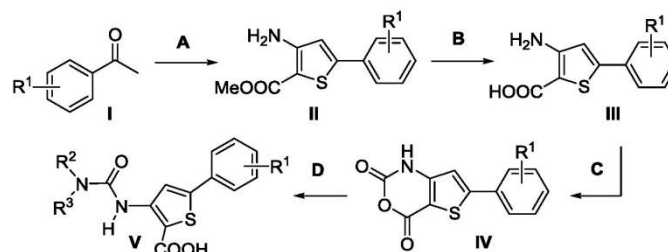
Contents:

a)	Chemistry:	
	Synthesis and spectroscopic data of compounds 1–25	S2–S23
	¹ H and ¹³ C NMR spectra of compounds 4, 10, 16, 21, 22, 24	S24–S35
	HPLC purities of compounds 1–25	S36
b)	Surface plasmon resonance (SPR)	S37
c)	References	S37–S38

a) CHEMISTRY

Synthesis and spectroscopic data of compounds 1–24

Scheme S1: General synthesis of 5-aryl-3-ureidothiophene-2-carboxylic acids.



Method A, general procedure for the synthesis of 5-Aryl-3-amino-2-carboxylic acid methylester (**II**) [1]:

POCl₃ (26.1 g, 0.17 mol) was added dropwise to DMF (24.9 g, 0.34 mol) maintaining the temperature beyond 25 °C (cooling in ice bath) and stirred for additional 15 min. The acetophenone **I** (85.0 mmol) was added slowly and the temperature was kept between 40 and 60 °C. After complete addition, the mixture was stirred for 30 minutes at room temperature. Hydroxylamine hydrochloride (23.6 g, 0.34 mol) was carefully added portionwise (exothermic reaction!) and the reaction was stirred for additional 30 min without heating. After cooling to room temperature, the mixture was poured into ice water (300 mL). The precipitated β-chloro-cinnamionitrile was collected by filtration, washed with H₂O (2 x 50 mL) and dried under reduced pressure over CaCl₂. In the next step sodium (1.93 g, 84.0 mmol) was dissolved in MeOH (85 mL) and methylthioglycolate (6.97 g, 65.6 mmol) was added to the stirred solution. The β-chloro-cinnamionitrile (61.1 mmol) was added and the mixture was heated to reflux for 30 min. After cooling to room temperature, the mixture was poured in ice water (300 mL). The precipitated solid was collected by filtration, washed with H₂O (2 x 50 mL) and dried under reduced pressure over CaCl₂. If necessary, recrystallisation was performed from EtOH.

Method B, general procedure for the synthesis of 5-Aryl-3-amino-2-carboxylic acid (**III**):

The 5-Aryl-3-amino-2-carboxylic acid methyl ester (16.6 mmol) was added to a solution of KOH (60 mL, 0.6 M in H₂O) and MeOH (60 mL). The mixture was heated to reflux for 3 h, concentrated, and washed with EtOAc (2 x 50 mL). The aqueous layer was cooled with ice and acidified with a saturated aqueous solution of KHSO₄. The precipitated solid was collected by filtration, washed with H₂O (2 x 30 mL) and dried under reduced pressure over CaCl₂.

Method C, general procedure for the synthesis of 5-Aryl-2-thioisatoic-anhydride (**IV**) [2,3]:

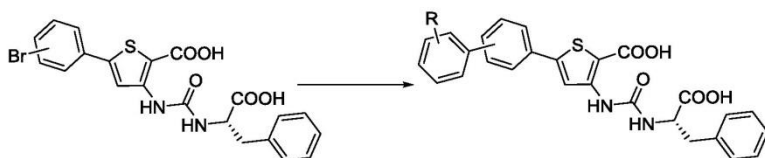
To a solution of the 5-Aryl-3-amino-2-carboxylic acid (**III**) (5.28 mmol) in THF (50 mL) a solution of phosgene (6.10 mL, 20 wt% in toluene, 11.6 mmol) was added dropwise

over a period of 30 min. The reaction mixture was stirred for 2 h at room temperature, followed by the addition of saturated aqueous solution of NaHCO₃ (30 mL) and H₂O (50 mL). The resulting mixture was extracted with EtOAc/THF (1:1, 3 x 100 mL). The organic layer was washed with saturated aqueous NaCl (100 mL), dried (MgSO₄) and concentrated. The crude material was suspended in a mixture of *n*-hexane/EtOAc (2:1, 50 mL) heated to 50 °C and after cooling to room temperature separated via filtration.

Method D, general procedure for the synthesis of 5-Aryl-3-ureidothiophene-2-carboxylic acid (**V**) [4]:

The 5-Aryl-2-thiaisatoic-anhydrid (**IV**) (0.46 mmol) was suspended in water (7.5 mL) and the appropriate amine (0.92 mmol) was added. After addition of triethylamine (1.84 mmol), the reaction mixture was stirred, heated to 100 °C and then cooled to room temperature. The reaction mixture was poured into a mixture of concentrated HCl and ice (1:1) and extracted with EtOAc/THF (1:1, 60 mL). The organic layer was washed with aqueous HCl (2M), followed by saturated aqueous NaCl (2 x 50 mL), dried (MgSO₄) and concentrated. The crude material was suspended in a mixture of *n*-hexane/EtOAc (2:1, 20 mL) heated to 50 °C and after cooling to room temperature separated *via* filtration.

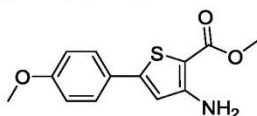
Scheme S2: General procedure for Suzuki coupling.



Method E, general procedure for the synthesis of (**VI**) [5]:

A mixture of the bromo-aryl compound (1 eq, 0.20 mmol), the boronic acid (2 eq, 0.40 mmol), Pd(PPh₃)₄ (0.1 eq, 0.02 mmol) and Na₂CO₃ (6 eq, 1.20 mmol) in H₂O (2 mL), THF (6 mL) and toluene (6 mL) were heated at 80°C under N₂ atmosphere overnight. The reaction mixture was poured into a mixture of concentrated HCl and ice (1:1, 50 mL) and extracted with EtOAc (2 x 50 mL). The organic layer was washed with H₂O, dried (MgSO₄) and evaporated. The crude product was purified using preparative HPLC.

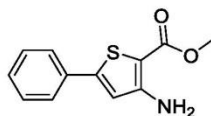
Methyl 3-amino-5-(4'-methoxyphenyl)thiophene-2-carboxylate (IIa).



The title compound was prepared from 4'-methoxyacetophenone according to general procedure **A** and used directly in the next step without further purification. ¹H NMR (DMSO-d₆, 500 MHz): δ = 7.56 (d, *J* = 8.8 Hz, 2H), 7.00 (d, *J* = 8.8 Hz, 2H), 6.86 (s, 1H), 6.56 (br. s, 2H), 3.79 (s, 3H, OCH₃), 3.72 (s, 3H, OCH₃) ppm. ¹³C NMR (DMSO-d₆, 125 MHz): δ = 163.9, 160.0, 155.7, 147.7, 127.0, 125.3, 114.9, 114.6, 95.7, 55.3, 50.8 ppm.

S3

Methyl 3-amino-5-phenylthiophene-2-carboxylate (IIb)

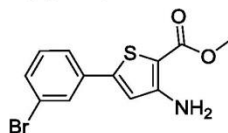


The title compound was prepared from acetophenone according to general procedure **A** and used directly in the next step without further purification. ^1H NMR (DMSO- d_6 , 500 MHz): δ = 7.61–7.64 (m, 2H), 7.43–7.47 (m, 2H), 7.38–7.42 (m, 1H), 6.98 (s, 1H), 6.59 (br. s, 2H), 3.73 (s, 3H) ppm. ^{13}C NMR (DMSO- d_6 , 125 MHz): δ = 163.9, 155.5, 147.5, 132.7, 129.2, 129.1, 125.5, 116.2, 96.6, 50.9 ppm.

Methyl 3-amino-7-methoxy-4,5-dihydronaphtho[1,2-*b*]thiophene-2-carboxylate (IIc).

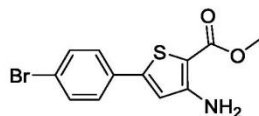
The title compound was prepared from 6-methoxy tetralone according to the following procedure:[6] The conversion to the β -chloro-cinnamionitrile was performed as described in the general procedure A. For the next step, sodium sulphite nonahydrate (10.9 g, 45.5 mmol) was suspended in DMF (50 mL) and heated to 40 °C for 30 min. A solution of the β -chloro-cinnamionitrile (5.00 g, 22.8 mmol) in DMF (20 mL) was added dropwise and the resulting mixture was stirred at 50 °C for 2 h. Methyl bromoacetate (6.96 g, 45.5 mmol) was dissolved in DMF (20 mL), slowly added and stirring was continued overnight. A solution Na (1.05 g, 45.5 mmol) in anhydrous EtOH (100 mL) was freshly prepared and added to the reaction mixture. After 1.5 h, the reaction was cooled to room temperature and diluted with cold H₂O (200 mL). The product appeared as a yellow solid and was filtered off. The product turned grey after washing with 100 mL cold H₂O and drying *in vacuo*. ^1H NMR (DMSO- d_6 , 300 MHz): δ = 7.28 (d, J = 8.4 Hz, 1H), 6.89 (s, 1H), 6.82 (dd, J = 2.4, 8.4 Hz, 1H), 6.50 (br. s, 2H), 3.78 (s, 3H), 3.73 (s, 3H), 2.90 (tt, J = 7.5, 8.1 Hz, 2H), 2.61 (tt, J = 7.5, 8.1 Hz, 2H) ppm. ^{13}C NMR (DMSO- d_6 , 75 MHz): δ = 164.2, 159.7, 153.3, 140.2, 137.6, 125.7, 124.6, 122.9, 113.9, 112.4, 94.7, 55.2, 50.8, 28.0, 20.3 ppm.

Methyl 3-amino-5-(3'-bromophenyl)thiophene-2-carboxylate (IIId).



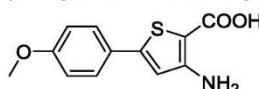
The title compound was prepared from 3'-bromoacetophenone according to general procedure **A** and used directly in the next step without further purification. ^1H NMR (DMSO- d_6 , 500 MHz): δ = 7.80 (t, J = 1.9 Hz, 1H), 7.63 (ddd, J = 0.9, 1.9, 7.9 Hz, 1H), 7.59 (ddd, J = 0.9, 1.9, 7.9 Hz, 1H), 7.40 (t, J = 7.9 Hz, 1H), 7.04 (s, 1H), 6.60 (br. s, 2H), 3.74 (s, 3H) ppm. ^{13}C NMR (DMSO- d_6 , 125 MHz): δ = 163.8, 155.3, 145.4, 135.0, 131.8, 131.3, 127.9, 124.7, 122.5, 117.3, 97.3, 51.0 ppm.

Methyl 3-amino-5-(4'-bromophenyl)thiophene-2-carboxylate (IIe).



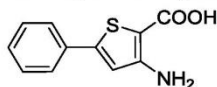
The title compound was prepared from 4'-bromoacetophenone according to general procedure **A** and used directly in the next step without further purification. ^1H NMR (CDCl_3 , 300 MHz): δ = 7.51 (d, J = 8.0 Hz, 2H), 7.43 (d, J = 8.0 Hz, 2H), 6.75 (s, 1H), 5.49 (br. s., 2H), 3.85 (s, 3H, OCH_3) ppm. ^{13}C NMR (CDCl_3 , 75 MHz): δ = 164.8, 154.2, 147.6, 132.3, 132.1, 127.3, 123.0, 115.8, 100.7, 51.3 ppm.

3-Amino-5-(4'-methoxyphenyl)thiophene-2-carboxylic acid (IIIa).



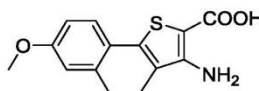
The title compound was prepared from **IIa** according to general procedure **B** and used directly in the next step without further purification. ^1H NMR (DMSO-d_6 , 300 MHz): δ = 7.55 (d, J = 8.8 Hz, 2H), 6.99 (d, J = 8.8 Hz, 2H), 6.84 (s, 1H), 3.79 (s, 3H, OCH_3) ppm. ^{13}C NMR (DMSO-d_6 , 75 MHz): δ = 165.3, 159.9, 155.3, 147.0, 127.0, 125.6, 115.0, 114.6, 97.1, 55.3 ppm.

3-Amino-5-phenylthiophene-2-carboxylic acid (IIIb).



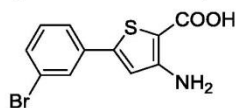
The title compound was prepared from **IIb** according to general procedure **B** and used directly in the next step without further purification. ^1H NMR (DMSO-d_6 , 500 MHz): δ = 7.56–7.69 (m, 2H), 7.33–7.50 (m, 3H), 6.96 (s, 1H) ppm. ^{13}C NMR (DMSO-d_6 , 125 MHz): δ = 165.2, 155.1, 146.8, 133.0, 129.2, 129.0, 125.5, 116.3, 98.1 ppm.

3-Amino-7-methoxy-4,5-dihydronaphtho[1,2-b]thiophene-2-carboxylic acid (IIIc).



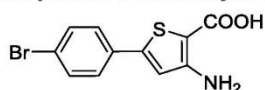
The title compound was prepared from **IIc** according to general procedure **B** and used directly in the next step without further purification. ^1H NMR (DMSO-d_6 , 300 MHz): δ = 7.27 (d, J = 8.2 Hz, 1H), 6.89 (br. s., 1H), 6.81 (d, J = 8.2 Hz, 1H), 3.77 (s, 3H), 2.89 (t, J = 7.0 Hz, 2H), 2.55–2.68 (m, 2H) ppm. ^{13}C NMR (DMSO-d_6 , 75 MHz): δ = 165.6, 159.5, 152.7, 139.3, 137.5, 125.9, 124.4, 123.1, 113.9, 112.4, 96.5, 55.2, 28.1, 20.4 ppm.

3-Amino-5-(3-bromophenyl)thiophene-2-carboxylic acid (IIIId).



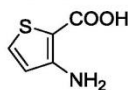
The title compound was prepared from **IId** according to general procedure **B** and used directly in the next step without further purification. ¹H NMR (DMSO-d₆, 500 MHz): δ = 7.79 (t, *J* = 1.9 Hz, 1H), 7.62 (ddd, *J* = 0.9, 1.9, 7.9 Hz, 1H), 7.58 (ddd, *J* = 0.9, 1.9, 7.9 Hz, 1H), 7.39 (t, *J* = 7.9 Hz, 1H), 7.03 (s, 1H) ppm. ¹³C NMR (DMSO-d₆, 125 MHz): δ = 165.2, 155.0, 144.7, 135.3, 131.6, 131.3, 127.8, 124.6, 122.4, 117.4, 98.8 ppm.

3-Amino-5-(4'-bromophenyl)thiophene-2-carboxylic acid (IIIe).



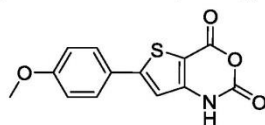
The title compound was prepared from **Ile** according to general procedure **B** and used directly in the next step without further purification. ¹H NMR (DMSO-d₆, 500 MHz): δ = 7.63 (d, *J* = 8.8 Hz, 2H), 7.57 (d, *J* = 8.8 Hz, 2H), 6.98 (s, 1H) ppm. ¹³C NMR (DMSO-d₆, 125 MHz): δ = 165.2, 155.1, 145.3, 132.2, 132.1, 127.5, 122.0, 116.8, 98.5 ppm.

3-Aminothiophene-2-carboxylic acid (IIIf).



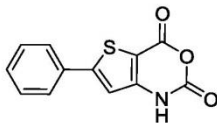
The title compound was prepared from Methyl 3-amino-2-thiophenecarboxylate according to general procedure **B** and used directly in the next step without further purification. ¹H NMR (DMSO-d₆, 300 MHz): δ = 7.47 (d, *J* = 5.4 Hz, 1H), 6.59 (d, *J* = 5.4 Hz, 1H) ppm.

6-(4'-Methoxyphenyl)-2,4-dihydro-1H-thieno[3,2-d][1,3]oxazine-2,4-dione (IVa).



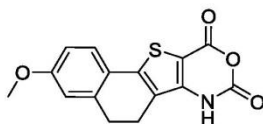
The title compound was prepared from **IIIa** according to general procedure **D** and used directly in the next step without further purification. ¹H NMR (DMSO-d₆, 300 MHz): δ = 12.28 (s, 1H), 7.74 (d, *J* = 8.9 Hz, 2H), 7.12 (s, 1H), 7.04 (d, *J* = 8.9 Hz, 2H), 3.82 (s, 3H, OCH₃) ppm. ¹³C NMR (DMSO-d₆, 75 MHz): δ = 161.1, 155.5, 155.0, 149.6, 148.6, 127.9, 124.1, 114.8, 111.2, 103.1, 55.4 ppm.

6-Phenyl-2H-thieno[3,2-d][1,3]oxazine-2,4(1H)-dione (IVb).



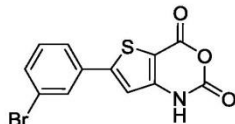
The title compound was prepared from **IIIb** according to general procedure **D** and used directly in the next step without further purification. ^1H NMR (DMSO- d_6 , 500 MHz): δ = 7.76–7.83 (m, 2H), 7.47–7.54 (m, 3H), 7.26 (s, 1H) ppm. ^{13}C NMR (DMSO- d_6 , 125 MHz): δ = 155.2, 155.1, 149.8, 148.6, 131.5, 130.5, 129.5, 126.3, 112.8, 104.4 ppm.

3-Methoxy-5,6-dihydro-8H-naphtho[2',1':4,5]thieno[3,2-d][1,3]oxazine-8,10(7H)-dione (IVc).



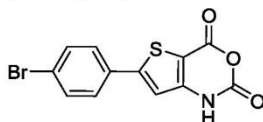
The title compound was prepared from **IIIc** according to general procedure **D** and used directly in the next step without further purification. ^1H NMR (DMSO- d_6 , 300 MHz): δ = 12.19 (br. s., 1H), 7.46 (d, J = 8.5 Hz, 1H), 6.95 (d, J = 2.3 Hz, 1H), 6.87 (dd, J = 2.3, 8.5 Hz, 1H), 3.80 (s, 3H), 2.94 (tt, J = 7.1, 7.8 Hz, 2H), 2.80 (tt, J = 7.1, 7.8 Hz, 2H) ppm. ^{13}C NMR (DMSO- d_6 , 75 MHz): δ = 160.8, 155.1, 149.0, 147.7, 147.4, 138.3, 125.6, 123.6, 121.8, 114.0, 112.9, 101.8, 55.4, 27.6, 20.1 ppm.

6-(3'-Bromophenyl)-2H-thieno[3,2-d][1,3]oxazine-2,4(1H)-dione (IVd).



The title compound was prepared from **IIIId** according to general procedure **D** and used directly in the next step without further purification. ^1H NMR (DMSO- d_6 , 500 MHz): δ = 12.41 (br. s., 1H), 8.05 (t, J = 1.7 Hz, 1H), 7.80 (ddd, J = 1.0, 1.9, 7.9 Hz, 1H), 7.69 (ddd, J = 1.0, 1.9, 7.9 Hz, 1H), 7.46 (t, J = 8.04 Hz, 1H), 7.36 (s, 1H) ppm. ^{13}C NMR (DMSO- d_6 , 125 MHz): δ = 155.1, 152.9, 149.3, 148.5, 133.8, 133.1, 131.5, 128.7, 125.5, 122.7, 113.9, 105.2 ppm.

6-(4-Bromophenyl)-2H-thieno[3,2-d][1,3]oxazine-2,4(1H)-dione (IVe).

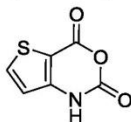


The title compound was prepared from **IIIe** according to general procedure **D** and used directly in the next step without further purification. ^1H NMR (DMSO- d_6 , 500 MHz): δ = 12.39 (br. s., 1H), 7.77 (d, J = 8.8 Hz, 2H), 7.70 (d, J = 8.8 Hz, 2H),

S7

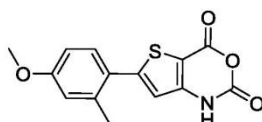
7.29 (s, 1H) ppm. ^{13}C NMR (DMSO- d_6 , 125 MHz): δ = 155.1, 153.5, 149.7, 148.6, 132.4, 130.8, 128.3, 123.8, 113.4, 104.7 ppm.

2H-Thieno[3,2-*d*][1,3]oxazine-2,4(1H)-dione (IVf).



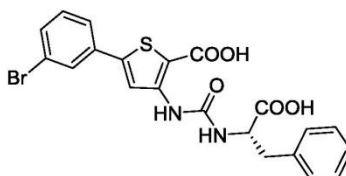
The title compound was prepared from **III f** according to general procedure **D** and used directly in the next step without further purification. ^1H NMR (DMSO- d_6 , 300 MHz): δ = 12.21 (br. s., 1H), 8.24 (d, J = 5.2 Hz, 1H), 6.94 (d, J = 5.2 Hz, 1H) ppm.

6-(4'-Methoxy-2'-methylphenyl)-2H-thieno[3,2-*d*][1,3]oxazine-2,4(1H)-dione (IVg).



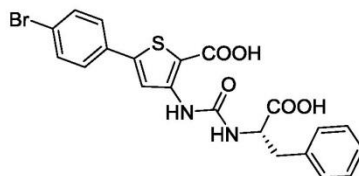
The title compound was prepared from **III g** according to general procedure **D** and used directly in the next step without further purification. ^1H NMR (DMSO- d_6 , 300 MHz): δ = 12.23 (br. s., 1H), 7.43 (d, J = 8.57 Hz, 1H), 6.84–7.01 (m, 3H), 3.80 (s, 3H), 2.41 (s, 3H) ppm. ^{13}C NMR (DMSO- d_6 , 75 MHz): δ = 160.3, 155.0, 154.9, 148.8, 148.5, 137.5, 131.2, 123.9, 116.6, 115.5, 112.1, 104.4, 55.3, 20.9 ppm.

(S)-5-(3'-Bromophenyl)-3-(3-(1-carboxy-2-phenylethyl)ureido)thiophene-2-carboxylic acid (Va).



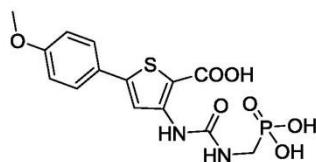
The title compound was prepared from **IV d** according to general procedure **E** and used directly in the next step without further purification. ^1H NMR (DMSO- d_6 , 500 MHz): δ = 12.88 (br. s., 2H), 9.42 (s, 1H), 8.23 (s, 1H), 8.18 (d, J = 7.9 Hz, 1H), 7.81 (t, J = 1.7 Hz, 1H), 7.64–7.69 (ddd, J = 1.0, 1.9, 7.9 Hz, 1H, 1H), 7.57–7.62 (ddd, J = 1.0, 1.9, 7.9 Hz, 1H, 1H), 7.25–7.33 (m, 4H), 7.17–7.25 (m, 1H), 4.39 (ddd, J = 4.6, 8.0, 9.5 Hz, 1H), 3.11 (dd, J = 4.8, 13.9 Hz, 1H), 2.88 (dd, J = 9.8, 13.9 Hz, 1H) ppm. ^{13}C NMR (DMSO- d_6 , 125 MHz): δ = 173.6, 164.5, 153.7, 145.5, 144.7, 137.7, 135.0, 131.8, 131.4, 129.1, 128.2, 128.0, 126.4, 124.8, 122.5, 119.0, 107.8, 54.4, 37.0 ppm.

(S)-5-(4'-Bromophenyl)-3-(3-(1-carboxy-2-phenylethyl)ureido)thiophene-2-carboxylic acid (Vb).



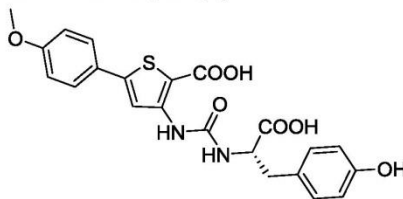
The title compound was prepared from **IVe** according to general procedure **E** and used directly in the next step without further purification. ^1H NMR (DMSO- d_6 , 300 MHz): δ = 12.93 (br. s., 2H), 9.42 (s, 1H), 8.23 (s, 1H), 8.17 (d, J = 7.9 Hz, 1H), 7.54–7.70 (m, 4H), 7.14–7.38 (m, 5H), 4.30–4.47 (m, 1H), 3.04–3.17 (m, 1H), 2.80–2.95 (m, 1H) ppm. ^{13}C NMR (DMSO- d_6 , 75 MHz): δ = 173.5, 164.5, 153.7, 145.7, 145.4, 137.7, 132.2, 132.0, 129.0, 128.2, 127.6, 126.4, 122.3, 118.5, 107.3, 54.4, 37.0 ppm.

5-(4-Methoxyphenyl)-3-(3-(phosphonomethyl)ureido)thiophene-2-carboxylic acid (1).



The title compound was prepared from **IVa** according to general procedure **D**. ^1H NMR (DMSO- d_6 , 300 MHz): δ = 9.43 (s, 1H), 8.15 (s, 1H), 7.89–8.09 (m, 1H), 7.60 (d, J = 8.6 Hz, 2H), 7.02 (d, J = 8.6 Hz, 2H), 3.80 (s, 3H), 3.25–3.50 (m, 2H) ppm. ^{13}C NMR (DMSO- d_6 , 75 MHz): δ = 164.5, 160.0, 153.9, 147.0, 146.1, 127.0, 125.4, 116.9, 114.7, 105.7, 55.3, 37.0 (d, J = 119.0 Hz, N-C-P) ppm. Melting point 199 °C. MS (ESI) m/z : 386.8 $[\text{M}+\text{H}]^+$

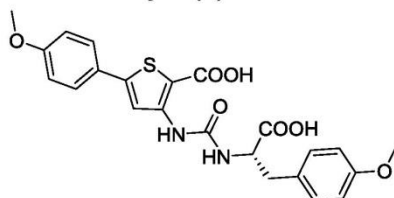
(S)-3-(3-(1-Carboxy-2-(4-hydroxyphenyl)ethyl)ureido)-5-(4-methoxyphenyl)thiophene-2-carboxylic acid (2).



The title compound was prepared from **IVa** according to general procedure **D**. ^1H NMR (DMSO- d_6 , 300 MHz): δ = 12.81 (br. s., 2H), 9.41 (s, 1H), 9.20 (br. s., 1H), 8.07–8.12 (m, 1H), 8.09 (s, 1H), 7.59 (d, J = 8.7 Hz, 2H), 7.06 (d, J = 8.3 Hz, 2H), 7.00 (d, J = 8.7 Hz, 1H), 6.68 (d, J = 8.3 Hz, 2H), 4.20–4.38 (m, 1H), 3.79 (s, 3H), 2.97 (dd, J = 4.4, 13.7 Hz, 1H), 2.76 (dd, J = 9.7, 13.7 Hz, 1H) ppm. ^{13}C NMR (DMSO- d_6 , 75 MHz): δ = 173.8, 164.6, 160.1, 155.9, 153.7, 147.1, 145.9, 130.0, 127.7, 127.1, 125.4, 116.8, 115.0, 114.7, 105.7, 55.3, 54.8, 36.2 ppm. Melting point 166 °C. MS (ESI) m/z : 456.9 $[\text{M}+\text{H}]^+$

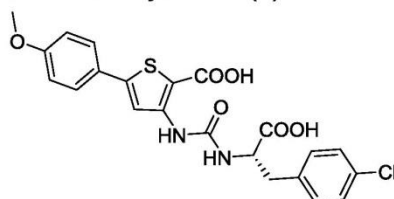
S9

(S)-3-(3-(1-Carboxy-2-(4-methoxyphenyl)ethyl)ureido)-5-(4-methoxyphenyl)thiophene-2-carboxylic (3).



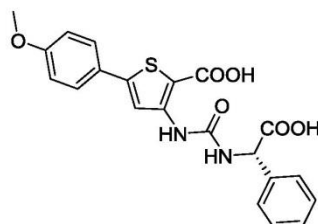
The title compound was prepared from **IVa** according to general procedure **D**. ^1H NMR (DMSO- d_6 , 300 MHz): δ = 12.83 (br. s., 2H), 9.41 (s, 1H), 8.12 (d, J = 8.01 Hz, 1H), 8.09 (s, 1H), 7.59 (d, J = 8.75 Hz, 2H), 7.19 (d, J = 8.50 Hz, 2H), 7.00 (d, J = 8.80 Hz, 2H), 6.86 (d, J = 8.57 Hz, 2H), 4.25–4.42 (m, 1H), 3.79 (s, 3H), 3.71 (s, 3H), 2.96–3.11 (m, 1H), 2.71–2.87 (m, 1H) ppm. ^{13}C NMR (DMSO- d_6 , 75 MHz): δ = 173.7, 164.6, 160.1, 157.9, 153.7, 147.1, 145.9, 130.1, 129.5, 127.1, 125.4, 116.7, 114.7, 113.7, 105.7, 55.3, 54.9, 54.7, 36.1 ppm. Melting point 154 °C. MS (ESI) m/z : 471.0 $[\text{M}+\text{H}]^+$

(S)-3-(3-(1-Carboxy-2-(4-chlorophenyl)ethyl)ureido)-5-(4-methoxyphenyl)thiophene-2-carboxylic acid (4).



The title compound was prepared from **IVa** according to general procedure **D**. ^1H NMR (DMSO- d_6 , 300 MHz): δ = 12.88 (br. s., 2H), 9.42 (s, 1H), 8.14 (d, J = 8.0 Hz, 1H), 8.08 (s, 1H), 7.59 (d, J = 8.8 Hz, 2H), 7.36 (d, J = 8.5 Hz, 2H), 7.29 (d, J = 8.5 Hz, 2H), 7.00 (d, J = 8.8 Hz, 2H), 4.29–4.47 (m, 1H), 3.79 (s, 3H), 3.03–3.15 (m, 1H), 2.80–2.97 (m, 1H) ppm. ^{13}C NMR (DMSO- d_6 , 75 MHz): δ = 173.4, 164.6, 160.1, 153.7, 147.2, 145.8, 136.7, 131.2, 131.0, 128.2, 127.1, 125.4, 116.7, 114.7, 105.8, 55.3, 54.2, 36.3 ppm. Melting point 190 °C. MS (ESI) m/z : 475.1 $[\text{M}+\text{H}]^+$

(S)-3-(3-(Carboxy(phenyl)methyl)ureido)-5-(4-methoxyphenyl)thiophene-2-carboxylic acid (5).

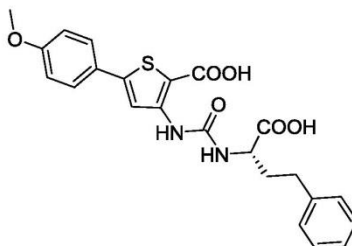


The title compound was prepared from **IVa** according to general procedure **D**. ^1H NMR (DMSO- d_6 , 300 MHz): δ = 12.90 (br. s., 2H), 9.55 (s, 1H), 8.60 (d, J = 7.0 Hz, 1H), 8.15 (s, 1H), 7.61 (d, J = 8.1 Hz, 2H), 7.25–7.53 (m, 5H), 7.01 (d, J = 8.1 Hz,

S10

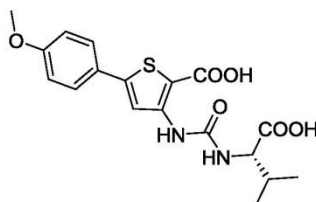
2H), 5.28 (d, $J = 7.0$ Hz, 1H), 3.80 (s, 3H) ppm. ^{13}C NMR (DMSO- d_6 , 75 MHz): $\delta = 172.4, 164.5, 160.1, 153.5, 147.1, 145.8, 137.4, 128.6, 128.0, 127.6, 127.1, 125.4, 116.9, 114.7, 106.1, 57.2, 55.3$ ppm. Melting point 186 °C. MS (ESI) m/z : 427.0 $[\text{M}+\text{H}]^+$

(S)-3-(3-(1-Carboxy-3-phenylpropyl)ureido)-5-(4-methoxyphenyl)thiophene-2-carboxylic acid (6).



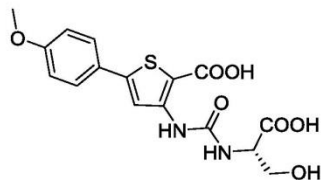
The title compound was prepared from **IVa** according to general procedure **D**. ^1H NMR (DMSO- d_6 , 300 MHz): $\delta = 12.82$ (br. s., 2H), 9.51 (s, 1H), 7.97–8.34 (m, 2H), 7.61 (d, $J = 8.5$ Hz, 2H), 7.12–7.39 (m, 5H), 7.01 (d, $J = 8.5$ Hz, 2H), 4.06–4.18 (m, 1H), 3.80 (s, 3H), 2.69 (t, $J = 7.1$ Hz, 2H), 1.76–2.16 (m, 2H) ppm. ^{13}C NMR (DMSO- d_6 , 75 MHz): $\delta = 174.2, 164.8, 160.1, 153.8, 147.3, 146.1, 141.0, 128.4, 128.3, 127.1, 126.0, 125.4, 116.7, 114.7, 105.6, 55.3, 52.3, 33.0, 31.5$ ppm. Melting point 163 °C. MS (ESI) m/z : 455.0 $[\text{M}+\text{H}]^+$

(S)-3-(3-(1-Carboxy-2-methylpropyl)ureido)-5-(4-methoxyphenyl)thiophene-2-carboxylic acid (7).



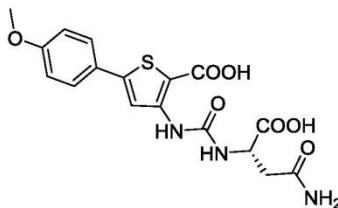
The title compound was prepared from **IVa** according to general procedure **D**. ^1H NMR (DMSO- d_6 , 300 MHz): $\delta = 12.72$ (br. s., 2H), 9.49 (s, 1H), 8.16 (s, 1H), 7.99 (d, $J = 8.4$ Hz, 1H), 7.60 (d, $J = 8.8$ Hz, 2H), 7.01 (d, $J = 8.8$ Hz, 2H), 4.07–4.15 (m, 1H), 3.80 (s, 3H), 2.04–2.17 (m, 1H), 0.85–1.01 (m, 6H) ppm. ^{13}C NMR (DMSO- d_6 , 75 MHz): $\delta = 173.6, 164.5, 160.0, 154.1, 147.0, 146.0, 127.1, 125.4, 117.0, 114.7, 105.8, 58.1, 55.3, 29.8, 19.2, 17.9$ ppm. Melting point 168 °C. MS (ESI) m/z : 392.9 $[\text{M}+\text{H}]^+$

(S)-3-(3-(1-Carboxy-2-hydroxyethyl)ureido)-5-(4-methoxyphenyl)thiophene-2-carboxylic acid (8).



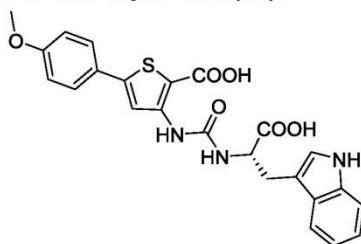
The title compound was prepared from **IVa** according to general procedure **D**. $^1\text{H NMR}$ (DMSO- d_6 , 300 MHz): δ = 12.77 (br. s., 2H), 9.50 (s, 1H), 8.01–8.23 (m, 2H), 7.60 (d, J = 8.8 Hz, 2H), 7.01 (d, J = 8.8 Hz, 2H), 5.00 (br. s., 1H), 4.17–4.29 (m, 1H), 3.80 (s, 3H), 3.62–3.77 (m, 2H) ppm. $^{13}\text{C NMR}$ (DMSO- d_6 , 75 MHz): δ = 172.5, 164.5, 160.0, 153.9, 147.0, 145.9, 127.0, 125.4, 116.9, 114.7, 105.9, 61.5, 55.5, 55.3 ppm. Melting point 185 °C. MS (ESI) m/z : 380.8 $[\text{M}+\text{H}]^+$

(S)-3-(3-(3-Amino-1-carboxy-3-oxopropyl)ureido)-5-(4-methoxyphenyl)thiophene-2-carboxylic acid (9).



The title compound was prepared from **IVa** according to general procedure **D**. $^1\text{H NMR}$ (DMSO- d_6 , 300 MHz): δ = 12.76 (br. s., 2H), 9.44 (s, 1H), 8.13 (s, 1H), 8.08 (d, J = 7.7 Hz, 1H), 7.61 (d, J = 8.8 Hz, 2H), 7.38 (br. s., 1H), 7.02 (d, J = 8.8 Hz, 2H), 6.92 (br. s., 1H), 4.40–4.56 (m, 1H), 3.80 (s, 3H), 2.55–2.64 (m, 1H), 2.45–2.55 (m, 1H) ppm. $^{13}\text{C NMR}$ (DMSO- d_6 , 75 MHz): δ = 173.4, 171.0, 164.6, 160.1, 153.6, 147.1, 146.0, 127.1, 125.4, 116.8, 114.7, 105.8, 55.3, 49.6, 37.0 ppm. Melting point 183 °C. MS (ESI) m/z : 407.9 $[\text{M}+\text{H}]^+$

(S)-3-(3-(1-Carboxy-2-(1H-indol-3-yl)ethyl)ureido)-5-(4-methoxyphenyl)thiophene-2-carboxylic acid (10).

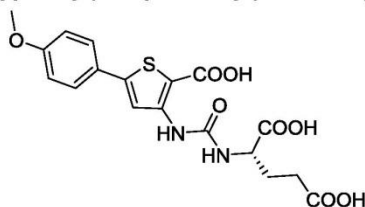


The title compound was prepared from **IVa** according to general procedure **D**. $^1\text{H NMR}$ (DMSO- d_6 , 300 MHz): δ = 12.80 (br. s., 2H), 10.85 (br. s., 1H), 9.43 (s, 1H), 8.15 (d, J = 7.7 Hz, 1H), 8.10 (s, 1H), 7.53–7.65 (m, 3H), 7.34 (d, J = 7.9 Hz, 1H), 7.17 (d, J = 2.0 Hz, 1H), 6.95–7.12 (m, 4H), 4.40–4.51 (m, 1H), 3.79 (s, 3H), 3.21

S12

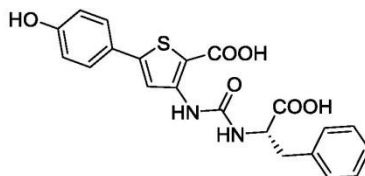
(dd, $J = 4.7, 14.7$ Hz, 1H), 3.03 (dd, $J = 9.0, 14.7$ Hz, 1H) ppm. ^{13}C NMR (DMSO- d_6 , 75 MHz): $\delta = 174.0, 164.6, 160.0, 153.7, 147.1, 145.9, 136.1, 127.1, 127.1, 125.4, 123.6, 120.9, 118.4, 118.1, 116.8, 114.7, 111.4, 109.9, 105.7, 55.3, 53.7, 27.3$ ppm. Melting point 173 °C. MS (ESI) m/z : 480.0 $[\text{M}+\text{H}]^+$

((2-Carboxy-5-(4-methoxyphenyl)thiophen-3-yl)carbamoyl)-L-glutamic acid (11).



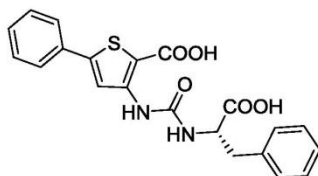
The title compound was prepared from **IVa** according to general procedure **D**. ^1H NMR (DMSO- d_6 , 300 MHz): $\delta = 12.59$ (br. s., 3H), 9.48 (s, 1H), 8.14 (s, 1H), 8.06 (d, $J = 7.64$ Hz, 1H), 7.61 (d, $J = 8.80$ Hz, 2H), 7.01 (d, $J = 8.85$ Hz, 2H), 4.10–4.23 (m, 1H), 3.80 (s, 3H), 2.23–2.44 (m, 2H), 1.93–2.07 (m, 1H), 1.72–1.89 (m, 1H) ppm. ^{13}C NMR (DMSO- d_6 , 75 MHz): $\delta = 173.9, 173.7, 164.8, 160.1, 153.8, 147.2, 146.0, 127.1, 125.4, 116.6, 114.7, 105.8, 55.4, 52.0, 30.1, 26.6$ ppm. Melting point 181 °C. MS (ESI) m/z : 423.0 $[\text{M}+\text{H}]^+$

(S)-3-(3-(1-Carboxy-2-phenylethyl)ureido)-5-(4-hydroxyphenyl)thiophene-2-carboxylic acid (12).



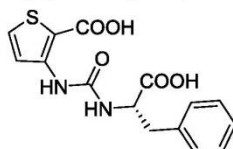
The title compound was prepared from **B** according to the following procedure: **B** (1 eq, 0.25 mmol) was filled in a crimp vial which was sealed afterwards. The vessel was evacuated and subsequently flushed with N_2 . This procedure was repeated three times. Anhydrous CH_2Cl_2 (5 mL) were added and the resulting solution was cooled to -78°C . BBr_3 (1 M solution in CH_2Cl_2 , 12 eq, 3.00 mmol) were added and the reaction was stirred for 48 h and allowed to warm to room temperature. Afterwards the reaction was cooled to -78°C again and quenched by the addition of MeOH (5 mL). After warming up to room temperature, 2 M HCl (5 mL) was added and the resulting mixture was extracted with EtOAc (3 x 20 mL). The organic layer was washed with brine (50 mL), dried (MgSO_4) and evaporated. The crude product was purified using preparative HPLC. ^1H NMR (DMSO- d_6 , 300 MHz): $\delta = 12.82$ (br. s., 2H), 9.87 (br. s., 1H), 9.41 (s, 1H), 8.14 (d, $J = 7.9$ Hz, 1H), 8.03 (s, 1H), 7.47 (d, $J = 8.5$ Hz, 2H), 7.14–7.35 (m, 5H), 6.82 (d, $J = 8.5$ Hz, 2H), 4.35–4.41 (m, 1H), 3.10 (dd, $J = 4.7, 13.9$ Hz, 1H), 2.87 (dd, $J = 9.7, 13.9$ Hz, 1H) ppm. ^{13}C NMR (DMSO- d_6 , 75 MHz): $\delta = 173.6, 164.6, 158.6, 153.7, 147.8, 145.9, 137.7, 129.0, 128.2, 127.1, 126.4, 123.8, 116.1, 116.0, 105.2, 54.4, 36.9$ ppm. Melting point 185 °C. MS (ESI) m/z : 426.8 $[\text{M}+\text{H}]^+$

(S)-3-(3-(1-Carboxy-2-phenylethyl)ureido)-5-phenylthiophene-2-carboxylic acid (13).



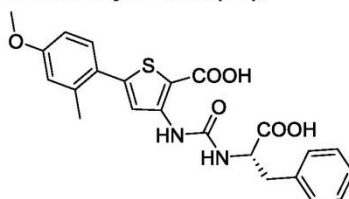
The title compound was prepared from **IVb** according to general procedure **D**. ^1H NMR (DMSO- d_6 , 300 MHz): δ = 12.89 (br. s., 2H), 9.42 (s, 1H), 8.21 (s, 1H), 8.17 (d, J = 7.9 Hz, 1H), 7.65 (d, J = 6.9 Hz, 2H), 7.36–7.54 (m, 3H), 7.16–7.35 (m, 5H), 4.33–4.47 (m, 1H), 3.10 (dd, J = 4.8, 13.9 Hz, 1H), 2.88 (dd, J = 9.7, 13.9 Hz, 1H) ppm. ^{13}C NMR (DMSO- d_6 , 75 MHz): δ = 173.6, 164.6, 153.7, 146.9, 145.7, 137.7, 132.7, 129.3, 129.2, 129.1, 128.2, 126.4, 125.6, 117.9, 106.9, 54.4, 37.0 ppm. Melting point 178 °C. MS (ESI) m/z : 411.0 $[\text{M}+\text{H}]^+$

(S)-3-(3-(1-Carboxy-2-phenylethyl)ureido)thiophene-2-carboxylic acid (14).



The title compound was prepared from **IVf** according to general procedure **D**. ^1H NMR (DMSO- d_6 , 300 MHz): δ = 12.84 (br. s., 2H), 9.38 (s, 1H), 8.10 (d, J = 8.0 Hz, 1H), 7.83 (d, J = 5.5 Hz, 1H), 7.69 (d, J = 5.5 Hz, 1H), 7.14–7.37 (m, 5H), 4.37 (dt, J = 3.4, 4.8 Hz, 1H), 3.09 (dd, J = 4.7, 13.9 Hz, 1H), 2.86 (dd, J = 9.7, 13.2 Hz, 1H) ppm. ^{13}C NMR (DMSO- d_6 , 75 MHz): δ = 173.6, 164.7, 153.7, 145.4, 137.7, 131.5, 129.0, 128.2, 126.4, 121.8, 107.8, 54.3, 37.0 ppm. Melting point 187 °C. MS (ESI) m/z : 335.0 $[\text{M}+\text{H}]^+$

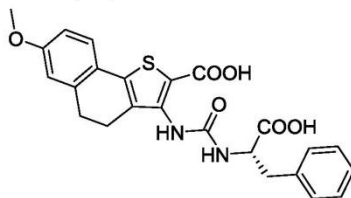
(S)-3-(3-(1-Carboxy-2-phenylethyl)ureido)-5-(4-methoxy-2-methylphenyl)thiophene-2-carboxylic acid (15).



The title compound was prepared from **IVg** according to general procedure **D**. ^1H NMR (DMSO- d_6 , 300 MHz): δ = 12.86 (br. s., 2H), 9.41 (s, 1H), 8.14 (d, J = 8.0 Hz, 1H), 7.86 (s, 1H), 7.33 (d, J = 8.6 Hz, 1H), 7.18–7.33 (m, 5H), 6.91 (d, J = 2.5 Hz, 1H), 6.84 (dd, J = 8.6, 2.6 Hz, 1H), 3.08 (dd, J = 14.1, 4.8 Hz, 1H), 2.86 (dd, J = 14.1, 9.7 Hz, 1H), 2.36 (s, 3H) ppm. ^{13}C NMR (DMSO- d_6 , 75 MHz): δ = 173.6, 164.6, 159.5, 153.7, 146.7, 145.0, 137.7, 137.0, 130.8, 129.0, 128.2, 126.4, 125.1, 120.9, 116.4, 111.9, 106.7, 55.2, 54.4, 36.9, 20.9 ppm. Melting point 119 °C. MS (ESI) m/z : 454.7 $[\text{M}+\text{H}]^+$

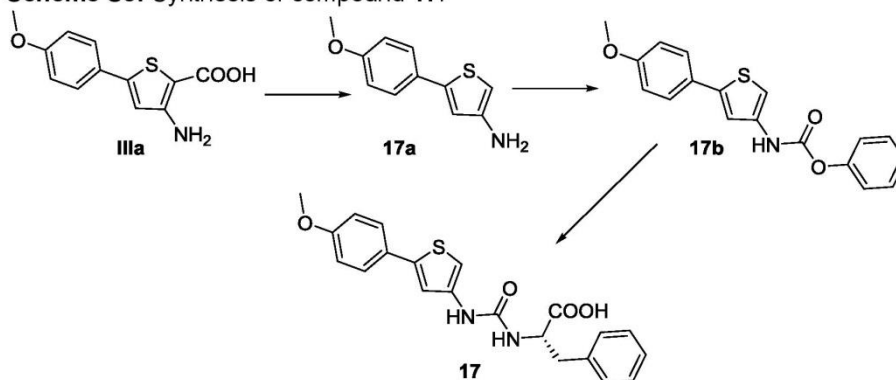
S14

(S)-3-(3-(1-Carboxy-2-phenylethyl)ureido)-7-methoxy-4,5-dihydronaphtho[1,2-*b*]thiophene-2-carboxylic acid (16).



The title compound was prepared from **IVc** according to general procedure **D**. ^1H NMR (DMSO- d_6 , 300 MHz): δ = 12.83 (br. s., 2H), 8.70 (s, 1H), 7.47 (d, J = 8.3 Hz, 1H), 7.34 (d, J = 8.3 Hz, 1H), 7.19–7.32 (m, 4H), 6.89 (d, J = 2.3 Hz, 1H), 6.83 (dd, J = 2.4, 8.3 Hz, 1H), 4.35–4.49 (m, 1H), 3.78 (s, 3H), 3.10 (dd, J = 4.7, 13.7 Hz, 1H), 2.88 (dd, J = 8.7, 13.7 Hz, 1H), 2.76 (app t, J = 7.6 Hz, 2H), 2.25–2.45 (m, 2H) ppm. ^{13}C NMR (DMSO- d_6 , 75 MHz): δ = 173.4, 164.0, 159.7, 154.0, 143.0, 139.3, 137.9, 137.4, 132.8, 129.3, 128.2, 126.4, 124.4, 123.1, 113.8, 112.5, 111.8, 55.2, 54.1, 37.6, 28.5, 23.3 ppm. Melting point 185 °C. MS (ESI) m/z : 466.8 $[\text{M}+\text{H}]^+$

Scheme S3: Synthesis of compound 17:



5-(4-Methoxyphenyl)thiophen-3-amine (17a) was prepared from **IIIa** according to the following procedure: To a solution of **IIIa** (4.4 mmol) in CH_2Cl_2 , was added HCl (2 M aq, 10 mL). The resulting mixture was heated to 80 °C for 18 h. The reaction was cooled to room temperature and alkalinized with 2 M KOH. The aqueous layer was extracted with CH_2Cl_2 (3 x 50 mL). The organic phase was washed with brine (1 x 100 mL), dried (MgSO_4) and evaporated to yield the title compound which was used in the next step without further purification.

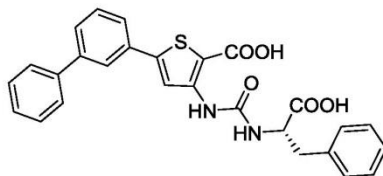
Phenyl (5-(4-methoxyphenyl)thiophen-3-yl)carbamate (17b) was prepared from **17a** according to the following procedure: To a solution of **17a** (3.4 mmol) in anhydrous CH_2Cl_2 (30 mL), pyridine (3.4 mmol) was added and the resulting mixture was cooled to 0 °C. Phenyl chloroformate (3.4 mmol) was added dropwise at 0 °C. The reaction was allowed to warm to room temperature and stirred until the reaction was completed (checked by TLC). The solvent was evaporated and the residue was suspended in ice water. After acidification with a saturated KHSO_4 solution, the aqueous layer was extracted with CH_2Cl_2 (3 x 50 mL). The organic phase was

S15

washed with an ice cold half saturated KHSO_4 solution (2 x 50 mL) and brine (1 x 50 mL), dried (MgSO_4) and evaporated to yield the title compound which was sufficiently pure to be used in the next step without further purification.

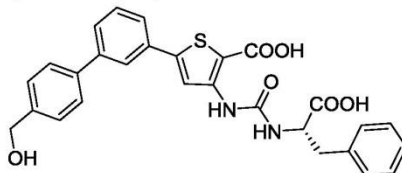
((5-(4-Methoxyphenyl)thiophen-3-yl)carbamoyl)-L-phenylalanine (17): The title compound was prepared from **17b** according to the following procedure: **17b** (1eq), triethylamine and L-phenylalanine were dissolved in anhydrous DMSO (7 mL) and stirred at 50°C for 50 h until the reaction was completed. The reaction mixture was poured into a mixture of concentrated HCl and ice (1:1) and extracted with EtOAc/THF (1:1, 60 mL). The organic layer was washed with aqueous HCl (2 M), followed by saturated aqueous NaCl (2 x 50 mL), dried (MgSO_4) and concentrated. The crude material was suspended in a mixture of *n*-hexane/EtOAc (2:1, 20 mL) heated to 50 °C and after cooling to room temperature separated *via* filtration. ^1H NMR (DMSO-d_6 , 300 MHz): δ = 12.78 (br. s., 1H), 8.90 (s, 1H), 7.51 (d, J = 8.8 Hz, 2H), 7.18–7.35 (m, 5H), 7.14 (d, J = 1.3 Hz, 1H), 7.03 (d, J = 1.3 Hz, 1H), 6.97 (d, J = 8.8 Hz, 2H), 6.35 (d, J = 8.0 Hz, 1H), 4.45 (dt, J = 5.2, 7.7 Hz, 1H), 3.78 (s, 3H), 3.03–3.16 (m, 1H), 2.87–3.03 (m, 1H) ppm. ^{13}C NMR (DMSO-d_6 , 75 MHz): δ = 173.5, 158.9, 154.5, 141.1, 138.2, 137.3, 129.2, 128.2, 126.5, 126.4, 126.3, 116.1, 114.5, 103.4, 55.2, 53.7, 37.3 ppm. Melting point 189 °C. MS (ESI) m/z : 397.0 $[\text{M}+\text{H}]^+$

(S)-5-([1,1'-Biphenyl]-3-yl)-3-(3-(1-carboxy-2-phenylethyl)ureido)thiophene-2-carboxylic acid (18).



The title compound was prepared from **Va** according to general procedure **E**. ^1H NMR (DMSO-d_6 , 500 MHz): δ = 12.90 (br. s., 2H), 9.44 (s, 1H), 8.28 (s, 1H), 8.19 (d, J = 7.9 Hz, 1H), 7.84 (t, J = 1.7 Hz, 1H), 7.71–7.75 (m, 2H), 7.69 (td, J = 1.7, 7.8 Hz, 1H), 7.65 (td, J = 1.7, 7.8 Hz, 1H), 7.53–7.57 (m, 1H), 7.47–7.52 (m, 2H), 7.39–7.43 (m, 1H), 7.26–7.33 (m, 4H), 7.20–7.24 (m, 1H), 4.40 (ddd, J = 4.7, 7.9, 9.7 Hz, 1H), 3.11 (dd, J = 4.7, 14.0 Hz, 1H), 2.88 (dd, J = 9.7, 14.0 Hz, 1H) ppm. ^{13}C NMR (DMSO-d_6 , 125 MHz): δ = 173.6, 164.6, 153.7, 146.7, 145.7, 141.3, 139.4, 137.7, 133.4, 130.0, 129.1, 129.0, 128.2, 127.9, 127.6, 126.9, 126.4, 124.8, 123.7, 118.3, 107.1, 54.4, 37.0 ppm. Melting point 185 °C. MS (ESI) m/z : 487.0 $[\text{M}+\text{H}]^+$

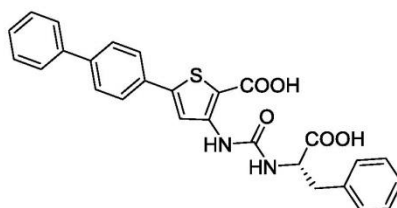
(S)-3-(3-(1-Carboxy-2-phenylethyl)ureido)-5-(4'-(hydroxymethyl)-[1,1'-biphenyl]-3-yl)thiophene-2-carboxylic acid (19).



S16

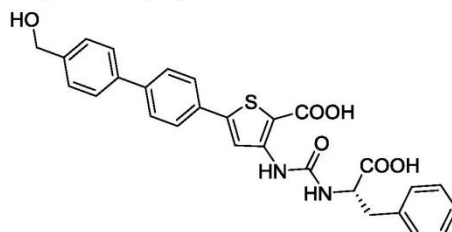
The title compound was prepared from **Va** according to general procedure **E**. ¹H NMR (DMSO-d₆, 500 MHz): δ = 12.99 (br. s., 2H), 9.44 (s, 1H), 8.28 (s, 1H), 8.19 (d, *J* = 7.9 Hz, 1H), 7.84 (t, *J* = 1.7 Hz, 1H), 7.67–7.71 (m, 3H), 7.62–7.65 (m, 1H), 7.51–7.56 (m, 1H), 7.43 (d, *J* = 8.5 Hz, 2H), 7.26–7.33 (m, 4H), 7.19–7.24 (m, 1H), 4.56 (s, 2H), 4.40 (ddd, *J* = 4.7, 8.1, 9.8 Hz, 1H), 3.11 (dd, *J* = 4.7, 13.9 Hz, 1H), 2.88 (dd, *J* = 9.8, 13.9 Hz, 1H) ppm. ¹³C NMR (DMSO-d₆, 125 MHz): δ = 173.6, 164.6, 153.7, 146.8, 145.7, 142.3, 141.2, 137.7, 137.7, 133.4, 130.0, 129.1, 128.2, 127.5, 127.1, 126.6, 126.4, 124.6, 123.6, 118.3, 107.1, 62.6, 54.4, 37.0 ppm. Melting point 176 °C. MS (ESI) *m/z*: 517.0 [M+H]⁺

(S)-5-([1,1'-Biphenyl]-4-yl)-3-(3-(1-carboxy-2-phenylethyl)ureido)thiophene-2-carboxylic acid (20).



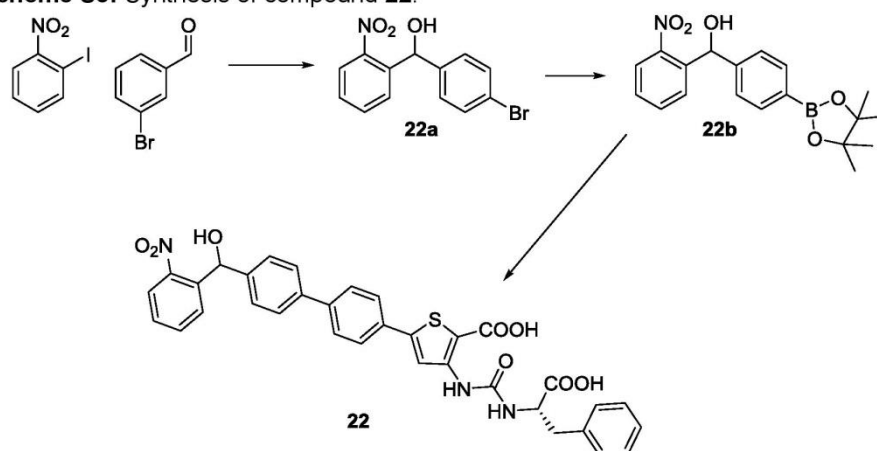
The title compound was prepared from **Vb** according to general procedure **E**. ¹H NMR (DMSO-d₆, 500 MHz): δ = 12.90 (br. s, 2H), 9.45 (s, 1H), 8.26 (s, 1H), 8.19 (d, *J* = 8.0 Hz, 1H), 7.73–7.78 (m, 4H), 7.69–7.73 (m, 2H), 7.46–7.51 (m, 2H), 7.37–7.41 (m, 1H), 7.27–7.33 (m, 4H), 7.19–7.24 (m, 1H), 4.41 (ddd, *J* = 4.8, 8.0, 9.7 Hz, 1H), 3.11 (dd, *J* = 4.8, 13.9 Hz, 1H), 2.89 (dd, *J* = 9.7, 13.9 Hz, 1H) ppm. ¹³C NMR (DMSO-d₆, 125 MHz): δ = 173.6, 164.6, 153.7, 146.4, 145.8, 140.7, 139.1, 137.7, 131.8, 129.0, 129.0, 128.2, 127.8, 127.4, 126.5, 126.4, 126.1, 117.9, 107.0, 54.4, 36.9 ppm. Melting point 185 °C. MS (ESI) *m/z*: 486.4 [M+H]⁺

(S)-3-(3-(1-Carboxy-2-phenylethyl)ureido)-5-(4'-(hydroxymethyl)-[1,1'-biphenyl]-4-yl)thiophene-2-carboxylic acid (21).



The title compound was prepared from **Vb** according to general procedure **E**. ¹H NMR (DMSO-d₆, 500 MHz): δ = 12.97 (br. s, 2H), 9.44 (s, 1H), 8.25 (s, 1H), 8.19 (d, *J* = 7.9 Hz, 1H), 7.76 (d, *J* = 8.7 Hz, 2H), 7.73 (d, *J* = 8.7 Hz, 2H), 7.68 (d, *J* = 8.2 Hz, 2H), 7.42 (d, *J* = 8.2 Hz, 2H), 7.26–7.33 (m, 4H), 7.19–7.24 (m, 1H), 4.55 (s, 2H), 4.35–4.45 (m, 1H), 3.11 (dd, *J* = 4.7, 14.0 Hz, 1H), 2.88 (dd, *J* = 9.8, 14.0 Hz, 3H) ppm. ¹³C NMR (DMSO-d₆, 125 MHz): δ = 173.6, 164.6, 153.7, 146.5, 145.8, 142.3, 140.6, 137.7, 137.4, 131.6, 129.1, 128.2, 127.3, 127.1, 126.4, 126.2, 126.1, 117.8, 106.8, 62.6, 54.4, 37.0 ppm. Melting point 117 °C. MS (ESI) *m/z*: 516.9 [M+H]⁺

Scheme S3: Synthesis of compound **22**:



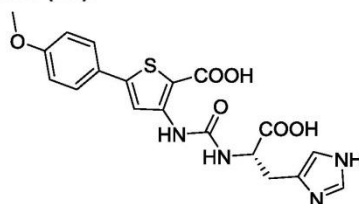
(4-Bromophenyl)(2-nitrophenyl)methanol (22a) was prepared according to the following procedure: A solution of 2-iodo-nitrobenzene (1.0 eq) in THF (10 mL/g reagent) was cooled to $-40\text{ }^{\circ}\text{C}$ and a solution of phenylmagnesium chloride (2 M in THF, 1.1 eq) was added dropwise. The solution was stirred for 30 min at $-40\text{ }^{\circ}\text{C}$, 3-bromobenzaldehyde was added and the reaction was completed at $-40\text{ }^{\circ}\text{C}$ (checked by TLC). The mixture was quenched with a saturated solution of NH_4Cl (5 mL) and diluted with water (5 mL). The aqueous phase was extracted with ethyl acetate (three times) and the combined organic layers were washed with brine, dried, and concentrated under reduced pressure. The residue was purified by column chromatography over silica gel to yield the desired product. $^1\text{H NMR}$ (CDCl_3 , 300 MHz): $\delta = 7.81$ (dd, $J = 1.3, 7.8$ Hz, 1H), 7.57 (dd, $J = 1.3, 7.8$ Hz, 1H), 7.52 (td, $J = 1.3, 7.8$ Hz, 1H), 7.32 (d, $J = 8.6$ Hz, 2H), 7.37 (td, $J = 1.3, 7.8$ Hz, 1H), 7.07 (d, $J = 8.6$ Hz, 2H), 6.23 (d, $J = 4.4$ Hz, 1H), 3.14 (d, $J = 4.4$ Hz, 1H) ppm. $^{13}\text{C NMR}$ (CDCl_3 , 75 MHz): $\delta = 148.0, 140.4, 137.9, 133.5, 131.5, 129.2, 128.7, 128.6, 124.7, 121.9, 70.7$ ppm.

(2-Nitrophenyl)(4-(4,4,5,5-tetramethyl-1,3,2-dioxaborolan-2-yl)phenyl)methanol (22b) was prepared from **22a** according to the following procedure: **22a** (1 eq), bis(pinakolato)diboron (1.2 eq) and potassium acetate (3 eq) were dissolved in anhydrous 1,4-dioxane (20 mL). The system was evacuated and subsequently flushed with nitrogen three times. [1,1'-Bis(diphenylphosphino)ferrocene]dichloro palladium (0.05 eq) was added and the resulting mixture was heated to $85\text{ }^{\circ}\text{C}$ for 24 h. The reaction was cooled to room temperature and the solvent was evaporated. The residue was dissolved in EtOAc (150 mL), the organic layer was washed with H_2O (1 x 100 mL) and brine (1 x 100 mL) and dried (MgSO_4). The solvent was evaporated and the crude product was purified by flash column chromatography (EtOAc/ hexane 1:6) to yield the title compound. $^1\text{H NMR}$ (CDCl_3 , 300 MHz): $\delta = 7.90$ (dd, $J = 1.3, 8.2$ Hz, 1H), 7.77 (d, $J = 8.0$ Hz, 2H), 7.68 (dd, $J = 1.3, 7.6$ Hz, 1H), 7.59 (dt, $J = 1.3, 7.6$ Hz, 1H), 7.42 (ddd, $J = 1.3, 7.6, 8.2$ Hz, 1H), 7.32 (d, $J = 8.0$ Hz, 2H), 6.41 (d, $J = 4.4$ Hz, 1H), 3.26 (d, $J = 4.4$ Hz, 1H), 1.33 (s, 12H) ppm. $^{13}\text{C NMR}$ (CDCl_3 , 75 MHz): $\delta = 148.3, 144.5, 138.3, 134.9, 133.3, 129.5, 128.4, 126.1, 124.6, 83.8, 71.2, 24.8$ ppm.

S18

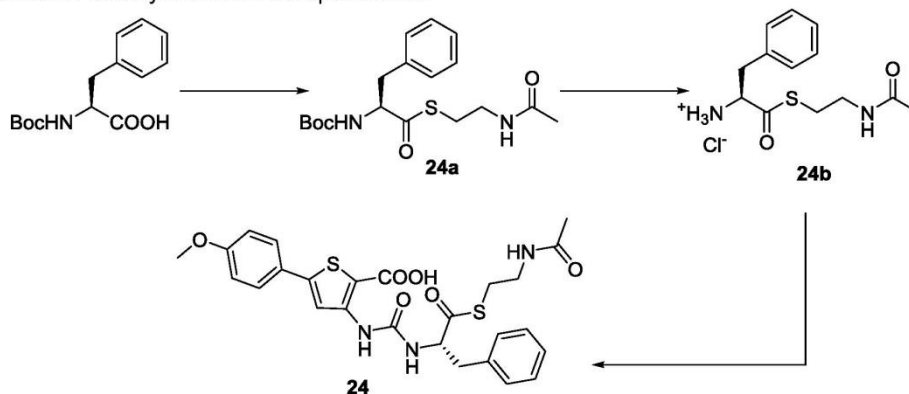
3-(3-((S)-1-Carboxy-2-phenylethyl)ureido)-5-(4'-(hydroxy(2-nitrophenyl)methyl)-[1,1'-biphenyl]-4-yl)thiophene-2-carboxylic acid (22) The title compound was prepared from **Va** and **22b** according to general procedure **E**. $^1\text{H NMR}$ (300 MHz, acetone- d_6): δ = 9.53 (s, 1H), 8.40 (s, 1H), 7.98 (dd, J = 1.2, 7.9 Hz, 1H), 7.93 (dd, J = 1.2, 8.2 Hz, 1H), 7.74–7.84 (m, 5H), 7.70 (d, J = 8.2 Hz, 2H), 7.53–7.60 (m, 1H), 7.47 (d, J = 8.2 Hz, 2H), 7.40 (d, J = 7.9 Hz, 1H), 7.26–7.37 (m, 4H), 7.18–7.25 (m, 1H), 6.51 (s, 1H), 4.69–4.80 (m, 1H), 3.29 (dd, J = 5.0, 14.0 Hz, 1H), 3.07 (dd, J = 8.85, 14.0 Hz, 1H) ppm. $^{13}\text{C NMR}$ (75 MHz, acetone- d_6): δ = 173.8, 165.6, 154.7, 149.5, 148.8, 148.1, 143.9, 142.1, 140.1, 140.0, 138.6, 134.1, 133.4, 130.3, 130.0, 129.3, 129.3, 128.7, 128.5, 127.6, 127.5, 127.3, 125.0, 118.9, 107.1, 70.8, 55.5, 38.6 ppm. Melting point 185 °C. MS (ESI) m/z : 637.9 $[\text{M}+\text{H}]^+$

(S)-3-(3-(1-Carboxy-2-(1H-imidazol-4-yl)ethyl)ureido)-5-(4-methoxyphenyl)thiophene-2-carboxylic acid (23).



The title compound was prepared from **IVa** according to general procedure **D**. $^1\text{H NMR}$ (DMSO- d_6 , 300 MHz): δ = 9.59 (br. s., 1H), 8.10 (d, J = 7.7 Hz, 1H), 8.00 (s, 1H), 7.82 (d, J = 0.7 Hz, 1H), 7.50 (d, J = 8.9 Hz, 2H), 6.88–6.95 (m, 3H), 4.27–4.41 (m, 1H), 3.71 (s, 3H), 2.98 (dd, J = 4.7, 15.0 Hz, 1H), 2.83 (dd, J = 9.3, 15.0 Hz, 1H) ppm. $^{13}\text{C NMR}$ (DMSO- d_6 , 75 MHz): δ = 173.5, 165.5, 159.9, 153.8, 146.0, 144.9, 134.3, 132.6, 126.9, 125.7, 116.9, 116.7, 114.7, 108.2, 55.3, 53.2, 28.5 ppm. Melting point 210 °C. MS (ESI) m/z : 430.9 $[\text{M}+\text{H}]^+$

Scheme S4: Synthesis of compound **24**:



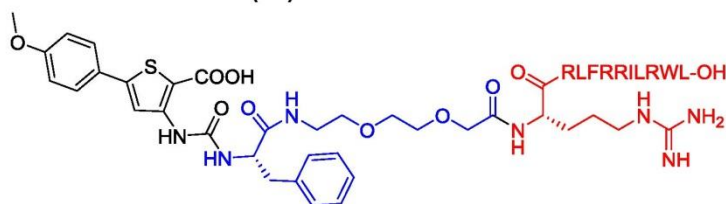
S-(2-Acetamidoethyl)(S)-2-((tert-butoxycarbonyl)amino)-3-phenylpropane thioate (24a) was prepared according to the following procedure:[7] A solution of boc-L-phenylalanine (400 mg, 1.50 mmol), N-acetylcysteamine (215 mg, 1.80 mmol) and DMAP (18.3 mg, 0.15 mmol) in anhydrous CH_2Cl_2 (10 mL) was cooled to 0°C.

S19

DCC (371 mg, 1.80 mmol), dissolved in CH₂Cl₂ (10 mL) was added dropwise and the ice bath was removed afterwards. Stirring was continued for 48 h until the reaction was completed. The solids were filtered off and rinsed with cold CH₂Cl₂ (10 mL). The filtrate was washed with 1 M HCl (30 mL), a saturated NaHCO₃ solution (30 mL), H₂O (30 mL) and brine (30 mL). After drying (MgSO₄), the solvent was evaporated and the residue was purified via column flash chromatography (100% EtOAc) to yield the desired product. ¹H NMR (Acetone-*d*₆, 300 MHz): δ = 7.18–7.35 (m, 5H), 6.63 (d, *J* = 8.5 Hz, 1H), 4.46 (ddd, *J* = 4.5, 8.5, 10.2 Hz, 1H), 3.33 (q, *J* = 6.9 Hz, 2H), 3.21 (dd, *J* = 4.5, 14.1 Hz, 1H), 2.98 (t, *J* = 6.9 Hz, 2H), 2.87–2.95 (m, 1H), 1.88 (s, 3H), 1.34 (s, 9H) ppm.

(S)-1-((2-Acetamidoethyl)thio)-1-oxo-3-phenylpropan-2-amonium chloride (24b) was prepared from **24a** according to the following procedure:[8] A solution of **24a** (475 mg, 1.30 mmol) in anhydrous CH₂Cl₂ (5 mL) was cooled to 0 °C. TFA (1.30 mL) was added very slowly and the resulting mixture was stirred at 0 °C for 2 h. The mixture was concentrated to about 2 mL, then diluted with 2 mL CH₂Cl₂ and again concentrated. This cycle was repeated three times and afterwards, the entire solvent was evaporated. The residue was dissolved in EtOAc (30 mL) and the resulting organic layer was washed with 1 M NaOH (10 mL). The solvent was evaporated again and the residue was treated with H₂O (2 mL) and 2 M HCl (2 mL). After washing the aqueous phase with EtOAc (2 x 2 mL), it was lyophilized to yield the title compound. ¹H NMR (DMSO-*d*₆, 300 MHz): δ = 7.23–7.37 (m, 5H), 7.13 (br. s., 3H), 4.34–4.49 (m, 1H), 3.04–3.28 (m, 4H), 2.90–3.00 (m, 2H), 1.79 (s, 3H) ppm. ¹³C NMR (DMSO-*d*₆, 75 MHz): δ = 196.0, 169.4, 134.4, 129.6, 128.6, 127.3, 59.5, 37.7, 36.8, 28.3, 22.5 ppm.

(S)-3-(3-(1-((2-Acetamidoethyl)thio)-1-oxo-3-phenylpropan-2-yl)ureido)-5-(4-methoxyphenyl)thiophene-2-carboxylic acid (24) The title compound was prepared from **24b** according to the following procedure: **24b** (52.0 mg, 0.19 mmol) and **Via** (63.0 mg, 0.21 mmol) were mixed in a reaction vial and capped. The system was evacuated and subsequently flushed with N₂. This cycle was repeated five times. Anhydrous DMSO (2 mL) was added and the reactants were dissolved under stirring. Anhydrous triethylamine (42.5 mg, 0.42 mmol) was added dropwise with a Hamilton syringe and the resulting mixture was stirred at room temperature for 2 h. The reaction mixture was poured into a mixture of concentrated HCl and ice (1:1, 50 mL) and extracted with EtOAc/THF (1:1, 3 x 60 mL). The organic layer was washed with 2 M HCl (2 x 50 mL), followed by brine (1 x 50 mL), dried (MgSO₄) and concentrated. The crude material was purified using preparative HPLC. ¹H NMR (500 MHz, DMSO-*d*₆): δ = 13.09 (br. s., 1H), 9.51 (s, 1H), 8.54 (d, *J* = 7.6 Hz, 1H), 8.07 (s, 1H), 8.03 (t, *J* = 5.5 Hz, 1H), 7.59 (d, *J* = 8.8 Hz, 2H), 7.26–7.33 (m, 4H), 7.18–7.25 (m, 1H), 7.00 (d, *J* = 8.8 Hz, 2H), 4.53 (ddd, *J* = 4.6, 7.7, 10.4 Hz, 1H), 3.79 (s, 3H), 3.07–3.21 (m, 3H), 2.80–2.95 (m, 3H), 1.78 (s, 3H) ppm. ¹³C NMR (125 MHz, DMSO-*d*₆): δ = 201.4, 169.2, 164.7, 160.1, 153.4, 147.4, 145.6, 137.2, 129.0, 128.3, 127.1, 126.6, 125.2, 116.5, 114.7, 106.0, 61.4, 55.3, 38.1, 37.0, 27.9, 22 ppm. Melting point 175 °C. MS (ESI) *m/z*: 541.8 [M+H]⁺

IVa-Phe-O2Oc-RRLFRRILRWL (25).

The title compound was prepared from **IV** in three steps. Firstly, the cell penetrating peptide main sequence (red) was produced using automated solid-phase peptide synthesis (SPPS). The linker (blue) was subsequently introduced *via* manual Fmoc-SPPS. In the last step, the whole peptide sequence was coupled with **IVa**.

Protocol for automated SPPS: The cell penetrating peptide main sequence (RRLFRRILRWL) was synthesized on a 100 μ mol scale on a Rapp S RAM resin linked with an amide bond to the peptide using a Syro I multiple peptide synthesizer (MultiSynTech, Witten, Germany), equipped with a reaction block containing 96 individual polypropylene reaction vessels of 1.4 mL volume with a polyethylene frit, arranged in a microtiter plate format.

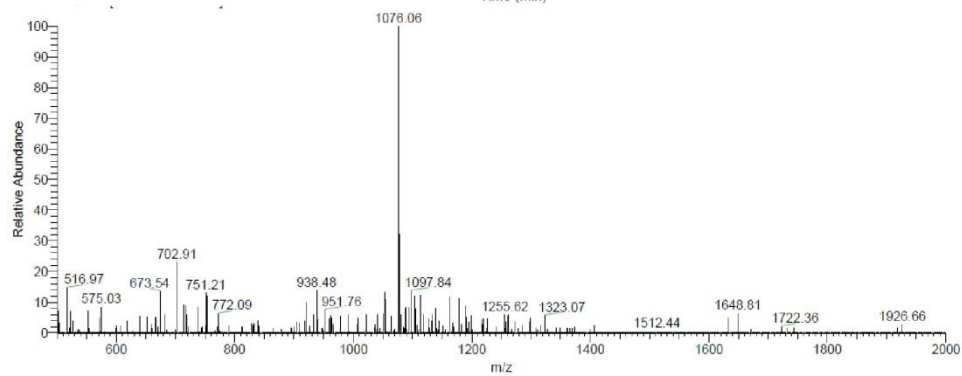
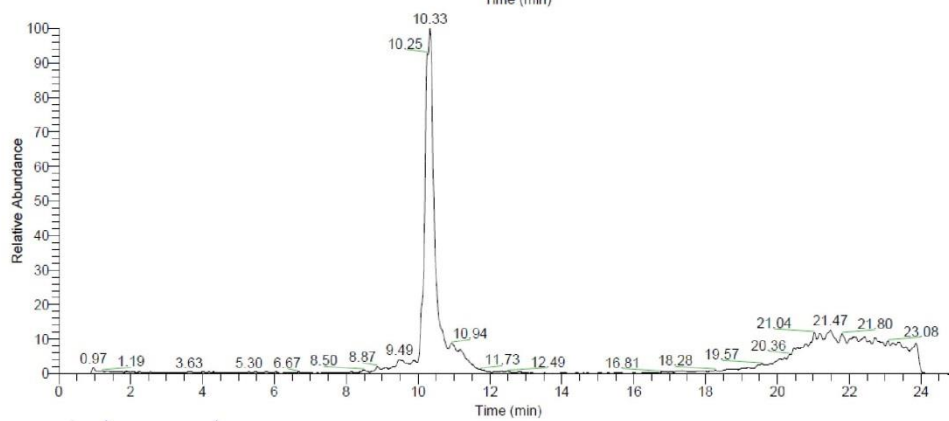
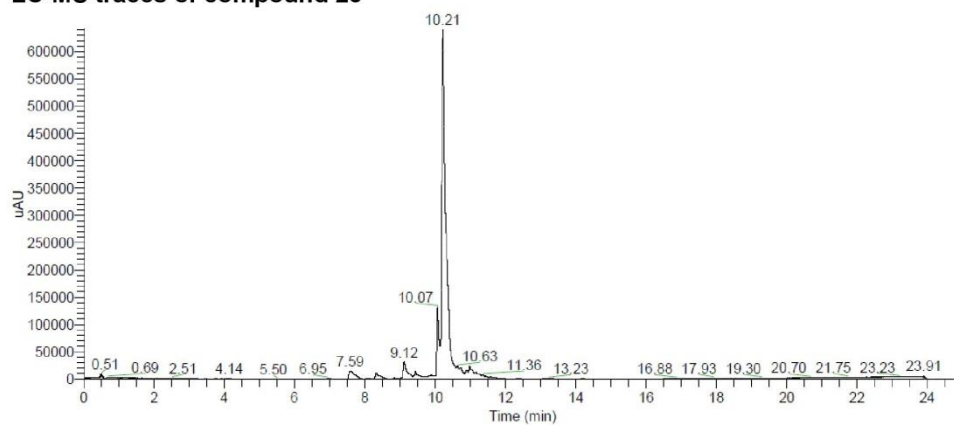
General Protocol for manual Fmoc-SPPS: 4.0 eq of the Fmoc-protected amino acid (scaled to the resin loading) and 3.9 eq of the coupling reagent (HATU) were dissolved in a minimal amount of DMF. Then, 8.0 eq DIEA were added for activation. After 15 min of pre-activation, the resulting mixture was added to the *N*-terminal deprotected peptide resin for 45 min. Excess reagents were removed by filtration and the peptide resin was washed thoroughly. These steps were repeated 3 times. The aforementioned steps were utilized for coupling of the O2Oc linker (8-amino-3,6-dioxa-octanoic acid) followed by phenylalanine. After each coupling step a micro cleavage was performed, in which the resins were washed with DMF (7 x), CH_2Cl_2 (3 x), and Et_2O (3 x), then stored in a desiccator and dried under vacuum. To cleave the assembled peptide off the resin and to achieve full deprotection of the amino acid side chain, the peptide resin was treated with a mixture of TFA/ H_2O /TIS 95:3:2 v/v for 3 h. The cleaved peptide was precipitated in cold MTBE, centrifuged and washed with MTBE (3x). Afterwards, the crude peptide was stored in a desiccator and dried under vacuum. Finally, the resulting peptide was injected into ESI-MS for mass determination (see below).

For the coupling of **IVa**, the same steps were performed except 2 eq. of **IVa** was used and no coupling agent was added as **IVa** innately possesses an activated asymmetric anhydride. The final conjugate was isolated using preparative HPLC. Melting point 199 °C.

Sequence	Expected mass [M+2H] ⁺	ESI-MS [M+2H] ⁺
RRLFRRILRWL	792.51	792.45
O2Oc-RRLFRRILRWL	865.54	865.07
Phe-O2Oc-RRLFRRILRWL	939.08	938.57
IVa-Phe-O2Oc-RRLFRRILRWL (25)	1077.59	1076.24

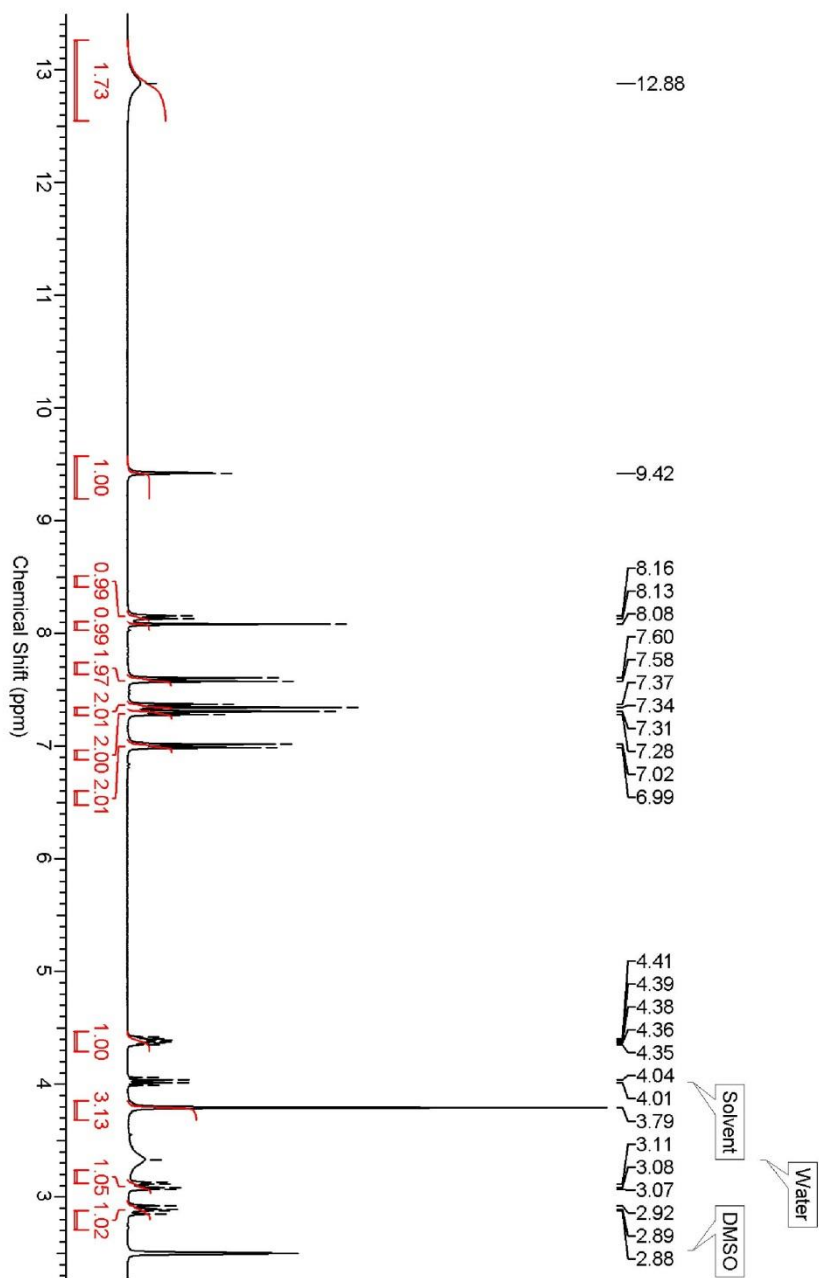
S21

LC-MS traces of compound 25



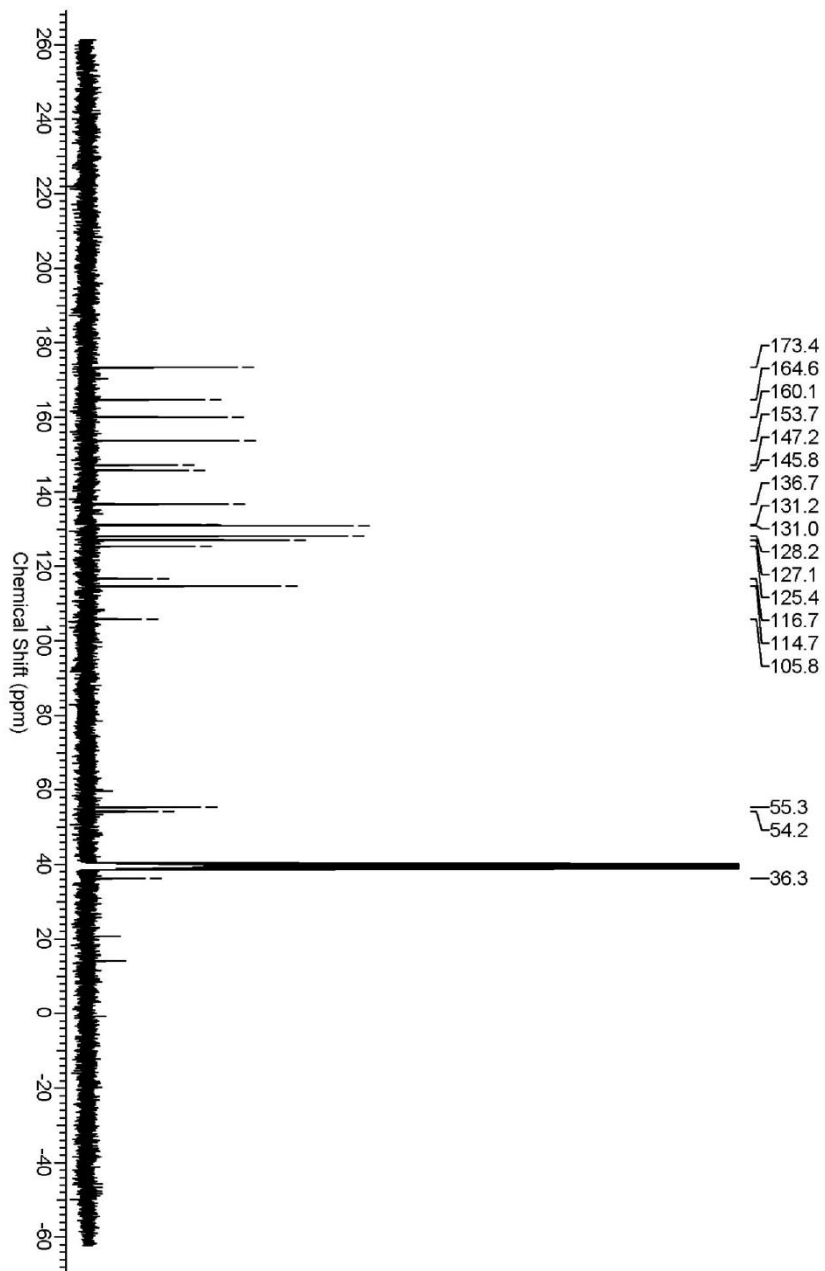
S22

¹H-NMR spectrum of compound 4

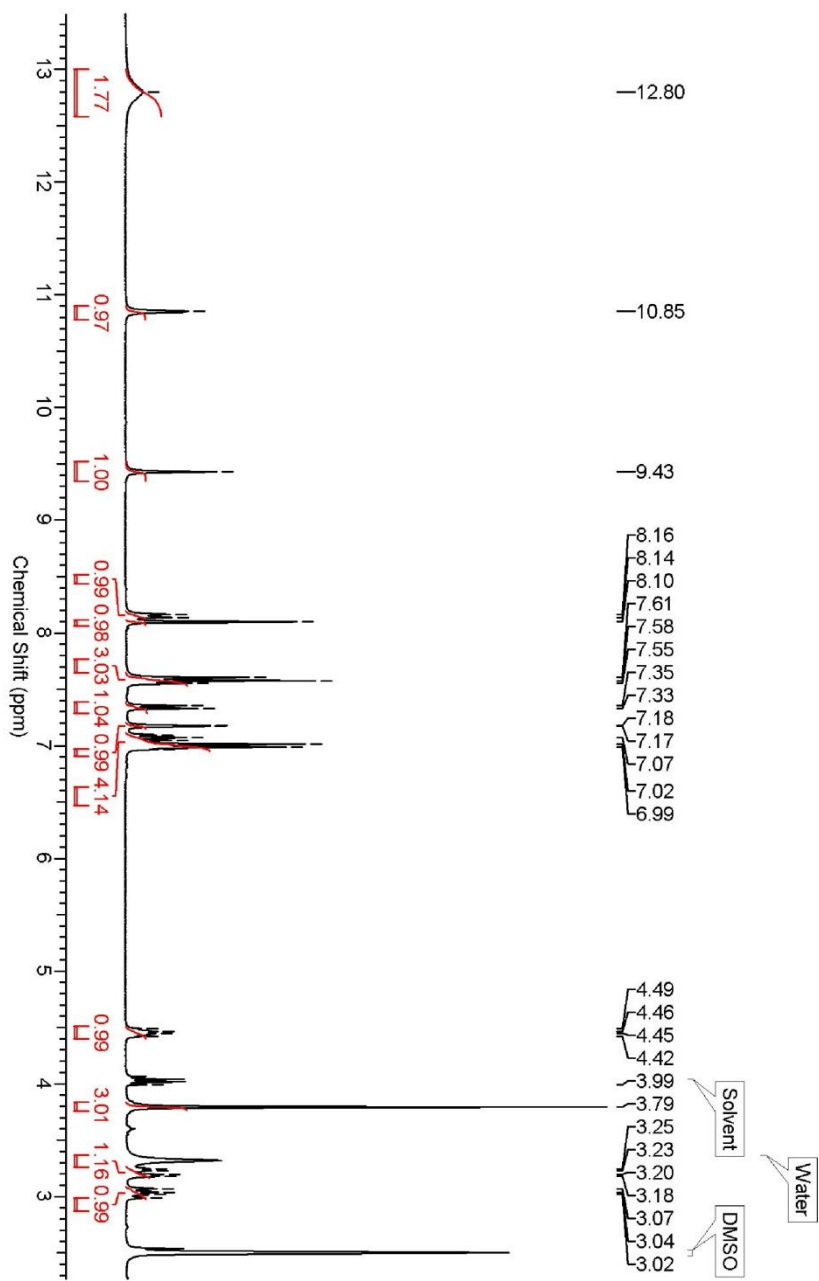


S23

¹³C-NMR spectrum of compound 4

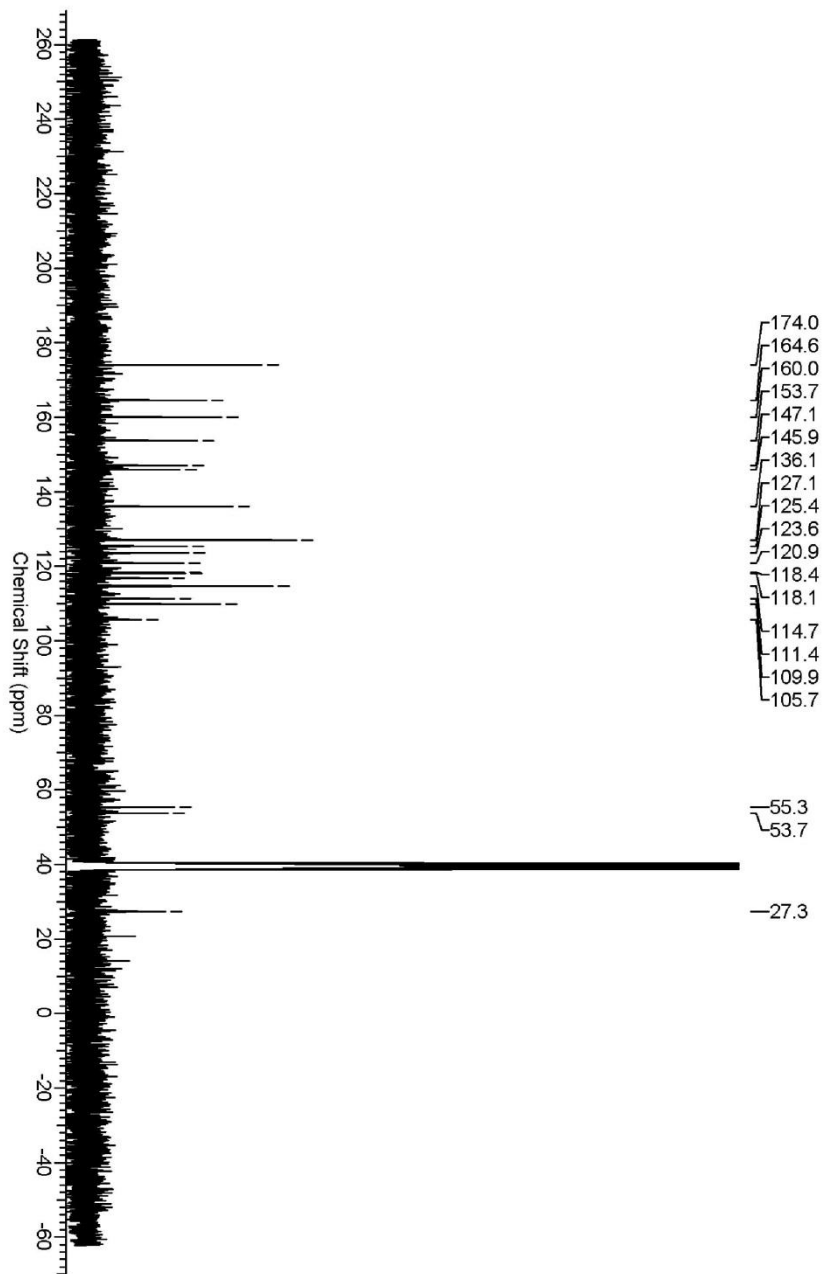


¹H-NMR spectrum of compound 10

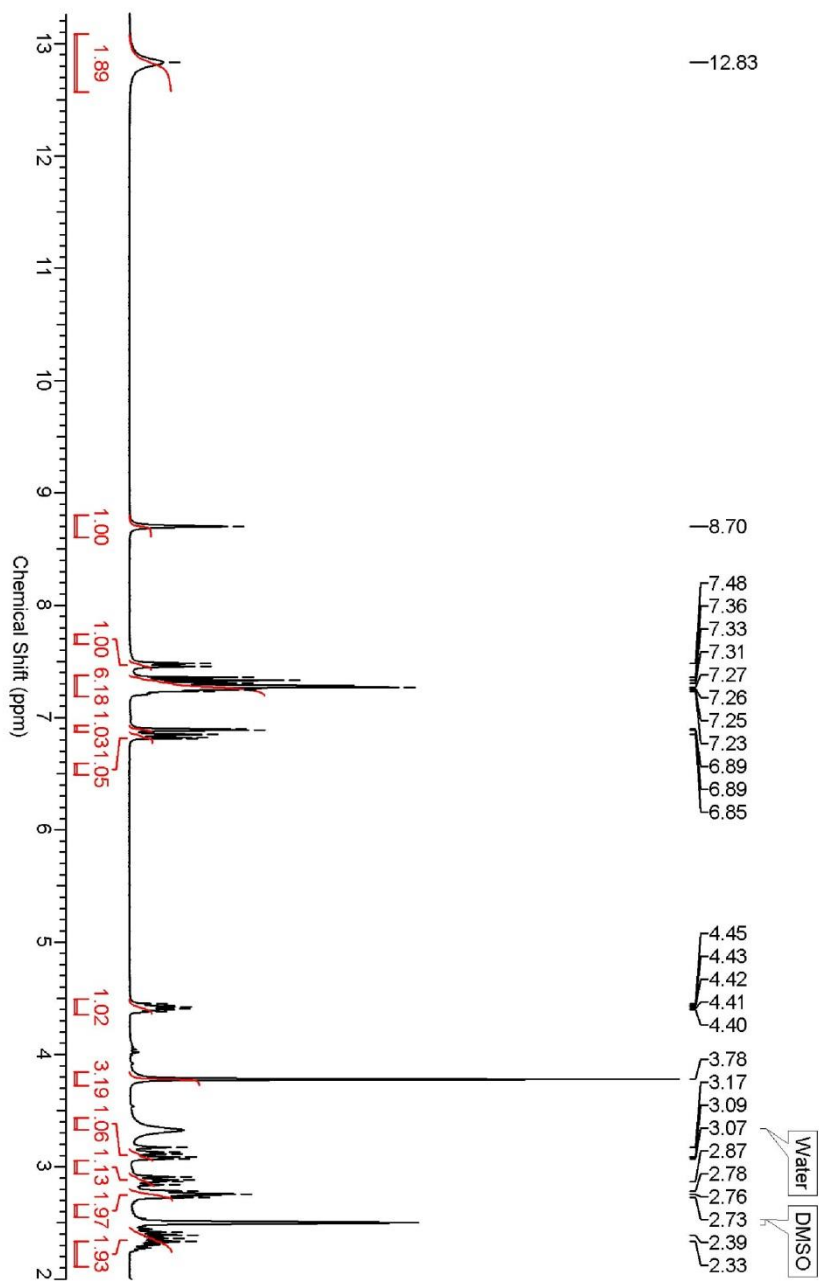


S25

¹³C-NMR spectrum of compound 10

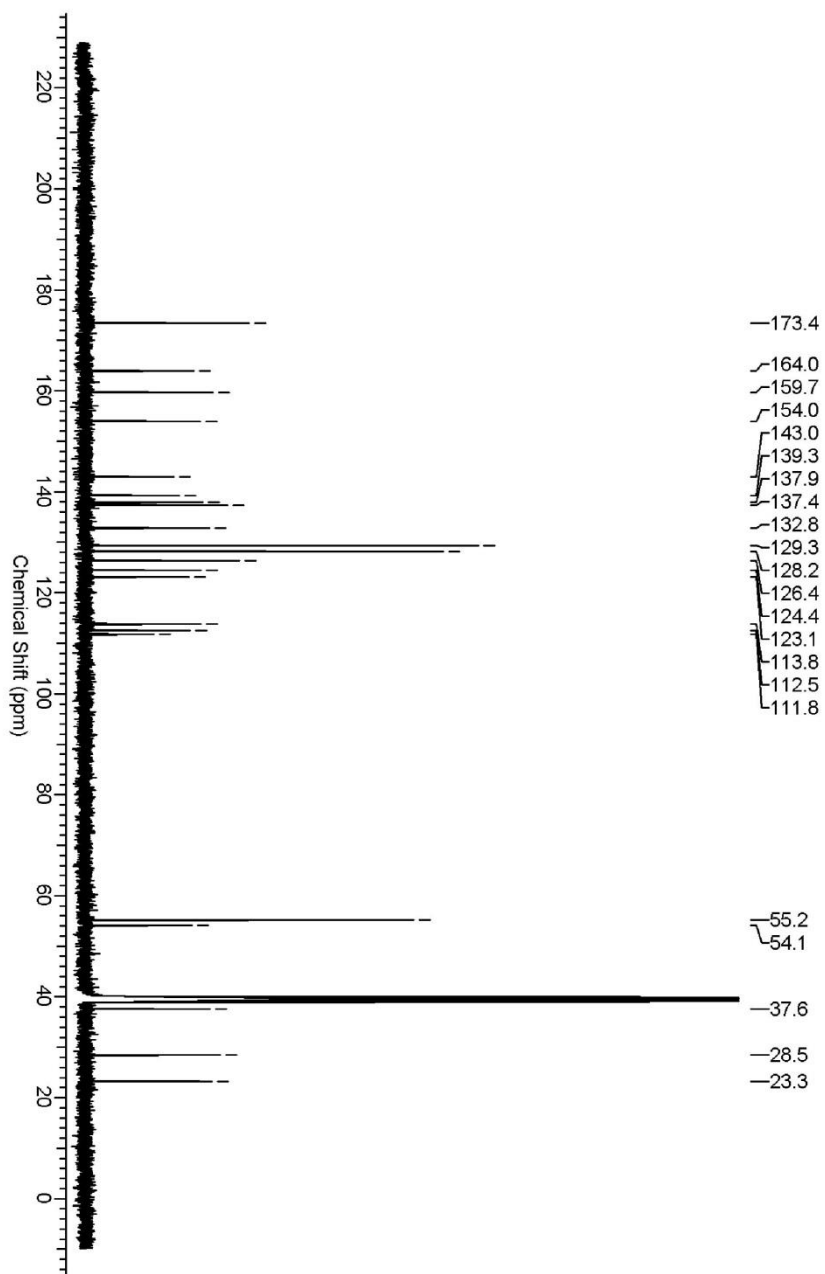


¹H-NMR spectrum of compound 16

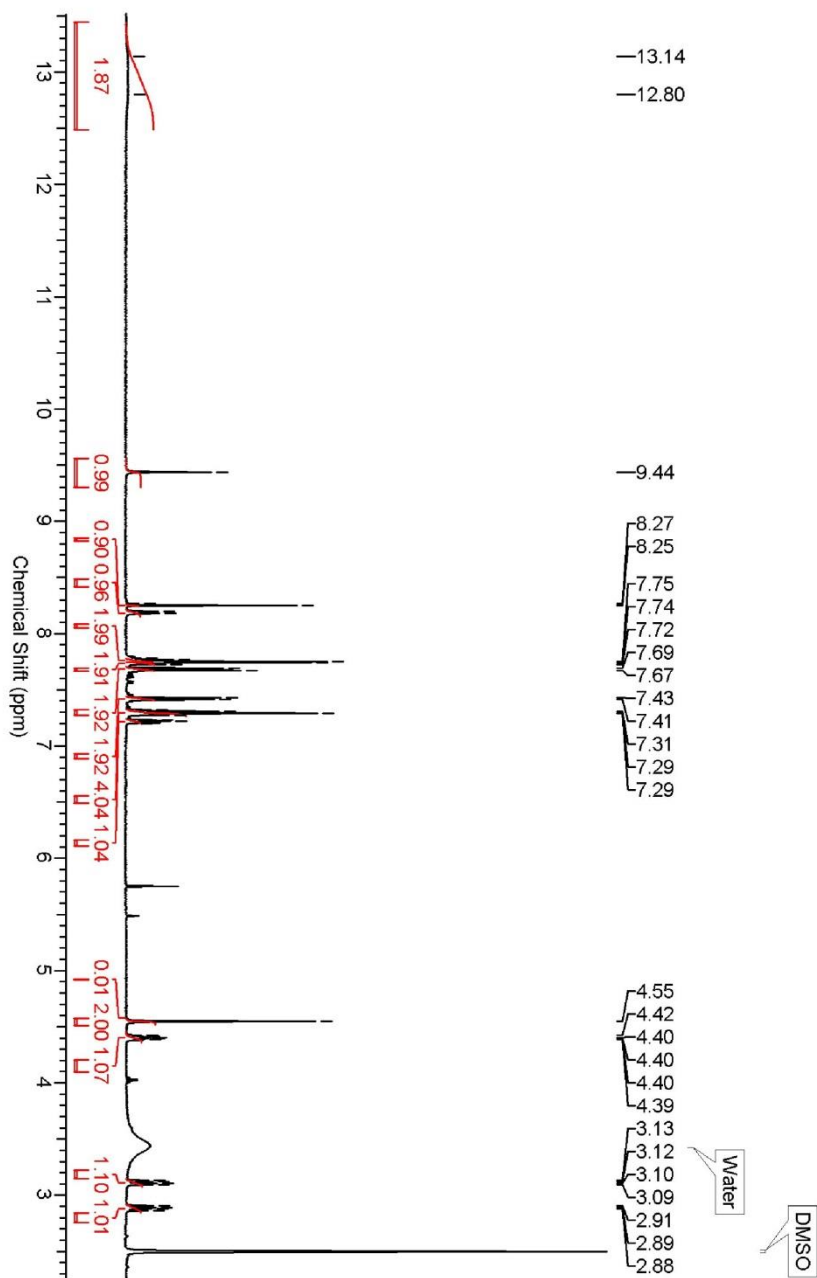


S27

¹³C-NMR spectrum of compound 16

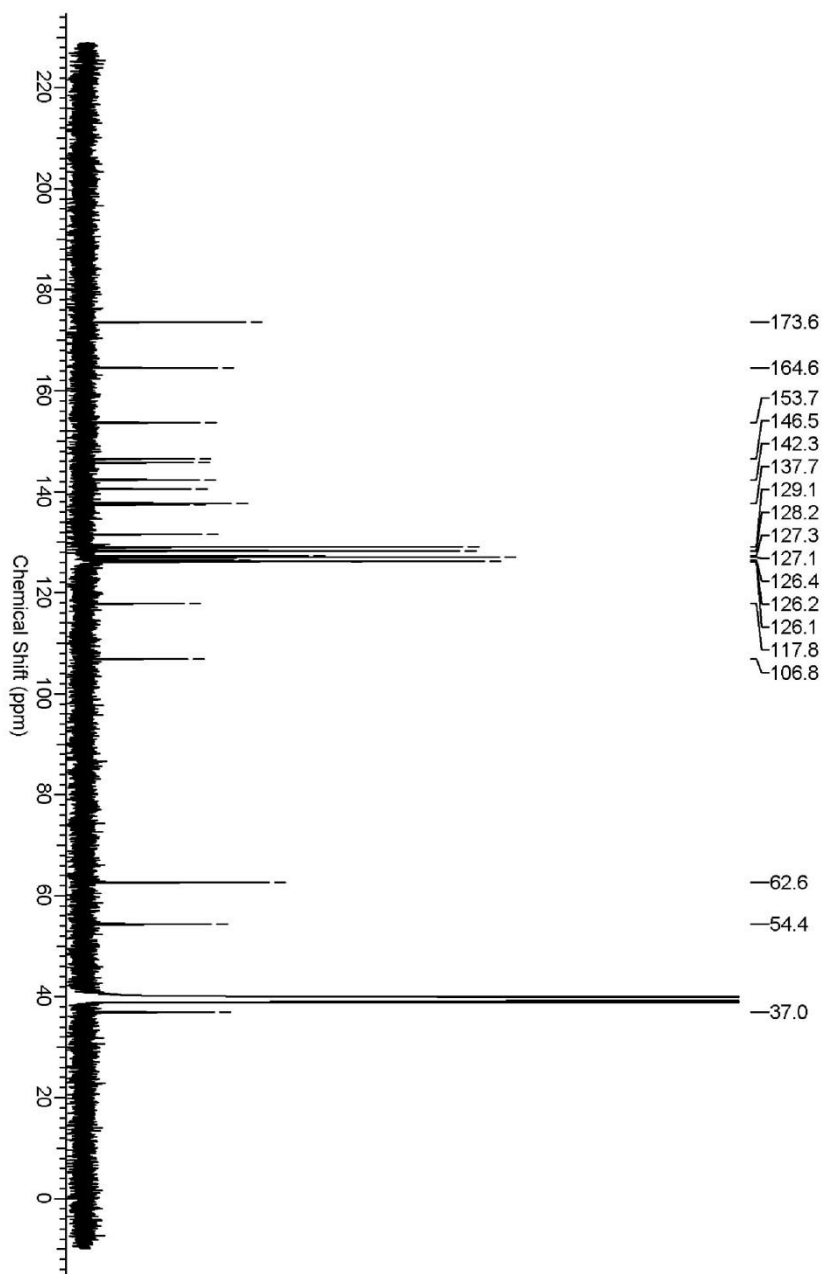


¹H-NMR spectrum of compound 21



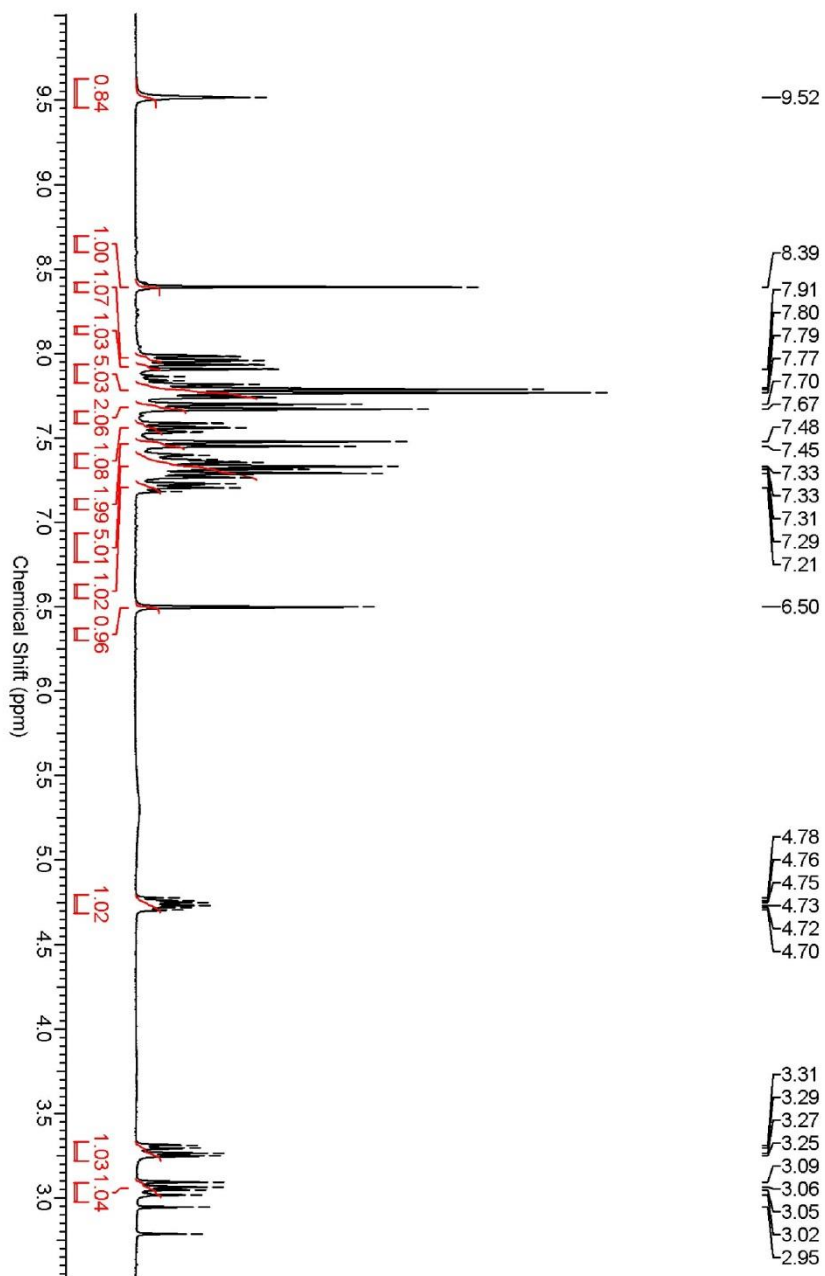
S29

¹³C-NMR spectrum of compound 21



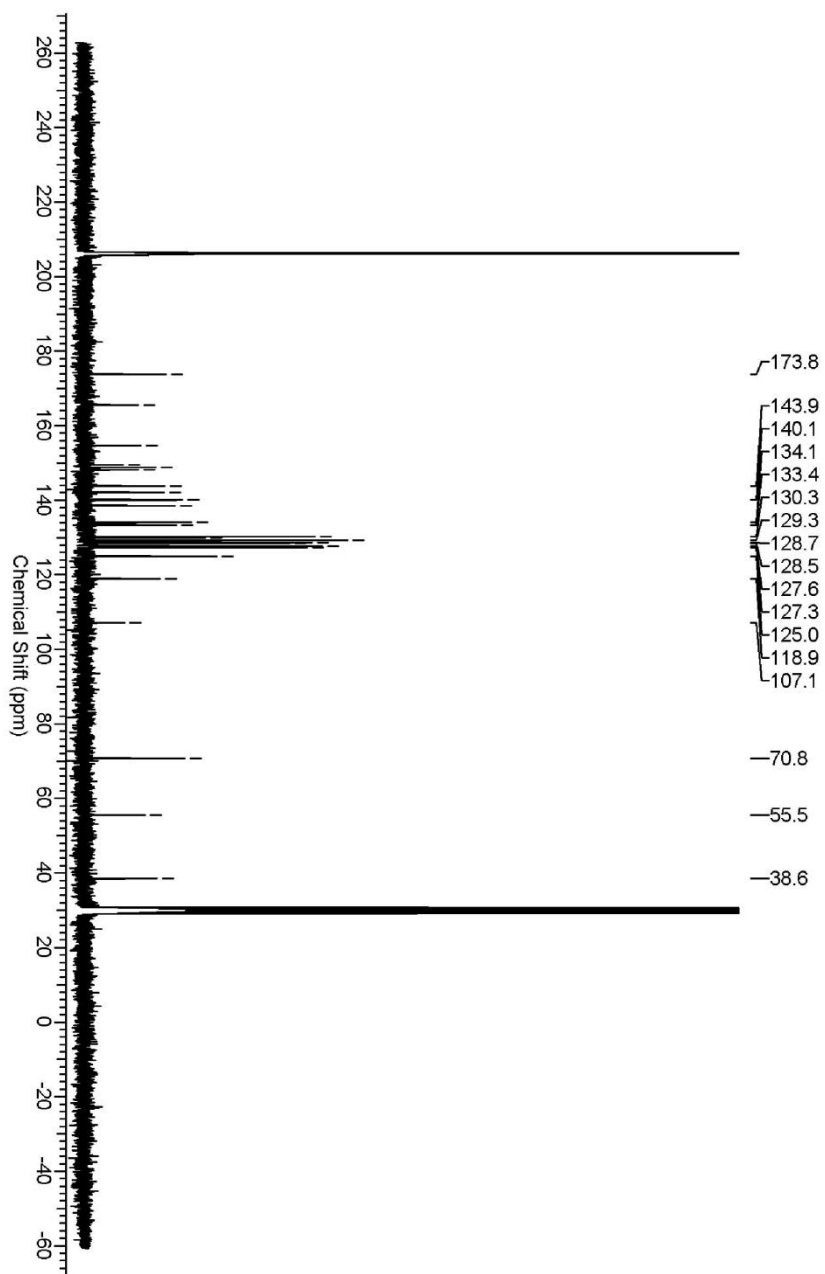
S30

¹H-NMR spectrum of compound 22

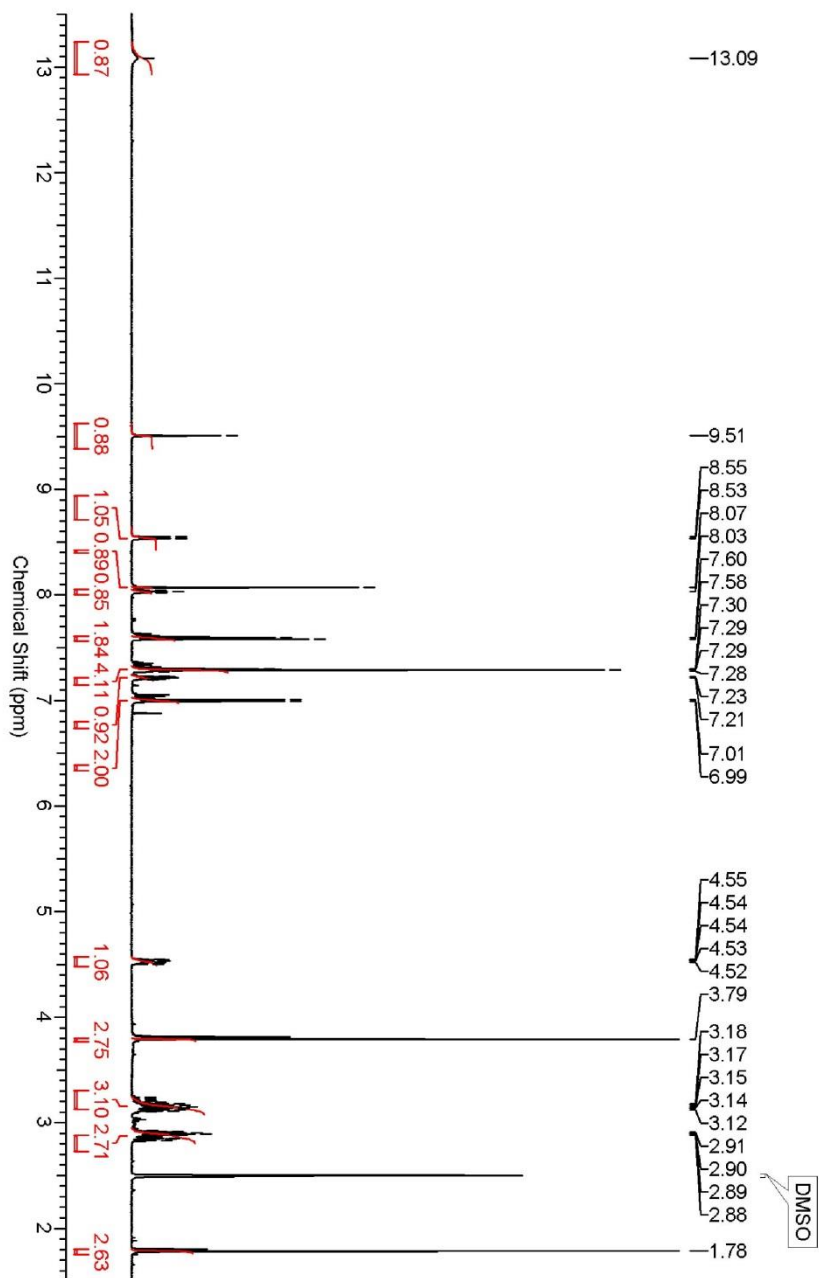


S31

¹³C-NMR spectrum of compound 22



¹H-NMR spectrum of compound 24



S33

¹³C-NMR spectrum of compound 24

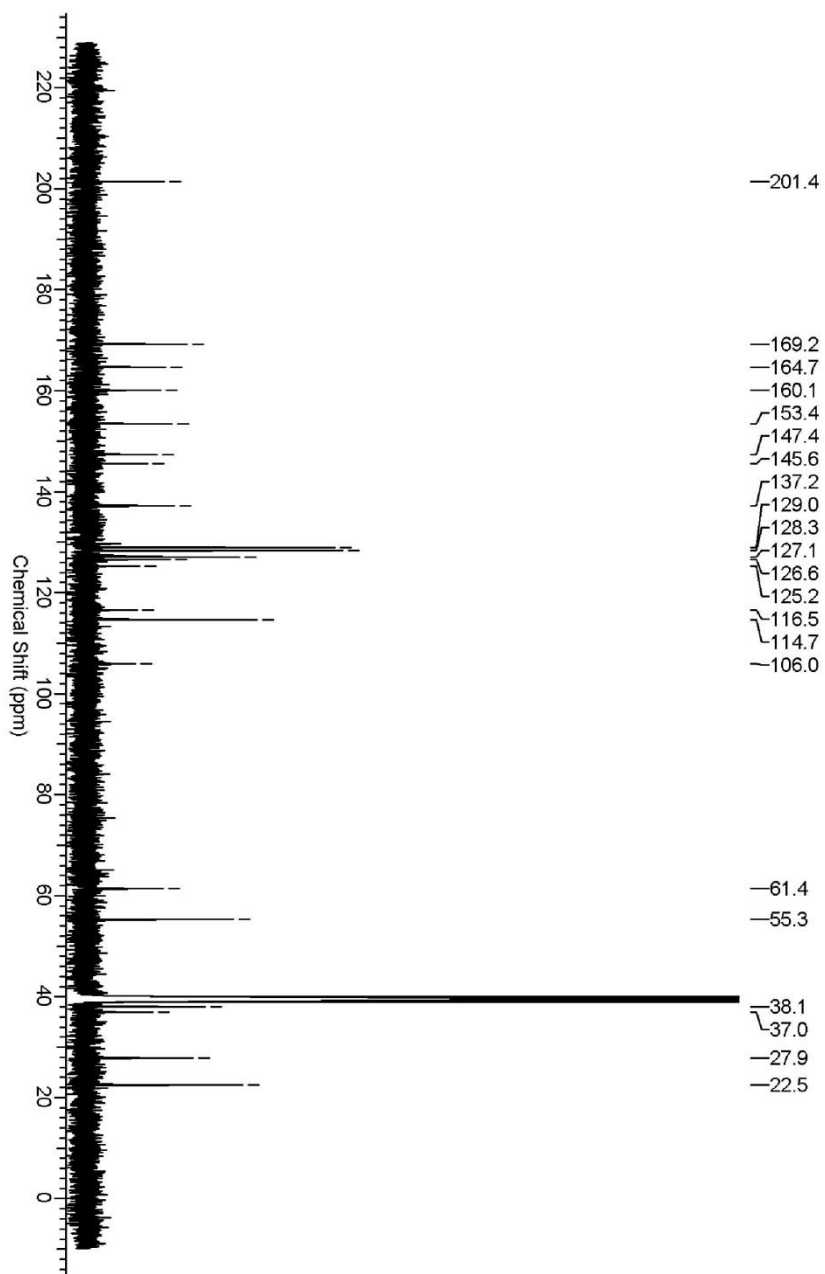


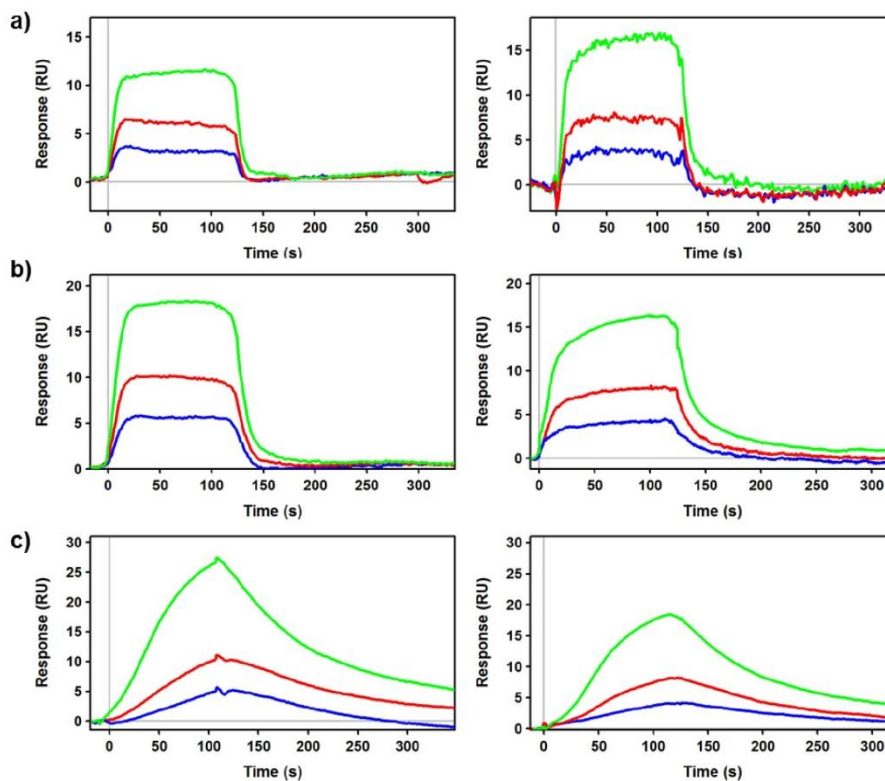
Table S1. Purity and retention times of compounds **1–25**.

Compound	UV - Purity [%]	Retention time [min] ^a
1	96	8.75
2	95	9.68
3	95	11.87
4	95	12.81
5	98	11.72
6	97	12.80
7	99	11.18
8	99	9.13
9	99	8.82
10	98	11.75
11	96	9.35
12	95	10.10
13	95	12.03
14	>99	9.43
15	97	12.40
16	99	11.94
17	97	12.27
18	97	14.30
19	96	11.71
20	99	14.35
21	99	11.92
22	96	13.53
23	99	8.41
24	96	12.50
25	90	10.21

^a In a gradient run the percentage of acetonitrile (containing 0.1% trifluoroacetic acid) was increased from a initial concentration of 0% at 0 min to 100% at 15 min and kept at 100% for 5 min.

b) Surface plasmon resonance (SPR)

Figure S1: SPR sensorgrams of **B** (Figure S1a), **21** (Figure S1b) and **22** (Figure S1c) at increasing concentrations (blue → red → green). Left panel: Before treatment with ACoA; Right panel: After treatment with ACoA.



c) References

- [1] H. Hartmann, J. Liebscher, A simple method for the synthesis of 5-aryl-3-amino-2-alkoxycarbonylthiophenes, *Synthesis* (1984) 275–276.
- [2] F. Fabis, S. Jolivet-Fouchet, M. Robba, H. Landelle, S. Rault, Thiaisatoic anhydrides: Efficient synthesis under microwave heating conditions and study of their reactivity, *Tetrahedron* 54 (1998) 10789–10800.
- [3] L. Foulon, E. Braud, F. Fabis, J.C. Lancelot, S. Rault, Synthesis and combinatorial approach of the reactivity of 6-and 7-arylthieno [3,2-d][1,3] oxazine-2,4-diones. *Tetrahedron* 59 (2003) 10051–10057.
- [4] F.X. Le Foulon, E. Braud, F. Fabis, J.C. Lancelot, S. Rault, Solution-phase parallel synthesis of a 1140-member ureidothiophene carboxylic acid library. *J. Comb. Chem.* 7 (2005) 253–257.
- [5] K. Sambasivarao, K. G. Arun, D. D. Kodrand, Synthesis of 9,10-Diarylanthracene Derivatives. *Synthesis* (2004) 549–557.
- [6] E. Perspicace, V. Jouan-Hureau, R. Ragno, F. Ballante, S. Sartini, C. La Motta, F. Da Settimo, B. Chen, G. Kirsch, S. Schneider, B. Faivre, S. Hesse,

S36

Design synthesis and biological evaluation of new classes of thieno[3,2-d]pyrimidine and thieno[1,2,3]triazine as inhibitor of vascular endothelial growth factor receptor-2 (VEGFR-2). *Eur. J. Med. Chem* (2013) 765–781.

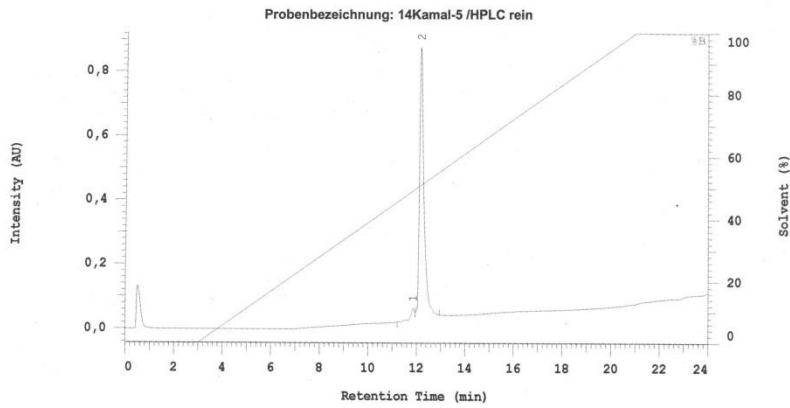
- [7] S. Flohr, V. Jungmann, H. Waldmann, Chemoenzymatic synthesis of nucleopeptides. *Chem. Eur. J.* (1999) 669–681.
- [8] R. Muchiri, K. D. Walker, Taxol biosynthesis: Tyrocidine Synthetase A catalyzes the production of phenylisoserinyl CoA and other amino phenylpropanoyl thioesters. (2012) 679–685.

6.3 Supporting information chapter C

Peptide No.	% Purity	Calculated Mass		ESI-MS	
		[M+H] ⁺	[M+2H] ⁺	[M+H] ⁺	[M+2H] ⁺
1	>99	2132.117		2132.093	
2	>90	2072.113		2072.035	
3	92.3	2090.070		2090.102	
4	87.6	2146.133	1073.570		1074.0
5	74.2	2090.070		2090.030	
6	81.9	2089.111		2089.042	
7	>90	2146.133		2146.266	
8	98.8	2074.111		2074.105	
9	97.7	2075.095		2075.133	
10	>75	2090.070		2089.996	
11	>95	2090.070		2089.974	
12	94.5	2088.127		2087.898	
13	96.3	2090.070	1045.539		1045.1
14	>90	2056.086		2056.057	
15	>90	2075.095		2075.081	
16	>90	2090.070		2090.050	
17	>90	2146.133		2146.107	
18	>85	2047.053	1024.039		1024.5
19	>90	2089.111		2089.065	
20	>90	2102.106		2102.078	
21	>99	2001.076	1001.042		1001.5
22	98.7	2114.160		2114.222	
23	98.7	2086.108	1043.558		1044.2
24	98.7	2031.069			2031.010
25	81	2154.112	1077.560		1077.73
26	85	2121.087	1061.047		1060.82
27	>99	2253.181	1127.094		1127.54
28	>99	2211.134	1106.071		1106.54
29	92	2154.112	1077.560		1077.49
30	91	2121.087	1061.047		1060.78
31	--	2253.181	1127.094		1127.67
32	>99	2211.134	1106.071		1106.48

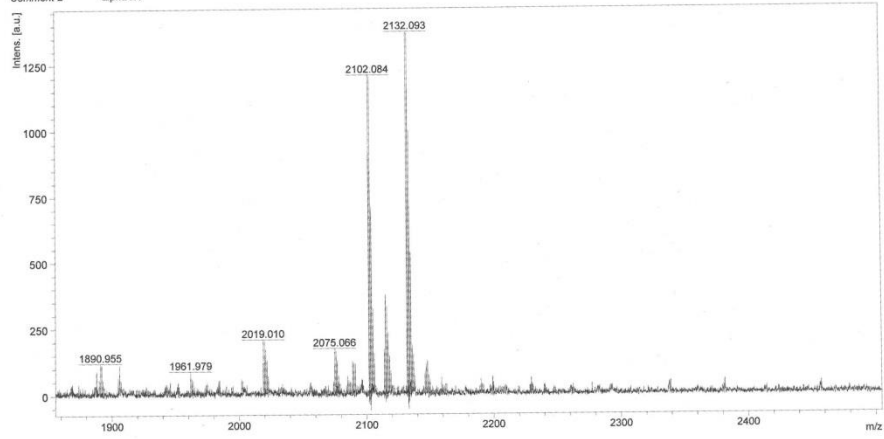
Table S1. Summary of peptides synthesized, purities, calculated mass and mass found.

Peptide 1



H:\LBKO14558\0_01711

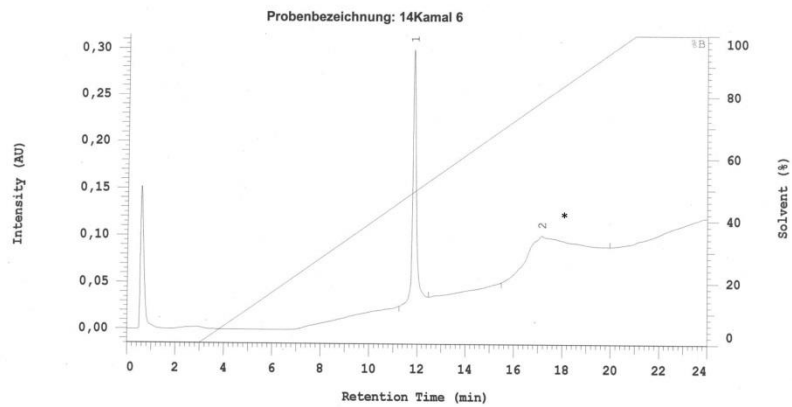
Comment 1 5
Comment 2 alphaCN



Bruker Daltonics flexAnalysis

printed: 13.05.2014 13:36:26

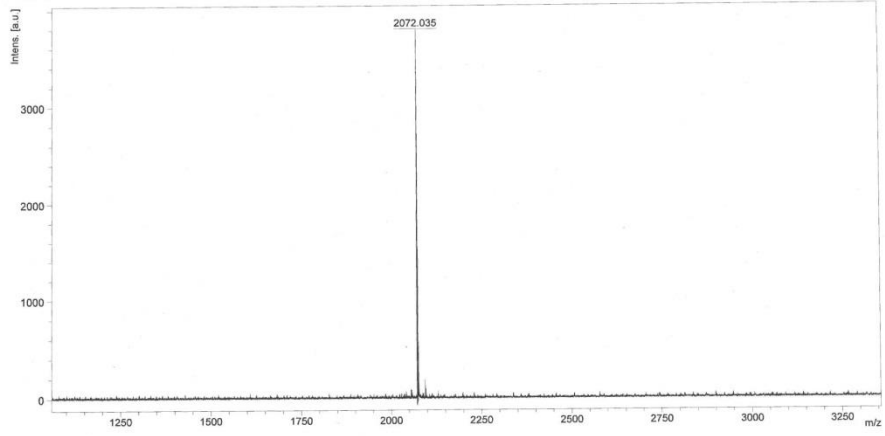
Peptide 2



* is an artifact from column

H:LBKO145710_C61

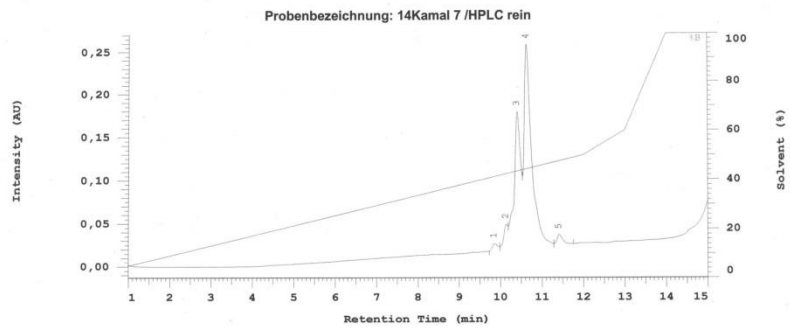
Comment 1 A
Comment 2 AlphaCN



Bruker Daltonics flexAnalysis

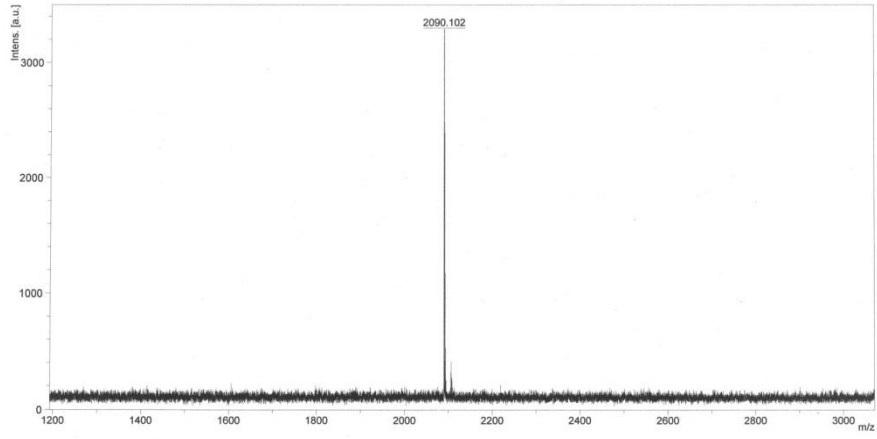
printed: 21.05.2014 09:27:06

Peptide 3



H:\LBKO145080_B2111

Comment 1 7/1
Comment 2 alphaCN

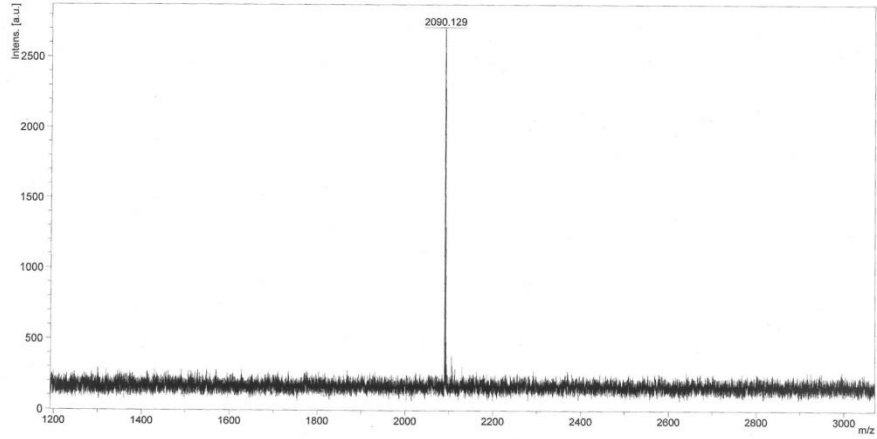


Bruker Daltonics flexAnalysis

printed: 04.04.2014 12:21:01

H:\LBKO145080_C2111

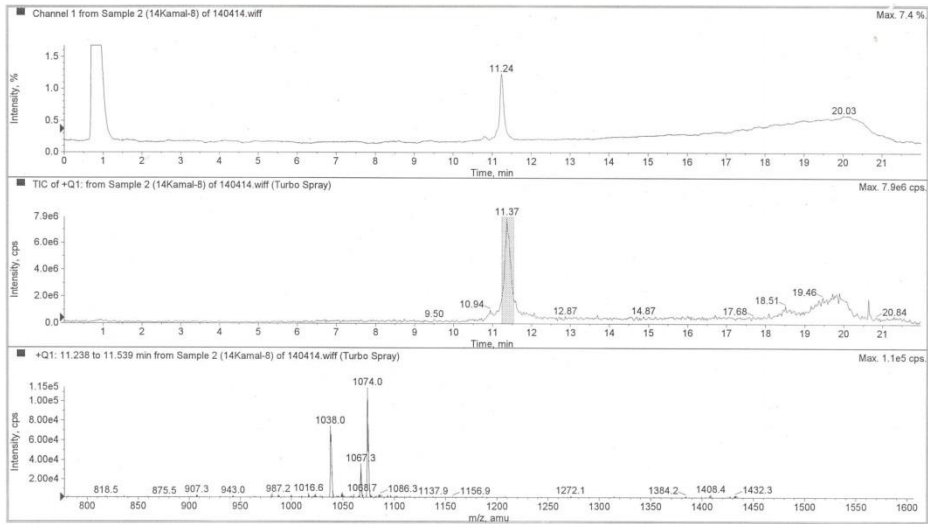
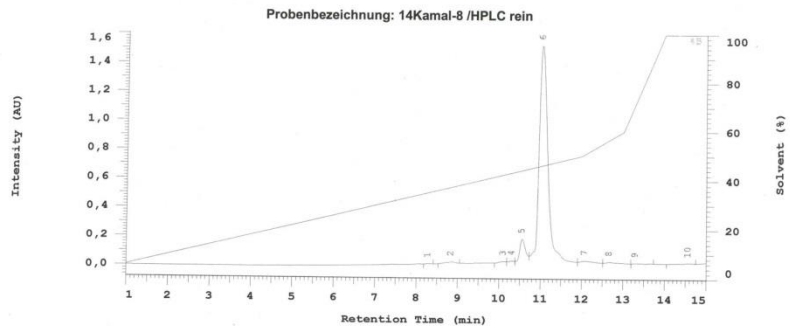
Comment 1 7/2
Comment 2 alphaCN



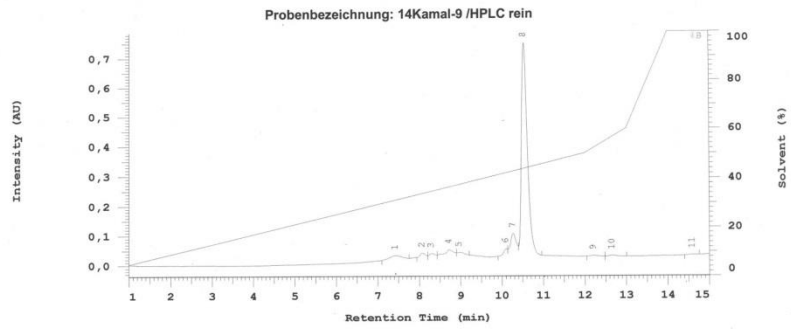
Bruker Daltonics flexAnalysis

printed: 04.04.2014 12:25:23

Peptide 4

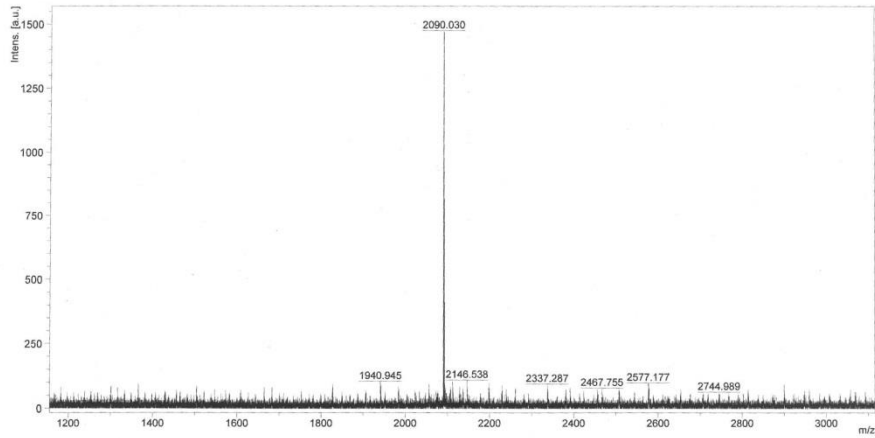


Peptide 5



H:\LBKO1449310_010.1

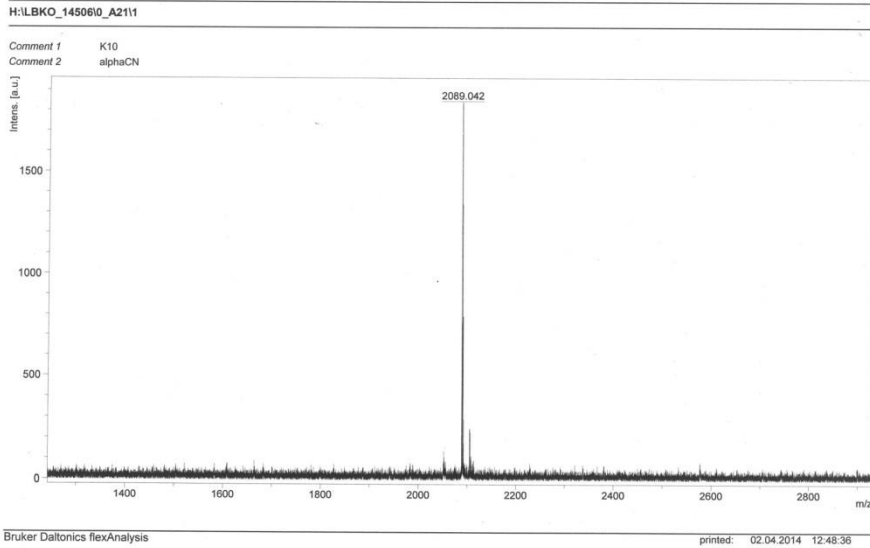
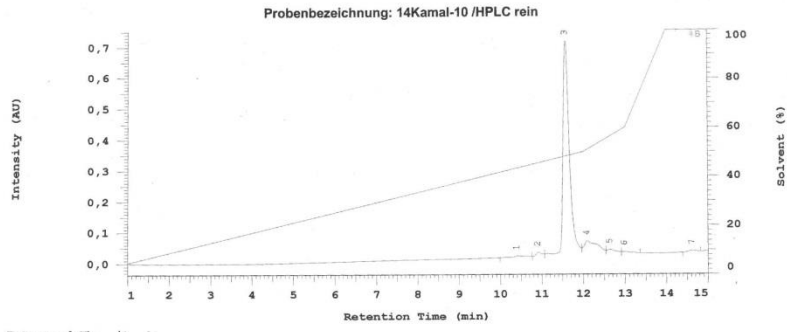
Comment 1 K9
Comment 2 alphaCN



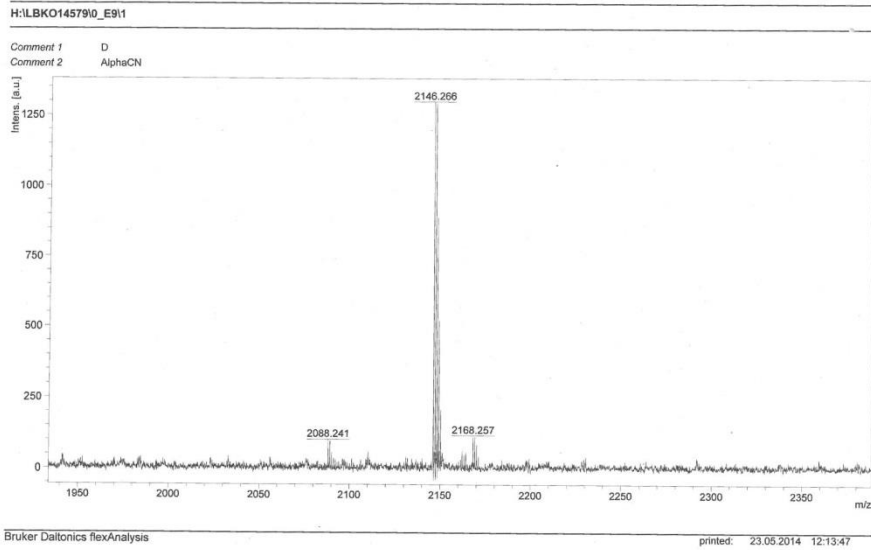
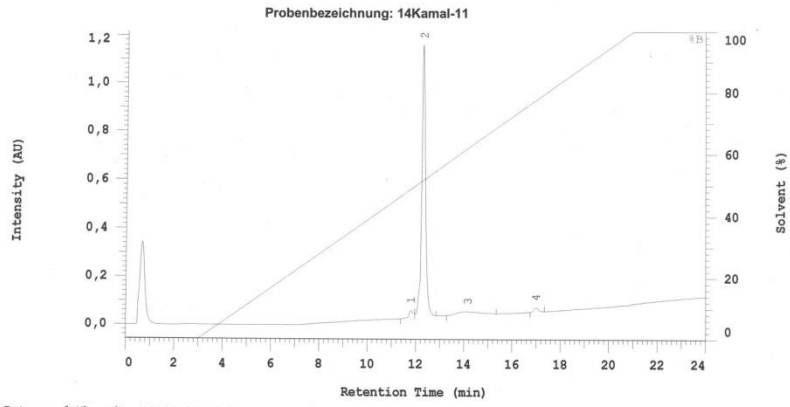
Bruker Daltonics flexAnalysis

printed: 27.03.2014 10:23:31

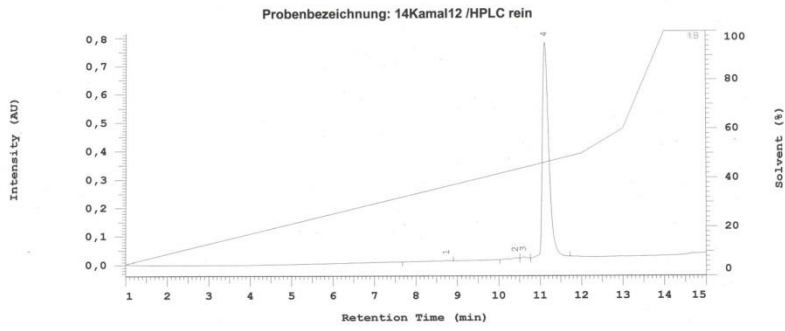
Peptide 6



Peptide 7

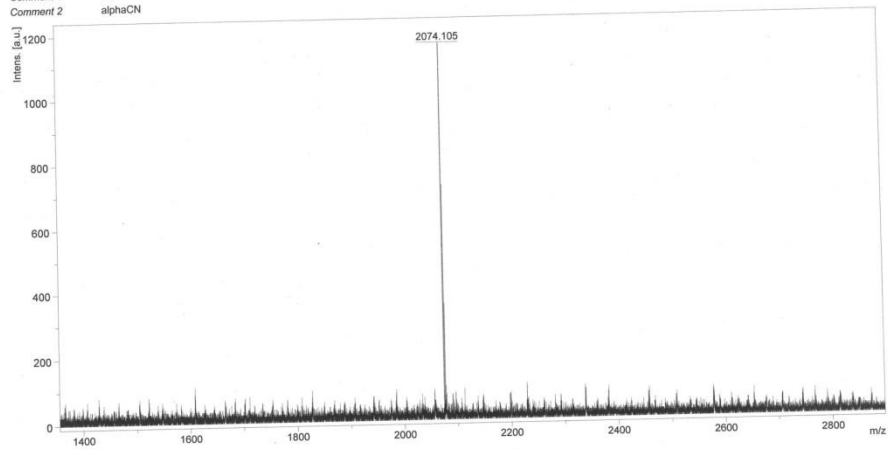


Peptide 8



H:\LBKO1448610_L1011

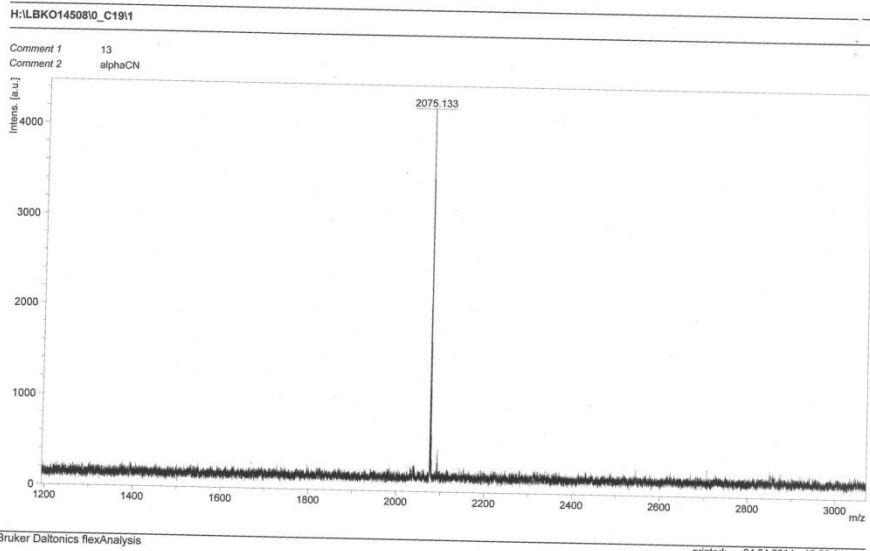
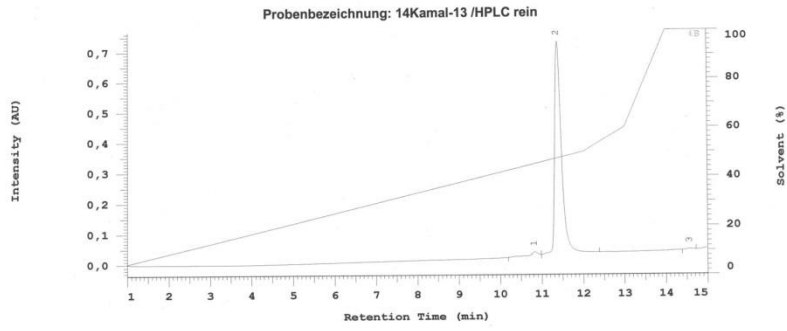
Comment 1 12
Comment 2 alphaCN



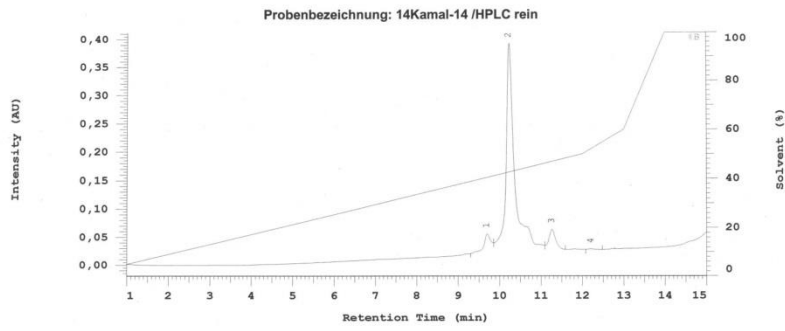
Bruker Daltonics flexAnalysis

printed: 24.03.2014 14:33:56

Peptide 9

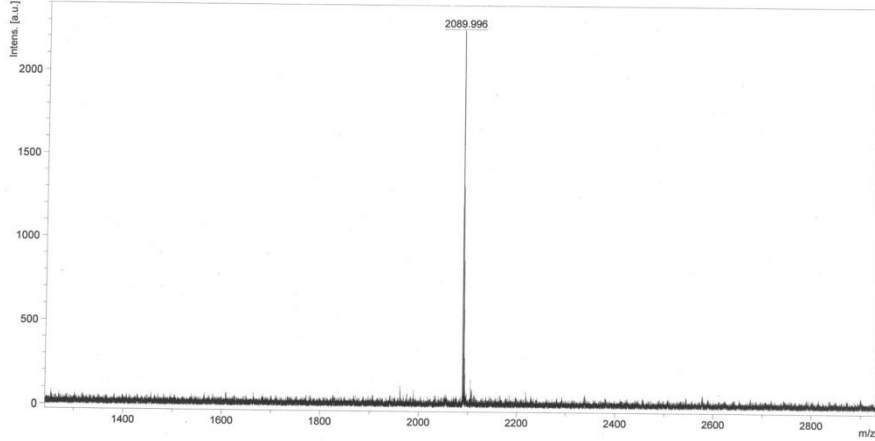


Peptide 10



H:\LBKO_1450610_A2011

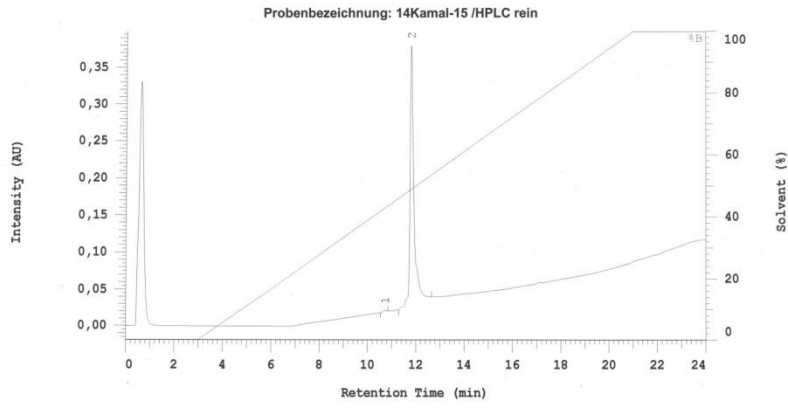
Comment 1 K14
Comment 2 alphaCN



Bruker Daltonics flexAnalysis

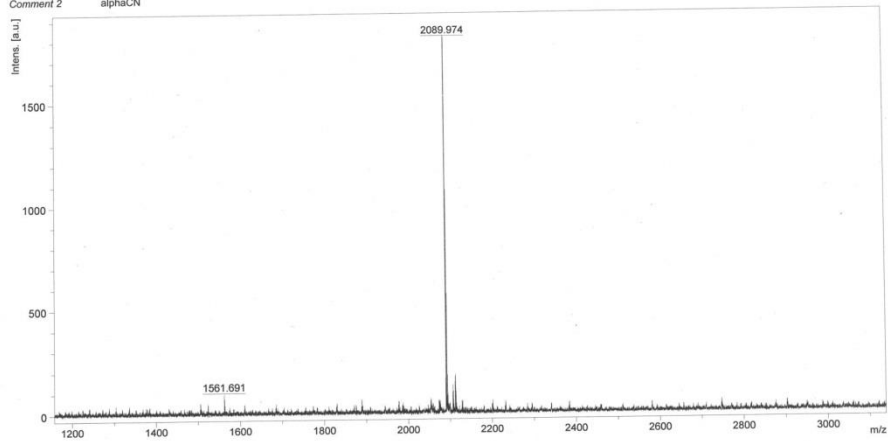
printed: 02.04.2014 12:46:42

Peptide 11



H:\LBK014550\0_M10\1

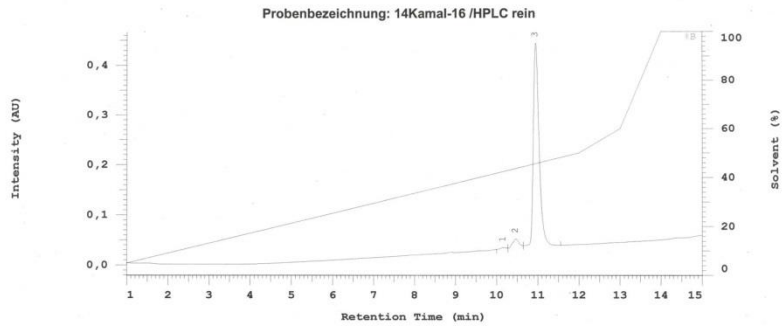
Comment 1 15
Comment 2 alphaCN



Bruker Daltonics flexAnalysis

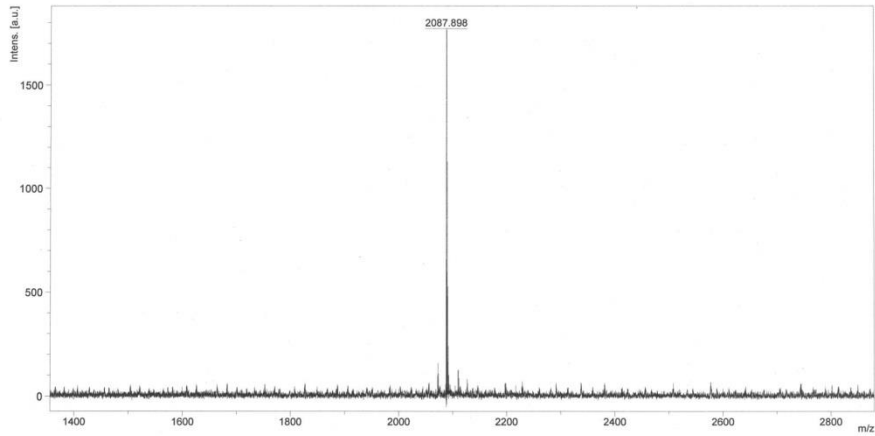
printed: 12.05.2014 08:06:27

Peptide 12



H:\LBKO145710_A711

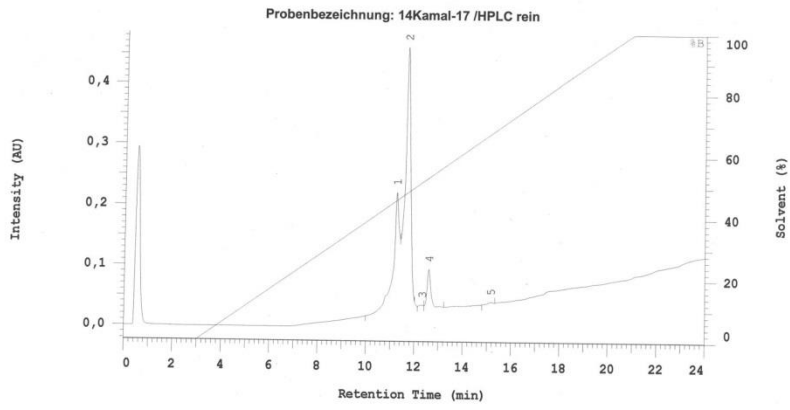
Comment 1 E
Comment 2 AlphaCN



Bruker Daltonics flexAnalysis

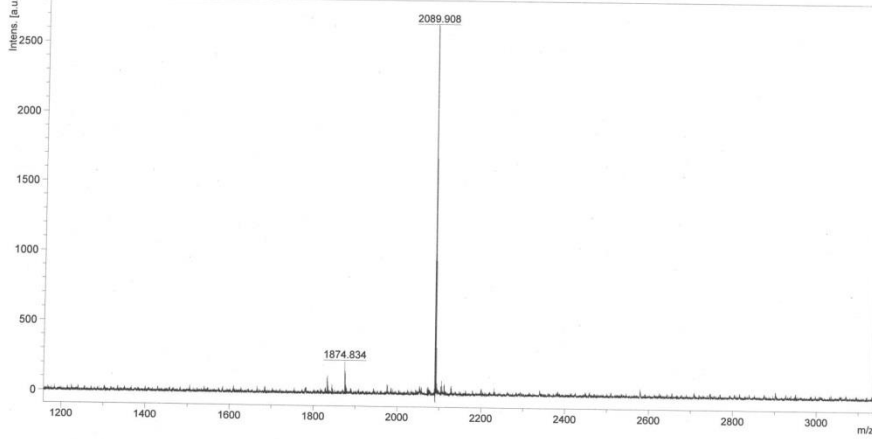
printed: 21.05.2014 07:37:44

Peptide 13



H:\LBKO14550\0_N1011

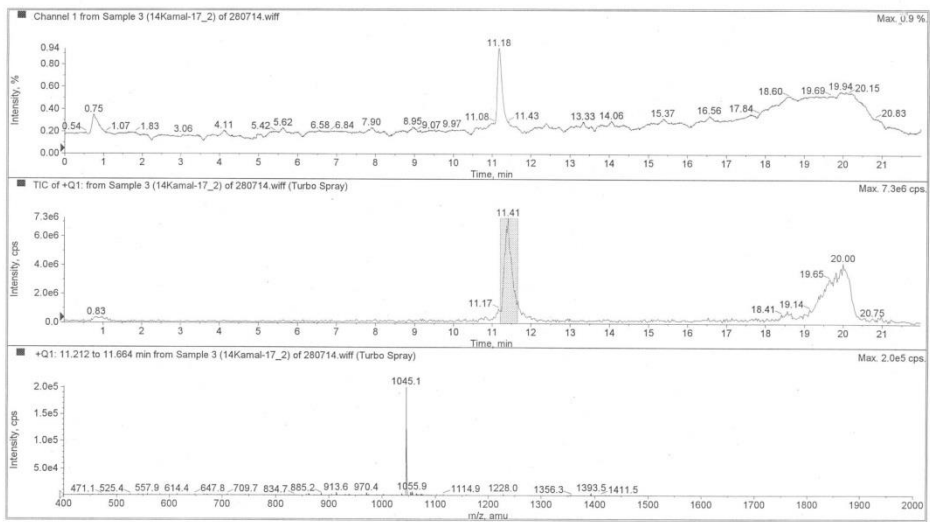
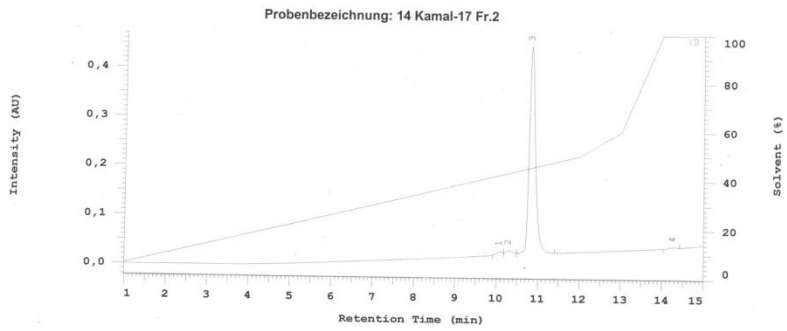
Comment 1 17
Comment 2 alphaCN



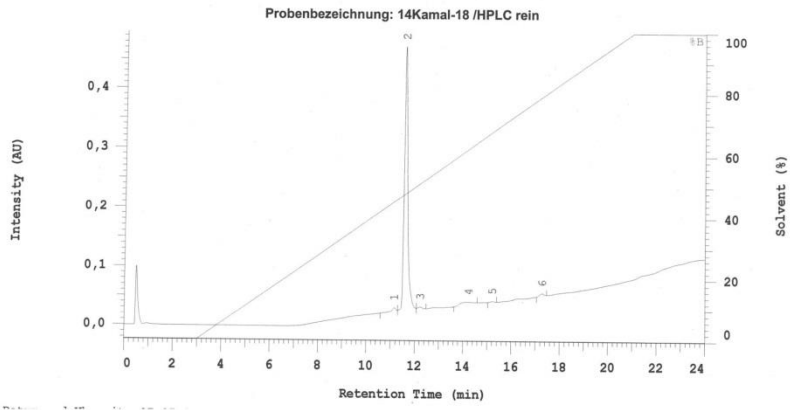
Bruker Daltonics flexAnalysis

printed: 12.05.2014 08:26:52

Peptide 14

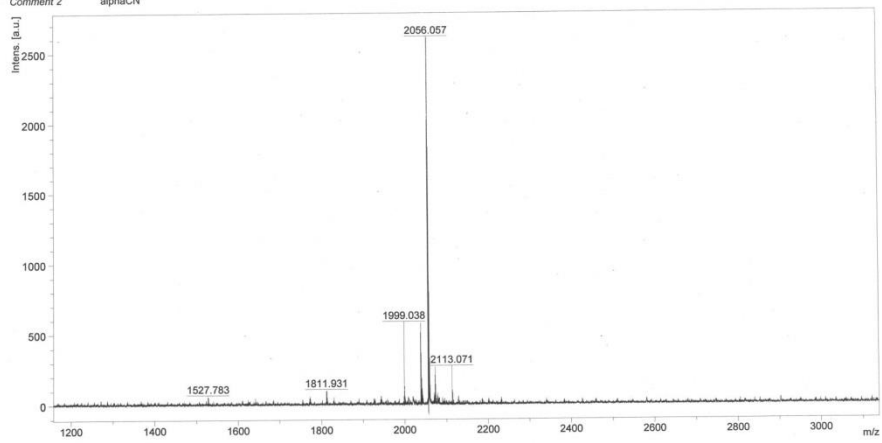


Peptide 15



H:\LBKO14550\0_M1111

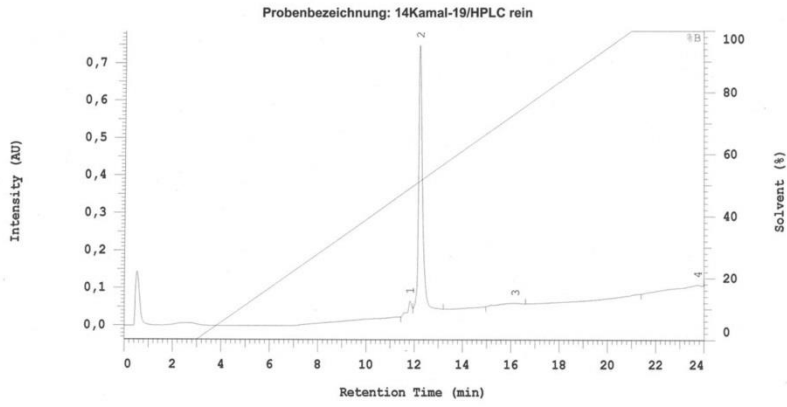
Comment 1 18
Comment 2 alphaCN



Bruker Daltonics flexAnalysis

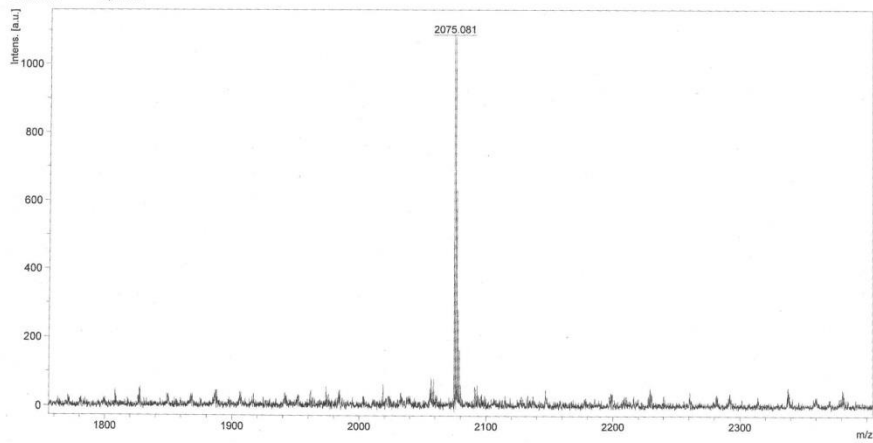
printed: 12.05.2014 08:07:54

Peptide 16



H:\LBKO14558\0_01611

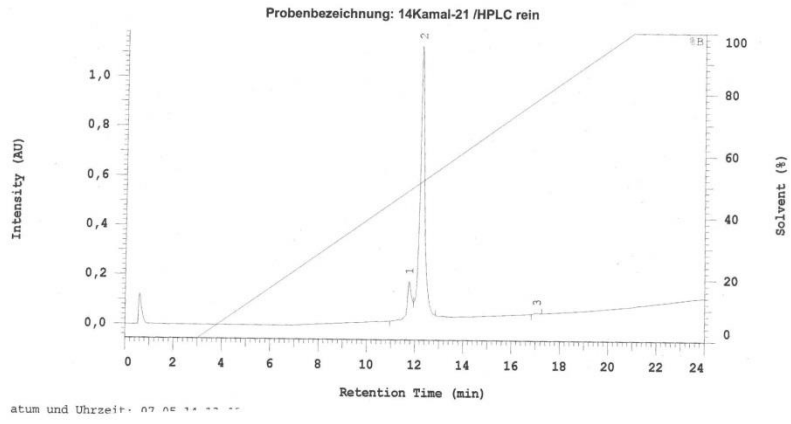
Comment 1 19
Comment 2 alphaCN



Bruker Daltonics flexAnalysis

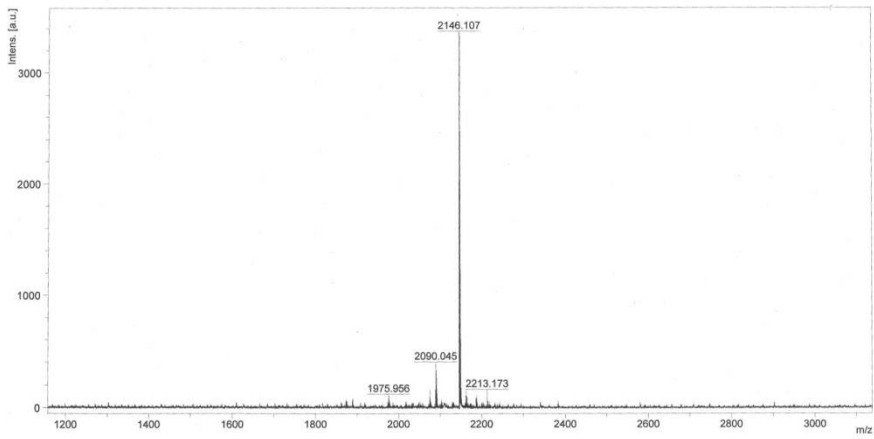
printed: 13.05.2014 13:34:44

Peptide 17



H:\LBK014550\0_N1211

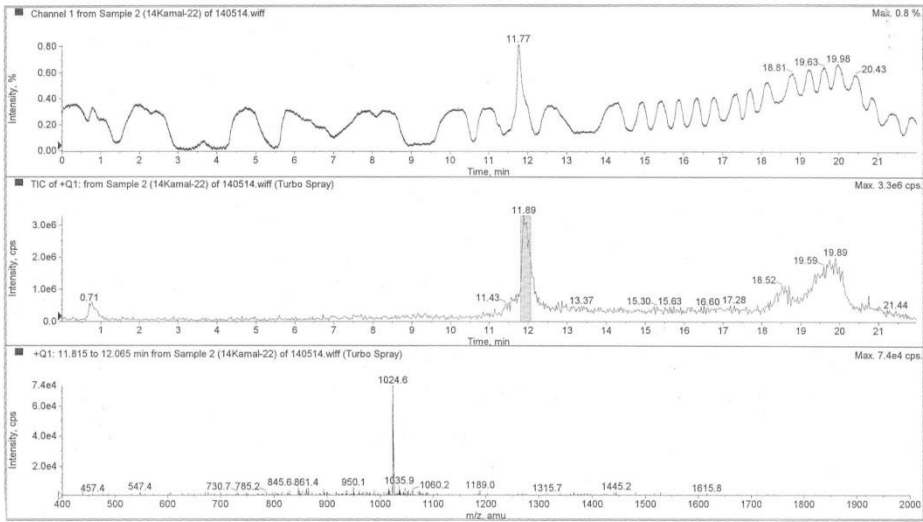
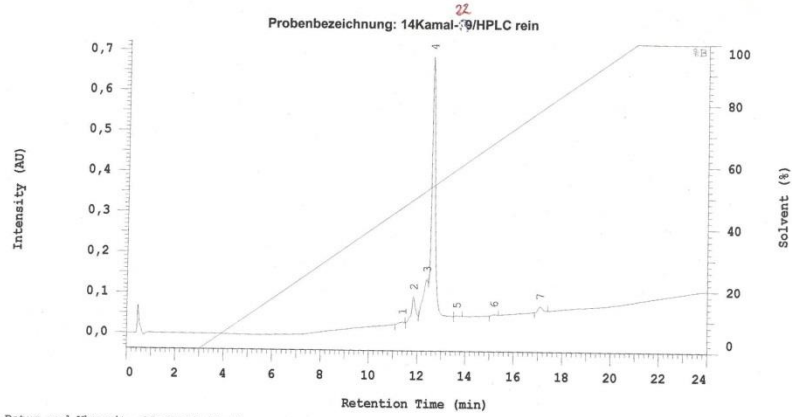
Comment 1 21
Comment 2 alphaCN



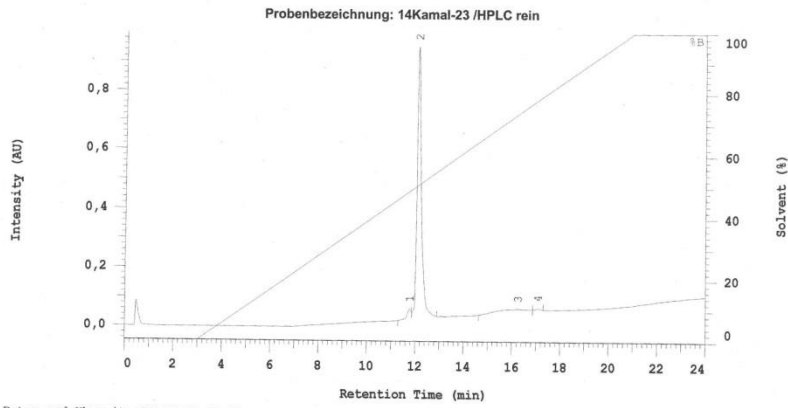
Bruker Daltonics flexAnalysis

printed: 12.05.2014 08:29:24

Peptide 18

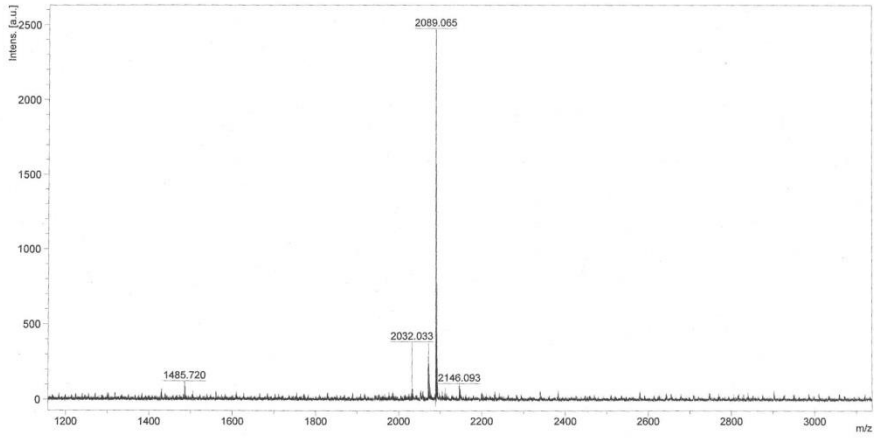


Peptide 19



H:\LBKO145500_M1311

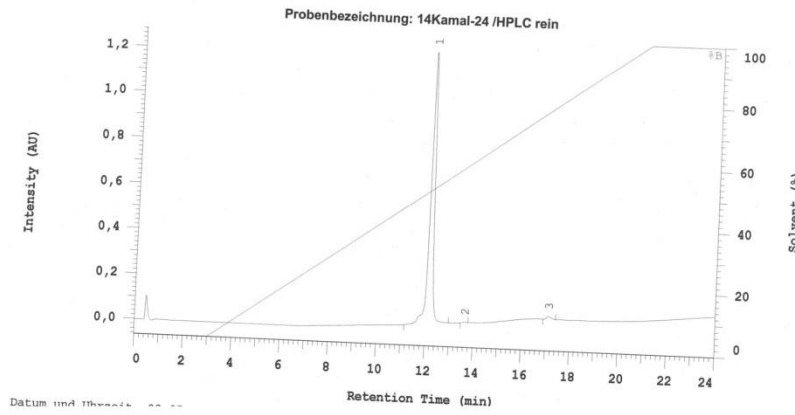
Comment 1 23
Comment 2 alphaCN



Bruker Daltonics flexAnalysis

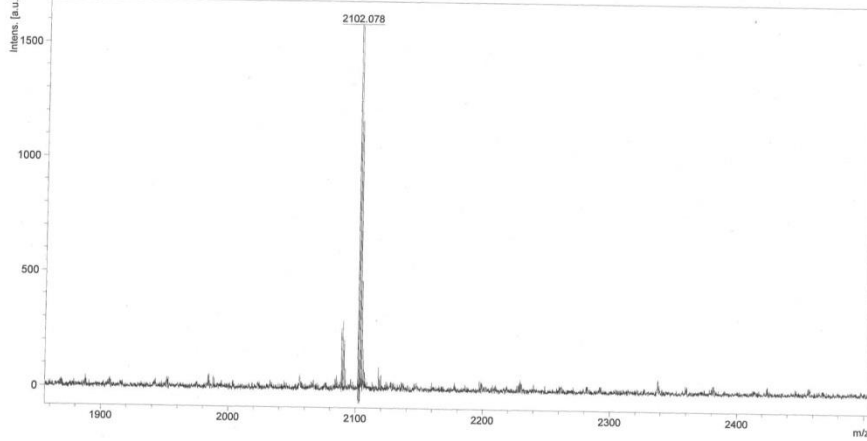
printed: 12.05.2014 08:10:29

Peptide 20



H:\LBKO14558\0_O1811

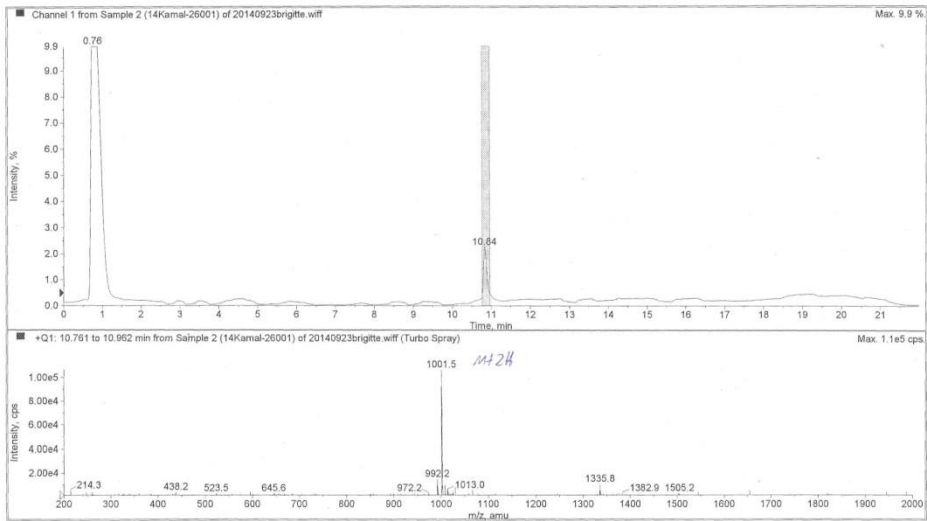
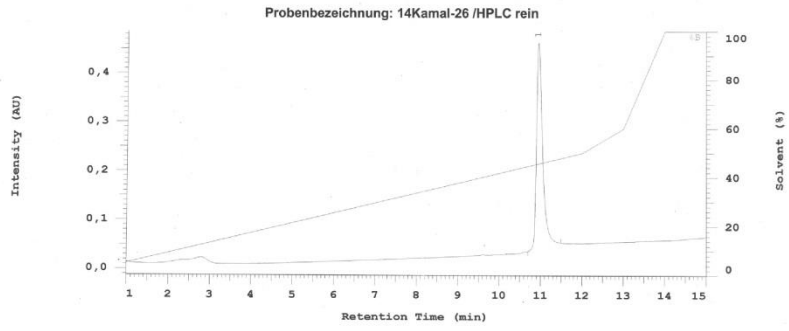
Comment 1 24
Comment 2 alphaCN



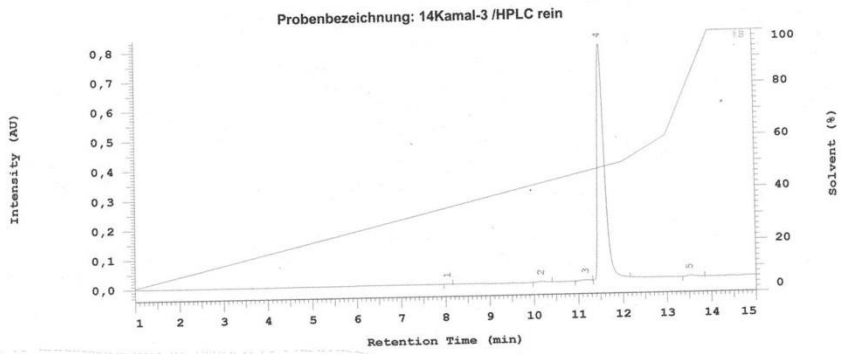
Bruker Daltonics flexAnalysis

printed: 13.05.2014 13:37:56

Peptide 21

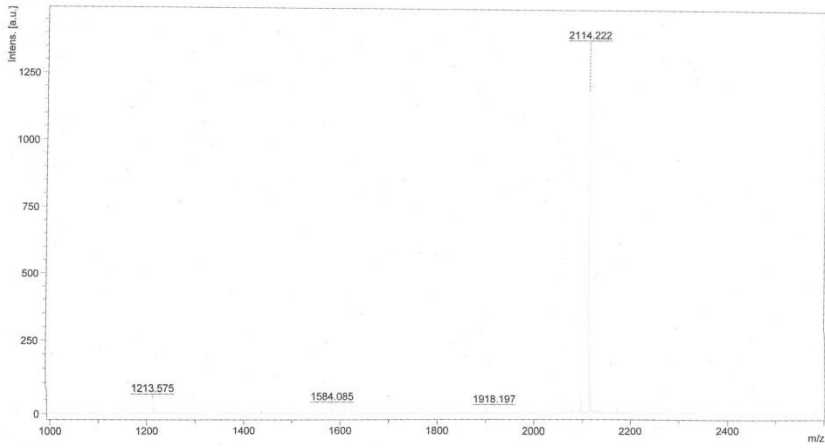


Peptide 22



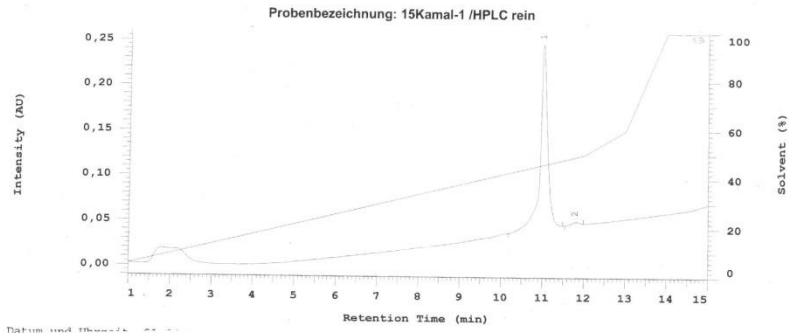
D:\Maldi_2014\LBKO144190_D5\1\1SRef

Comment 1 K3
Comment 2 alphaCN



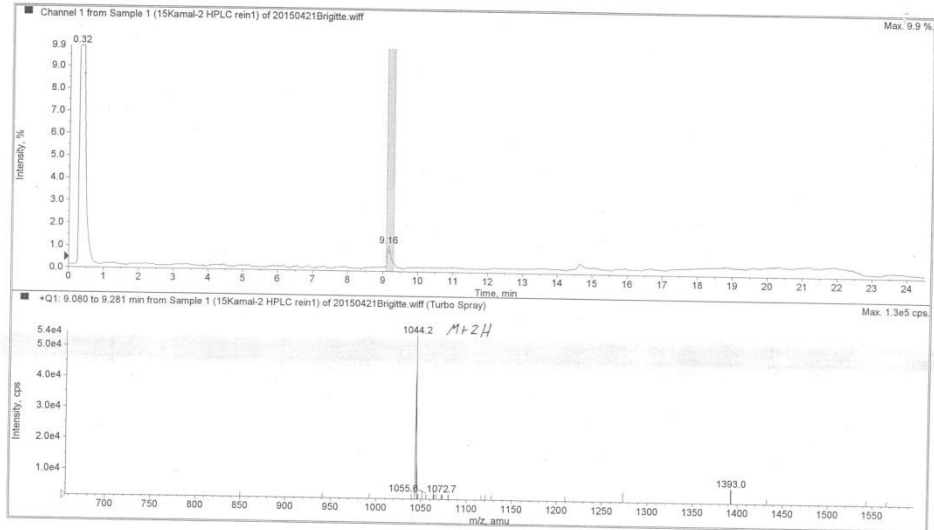
printed: 2/3/2014 10:23:21

Peptide 23

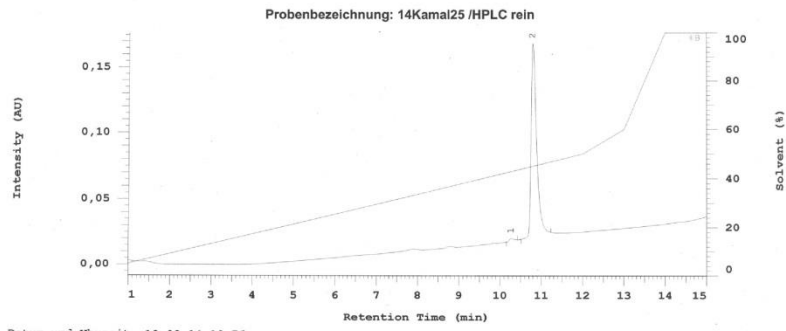


Acq. File: 20150421Brigitte.wiff

Sample Name: 15Kamal-2 HPLC rein
Sample Number: N/A

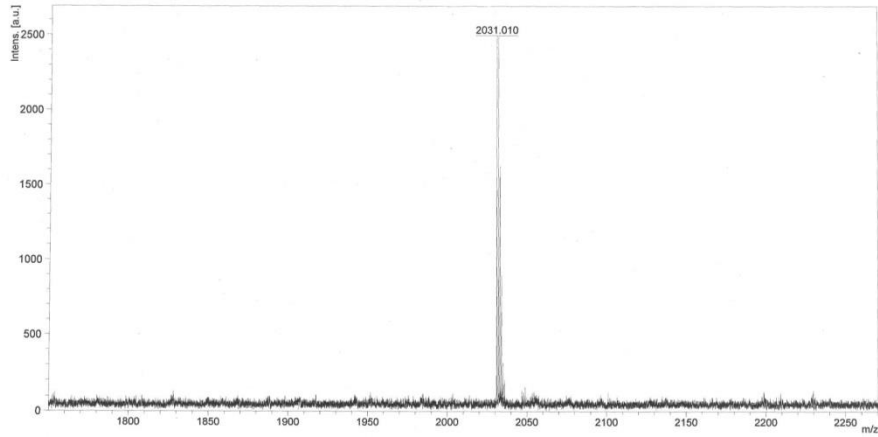


Peptide 24



H:\LBKO_14682\0_M20\1

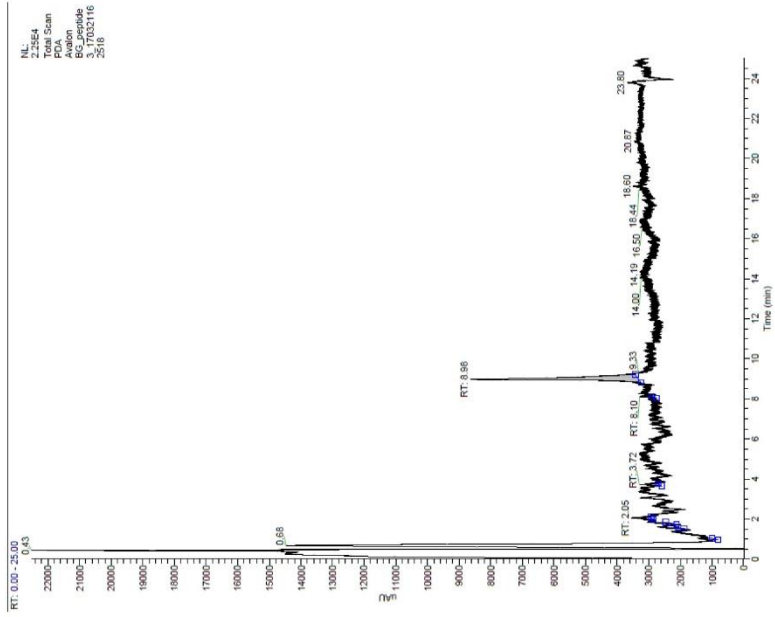
Comment 1 2 25
Comment 2 alphaCN



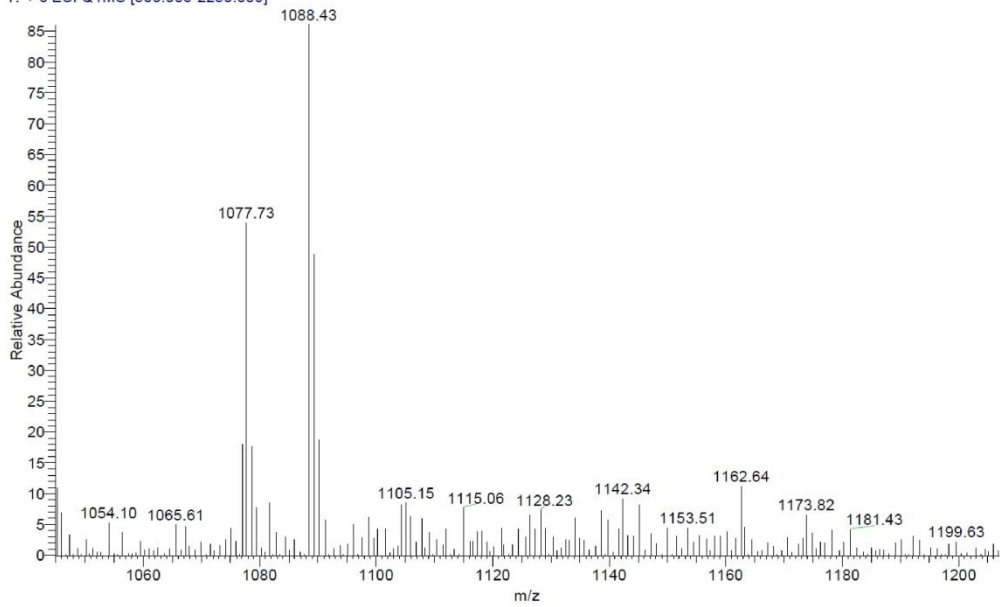
Bruker Daltonics flexAnalysis

printed: 30.09.2014 13:03:09

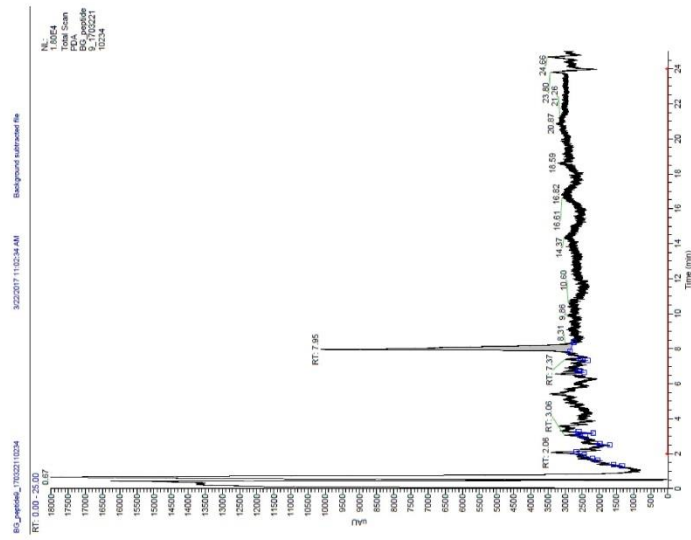
Peptide 25



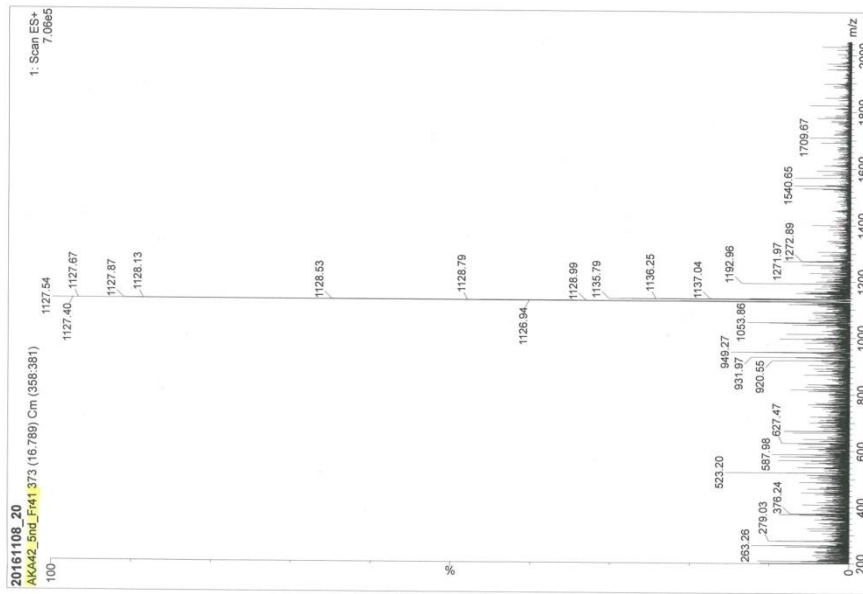
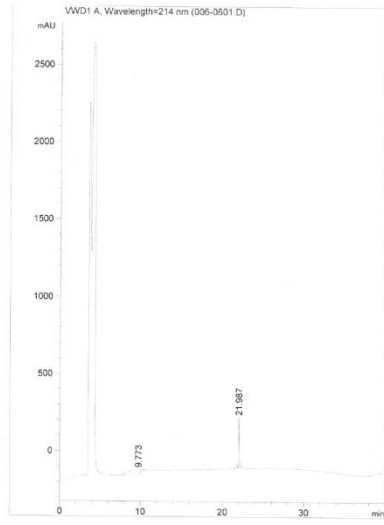
peptide 3 #493-505 RT: 8.87-9.09 AV: 13 NL: 7.57E4
T: + c ESI Q1MS [500.000-2250.000]



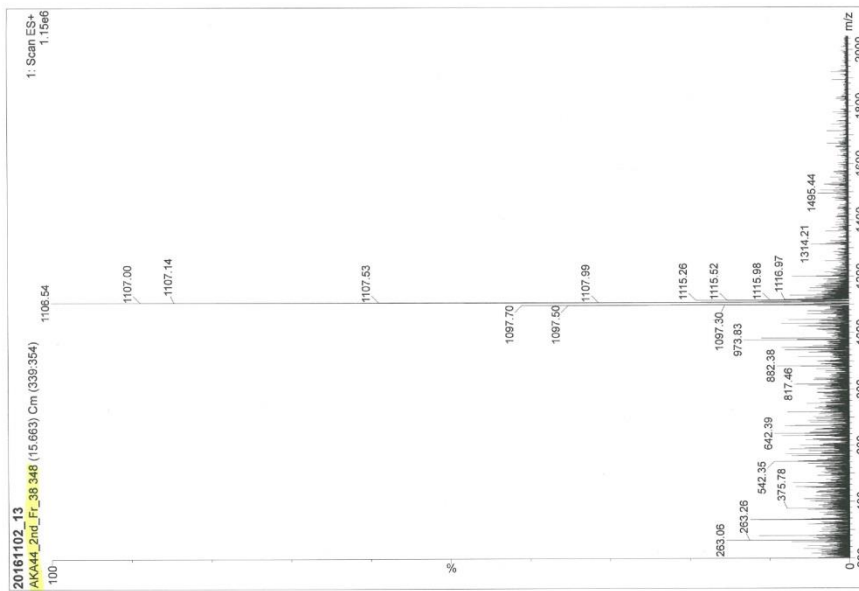
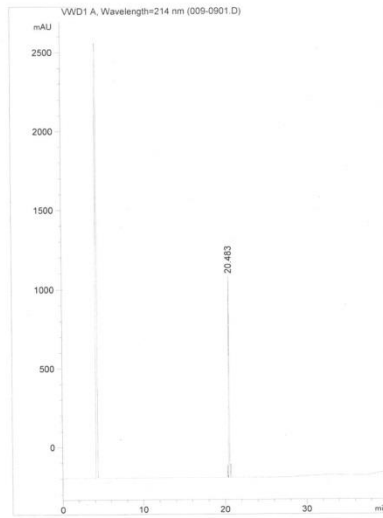
Peptide 26



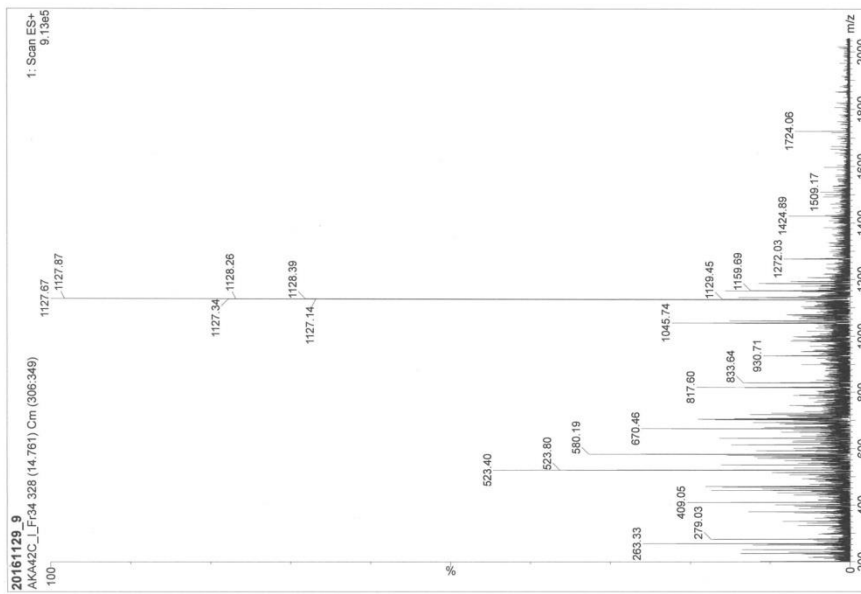
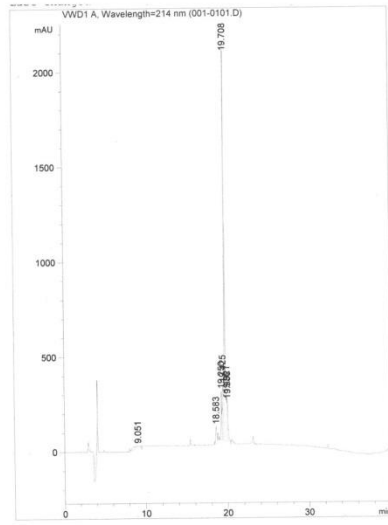
Peptide 27



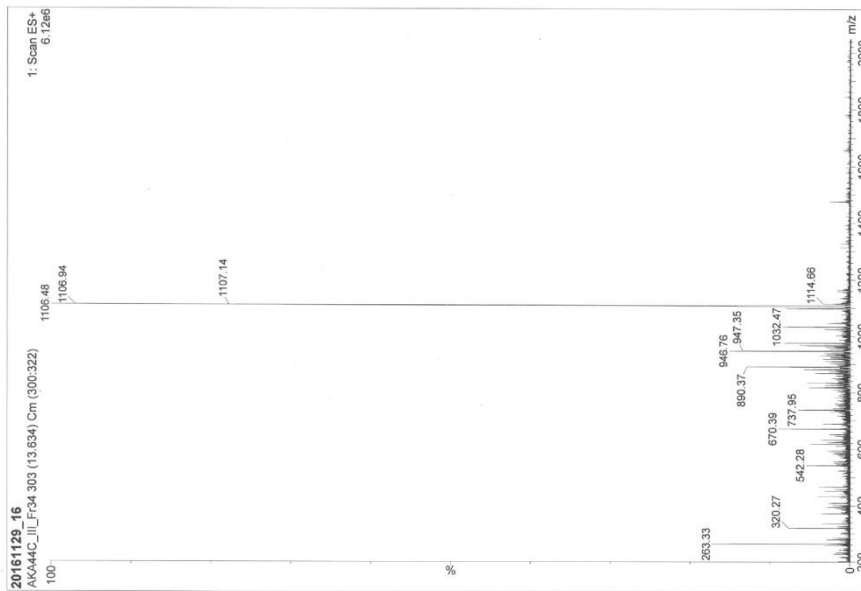
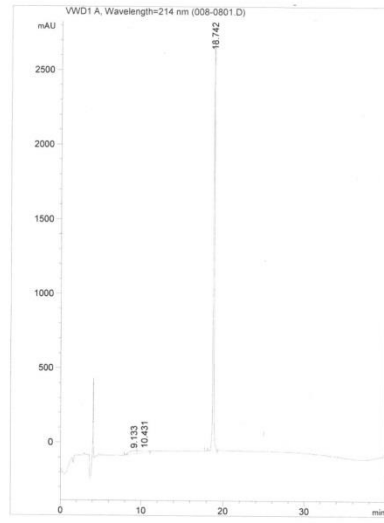
Peptide 28



Peptide 31

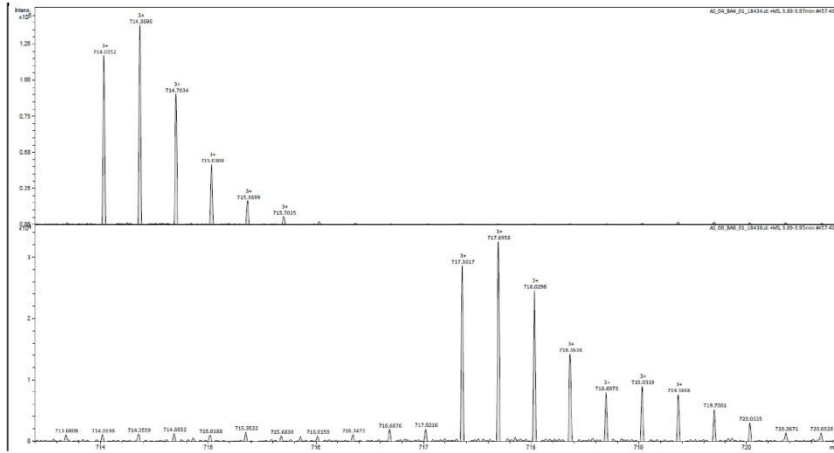


Peptide 32

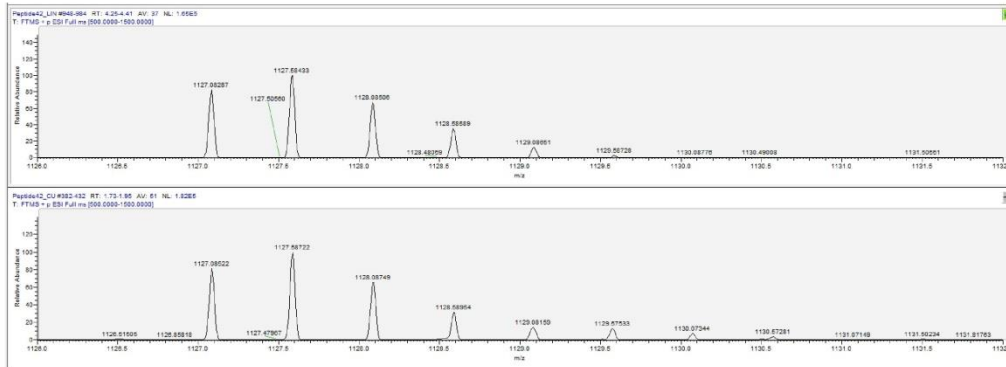


HRMS data

Peptide 25 (top) and peptide 29 (bottom)

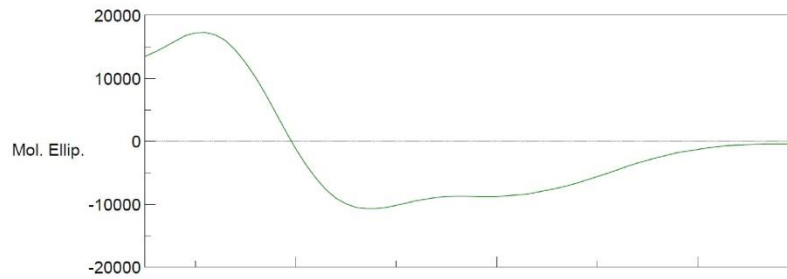


Peptide 27 (top) and peptide 31 (bottom)

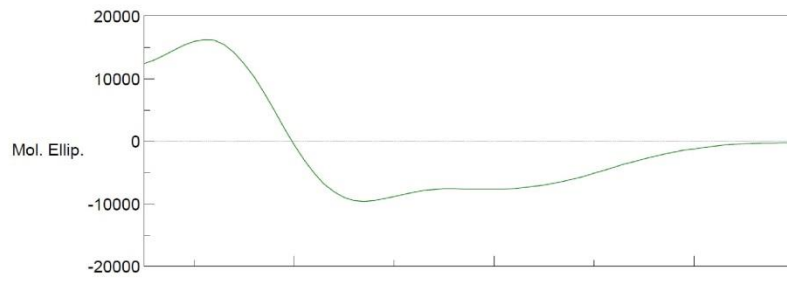


CD spectroscopy

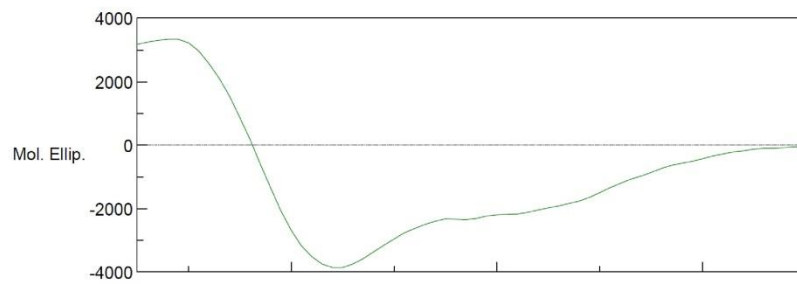
Peptide 1



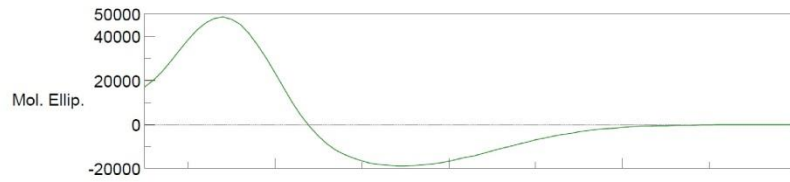
Peptide 25



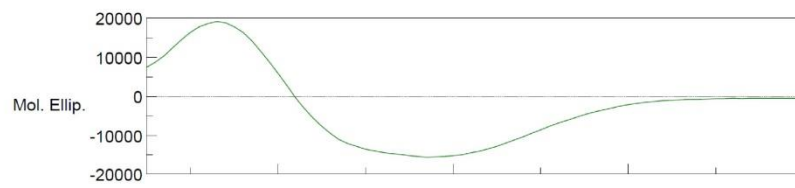
Peptide 26



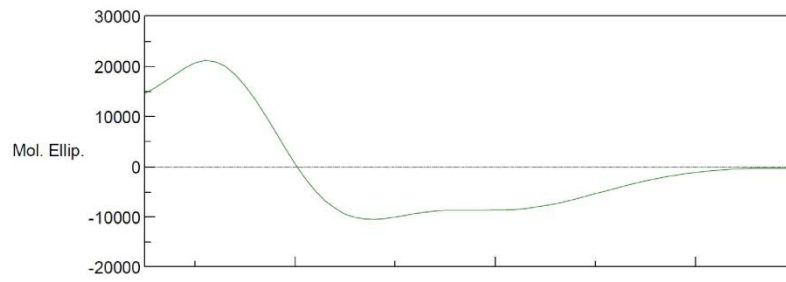
Peptide 27



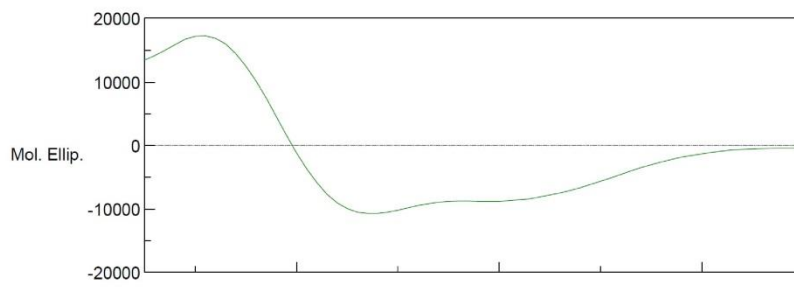
Peptide 28



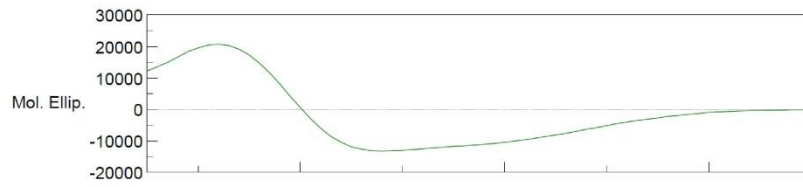
Peptide 29



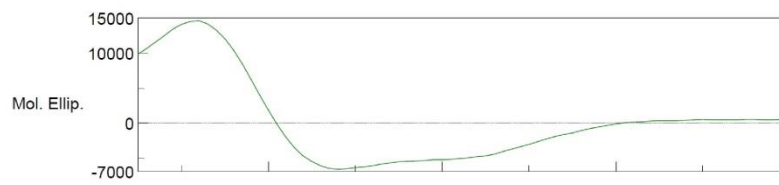
Peptide 30



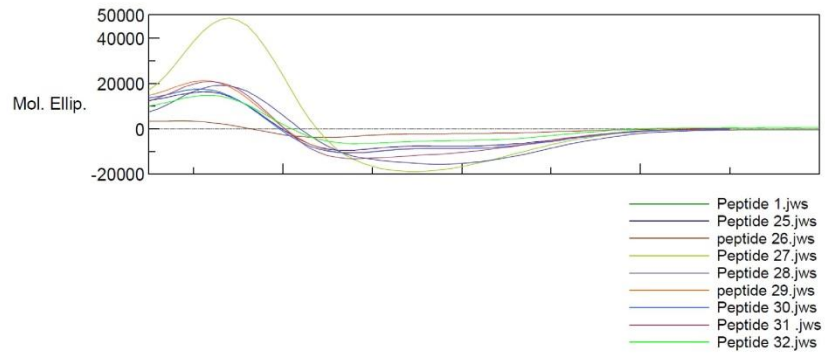
Peptide 31



Peptide 32

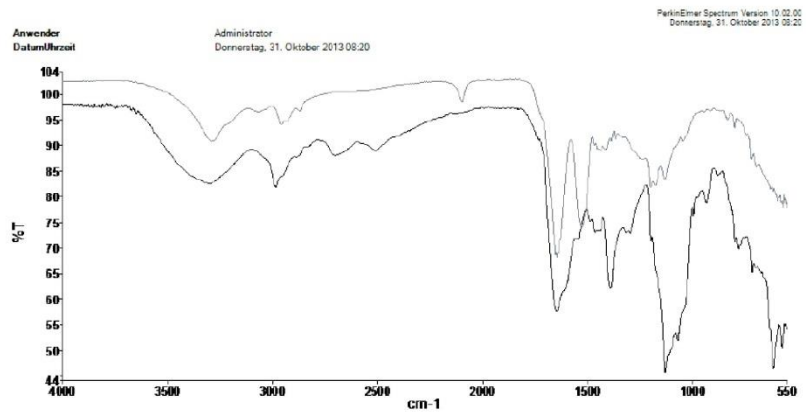


Overlay of peptide 1 and peptides 25-32

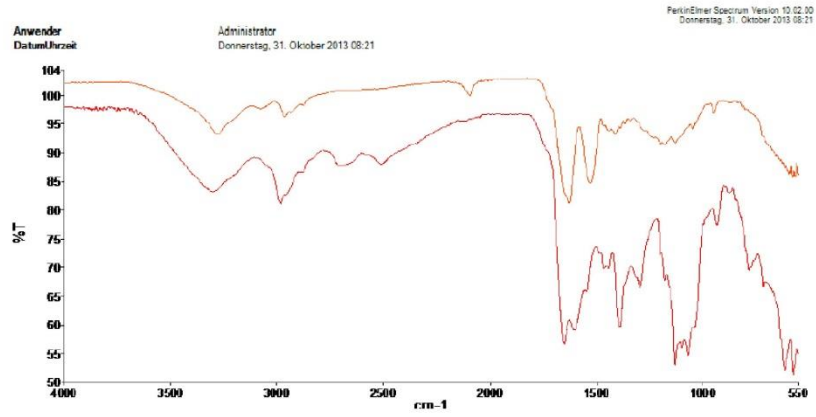


IR

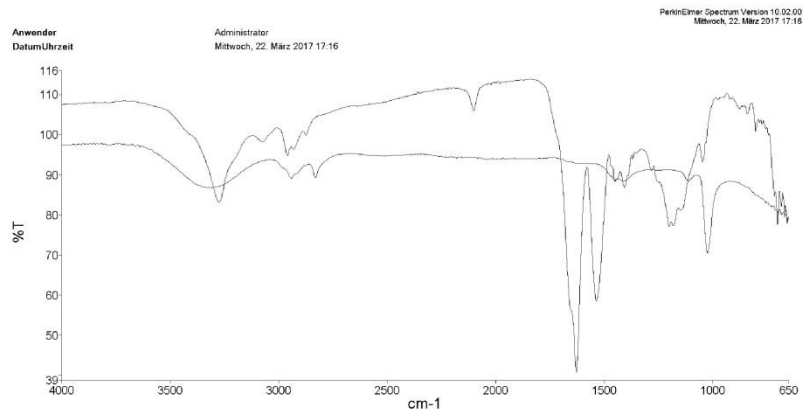
Peptide 25 (gray) and peptide 29 (black)



Peptide 26 (orange) and peptide 30 (red)



Peptide 27 (top) and peptide 31 (bottom)



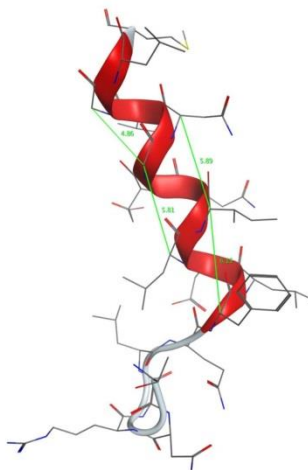
Aggregation Test

Concentration (µM)	Peptide 14 (10 Min)	Peptide 14 (24 Hrs)	Peptide 5 (10 Min)	Peptide 5 (24 Hrs)	Negative control (10 Min)	Negative control (24 Hrs)
100	0,041	0,044	0,058	0,054	0,043	0,043
25	0,048	0,046	0,049	0,05	0,042	0,043
12,5	0,04	0,042	0,049	0,053		
6,25	0,04	0,041	0,04	0,042		
3,125	0,04	0,041	0,042	0,043		

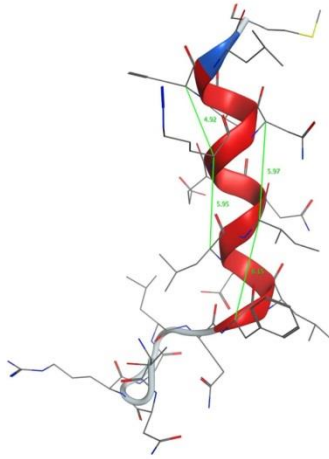
Table S2. Absorbance values at 600 nm acquired from aggregation test.

Molecular modeling of peptides 1 and 25-32 showing the distances between the amino acids used for macrocyclization.

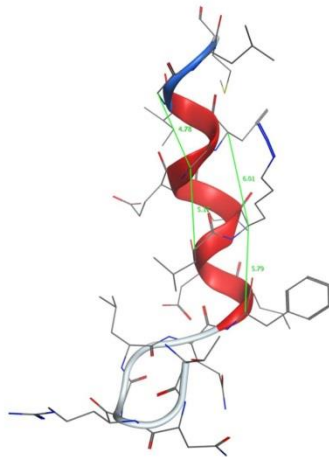
Peptide 1



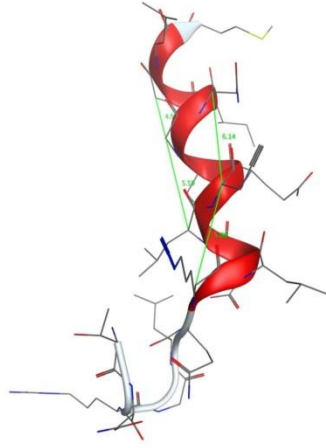
Peptide 25



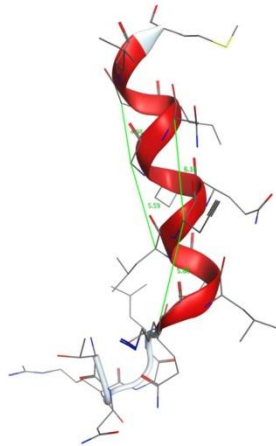
Peptide 26



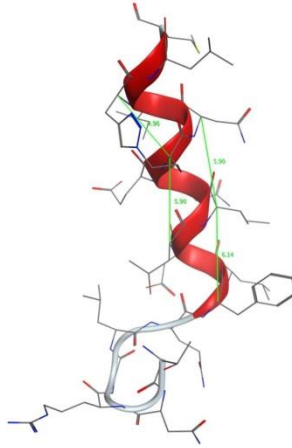
Peptide 27



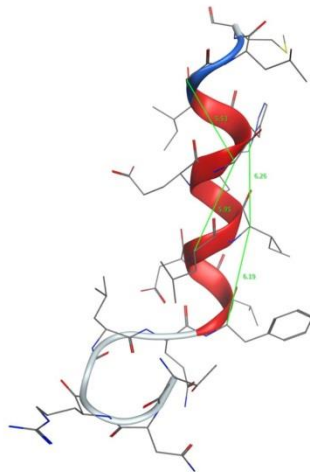
Peptide 28



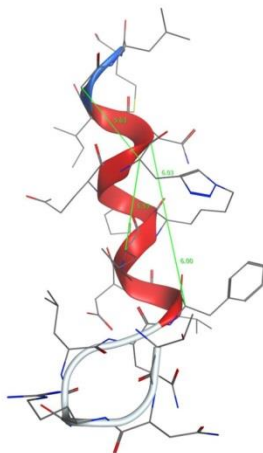
Peptide 29



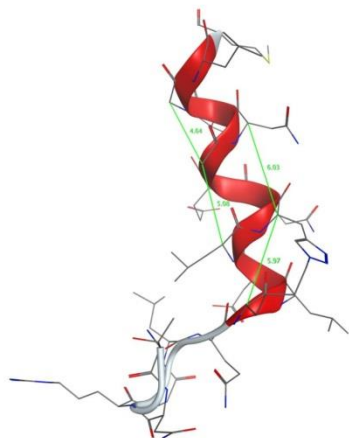
Peptide 30



Peptide 31



Peptide 32



7. Curriculum Vitæ

Personal Information

Full Name: Ahmed Ashraf Moustafa Kamal
Email: ahmed.ashraf.moustafa@gmail.com
Date/Place of Birth: 09.05.1989, Cairo, Egypt
Nationality: Egyptian
Marital Status: Single

Education

Jan 2014 – to date **Doctor Rerum Naturalium (Ph.D.)**
Helmholtz Institute for Pharmaceutical Research Saarland and Saarland University, Saarbrücken, Germany.
Prof. Dr. Rolf W. Hartmann

Feb. 2013 – Dec. 2013 **Diplom-Pharmazeut (Master thesis)**
Helmholtz Institute for Pharmaceutical Research Saarland and Saarland University, Saarbrücken, Germany.
Prof. Dr. Rolf W. Hartmann
Thesis Grade: 1.3

Sep. 2006 - May 2011 **Bachelors of Pharmaceutical Sciences**
Faculty of Pharmacy, Cairo University, Egypt,
Grade Excellent with Honors (Top 5% of Class)

Work Experience

Jan 2014 – to date **Doctoral Researcher**
Helmholtz Institute for Pharmaceutical Research Saarland Saarbrücken, Germany

Feb. 2013 – Dec. 2013 **Research Assistant**
Saarland University, Saarbrücken, Germany

Dec. 2012 – Feb. 2013 **Quality Control Analyst**
National Organization for Drug Control and Research, Egypt

Oct. 2011–Dec. 2012 **Hospital Pharmacist (Military Service)**
Heliopolis Military Hospital, Egypt

Linguistic skills

Arabic: Mother Tongue
English: Full professional proficiency
German: Professional working proficiency
French: Elementary proficiency



8. Further publications of the author that is not part of this dissertation

A) Quorum Sensing Inhibitors as Pathoblockers for *Pseudomonas aeruginosa* Infections: A New Concept in Anti-Infective Drug Discovery

Kamal, A.A.M.; Maurer, C.K.; Allegretta, G.; Haupenthal, J.; Empting, M.; Hartmann, R.W. *Topics in Medicinal Chemistry* **2017**, 1–26.

B) Biophysical Screening of a Focused Library for the Discovery of CYP121 Inhibitors as Novel Antimycobacterials

Brengel, C.; Thomann, A.; Schiffrin, A.; Allegretta, G.; Kamal, A.A.M.; Haupenthal, J.; Schnorr, I.; Cho, S.H.; Franzblau, S.G.; Empting, M.; Eberhard, J.; Hartmann, R.W. *ChemMedChem* **2017**.

C) Discovery of novel non-ATP competitive inhibitors of protein kinase CK2,

Bestgen, B.; Krimmf, I.; Kufarevag, I.; Kamal, A.A.M.; Abagyang, R.; Cochet, C.; Hartmann, R.W.; Le Borgne, M.; Lomberget, T.; Engel, M, *Manuscript in preparation*

